



HAL
open science

Structures en treillis avec poutres pivotantes : homogénéisation et résultats d'élasticité non-linéaire

Alessandro Della Corte

► **To cite this version:**

Alessandro Della Corte. Structures en treillis avec poutres pivotantes : homogénéisation et résultats d'élasticité non-linéaire. Mécanique des solides [physics.class-ph]. Université de Toulon; Università degli studi La Sapienza (Rome). Dipartimento di Ingegneria Meccanica e Aerospaziale, 2017. Français. NNT : 2017TOUL0019 . tel-01982096

HAL Id: tel-01982096

<https://theses.hal.science/tel-01982096>

Submitted on 15 Jan 2019

HAL is a multi-disciplinary open access archive for the deposit and dissemination of scientific research documents, whether they are published or not. The documents may come from teaching and research institutions in France or abroad, or from public or private research centers.

L'archive ouverte pluridisciplinaire **HAL**, est destinée au dépôt et à la diffusion de documents scientifiques de niveau recherche, publiés ou non, émanant des établissements d'enseignement et de recherche français ou étrangers, des laboratoires publics ou privés.

ÉCOLE DOCTORALE
**MÉCANIQUE DES SOLIDES, GÉNIE MÉCANIQUE, PRODUCTIQUE,
TRANSPORT ET GÉNIE CIVIL**

THÈSE présentée par :
Alessandro DELLA CORTE

soutenue le : **15 Décembre 2017**

pour obtenir le grade de Docteur en Mécanique des solides
Spécialité : Homogénéisation et élasticité non-linéaire

**STRUCTURES EN TREILLIS AVEC POUTRES
PIVOTANTES: HOMOGENÉISATION ET
RÉSULTATS D'ÉLASTICITÉ NON-LINÉAIRE**

THÈSE dirigée par :

M. DELL'ISOLA Francesco	Professor, M&MoCS, Università degli Studi dell'Aquila
M. SEPPECHER Pierre	Professor, IMATH, Université de Toulon

JURY :

M. MARCATI Pierangelo	Professor, Università degli Studi dell'Aquila
M. LEBON Frédéric	Fonctions, Aix-Marseille Université
M. REMOND Yves	Professor, Université de Strasbourg
M. PEREGO Umberto	Professor, Politecnico di Milano
M. DELL'ISOLA Francesco	Professor, Università degli Studi dell'Aquila
M. SEPPECHER Pierre	Professor, Université de Toulon

PhD THESIS

LATTICE STRUCTURES WITH PIVOTED BEAMS:
HOMOGENIZATION AND
NONLINEAR ELASTICITY RESULTS

Submitted by

Alessandro Della Corte

Sapienza Università di Roma

Dipartimento di Ingegneria
Meccanica e Aerospaziale

Co-supervisor:

Prof. Francesco dell'Isola

Université de Toulon

Institute de Mathématiques

Co-supervisor:

Prof. Pierre Seppecher

2017

Abstract:

This thesis focuses on the mathematical modeling of fibrous structures having some peculiar properties (high strength-to-weight ratio and very good toughness in fracture), whose mechanical behavior escapes from standard Cauchy elasticity. In particular, it addresses cases in which the presence of a microstructure, consisting of regularly spaced pivoted beams, entails effects that are well described by generalized continuum models, i.e. models in which the deformation energy density depends not only on the gradient of the placement but also on the second (and possibly higher) gradients of it. In the Introduction, the state of the art concerning generalized continua and their applications for the description of fibrous structures is described and some relevant open problems are highlighted. In Chapter 1 and 2 a rigorous homogenization procedure based on Gamma-convergence arguments is performed for a lattice (truss-like) structure and for a discrete 1D system (Hencky-type beam model). In Chapter 3, a variational treatment is employed to formulate a computationally convenient approach. In Chapter 4 some experimental results concerning the behavior of the structure in various kinds of deformation are discussed. This motivated the investigation performed in Chapter 5, in which Direct Methods of Calculus of Variations are applied to Euler beams in large deformations under distributed load.

Keywords: Generalized continua, Direct methods of calculus of variations, Gamma-convergence.

Titre en français : Structures en treillis avec poutres pivotantes: homogénéisation et résultats d'élasticité non-linéaire.

Résumé:

Cette thèse est consacrée à la modélisation des structures fibreuses avec des milieux continus généralisés. Dans l'Introduction, l'état de l'art concernant les milieux continus généralisés et applications aux structures fibreuses sont décrits et les problèmes ouverts pertinents sont mis en évidence. Dans le Chapitre 1 et 2, une procédure d'homogénéisation rigoureuse basée sur des arguments de Gamma-convergence est appliquée à une structure en treillis et à un modèle de poutre discrétisé. Dans le Chapitre 3, un traitement variationnel est utilisé pour formuler une approche favorable du point de vue numérique. Dans le Chapitre 4 sont discutées les résultats expérimentaux concernant le comportement de la structure dans différents types de déformation. Cela a motivé les études effectuées dans le Chapitre 5, où les Méthodes directes de calcul des variations sont appliquées à des poutres d'Euler en grandes déformations.

Mot clés: Milieux continus généralisés, Méthode directe du calcul des variations, Gamma-convergence.

Contents:

Foreword	p. 5
Introduction	p. 8
Chapter 1	p. 30
Chapter 2	p. 47
Chapter 3	p. 67
Chapter 4	p. 115
Chapter 5	p. 126
Appendix	p. 158

Foreword

The present thesis is based on the following papers:

1. dell'Isola, F., Steigmann, D., **Della Corte, A.** (2016). Synthesis of fibrous complex structures: designing microstructure to deliver targeted macroscale response. *Applied Mechanics Reviews*, 67(6), 21-pages.
2. Alibert, J. J., **Della Corte, A.** (2015). Second-gradient continua as homogenized limit of pantographic microstructured plates: a rigorous proof. *Zeitschrift für angewandte Mathematik und Physik*, 66(5), 2855-2870.
3. Alibert, J. J., **Della Corte, A.**, Giorgio, I., Battista, A. (2017). Extensional Elastica in large deformation as Gamma-limit of a discrete 1D mechanical system. *Zeitschrift für angewandte Mathematik und Physik*, 68(2), 42.
4. dell'Isola, F., **Della Corte, A.**, Greco, L., Luongo, A. (2016). Plane bias extension test for a continuum with two inextensible families of fibers: A variational treatment with Lagrange multipliers and a perturbation solution. *International Journal of Solids and Structures*, 81, 1-12.
5. **Della Corte, A.**, dell'Isola, F., Esposito, R., Pulvirenti, M. (2016). Equilibria of a clamped Euler beam (Elastica) with distributed load: Large deformations. *Mathematical Models and Methods in Applied Sciences*, 1-31.

These papers investigate, from different points of view, pantographic structures, i.e. lattice structures in which two families of fibers are interconnected by means of torsional pivots. The geometry of the system, in the simplest case in which the pivots are regularly spaced and the fibers are parallel and straight in the reference configuration, is represented in Fig. 1.

These objects can be easily manufactured by means of computed-aided techniques such as 3D-printing. Concerning potential applications, the main advantages of pantographic structures (which of course will be discussed in detail later) can be quickly summarized as follows:

- Lightness
- Resilience
- Toughness in fracture
- Contained manufacturing costs

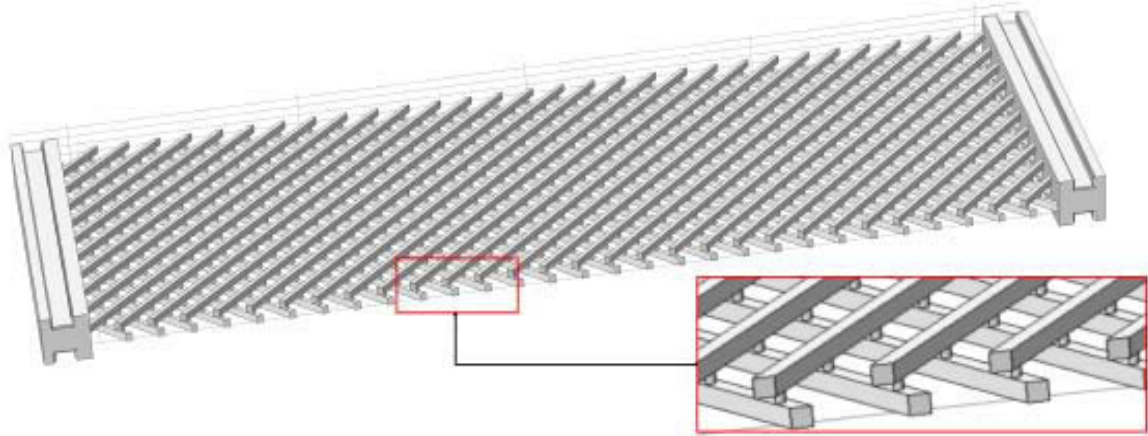


Fig. 1: The geometry of a pantographic sheet. Two families of parallel fibers are connected by means of short cylinders, which undergo torsional deformation when the angle between the fibers changes. The fibers are slender enough to be modeled as Euler beams. Depending on the particular shape ratio and on the particular deformation under consideration, the extensible or inextensible beam model can be adopted. A 2D homogenized model must take into account effects that cannot be captured by classical Cauchy continua, and for which second gradient energy models are needed.

The theoretical and numerical investigation of such kind of structures is by no means trivial. Indeed, as it will be shown, generalized continuum models are called for if one wants to model the behavior of pantographic sheets in a convenient and efficient way. Moreover, rigorous homogenization results for lattice structures can be established by means of Gamma-convergence arguments, and they prove that in general the deformation energy density of the homogenized limit has to involve the second gradient of the placement. Finally, the problem of geometrically nonlinear deformation of Euler beams under distributed load arises naturally when studying these objects at the meso-scale, and the relative rigorous treatment involves techniques from calculus of variations and convex analysis.

The thesis is organized as follows: the Introduction (paper 1) is devoted to the general description of metamaterials (with a special focus on fibrous systems) and of their mathematical modeling by means of generalized continuum models; pantographic structures are introduced as a model case in Section 7. Chapter 1 (paper 2) proves the Gamma-convergence of a lattice (truss-like) structure to a generalized continuum model, as the lattice step goes to zero; it is the first rigorous homogenization result involving a pure second gradient energy model as homogenized limit. Chapter 2 (paper 3) proves the Gamma-convergence of a discretized beam model consisting of extensional springs connected by rotational springs (Hencky-type beam model) towards the extensible Euler beam in large deformations, thus providing a rigorous basis for a discretization that is commonly employed in computational mechanics; moreover, it is particularly relevant to our aims since the fibers of the pantographic

sheet undergo large deformation in the experimental tests which we will consider later. In Chapter 3 (paper 4) a variational treatment is employed to deduce the nonlinear integral equations describing fibers directions for a large class of deformation energies associated to the variation of the angle between the fibers of the pantographic sheet. In Chapter 4 (based on the paper [1], in preparation) some experimental evidence, based on extension tests performed on polyamide samples, is provided, discussed and compared to numerical results. Chapter 5 (paper 5) provides rigorous results on the large deformations of an inextensible Euler beam model under distributed load; this kind of load is intended as a reasonable approximation of the load which the fibers of the pantograph are submitted to when the lattice step is small enough; the existence of a global minimizer and of local minima of the energy are proven, qualitative properties of the solutions are established and some stability results are also provided. Finally, in the Appendix some (still unpublished) results on the qualitative behavior of an Euler beam in large deformations in the extensible case are proven, and in particular it is established that equilibrium configurations exhibiting multiple turns around the clamped edge are not possible.

[1] Andreaus U., Spagnuolo M., **Della Corte, A.** et al. Discrete geometrically nonlinear pantographic structures: numerics and experiments (2017) [*In preparation*].

Introduction

Synthesis of Fibrous Complex Structures:
Designing Microstructure to Deliver Targeted
Macroscale Response

Synthesis of Fibrous Complex Structures: Designing Microstructure to Deliver Targeted Macroscale Response

Francesco dell'Isola

DISG,
University of Rome La Sapienza,
Rome 00184, Italy
e-mail: francesco.dellisola@uniroma1.it

David Steigmann

Faculty of Mechanical Engineering,
University of California,
Berkeley, CA 94720-1740
e-mail: dsteigmann@berkeley.edu

Alessandro Della Corte¹

DIMA,
University of Rome La Sapienza,
Rome 00185, Italy
e-mail: alessandro.dellacorte@uniroma1.it

In Mechanics, material properties are most often regarded as being given, and based on this, many technical solutions are usually conceived and constructed. However, nowadays manufacturing processes have advanced to the point that metamaterials having selected properties can be designed and fabricated. Three-dimensional printing, electrospinning, self-assembly, and many other advanced manufacturing techniques are raising a number of scientific questions which must be addressed if the potential of these new technologies is to be fully realized. In this work, we report on the status of modeling and analysis of metamaterials exhibiting a rich and varied macroscopic response conferred by complex microstructures and particularly focus on strongly interacting inextensible or nearly inextensible fibers. The principal aim is to furnish a framework in which the mechanics of 3D rapid prototyping of microstructured lattices and fabrics can be clearly understood and exploited. Moreover, several-related open questions will be identified and discussed, and some methodological considerations of general interest are provided.

[DOI: 10.1115/1.4032206]

1 Introduction

1.1 Past Achievements and New Challenges. Since its birth, hard science has developed in close relation with emerging technology [1]. It is indeed a *leitmotiv* in the History of Science that the increase of phenomenological evidence entailed by the development of new technological possibilities has first put in crisis the existing scientific paradigms and then gradually led to new ones. This was exactly what happened, for instance, when scientific technology was born in the Hellenistic World, when modern Mechanics arose in the age of Galileo or when thermodynamics was elaborated in the early 19th century. In all these cases, the most evident sign of the success of the conceptual revolution is the fact that the new ideas which were elaborated to describe and design technological novelties (as, for instance, catapults, bombs, or steam engines) are nowadays integrated in the same theoretical framework of so-called *classical physics*. However, one should not forget the long and troublesome process that led to this integration.

In our opinion, Mechanics is about to experience a similar conceptual revolution. The newly arisen technological possibilities in controlling the properties of materials at the micro- and nanoscale are pushing for the development of new theoretical models. In particular, the novelties made possible by advanced manufacturing techniques developed in the recent past are forcing us to reconsider our ideas about the position of theoretical and applied mechanics in relation to technology. The behavior of objects produced by means of these methods, more often than not, is indeed exotic and peculiar from the classical point of view.

Whereas for thousands of years, material properties have been regarded as being given, it is clear that manufacturing processes have now advanced to the point that one can design and fabricate materials exhibiting properties that are not directly found in nature, i.e., so-called metamaterials. Three-dimensional printing, electrospinning, self-assembly, and many other advanced

manufacturing techniques are raising a number of scientific questions, which have to be answered if the potential of existing and foreseeable developments in manufacturing is to be fully realized. One has to admit that, as sometimes happens in the History of Science, technological innovation is today ahead of scientific modeling in this regard. Multiscale and multiphysics structures are able to exhibit a wide range of peculiar behaviors and may involve an extraordinary level of complexity in their internal organization. The need to design and construct metamaterials calls thus for major advancements in the mechanics and physics of solids and fluids, in mathematical and numerical modeling, and in advanced computer-aided technology. Moreover, to meet this challenge, a strong theoretical foundation and a realistic and up-to-date knowledge of what is concretely feasible today are essential.

The present work is mainly intended as a review on fabrics and in general on fibrous materials. However, when speaking of metamaterials, many different systems come to mind, as, for instance, acoustoelastic metamaterials intended for wave manipulation (photonic, phononic effects, etc.) and others (e.g., truss networks, composites, mechanical metamaterials, etc.). In order to outline a much more general picture, we will provide some example of metamaterials from a broader class than fabrics which, without any claim of exhaustiveness, can help the reader to get a better understanding of a very large research area.

From the point of view of a theoretical approach, one of the main ideas emerging up to the present time is a unifying variational approach, which is applicable to a wide and diverse range of problems. On this subject, Refs. [2–9] are classical references; a recent overview is provided in Refs. [10,11], while interesting recent results related to complex materials are provided in Refs. [12–19]. Existence and uniqueness of solutions in the variational setting are studied in Refs. [20–22] concerning surface effects, in Ref. [23] in case of micropolar continua, and in Ref. [24] in a more general context. Moreover, inelastic processes have also been described within the variational framework, and in this connection, relevant contributions are given in Ref. [25], where aspects, such as plastic deformation, non-Newtonian viscosity, rate sensitivity of plastic flow, and hardening, are covered.

¹Corresponding author.

Manuscript received July 24, 2015; final manuscript received December 7, 2015; published online January 6, 2016. Assoc. Editor: Rui Huang.

1.2 The Need to Reorganize a Complex Subject. The absence of a general order founded on a common framework is a common feature of emerging topics and novel research fields. This is exemplified by the design of metamaterials; this is not a mere problem of terminology, but may also form barriers to communication between different groups of researchers; this is indeed one of the major problems of modern science.

A primary purpose of the present review is to show that problems attacked by means of a variety of approaches, in seemingly different research fields are, under the surface, just different aspects of the same general problem.

Among the most used “labels” for today’s research in applied mechanics we indeed find:

- advanced materials [26–29],
- architected materials [30–36],
- optimized materials [37–39],
- metamaterials [40–44],
- smart materials [45–49],
- multiscale materials [50–53],
- multiphysics materials [54–68],
- materials with negative mechanical constitutive coefficients (stiffness, modulus, Poisson ratio, etc.) [69–73],
- composite materials [74–78], and
- complex materials [79–85].

Regarding theoretical counterparts, we have, for instance:

- generalized continua [86–94],
- microstructured continua [2,95–109],
- continua with microstrains [110,111]
- higher gradient continua [112–119],
- Cosserat continua [120–127], and
- micropolar continua [128–131].

Of course, it would be wrong to say that all these labels refer to exactly the same scientific content, even if in some cases, as for instance the last two, they are almost exact synonyms (for works explicitly aimed at the identification of intersections between some of the previous fields, reference may be made to, e.g., Refs. [89,132–138]). Rather, we want to underline the common *motivations* behind their origins, together with their shared goals.

In the opinion of the authors, the real challenge for today’s theoretical and applied mechanics is expressed by the following:

Mission statement—to select the desired behavior of a material by means of the choice of its governing equations, and subsequently to synthesize and manufacture a microstructure or a complex multiphysics system whose behavior is suitably described by the chosen equations.

This mission statement is, sometimes in an indirect way, at the basis of the fields identified by the previous labels and constitutes their common underlying foundation. In our opinion, this kind of perspective provides a needed guide in what seems to be a very complicated spectrum of problems. If one keeps clear the ultimate target, the subtleties and the technicalities which distinguish one label from the other will not distract attention from the actual scientific content, and it will be much easier to translate methods and tools from one area to another, thereby strengthening the arsenal for meeting the challenges.

2 The Hypotheses at the Basis of Mechanics and Their Relation With Existing Technology

Mathematical modeling capabilities have shaped the technologies of every advanced society [1]. The great advancement of Illuministic engineering was based on solid mathematical grounds and produced a grand economical and technological development. Western civilization was characterized by an Archimedean mathematical description of both phenomena and engineering artifacts. However, until very recent times, mathematical modeling has been limited to the description of pre-existing materials (see Ref. [139] for a general introduction in material selection).

Therefore, the simplifying assumptions which were the basis of engineering in the Illuministic era and in the subsequent Industrial Revolution were deeply founded in the observed phenomenology and became a paradigm of scientific and technological thought. The assumptions conjectured by the founders of modern engineering sciences (Cauchy, Poisson, Navier, Maxwell, Piola, etc.) were so deeply rooted in the minds of scientists and engineers that they became basic doctrine.

Indeed, several lines of inquiry have ceased to evolve, precisely because of the depth of these roots, even if the emergence of computer-aided manufacturing rendered them rather obsolete (for a general reference on the topic, see Ref. [140]). An important example is that of external contact action. For scientists accustomed to classical Cauchy continua, whose deformation energy depends on the first gradient of the displacement, external contact actions are essentially surface forces; however, when dealing with complex microstructures which lead, in their homogenized limit, to higher gradient models (refer to Sec. 1.1), the set of possible external contact actions is richer and may include line forces, concentrated forces, double forces, and objects of higher order [141]. Another way to express the previous statement is: once you can manufacture (by 3D printing, electrospinning, or any other novel technical possibility) an object with a microstructure which, macroscopically seen as a continuum, can sustain double forces (or higher order ones), you cannot anymore neglect them in your theoretical constructions. This means that you have to rebuild your set of assumptions in order to enrich the consequences you can deduce from them. It is a clear example of what is intended by the title of the present section: the technological possibilities, as already observed in Sec. 1, determine the most appropriate set of hypotheses to be assumed as a foundation for the theoretical construction of mechanics. As a consequence, it is insufficient to be limited to a certain formulation for purely abstract reasons, without taking into consideration the effects of the introduction of novel technologies. A notable example is given in Ref. [142], where materials with unusual response to elastic waves (requiring a suitable generalization of elementary dynamics’ concepts) are investigated.

An important conceptual revolution in connection with the emergence of new technology, methodologically not too different from what we are discussing, has already occurred. In the early 1940s of the 20th century, the competition between analog computers and Turing-von Neumann machines forced the supporters of analog computing to change their paradigms. Inspired by the need to obtain solutions to complex partial differential equations (PDEs) or ordinary differential equations (ODEs) needed for the construction of scientific experiments (see, for instance, Ref. [143]) or for large-scale production designing [144], many scientists could not wait for the final establishment of the superiority of digital computers and were obliged to build, or, as they often said, to synthesize analogous electric circuits governed by a given set of mathematical equations for the purpose of computing.

This process, which was historically important in the emergence of modern computing, is methodologically analogous to the approach entailed by the aforementioned mission statement, whose aim is indeed to choose the desired behavior of the materials by means of the choice of its governing equations, and subsequently to synthesize a microstructure or a complex multiphysics system whose behavior is suitably described by the chosen equations. The main difference lies in the wider generality of the systems to be considered today, and, as a consequence, the greater sophistication of the necessary theoretical tools.

3 Three Approaches to Accomplish the Objective

In the context of Applied Mechanics, three different approaches can be used to meet the challenge expressed by the foregoing mission statement.

3.1 Physical Modeling. This approach consists of conjecturing, by means of physical intuition and experience, the structure

of a system performing a given task and then proving the validity of the conjecture by means of prototyping and experimental evidence. Of course, in this approach the proper use of numerical simulations is very important to direct physical intuition toward the most promising cases. Powerful methods allowing rapid assessment of the main quantitative characteristics of complex mechanical systems are today available, and among them one of the most universal is the Finite-Element Analysis, whose flexibility is ideal for dealing with geometrically complex systems such as those related to metamaterials (see Ref. [145] for a historically important reference, and Refs. [146–154] for interesting recent applications). Finite elements with suitable interfaces can also be employed for modeling fracture phenomena, as done in Refs. [155,156]. Finally, especially useful can be the introduction of elements with high regularity properties as, for instance, those used in isogeometric analysis (see, e.g., Refs. [157–164]). Another very successful computational tool is represented by Molecular Dynamics, which is based on the numerical study of systems constituted by a very large number N of elements. The numerical computation of the trajectories of particles in the ordinary $6N$ -dimensional phase space of positions and momenta employs the classical mechanics laws of motion (for an introduction, see Ref. [165]). Finally, especially concerning inelasticity, very important are computational scale-bridging methods (such as CADD, QC, MADD, and DDD, see Ref. [166] for an example with the discussion of some general problems in models comparison), which have emerged from the need to apply classical mechanics to small-scale systems.

3.2 Models of Generalized Continua. The foregoing approach is probably most effective when a major advance has already been achieved, and only simple refinements remain to be performed. When, instead, completely new concepts are to be applied to achieve technological progress, a true change of paradigm is needed, and such a change can be obtained only by re-examining a substantial part of engineering science. It seems that to this end the basis of continuum mechanics must be revisited, to effectively restart a line of research initiated by Piola [167]. Even if seemingly not consciously, the revival of Piola’s ideas is already in progress. The currently active field of Peridynamics furnishes a particularly fruitful example (see, for instance, Refs. [168–172] for relevant results and Ref. [134] for a historical perspective). Peridynamics is indeed the modern name given to Piola’s most general continuum mechanics proposed by him as a sound tool for investigating the mechanics of deformable bodies. Standard continuum mechanics, though providing a most powerful conceptual framework, seems to have exhausted its propulsive thrust, at least insofar as macromodeling is concerned. Naturally, once suitable continuum models have been introduced on the basis of the known smaller-scale structure, then only discrete numerical methods will be able, in the general case, to furnish detailed predictions of the relevant phenomena occurring in the contemplated technologies. Some purely academic exercises can be solved with analytical or semi-analytical methods, but their impact cannot be regarded as being substantially relevant in technological applications. Rather, their importance stems mainly from the fact that they furnish benchmarks for numerical codes.

3.3 Dimension Reduction of Discrete Models. Once the relevant small-scale substructure has been identified, providing a purely conceptual basis for the theoretical description of a complex system, the most important modeling step consists in finding a discrete model to represent the important aspects of the phenomenology. Normally, such a discrete system has a very large number of degrees-of-freedom, say $q_i (i = 1, \dots, N)$, and even if very powerful supercomputers could apply them to a few cases of academic interest, their systematic application to engineering problems is still not feasible. Therefore, one contemplates the introduction of a lower dimensional discrete model (having coordinates $Q_h, h = 1, \dots, n$, with $n \ll N$) and a reduction kinematic

map (also known as a “handshake step” in multiscale modeling), allowing for the determination of all of the q_i once the Q_h are given (interesting results along these lines may be found in Ref. [173]). All of the capabilities of the modeler are, in this context, bound to the fidelity of this reduction map. If both systems are Lagrangian (possibly extended to include a Hamilton–Rayleigh dissipation potential), the reduction map will immediately produce the Lagrangian of the reduced system and will provide a useful computational tool. In some cases, rigorous mathematical results may also be available to prove that when one or more parameters tend to zero, the introduced procedure actually yields a suitable approximation.

3.4 An Overview of the Three Approaches. Each one of the aforementioned approaches finds a natural role in the research work according to its intrinsic merits. In most of the cases, the synergistic interaction of all of them, which is the basis of the Archimedean–Galilean method, is a necessary condition for scientific progress. A way to concretely realize the purposes described concisely in Secs. 3.1, 3.2 and 3.3 can consist in setting up a program for producing 3D-printed prototypes, such as that shown in Fig. 1 (see below for details). The inspiration for the fine structure of the printed specimens can often be drawn from the available technology of fiber-reinforced composites and the available literature in the field of architected materials [32,109,139,174]. Suitable modifications and parameter variations can be tested by measuring the mechanical properties of prototypes. Further, simple piezoelectromechanical systems with actuators of smaller size than those used in Refs. [175–177] can be constructed to test the feasibility of exploiting multiphysics to achieve desired global macroscale properties. Of course, the characteristic length scale that can be attained with the aforementioned methods cannot reach nanodimensions. However, the conceived prototyping, once guided by a suitable rescaling theoretical methodology, could yield important insights into the effectiveness of the considered concepts. For example, it is well known that electrospinning cannot currently produce precisely designed complex fabrics at the nanoscale. However, it can be usefully employed to explore some nanophenomenology and to yield an understanding of some relevant properties (for a discussion concerning size-related surface effects, see Sec. 6).

4 Examples of Possible Implementations of the Mission Statement

The Mission Statement above expressed in its general form can be realized in several concrete ways. A classical challenge, and

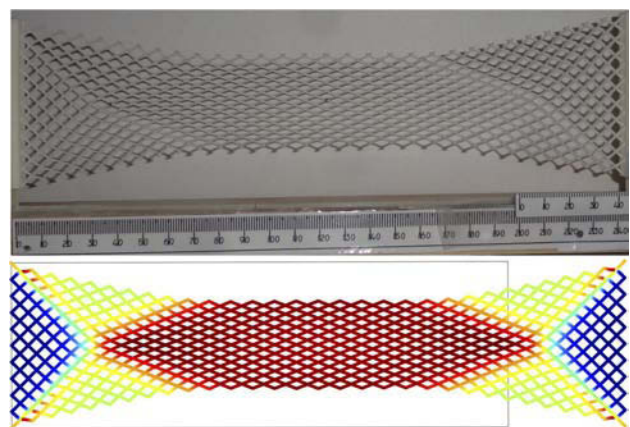


Fig. 1 Bias test on a 3D-printed pantographic sheet (top) and simulation, as studied in Ref. [358] (original picture by the authors); we remark that the picture is relative to a continuum simulation, and that the curves represent sets of material points which are straight lines in the reference configuration

still one of the most important ones, is to find materials with prescribed/optimized constitutive characteristics (e.g., stiffness, strength, toughness, dispersions relations, etc.). Moreover, several other problems can nowadays be addressed:

- (1) To find a material which is able to damp mechanical vibrations by means of a granular microstructure [178] or by transforming mechanical energy into electromagnetic energy via piezoelectric transduction [175,179–185].
- (2) To find a material which exhibits, at least in some directions, a large ratio between weight and fracture toughness [186–195].
- (3) To find a deformable porous material saturated by an electrically or magnetically active nematic fluid, to enhance Darcy dissipation to control the propagation of electro- or magneto-nematic waves [196–199].
- (4) To find an adaptive material endowed with an embedded sensing system activating variations in mechanical constitutive parameters; for example: a beam with a section moment of inertia that can be modified by the actuation driven by mechanical wave propagation or by an electrical signal, or other kinds of smart materials for bone fracture repair purposes [200–214].
- (5) To design a multiscale fabric constituted by a beamlike substructure whose deformation energy depends on n th gradient of displacement field, and to exploit these structural elements to form materials exhibiting nonstandard dispersion effects, possibly including frequency band gaps.
- (6) To find a material constituted by nearly inextensible fibers, which is able to resist shear and elongation by storing deformation energy in the form of fiber bending energy [215].

For each one of the previous targets, some results and potentially useful tools are already available in the literature, and the references provided were intended as a (partial) coverage of them. In addition, it should also be pointed out that, in almost every one of the considered problems, the elementary theory of the beam can still play a fundamental role. It is indeed by suitably generalizing classical beam models that richer theories, required for the study of metamaterials, are often developed (on generalized beam theory, see, e.g., Refs. [216–219]).

5 Standard Methods in Material Designing and Related Challenges

The usual procedure, when dealing with the mathematical design and description of new technology, in particular considering microstructured objects, consists of the following steps:

- (1) To select a promising microstructure which is practically realizable by means of existing (or foreseeable) manufacturing techniques; this may be done by means of intuition, experience, or by the methods of structural optimization [32,109,139].
- (2) To identify the smallest length scale at which a field model could be introduced, at least in principle. This field theory can be classical or based on molecular dynamics, depending on the characteristic structural length scale and the required accuracy. Usually, this model cannot be employed to make predictions because of the enormous computational effort required.
- (3) To use a discrete mesoscale model for describing the behavior of the considered complex system in an approximate way; this mesomodel must incorporate the most relevant overall behavior of the previously introduced smallest length-scale model.
- (4) To build an averaged continuous macromodel based on a certain set of simplifying assumptions, using an appropriate homogenization process, asymptotic expansions, and perturbative analyses, as done, for instance, in Ref. [192] in the case of pantographic structures (see below; useful

general results based on perturbative methods are provided in Refs. [220–223]).

- (5) To study the continuous model via numerical methods; i.e., to discretize it with one of the standard techniques (finite-difference method or finite-element method (FEM), isogeometric, etc.).
- (6) To compare the numerical solutions with experimental data and to refine the model accordingly.

The previous scheme, going from micro- to macroscale, is not the only one possible, and indeed other kinds of approaches exist (e.g., the so-called “scale-bridging” models, where two different scales, a coarser one and a finer one, are used for the description of the system [224]).

Concerning the aforementioned scheme, it is at least reasonable to question the universal validity of the aforementioned procedure. It can be conjectured, indeed, that the passages 3–5 could be made shorter by avoiding the intermediate continuum model.

Let us discuss this point in detail. Because of the high degree of complexity of the structures which can be produced today, it is almost always impossible to find analytical or semi-analytical solutions to the equations governing the micromodel (discussed in point 2), and in fact numerical analysis (point 5) has gradually become the only means by which the model interacts with experiments. While in the previous two or more centuries, in the engineering sciences the continuous model has been viewed as the most appropriate scientific image of reality, currently the awareness of the importance of the discrete nature of both the matter and the employed computational tools has led to the emergence of a novel epistemological picture. The role of continuous modeling and of homogenization methods is indeed still very important (a useful general references are provided in Refs. [225–227]; recent relevant results are Refs. [136,228–232]; on related numerical schemes see Ref. [233]), but it has a different motivation: namely, continuous models are very powerful for saving computational time. Indeed, one can succeed, by means of homogenization techniques, in:

- (1) Capturing all the important features of a given discrete system [234].
- (2) Filtering out phenomena occurring at a too small a length scale to be regarded as characteristic of the structure as a whole.
- (3) “Cleansing” the system from characteristics that are not interesting for a certain class of applications.
- (4) The equations obtained by means of this procedure can be simpler than those coming from discrete modeling, and so they are within reach of existing numerical methods.

This means that the entire passage: (a) discrete microstructure → (b) continuous model → (c) discrete numerical formulation has the meaning of revealing the essential physical features of the considered structures.

The micro–meso–macro identification, which confers concrete meaning to the mesoscale and to the homogenized models with respect to the micromodel, is characterized by a complex and complementary relationship between classical mechanical models and more sophisticated and rich ones; this point is worth to be discussed in some detail. As long as one does not reach a length scale at which quantum effects are relevant, it is in principle possible to study a structure, at the microlevel, by means of the standard Cauchy continuum model (see Sec. 6, for some observation on classical size-related effects at the nanoscale). The problem of this approach, as already explained, is the enormous computational cost it entails. It is easy, when trying to perform numerical simulations in which the micromodel of a complex structure is directly studied (see below, Fig. 2), that the computational possibilities of the most advanced hardware and software available today are overcome, and that consequently even powerful workstations may be led (and actually were, in the research experience of the

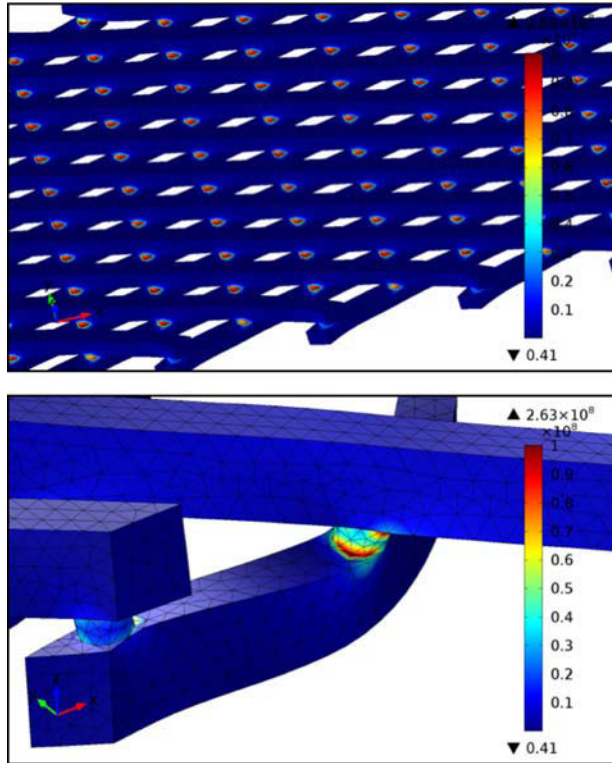


Fig. 2 Three-dimensional simulation for a pantographic structure as studied in Ref. [359]. Top: the deformation energy is stored in the pivots; bottom: the employed mesh is visible (original picture by the authors).

authors!) to a physical breakdown. A mesomodel, in which simpler objects (e.g., beams, chords, Saint-Venant cylinders, etc.) replace Cauchy continua, is in general much less computationally expensive and can therefore be precious once one has successfully established that the simplifying assumptions introduced do not involve the loss of relevant physical information (which is in general not easy). In this process, the generalization/adaptation of existing models, as, for instance, the introduction of a suitable nonlinear model for the beam (see, e.g., Refs. [91,235,236]), is often required. The computational advantage achieved in this way can be of several orders of magnitude, which means that problems requiring computational times of the order of weeks can be dealt with in hours or minutes. Obviously, an even more advantageous result is obtained by identifying the correct homogenized model for the considered system. In this case, usually, one cannot simply adjust existing models, but has to introduce new and more sophisticated generalized continua. Finally, it has to be noted that proving the convergence of the micromodel to the conjectured homogenized one, and even to select the most suitable kind of convergence to be considered, is in general a far from trivial operation [93,237].

5.1 Perspectives for Extension and Generalization of Available Results. Lagrangian mechanics has been formulated for both finite and infinite dimensional systems and is based on stationary principles, exemplified by the principle of virtual work. Because of the intrinsically discrete nature of Turing-von Neumann machines, also infinite dimensional Lagrangian systems must—if they are to produce predictions to be compared with experimental evidence—be approximated by discrete ones. A critical research field concerns the search for discrete simplified Lagrangian systems approximating discrete but more complex ones, without passing through homogenized continuous field models. General results in this context have never been applied to

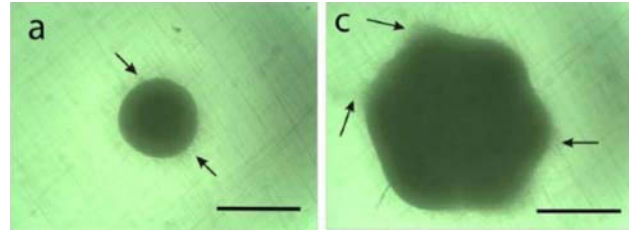


Fig. 3 A prestretched electrospun polyurethane metamaterial used as a scaffold for tissue growth; left: single tissue spheroid attached to the electrospun scaffold; right: seven fused tissue spheroids attached to the scaffold. Arrows indicate the areas of attachment-dependent cell and tissue spreading; scale-bar 300 μm (from Ref. [274]; free licence from SAGE webpage²).

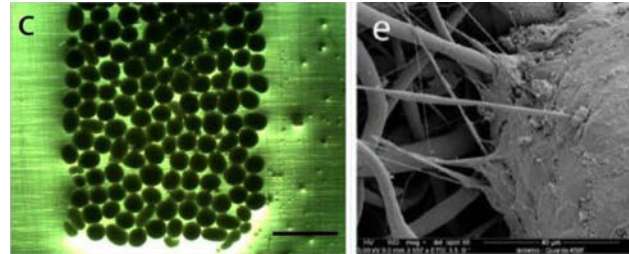


Fig. 4 Left: tissue spheroids adherent to the electrospun scaffold; right: SEM image of the adhesion of tissue spheroids to the electrospun matrix (from Ref. [274]; free licence from SAGE webpage³)

material and structural mechanics and may offer a major opportunity to advance the application of discrete mathematics.

From an historical point of view, it has to be deeply investigated the reason for which the founders of analytical mechanics, i.e., Navier, Poisson, Cauchy, Piola, Boltzmann, and all their successors, even if being strongly persuaded that the “true” ultimate nature of matter was discrete, still wanted to introduce a continuous model for deformable bodies. It could be that this choice was dictated simply by the deeply rooted habit of looking for analytical solutions using the methods of classical mathematical analysis, or by using semi-analytical methods as those developed by means of every kind of series expansion. It cannot be excluded, however, that these pioneers were aware of the importance of continuous models when the global behavior of a structure has to be investigated. The standard classification of PDEs in parabolic, hyperbolic, and elliptic may support such an epistemological point of view. For instance, a set of masses connected by nonlinear springs may exhibit many chaotic and extremely unlikely (or macroscopically irrelevant) kinds of time evolution. However, proving that in the regime of small deformations they are governed by the hyperbolic D’Alembert wave equation allows for a deep understanding of their overall behavior. One of the main expected results of the forthcoming researches is that many more exotic global behaviors will be obtained simply interconnecting elementary structural elements. In particular, the results obtained for 1D systems [135] can be generalized by showing how to synthesize microstructures whose continuous counterparts exhibit “forbidden” frequencies for wave propagation [238], the onset of trapping boundary layers or energy trapping at the microscopic level and consequent enhanced damping [239,240]. Exemplifying this multiscale structure is the model for fabrics conceived in Ref. [241], which,

²<http://www.ncbi.nlm.nih.gov/pmc/articles/PMC4229054/figure/fig3-2041731414556561/>

³<http://www.ncbi.nlm.nih.gov/pmc/articles/PMC4229054/figure/fig3-2041731414556561/>

however, is concerned only with static problems. The most interesting extensions of these researches involve:

- (1) The introduction of kinetic effects at the smaller scale.
- (2) The extension to 2D (see Ref. [136]) and 3D structures.
- (3) The introduction of multiphysics effects via the introduction of suitable transducers, as, for instance, those based on the piezoelectric effect [242–244].

Another field in which new results are needed because of newly arisen technological possibilities is related to the study of instabilities. Indeed, it is easily understood that instabilities in the microstructure of a complex system may imply “macro” effects of various kinds, including phase transitions [245,246] and other kinds of overall behaviors. The study of complex types of instabilities is therefore of crucial importance in order to fully exploit the potential afforded by complex microstructures. In this regard, relevant results are available in the literature concerning both general aspects [247–260] and more specific issues related to the behavior of the microstructure [261–264].

5.2 Experimental Features. As already observed, the emergence of computer-aided manufacturing is having deep consequences for the evolution of Mechanics, which also involve numerical and theoretical developments. Indeed, it can be observed that a very remarkable feature of computer-aided manufacturing is that one can employ the same code (or compatible versions of the same code in different software) for both producing a sample and establishing the topology for performing numerical simulations. This feature has very deep consequences of a methodological and even epistemological nature. The concept of “description of reality through a theoretical model” seems in this case more powerful, as most of the approximate character of the numerical study is sidestepped by the aforementioned identification between the model for numerical investigation and the one for realizing the object.

Concerning experimental work, some specifications have to be made between different kinds of computer-aided manufacturing. Indeed, while 3D printing allows for the construction of very

specific multiscale fabrics (see, e.g., Refs. [140,265,266]) whose quality can be very precisely controlled (at least at the level of 10^{-2} mm), the technology of electrospinning allows for the construction of micro- and even nanostructures, but with a much more limited precision (see, e.g., Refs. [267–271]). In this context, the improvement of electrospinning control capability is one of the most interesting problems. It is conceivable to design, for example, better devices which exploit the dependence of surface tension on the curvature of the outer interface of the injected filament [272]. Moreover, a sensitivity analysis to estimate the effect of nano- and micro-imperfections on the global behavior of the considered fabrics would also be of great interest, and increase the already considerable potential that electrospinning techniques have in several fields, including tissue engineering (see Ref. [273]). Concerning these applications, a notable example is the construction of polyurethane biomimetic scaffolds for driving the growth of cell tissues. In Ref. [274], specifically, a thin pre-stretched elastic polyurethane electrospun scaffold has been shown to serve as a supporting template for rapid biofabrication of thick tissue-engineered constructs (see Figs. 3 and 4).

Besides technical difficulties in achieving the desired degree of accuracy at the nanoscale, deeper problems connected with nano-sized objects concern the presence of size-related effects which are not observable at macro- and microscale. Among them there are problems which depend on the intrinsic nature of the physics laws (classical or quantum ones) governing phenomena at a given length scale; in addition, there are also specific size-related effects which are completely captured even by a classical approach, and which start to play a relevant role, as the length scale decreases, well before quantum mechanics is required. Given the importance of these last effects for the experimental and theoretical study of metamaterials and for the exploitation of their characteristics, an overview of them is provided in Sec. 6.

We conclude this section by remarking that computer-aided manufacturing techniques and other advanced manufacturing procedures are not the only ones able to produce new interesting metamaterials. Indeed, the research is by any means confined to them, and many interesting cases of metamaterials exhibiting new and promising behaviors are indeed being realized through

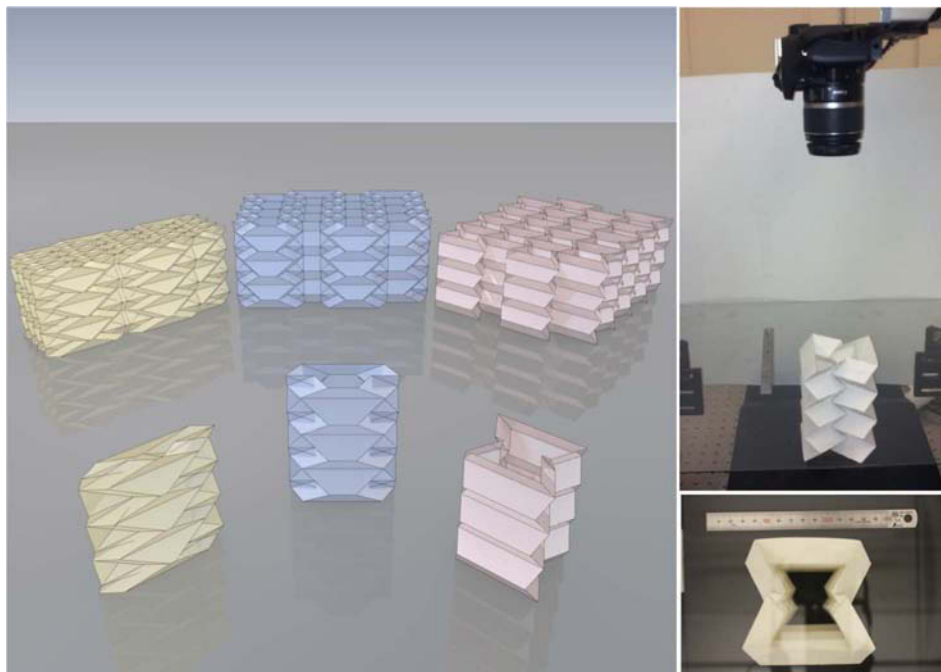


Fig. 5 Handicraft metamaterial exhibiting interesting mechanical properties (high damping, negative stiffness, snap-through, etc.): Tachi-Miura polyhedron realized by means of origami structures made of paper as studied in Ref. [275]. Left: digital image of the prototypes; right: photo of the top of the prototype (original pictures by the authors).

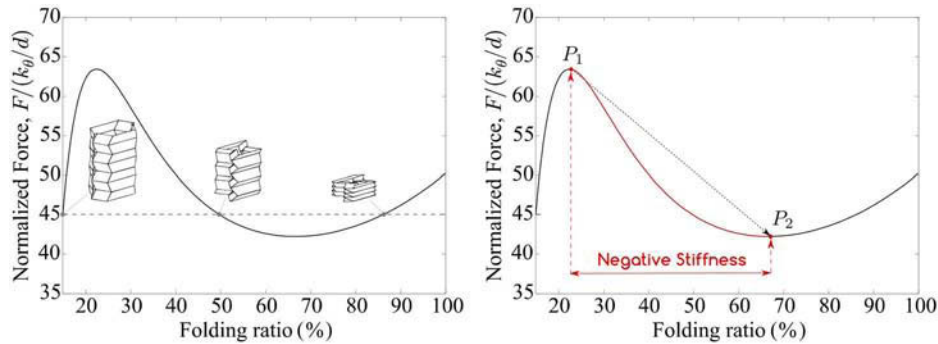


Fig. 6 Left: three different configurations of the papermade Tachi-Miura polyhedron (studied in Ref. [275]) under the same normalized force; right: force-folding ratio relationship and snap-through response (original rendering of pictures provided by the authors)



Fig. 7 Another example of handcraft metamaterial: hollow plastic spheres (138 mm high) with a central impervious cylinder studied in Ref. [276]. Spheres might be impervious hollow spheres, or resonators, or both (see Table 1 in the reference paper for details). The interspheres space might be occupied either by air or filled by a granular medium. Left: geometry of the prototype; middle: a prototype; right: cut of the two types of Helmholtz resonators (original pictures by Professor Claude Boutin).

ordinary industrial procedures, and even (at least in the prototyping phase) through handcraft methods. An interesting example of this kind is provided in Ref. [275], where a Tachi-Miura polyhedron made of paper is realized and studied (see Fig. 5). The authors measured cross-sectional area of the structure and studied how mechanical properties depend on it. In Fig. 6—right panel, the normalized force (i.e., the applied force divided by a density of torsional stiffness) is represented versus the folding ratio, and the loading and unloading behaviors show that the system can achieve hysteresis effect under dynamical circumstances, which can be exploited for building structures with promising damping properties. In Fig. 6—left panel, three different configurations reached by the system under the same value of the normalized force, having significantly different folding ratio, are graphically shown. Another interesting case of handcraft metamaterial is the one realized and studied by Boutin and Becot [276]. The authors investigate theoretically and experimentally the acoustics of gas-saturated rigid porous media with inner resonance effects. By realizing a prototype made by cutting hollow plastic spheres and packing them with an approximately cubic geometry (see Fig. 7), they confirmed experimentally that the resonators essentially modify the effective bulk modulus of the medium inducing strong velocity dispersion and high attenuation in the frequency range of

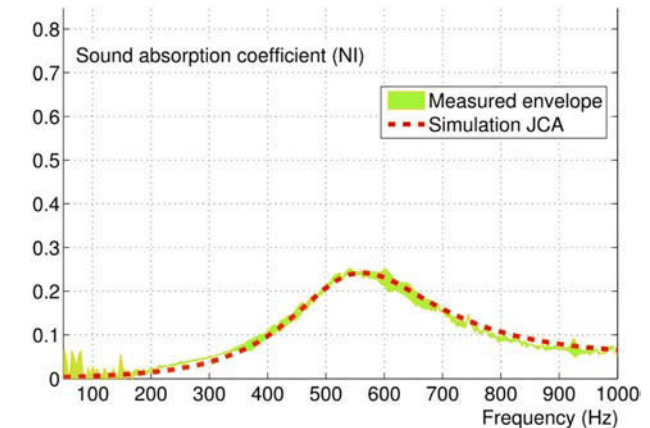


Fig. 8 Sound absorption coefficient at ambient condition of temperature and pressure for the system studied in Ref. [276] and represented in Fig. 7. Measurement is represented by the thick line and simulation by the dashed one (original picture by Professor Claude Boutin).

the theoretical band gaps. In Fig. 8, sound absorption coefficient of the sphere packing shown in Fig. 7 can be seen at ambient condition of temperature and pressure. Measurement is represented by the thick line and simulation by the dashed one. A very similar kind of investigation concerning the bulk effects of microstructure resonance is carried in Ref. [277] (for related researches, see also Refs. [278–281]) with respect to a structure constituted by a shaking table equipped with aluminum sheets acting as resonators (see Fig. 9). The effect on resonance of the addition of 1 and 37 sheets is represented in Fig. 10; as one can see, very sharp changes in the resonance properties of the structure result from the addition of 37 resonators. This last research was a particular case of a more general research line involving locally resonant mechanical metamaterials (see, for instance, Refs. [282,283]).

6 Micro- and Nanostructured Materials Presenting Surface-Related Effects

A case in which microstructure can affect significantly the behavior of a mechanical system is the presence of surface- and interface-related effects (see, for instance, Refs. [284,285]). At the moment, we do not have yet a general and comprehensive theoretical framework which is able to cover this topic in a satisfactory way, and a big amount of effort by researchers from different fields is being made to achieve it, or at least to add some pieces to the puzzle. We will try to briefly illustrate where the line separating already understood phenomena and open problems lies.

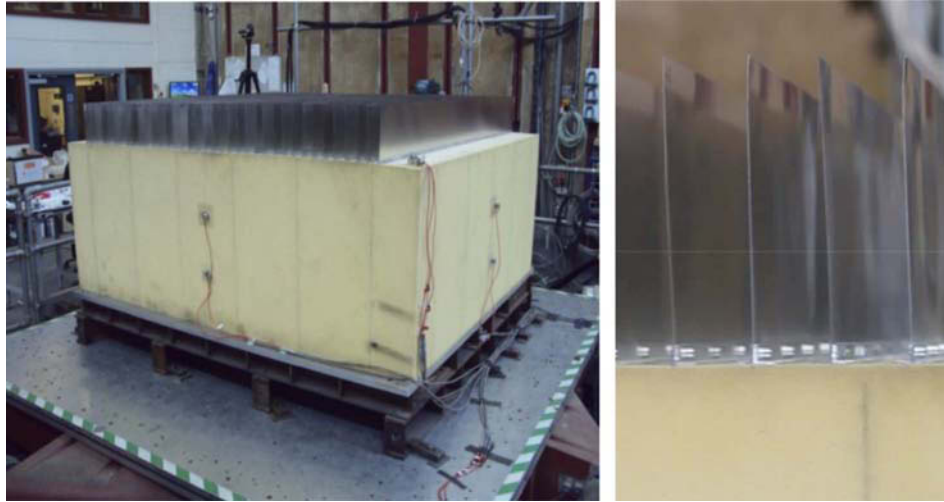


Fig. 9 Left: shaking table (Bristol Laboratory for Advanced Dynamics Engineering) equipped with aluminum sheets acting as resonators as studied in Ref. [277]; right: zoom on the sheets (original pictures by Professor Claude Boutin)

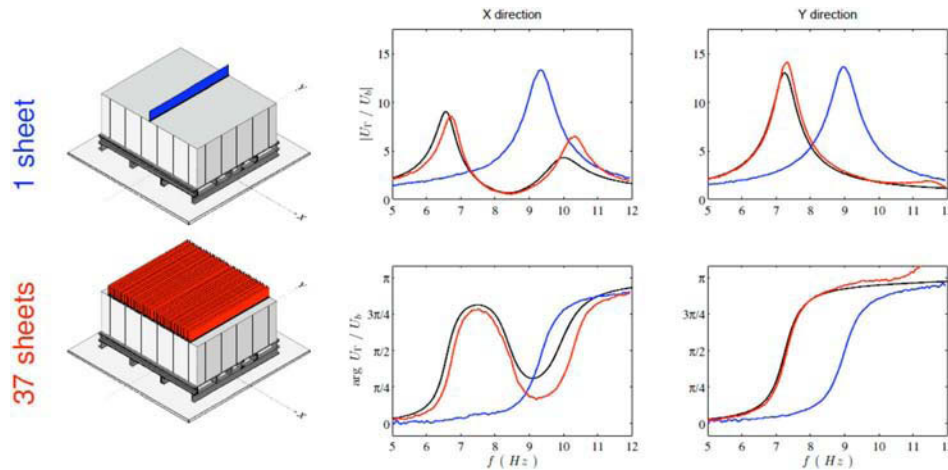


Fig. 10 Changes in spectrum surface/table for the system studied in Ref. [277] and shown in Fig. 9. The curve for one resonator is very close to usual layer's resonance; the curve corresponding to 37 resonators shows drastic changes in layer's resonance in x resonant direction and usual resonance peak in y inert direction; in black: standard impedance analysis is also shown; U_T and U_b are, respectively, the displacements of the material points belonging to the upper surface and to the base of the sample (original picture by Prof. Claude Boutin).

The general concept is that, in the presence of complex micro- or nanostructures, surface effects are the most relevant factor in determining size-related behaviors. The development of micro- and nanotechnology is indeed making even more acute the need for new theoretical developments. There are several examples of new materials which try to exploit the specific characteristics that surface-related effects can have in the presence of complex microstructures. In the literature (see, e.g., Ref. [286]), a distinction is made between “extrinsic” and “intrinsic” size effects, i.e., the dependence of the bulk properties, respectively, on the size of a sample or on the micro- and nanostructure. Examples of the two types are provided, respectively, in Refs. [287–291,292,293].

Concerning the geometry of the surfaces, we can start by mentioning the simplest case, i.e., the so-called “perfect” surfaces. These are the ones that can be described by the tools of standard differential geometry with the simple addition of some special physical properties (see, for example, the surface of the nanocrystals and nanotubes made of ZnO shown in Fig. 11 and studied in Ref. [294]). This, however, is just a very special case. There are indeed several cases of largely irregular geometry even in the

presence a microstructure constituted by nanotubes or nanocrystals, since their spatial configuration can be very far from uniform, as shown in Fig. 12. Materials with this type of surfaces can be employed for many applications, including the production of sensors, actuators, and other elements of micro- and nanoelectromechanical systems (see, for example, Refs. [295–301]). For this type of surfaces, it is completely pointless to aim at a detailed mathematical description, and instead suitable averaged models have to be developed; this is in the opinion of the authors of one of the most promising research directions. An application which is important for the development of energetically advantageous solar cells is provided by the so-called Black Silicon (see Ref. [301] and Fig. 13); another example of results having application to photovoltaic technology is the theory of layered plates and shells provided in Ref. [302]. Self-cleaning and bactericide coatings provide other examples of highly irregular surfaces exploited to obtain specific properties (see, e.g., Refs. [303–313]).

The concept of surface tension for solids, introduced by Gibbs [314], is still an active research field (for a coverage of recent

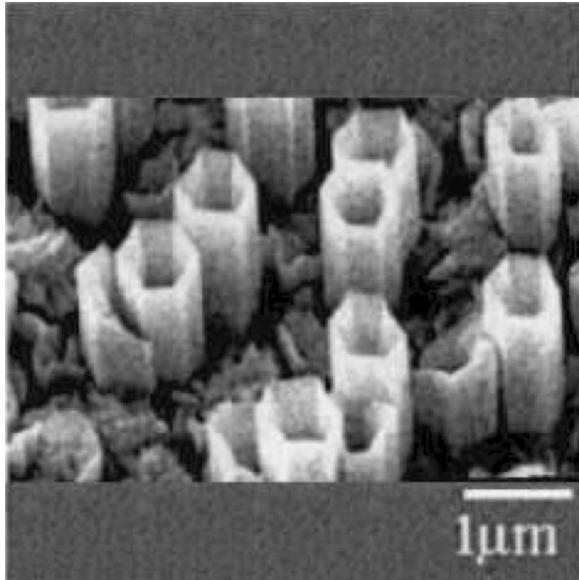


Fig. 11 ZnO crystal and ZnO nanotubes (Reproduced with permission from Özgür et al. [294]. Copyright 2005 by AIP.)

literature, the reader can see Refs. [315,316] and the works there cited). Gurtin and Murdoch introduced in Refs. [317,318] a model in which a nonlinear elastic solid is equipped with a prestressed membrane on the surface to account for surface tension. This model found applications in micro- and nanomechanics (see, e.g., Refs. [319–321]), and in particular proved capable of describing size-related differences in mechanical properties, as

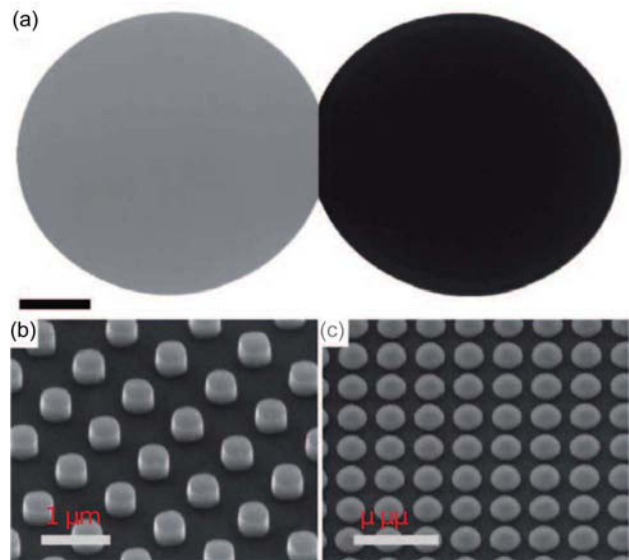


Fig. 13 “Black silicon” for solar cells (Reproduced with permission from Spinelli et al. [301]. Copyright 2012 by Nature Publishing Group.)

observed, for instance, in Ref. [322]. The importance of this model can also be appreciated considering that many generalizations were proposed for it, for instance, adding bending stiffness for the external membrane and accounting for thermoelasticity or fracture (see Refs. [323–328]). In this framework, it is of course very useful to provide solutions to initial value problems (IVPs)

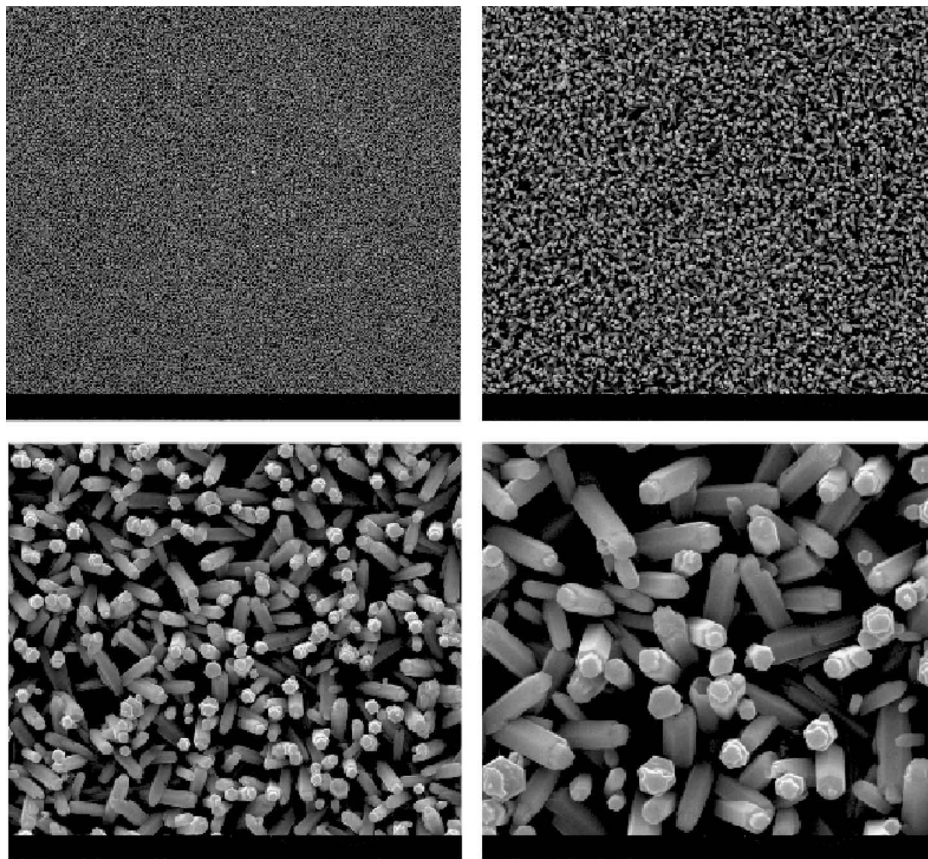


Fig. 12 ZnO nanoarray (respectively, 300×, 1200×, 5000×, and 10,000× from top left to bottom right) (Reproduced with permission from Ma et al. [298]. Copyright 2008 by Elsevier.)

and boundary value problems (BVPs) which are met in surface elasticity; related results are provided in Refs. [20,21,329,330].

Surface elasticity influences the properties of the material, as shown in Refs. [319,320]. A remarkable theoretical result is that, in linear surface elasticity, the presence of surface stresses leads to a stiffening of the material (see, for example, Refs. [21,331–335]). This general result helps understanding the fact that, in fracture mechanics, the presence of surface reinforcements can change the behavior of solutions in proximity of cracks, holes, and other kind of singularities, as it was shown in Refs. [327,328].

To complete the picture concerning surface stresses and effects, we add a list of other related topics developed in recent literature:

- (1) The influence of surface stresses on the free vibrations of materials is investigated in Refs. [336–340].
- (2) The finite deformations of elastic solids in the Gurtin–Murdoch model is studied in Refs. [341–344].
- (3) The study of BVPs in case of linear elasticity with surface stresses is performed in Refs. [20,21,24,329,330].
- (4) Numerical study (based on FEM) of bodies with surface stresses is provided in Refs. [345–347].
- (5) Ab initio methods and other atomistic simulations are covered in Refs. [348–351].
- (6) Surface energy introduced by means of the evaluation of the excess of bulk energy close to the surface is investigated in Ref. [352].
- (7) Models of higher gradient continua capable to include surface stresses are presented in Refs. [315,353–356].

7 Example: Pantographic Structures

As a model case of a structure which can be 3D printed and studied by means of the approaches proposed in Sec. 3, we will briefly describe pantographic sheets. By this, we mean a structure constituted by long fibers, which can be modeled as Euler or Timoshenko beams, inextensible chords, or in other ways according to the particular application at hand (see Fig. 1). The fibers form parallel arrays orthogonal to each other, and each fiber belonging to an array is interconnected via internal pivots to all the fibers of the other array (see Refs. [190,240]).

This system appears rather simple in its geometry and in the mechanics of its basic substructure, but nevertheless is capable of very rich macroscopic behavior which poses great challenges to its theoretical characterization, due primarily to: (i) the need to account for special constraints, such as inextensibility and (ii) the presence of “floppy modes”; i.e., macrodeformations to which no strain energy is associated. Moreover, it is clearly of a multiscale nature, as it is characterized by four different length scales: the diameter of the fibers, the spacing between the fibers, the distance between the closest pivots, and the size of the pivots.

This structure can have a very advantageous strength/weight ratio, and it is experimentally proved that it exhibits a particularly safe behavior in fracture [357], since it is capable of sustaining load in a stable fashion long after the inception of fracture: the part of energy absorbed by the system between the end of the elastic regime and the ultimate failure is comparable to that stored as elastic deformation energy. These features make it a very promising candidate for applications in the aeronautical and aerospace industries.

A basic version of this structure has already been printed and experimentally studied in recent research activity [357–359]; in Fig. 1 (top) the result of a so-called “bias test” is shown. One can clearly observe the presence of different “phases”; i.e., regions in which the shear deformation is more or less constant, with almost vanishing bending of the fibers, separated by thin layers in which bending is concentrated. This qualitative behavior was accurately reproduced by introducing a continuum model (Fig. 1 (bottom)), where shear deformation is represented on the vertical axis. We

remark that this picture is relative to a continuum simulation, and that the curves represent sets of material points which are straight lines in the reference configuration. For the continuum model, a placement \mathbf{r} can be considered which is a vector function defined over the planar domain corresponding to the reference configuration of the sample, taking values in \mathbb{R}^3

$$\mathbf{r} = X_\alpha \mathbf{e}_\alpha + u_i(X_\alpha) \mathbf{e}_i$$

with Latin indexes ranging from 1 to 3 and Greek indexes from 1 to 2; the u_i are the three components of displacement.

The strain-energy function of the model is

$$W = W_1(C_{\alpha\beta}) + W_2 \quad (1)$$

where

$$C_{\alpha\beta} = r_{i,\alpha} r_{i,\beta} \quad E_{\alpha\beta} = \frac{1}{2}(C_{\alpha\beta} - \delta_{\alpha\beta}) \quad (2)$$

$$W_1 = \frac{1}{2} Y_L (L_\alpha L_\beta E_{\alpha\beta})^2 + \frac{1}{2} Y_M (M_\alpha M_\beta E_{\alpha\beta})^2 + \mu (L_\alpha M_\beta E_{\alpha\beta})^2 \quad (3)$$

$$W_2 = \frac{1}{2} A_L |L_\alpha L_\beta \mathbf{r}_{,\alpha\beta}|^2 + \frac{1}{2} A_M |M_\alpha M_\beta \mathbf{r}_{,\alpha\beta}|^2 + \frac{1}{2} A_T |L_\alpha M_\beta \mathbf{r}_{,\alpha\beta}|^2 \quad (4)$$

and

$$\begin{aligned} \mathbf{L} &= \frac{1}{\sqrt{2}} (\hat{e}_1 + \hat{e}_2) \\ \mathbf{M} &= \frac{1}{\sqrt{2}} (\hat{e}_1 - \hat{e}_2) \end{aligned} \quad (5)$$

This is in many aspects the simplest choice for the constitutive model, as (for instance) the same stiffness coefficient is assumed for normal and geodesic bending, and yet it is able to reproduce exceptionally well the experimental evidence. We can expect that subsequent refinement of the model will lead to even better quantitative predictions.

The continuum model was conceived to account for energy related to microstructural in-plane bending, which manifests itself macroscopically as geodesic curvature. It is not possible to model the response to this kind of deformation without introducing a second gradient contribution to the energy density. This is clearly established by the very good fidelity exhibited by the numerical simulations based on the foregoing theoretical model with respect to the patterns observed in the actual test.

In addition to the simulations based on the continuum model, mesoscale simulations based on an averaged model in which the energy (thought as dependent only on the angles between the fibers) is concentrated in the nodes of a lattice were performed (see Ref. [359]). In Figs. 14 and 15, the angular variation between

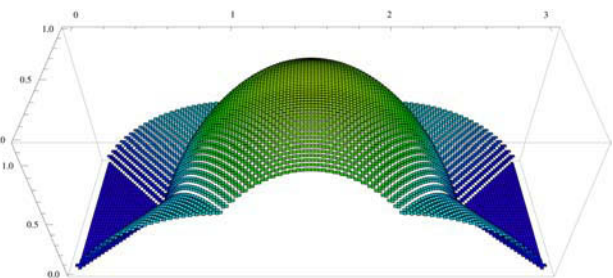


Fig. 14 Deformation energy for a second gradient lattice mesoscale model of a sheet with inextensible fibers, with an imposed elongation of 60%, as studied in Ref. [359] (original picture by the authors)

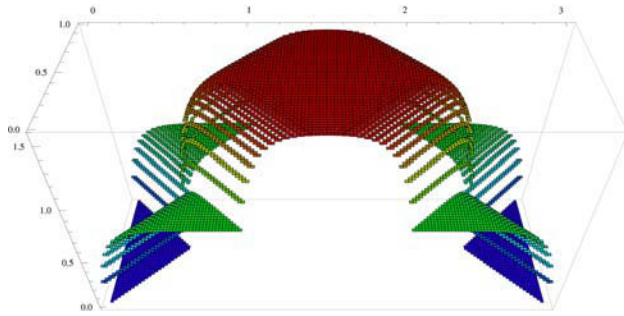


Fig. 15 Deformation energy for a mixed first and second gradient lattice mesomodel of a sheet with inextensible fibers, with an imposed elongation of 80%, as studied in Ref. [359] (original picture by the authors)

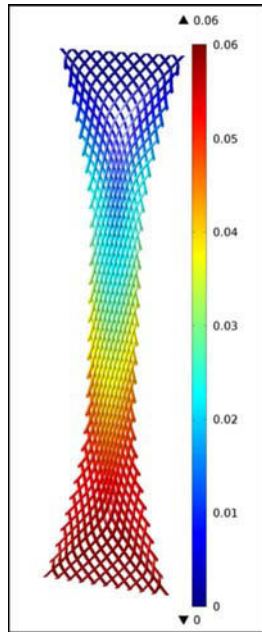


Fig. 16 Three-dimensional simulation for a pantographic structure in traction as studied in Ref. [359] (original picture by the authors)

the inextensible fibers with respect to the undeformed configuration is plotted, resulting in well visible boundary layers and undeformed triangular regions close to the shortest sides. Finally, large-scale simulations of the actual 3D structure were also conducted (see Ref. [358]; this is a particular case of the general feature that was already discussed before, i.e., with 3D-printing, one can employ the same code for both producing the sample and establishing the topology for performing numerical simulations. It is worth noting, recalling what was mentioned in Sec. 5, that the previous mesoscale simulations required a computation time approximately 10^4 times smaller than these last ones.

In Fig. 16, we show 3D numerical simulations based on the same code used for manufacturing the object shown in the previous figure; a numerical bias test is shown (norm of absolute displacement is plotted by means of a color map). In Fig. 2—top, the strain-energy density is shown in a more restricted region, and one can observe that almost all the energy is stored in the pivots as torsional energy. In Fig. 2—bottom, a sharper resolution is shown, which is particularly fine at the pivots.

This 3D model represents the micromodel of the considered structure, while its eventual homogenization by means of a

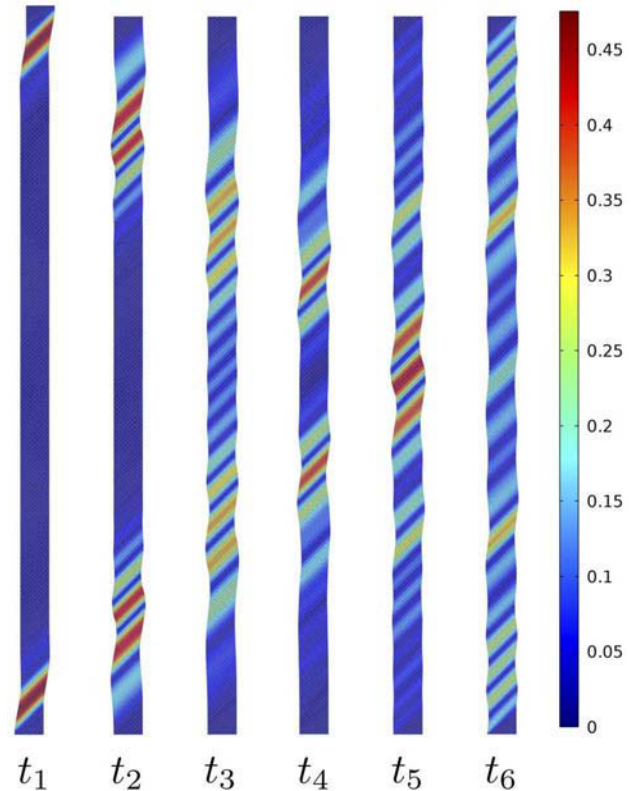


Fig. 17 Waves traveling in opposite directions in a pantographic structure (Reproduced with permission from Madeo et al. [240]. Copyright 2014 by Proceedings of the Estonian Academy of Sciences.)

suitable continuum model will represent the “macro” approach. Between them, a mesomodel in which the Euler beam model will account for the description of the fibers can also be introduced.

Concerning the theoretical formulation of the problem, we confine ourselves to an outline of some relevant concepts for the purpose of illustrating the difficulties that can arise. For example, the introduction of fiber inextensibility entails the presence, in the Lagrangian of the system, of terms expressed by means of nonlocal (integral) operators representing the constraint [193], leading to mathematical problems that are much more complex than those associated with local constraints. For example, in a test with a diagonal displacement at 45 deg with respect to the sides of a rectangular sample, with boundary displacements u_{01} and u_{02} , one has the following integral conditions in case of inextensible flexural beams with internal hinges [192]:

$$\begin{cases} \int_1^3 (\cos(\vartheta_1(\eta)) + \sin(\vartheta_2(\eta))) d\eta = 2 + u_{01} \\ \int_1^3 (\cos(\vartheta_2(\eta)) + \sin(\vartheta_1(\eta))) d\eta = 2 + u_{02} \end{cases} \quad (6)$$

where η is the curvilinear abscissa along the fibers in the reference configuration, ϑ_i are the kinematical descriptors representing the angular variation of the two families of fibers with respect to the reference configuration, and the value 2 is due to the shape ratio (3:1) of the sample (for details, see Ref. [189]). More complicated integral conditions will appear in the resulting evolution equations in the case of a more general imposed displacement.

The dynamics of such systems is expected to be very rich and to exhibit unusual features, including the presence of nonstandard interaction between opposing waves (Fig. 17) and energy entrapment by means of filters constituted by an array of springs

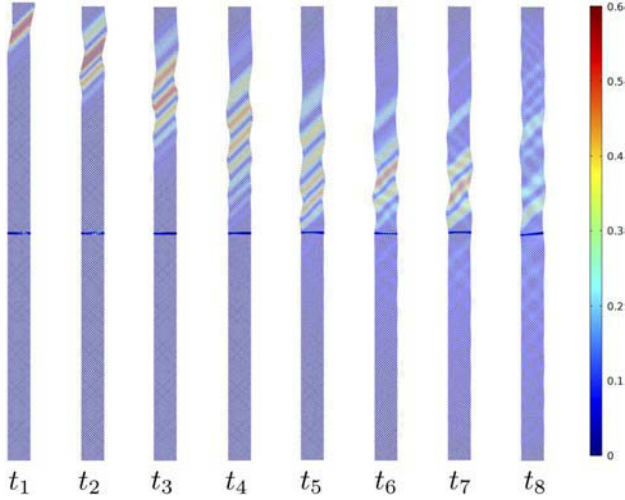


Fig. 18 Damping of a wave by means of an array of vertical springs in a pantographic structure (Reproduced with permission from Madeo et al. [240]. Copyright 2014 by Proceedings of the Estonian Academy of Sciences.)

(Fig. 18) [190]. Selecting different stiffnesses for the two families of parallel beams, the system can yield different dispersion coefficients in different directions. The homogenized continuum theory, to be developed, must be rich enough to account for this kind of behavior, which, together with the exploitation of possible soft-modes, can aid in the realization of acoustic (cloaking) applications.

Further, the foregoing continuum model may be extended to accommodate three-dimensional deformations of the elastic lattice in space. To this end, additional terms are included in the strain-energy function W of the model to account for surface flexure and twist. In such a deformation, we have (see Eq. (4))

$$\begin{aligned} L_{\alpha}L_{\beta}\mathbf{r}_{,\alpha\beta} &= \mathbf{g}_l + K_L\mathbf{n}, & M_{\alpha}M_{\beta}\mathbf{r}_{,\alpha\beta} &= \mathbf{g}_m + K_M\mathbf{n} \\ L_{\alpha}M_{\beta}\mathbf{r}_{,\alpha\beta} &= \mathbf{\Gamma} + T\mathbf{n} \end{aligned} \quad (7)$$

where $\mathbf{g}_{l,m}$ and $\mathbf{\Gamma}$ account for geodesic bending in the tangent plane of the deformed surfaces, as before, and \mathbf{n} is the (variable) unit normal to the evolving deformed curved surface. The variables $K_{L,M}$ and T are the normal curvatures of the embedded fibers and the twist induced by the bending of the surface in three-space.

To help understanding of how these effects should be manifested in the constitutive theory, the strain-energy function may be nondimensionalized by introducing a local length scale. Candidates for this are the thickness of the actual sheet represented by our surface model, the characteristic spacing of the internal pivot points of the actual pantographic lattice or the widths of the constituent fibers. If any of these is used as the length scale, then in typical applications the nondimensionalized vectors \mathbf{g}_l , \mathbf{g}_m and $\mathbf{\Gamma}$ are small enough that the dependence of the strain energy on them is quadratic at leading order, provided that the associated couple stresses and bending/twisting moments vanish when the fibers are straight and untwisted. A simple strain-energy function of this type, incorporating the orthotropic symmetry conferred by the initial fiber geometry, is

$$\begin{aligned} W &= w(\lambda, \mu, J) \\ &+ \frac{1}{2} \left(A_l |\mathbf{g}_l|^2 + A_m |\mathbf{g}_m|^2 + A_{\Gamma} |\mathbf{\Gamma}|^2 + k_L K_L^2 + k_M K_M^2 + k_T T^2 \right) \end{aligned} \quad (8)$$

where the coefficients $A_{l,m,\Gamma}$ and $k_{L,M,T}$ are constants; this form is assumed for the sake of definiteness and tractability. Other forms are, of course, possible. Here, we take $A_{l,m,\Gamma}$ and $k_{L,M,T}$ to be strictly positive and observe that the part of the energy depending on the second gradient $\nabla\nabla\mathbf{r}$ is then nonnegative, vanishing if and only if \mathbf{g}_l , \mathbf{g}_m , $\mathbf{\Gamma}$, K_L , K_M and T all vanish simultaneously. It is thus a convex function of $\nabla\nabla\mathbf{r}$, which is enough to secure the existence of energy-minimizing deformations in conservative boundary-value problems via the direct method of the calculus of variations [360]. The resulting model is therefore ideally suited to finite-element analysis.

The constitutive sensitivity to the geodesic and normal curvatures is easily understood in terms of the mechanics of the constituent fibers. In particular, fibers are expected to offer resistance to any mode of bending, be it of the geodesic type or the type induced by surface flexure. Regarding fiber twist, in the present model this is determined by the twist of the surface because of the connectivity of the pantographic lattice substructure. Specifically, both families of intersecting fibers of the lattice are assumed to be pivoted about the current surface normal. This constraint implies that fiber twist is controlled entirely by surface geometry and is therefore not an independent kinematic variable [213].

For the strain-dependent function w , we may adopt

$$w(\lambda, \mu, J) = \frac{1}{2} (E_L \varepsilon_L^2 + E_M \varepsilon_M^2) - G(\ln J + 1 - J) \quad (9)$$

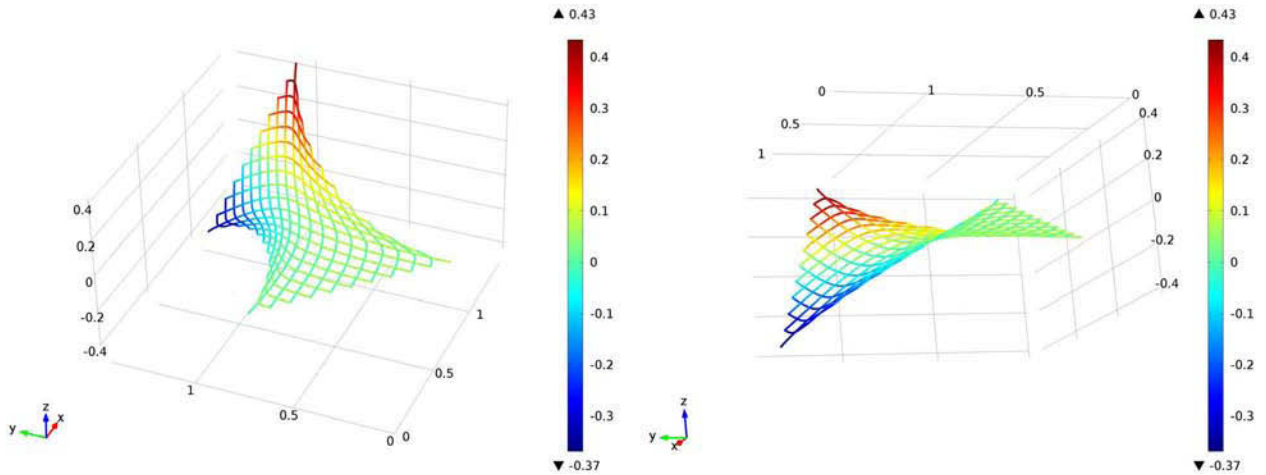


Fig. 19 Out-of-plane twisting of a squared pantographic sheet as studied in Ref. [358]. The picture is relative to a continuum simulation, and that the curves represent sets of material points which are straight lines in the reference configuration (original picture by the authors).

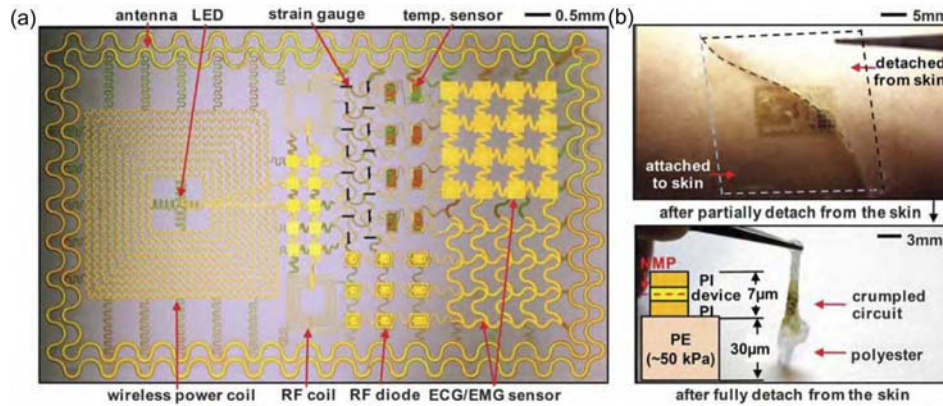


Fig. 20 Epidermal flexible plate (Reproduced with permission from Kim et al. [361]. Copyright 2011 by AAAS.)

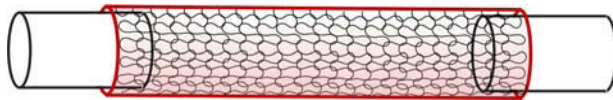


Fig. 21 An architected material employed for a vascular implant made of NiTi knitted fabric and inserted in a silicone elastomer (original rendering of a photo from Ref. [369])

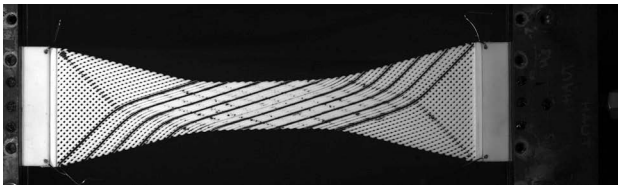


Fig. 22 A pantographic sheet under extensional bias test as studied in Ref. [358]: a concept for a new lightweight, extremely resistant and safe in failure architected material (original picture by the authors)

where

$$\varepsilon_L = \frac{1}{2}(\lambda^2 - 1), \quad \varepsilon_M = \frac{1}{2}(\mu^2 - 1) \quad (10)$$

are the extensional fiber strains, and $E_{L,M}$ and G are the positive constants. This energy does not include a term proportional to $\varepsilon_L \varepsilon_M$ and therefore does not accommodate a Poisson effect with respect to the fiber axes. Poisson effects are generally non-negligible in woven fabrics due to fiber crimping and decrimping [193,213], but this mechanism is absent in pantographic lattices. Finally, the term involving J penalizes fiber collapse ($J \rightarrow 0$) by requiring unbounded growth of the associated energy.

Figure 19 illustrates a simulation based on this theory in which one edge of the lattice is fixed and the opposite end undergoes a relative displacement and twist in three dimensions (we again remark that the picture represents a 2D continuum simulation; see the caption). The effect is to introduce substantial bending and twisting of the lattice without disturbing the aforementioned phase segregation pattern. This generalization of the model is important in providing a capability to model the potentially complex three-dimensional deformations of real lattice substructures. It may be further extended through refinement of the constitutive equations and the introduction of kinetic effects to capture wave propagation and structural vibrational modes. The latter are expected to be

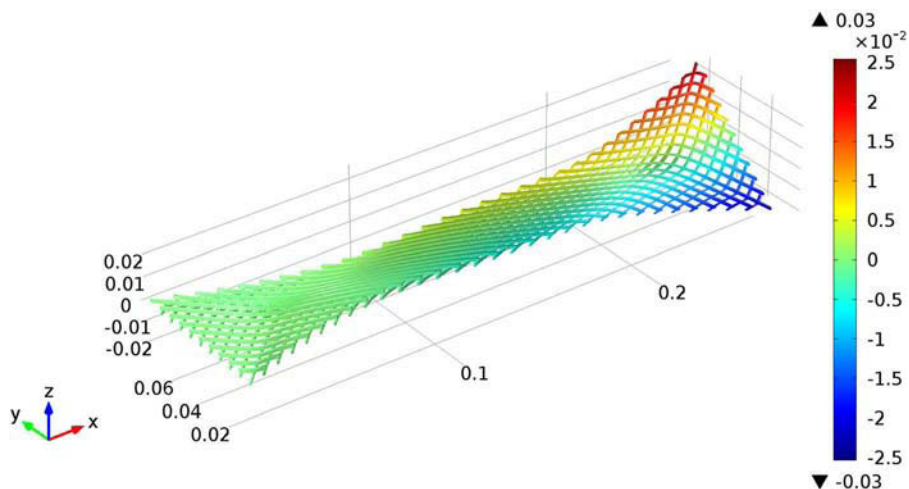


Fig. 23 Three-dimensional simulation for a pantographic structure in traction and torsion as studied in Ref. [359] (original picture by the authors)

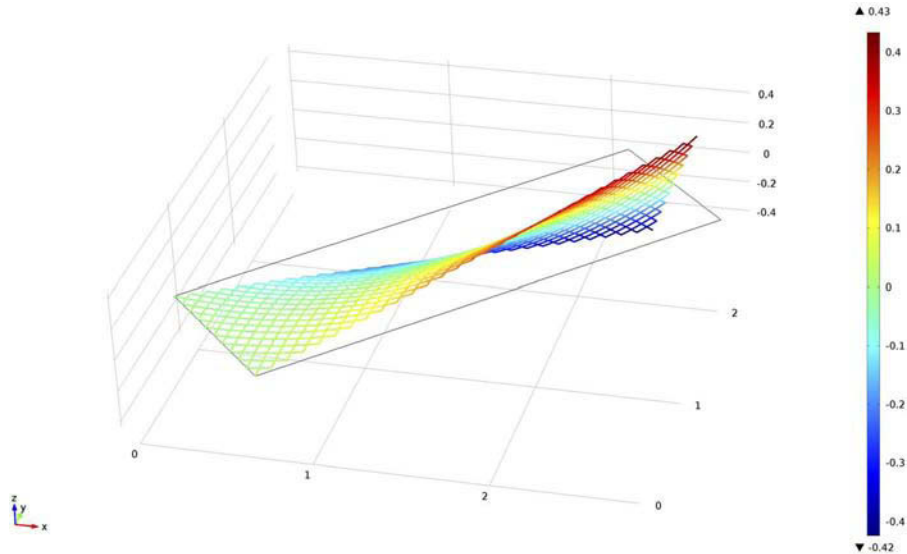


Fig. 24 Out-of-plane twisting of a pantographic sheet with combined traction and torsion as studied in Ref. [358]. The picture is relative to a continuum simulation, and that the curves represent sets of material points which are straight lines in the reference configuration (original picture by the authors).

coupled due to the interplay among strain, normal bending, twisting, and geodesic bending.

One very ambitious field of application in this field of research is the analysis of the response of recently developed bio-inspired flexible electronics for health-monitoring purposes, such as those developed by the group led by Nanshu Lu (see, for instance, Ref. [361]). In this research, a generalization of the aforementioned pantographic structure is proposed (see Fig. 20), which conforms mechanically to skin tissue (for details on this topic, see Refs. [362–368]), i.e., electronic systems that remain congruent to the epidermis as it deforms. These structures may exhibit complex large-deformation behavior, including out-of-plane buckling induced by in-plane extension. Their mechanical behavior is such that other soft-tissue biomimetic applications are possible (see Fig. 21 for the employment of a similarly conceived architected material for a vascular prosthesis). Understanding the mechanics of these kinds of structures, as well as deepening our knowledge of mechanophysiology of the skin, will be crucial in order to exploit their potential (Figs. 22–24).

8 Conclusions

Modern technology is experiencing a tumultuous growth. This growth is producing wonderful and unexpected devices, mechanisms, tools, and some solutions to many among the problems humankind is facing since its appearance on Earth. All these developments are based on what can be considered the deepest and most detailed scientific understanding of Nature ever attained. The situation is very similar to what experienced during the Renaissance when, based on the rediscovery (see again Ref. [1]) of Hellenistic science, Italian (and in general Western) scientists started to shape the modern human society, which systematically exploits innovation, scientific knowledge, and technological transfer to increase its productive capability and, at the end, the quality of life of humankind.

It is therefore suitable even nowadays to address the methodological considerations and innovation thrusts which animated all Renaissance men, and, first among them, Galileo Galilei. In Galileo's *Il Saggiatore* (Ref. [370], p. 232), we can read:⁴

⁴The authors want to note that it is unfortunate that it is not easy to find a complete translation into English of all the works by Galileo.

La filosofia è scritta in questo grandissimo libro che continuamente ci sta aperto innanzi a gli occhi (io dico l'universo) ma non si può intendere se prima non s'impara a intender la lingua, e conoscer i caratteri, ne' quali è scritto. Egli è scritto in lingua matematica, e i caratteri son triangoli, cerchi ed altre figura geometriche, senza i quali mezzi è impossibile a intenderne umanamente parola; senza questi è un aggirarsi vanamente per un oscuro laberinto.

Which is translated by Stillman Drake (in Ref. [371]) as:

Philosophy is written in this grand book, the universe, which stands continually open to our gaze. But the book cannot be understood unless one first learns to comprehend the language and read the letters in which it is composed. It is written in the language of mathematics, and its characters are triangles, circles, and other geometric figures without which it is humanly impossible to understand a single word of it; without these, one wanders about in a dark labyrinth.

One should not believe that Galileo is accepting the philosophical vision which is currently known as "Platonistic." Galileo (and ourselves) did not believe that mathematics is a reality outside our mind: he claims indeed that "Philosophy" is written in the language of mathematics and that the universe can be understood only when using a philosophy which exploits the scientific logical-deductive method and the tools given to us by mathematics.

Engineering sciences must be based on a preliminary deep understanding of the nature of the phenomena which it intends to exploit for developing its applications. Therefore, mathematical formulation of predictive models is essential in Engineering. Moreover, the attentive observer will discover that, indeed, mathematics and mathematical knowledge have shaped and are shaping our environment, our world or, if you like, our "ecological niche" via the engineering applications and technology which they ultimately make possible. It is not the world which is written in mathematical symbols: it is our mind which shapes the world using mathematics as a fundamental tool for understanding, predicting, and controlling the phenomena, and for designing the artifacts which surround us. It is therefore natural that one recognizes in the artifacts the mathematics which is behind them. One instance will clarify the issue: even if Navier's effort to design a suspension bridge based on mathematical modeling failed because of lack of knowledge about the mechanical behavior of

foundations (and this failure pushed the development of geotechnics), when Navier “Mathematizes” the study of suspension bridges he establishes the methods needed to cross large spans without intermediate pillars and therefore changes the shape of our cities, our highways, and our railways (see, for instance, Ref. [372] and [373]). Similarly, the concept of tube-frame structural system, based on the highly mathematically based theory of structures, was developed, among the others, by Fazlur Rahman Khan and was used to build the twin towers and many subsequent skyscrapers. Moreover, it is also to be pointed out that our failures in understanding mathematical problems play an important role as our successes in determining our technology. For example, it is well known that Warren bridge was mainly chosen, among many possible structures, because of the fact that having loads concentrated on the nodes (usually modeled by means of ideal hinges) heavily cuts the computational costs, making the problem solvable even in an age in which computers were not yet available; this is the reason for which, still today, this kind of structures is so often employed even if our software can easily deal with the computation needed by distributed bending loads in most of the cases.

In the present review, we wanted to stress that mathematics is starting to shape novel “exotic” fabric materials. Indeed their structure is determined “a priori” via the mathematical equations which one decides must be those governing their physical behavior. The limits in this design and conception process coincide with the limits of the mathematics which we are able to handle. Exactly as happened during Navier’s age, when the lack of mathematical and mechanical knowledge limited the capability of building bridges, nowadays the limits of the mathematical and mechanical theories and models risk to impose restrictions on the technological capabilities of humankind, and in particular on the materials which are available for our engineering applications. To be able to improve the performances of materials, to increase their capacity to sustain thermal, mechanical, or electrical external actions, one needs to develop new and more powerful mathematical, mechanical, and numerical methods. In this sense, mathematics is one of the most practical tools which are available to the engineer. Moreover, the field of novel engineered materials systems requires new and powerful experimental techniques in order to validate and to inform any of the developed theories and models.

The authors hope that this review will contribute to the achievement of an effective overview of what has been done and what remains to be done in a part of the vast field of complex mechanical metamaterials design and prototyping.

Acknowledgment

The authors would like to thank Professor Claude Boutin, Professor Victor Eremeyev, Professor Angelo Luongo, and Professor Pierre Seppecher for the precious help provided while working on the manuscript as well as in long years of fruitful scientific discussions.

References

- [1] Russo, L., 2004, “The Forgotten Revolution. How Science Was Born in 300 BC and Why it Had to be Reinvented,” *Übersetzung aus dem Italienischen von Silvio Levy*, Springer, Berlin.
- [2] Germain, P., 1973, “The Method of Virtual Power in Continuum Mechanics. Part 2: Microstructure,” *SIAM J. Appl. Math.*, **25**(3), pp. 556–575.
- [3] Maugin, G., and Tricarico, C., 1992, “Pseudomomentum and Material Forces in Nonlinear Elasticity: Variational Formulations and Application to Brittle Fracture,” *Acta Mech.*, **94**(1–2), pp. 1–28.
- [4] Maugin, G. A., and Tricarico, C., 1992, “Note on a Mixed Variational Principle in Finite Elasticity,” *Atti Accad. Naz. Lincei, Cl. Sci. Fis., Mat. Nat., Rend. Lincei, Mat. Appl.*, **3**(1), pp. 69–74.
- [5] Arnold, V. I., 1989, *Mathematical Methods of Classical Mechanics*, Vol. 60, Springer Science & Business Media, New York.
- [6] Maugin, G., 1980, “The Method of Virtual Power in Continuum Mechanics: Application to Coupled Fields,” *Acta Mech.*, **35**(1–2), pp. 1–70.
- [7] Toupin, R. A., 1965, “Saint-Venant’s Principle,” *Arch. Ration. Mech. Anal.*, **18**(2), pp. 83–96.
- [8] Mühlhaus, H.-B., and Alfantis, E., 1991, “A Variational Principle for Gradient Plasticity,” *Int. J. Solids Struct.*, **28**(7), pp. 845–857.
- [9] Edelen, D. G., 1969, “Non-Local Variational Mechanics Variational Imbedding, Adjoint Theorems and Existence,” *Int. J. Eng. Sci.*, **7**(4), pp. 401–415.
- [10] dell’Isola, F., and Placidi, L., 2012, “Variational Principles are a Powerful Tool Also for Formulating Field Theories,” *Variational Models and Methods in Solid and Fluid Mechanics*, Springer Science & Business Media, Vienna, Austria.
- [11] Kirchner, N., and Steinmann, P., 2005, “A Unifying Treatise on Variational Principles for Gradient and Micromorphic Continua,” *Philos. Mag.*, **85**(33–35), pp. 3875–3895.
- [12] Placidi, L., “A Variational Approach for a Nonlinear One-Dimensional Damage-Elasto-Plastic Second-Gradient Continuum Model,” *Continuum Mech. Thermodyn.*, epub.
- [13] Placidi, L., “A Variational Approach for a Nonlinear 1-Dimensional Second Gradient Continuum Damage Model,” *Continuum Mech. Thermodyn.*, **27**(4–5), pp. 623–638.
- [14] Rahouadj, R., Ganghoffer, J.-F., and Cunat, C., 2003, “A Thermodynamic Approach With Internal Variables Using Lagrange Formalism. Part I: General Framework,” *Mech. Res. Commun.*, **30**(2), pp. 109–117.
- [15] Eremeyev, V. A., and Pietraszkiewicz, W., 2004, “The Nonlinear Theory of Elastic Shells With Phase Transitions,” *J. Elasticity*, **74**(1), pp. 67–86.
- [16] Rahouadj, R., Ganghoffer, J.-F., and Cunat, C., 2003, “A Thermodynamic Approach With Internal Variables Using Lagrange Formalism. Part II. Continuous Symmetries in the Case of the Time–Temperature Equivalence,” *Mech. Res. Commun.*, **30**(2), pp. 119–123.
- [17] Ganghoffer, J., 2012, “Extremum Principles for Biological Continuous Bodies Undergoing Volumetric and Surface Growth,” *Bull. Pol. Acad. Sci.*, **60**(2), pp. 259–263.
- [18] Serrano, H., 2014, “A Variational Approach to the Homogenization of Laminated Metamaterials,” *Nonlinear Anal.*, **18**, pp. 75–85.
- [19] Deü, J. F., Larbi, W., and Ohayon, R., 2008, “Piezoelectric Structural Acoustic Problems: Symmetric Variational Formulations and Finite Element Results,” *Comp. Meth. Appl. Mech. Eng.*, **197**(19), pp. 1715–1724.
- [20] Altenbach, H., Eremeyev, V. A., and Lebedev, L. P., 2010, “On the Existence of Solution in the Linear Elasticity With Surface Stresses,” *J. Appl. Math. Mech./Z. Angew. Math. Mech.*, **90**(3), pp. 231–240.
- [21] Altenbach, H., Eremeyev, V. A., and Lebedev, L. P., 2011, “On the Spectrum and Stiffness of an Elastic Body With Surface Stresses,” *J. Appl. Math. Mech./Z. Angew. Math. Mech.*, **91**(9), pp. 699–710.
- [22] Eremeyev, V. A., and Lebedev, L. P., 2015, “Mathematical Study of Boundary-Value Problems Within the Framework of Steigmann–Ogden Model of Surface Elasticity,” *Continuum Mech. Thermodyn.*, epub.
- [23] Eremeyev, V. A., and Lebedev, L. P., 2011, “Existence Theorems in the Linear Theory of Micropolar Shells,” *J. Appl. Math. Mech./Z. Angew. Math. Mech.*, **91**(6), pp. 468–476.
- [24] Eremeyev, V. A., and Lebedev, L. P., 2013, “Existence of Weak Solutions in Elasticity,” *Math. Mech. Solids*, **18**(2), pp. 204–217.
- [25] Ortiz, M., and Stainier, L., 1999, “The Variational Formulation of Viscoplastic Constitutive Updates,” *Comput. Methods Appl. Mech. Eng.*, **171**(3), pp. 419–444.
- [26] Liu, C., Li, F., Ma, L.-P., and Cheng, H.-M., 2010, “Advanced Materials for Energy Storage,” *Adv. Mater.*, **22**(8), pp. E28–E62.
- [27] Caruso, F., 2001, “Nanoengineering of Particle Surfaces,” *Adv. Mater.*, **13**(1), pp. 11–22.
- [28] Coleman, J. N., Khan, U., and Gun’ko, Y. K., 2006, “Mechanical Reinforcement of Polymers Using Carbon Nanotubes,” *Adv. Mater.*, **18**(6), pp. 689–706.
- [29] Hammond, P. T., 2004, “Form and Function in Multilayer Assembly: New Applications at the Nanoscale,” *Adv. Mater.*, **16**(15), pp. 1271–1293.
- [30] Fleck, N., Deshpande, V., and Ashby, M., 2010, “Micro-Architected Materials: Past, Present and Future,” *Proc. R. Soc. London A*, **466**(2121), pp. 2495–2516.
- [31] Dunlop, J. W., and Fratzl, P., 2013, “Multilevel Architectures in Natural Materials,” *Scr. Mater.*, **68**(1), pp. 8–12.
- [32] Brechet, Y., and Embury, J., 2013, “Architected Materials: Expanding Materials Space,” *Scr. Mater.*, **68**(1), pp. 1–3.
- [33] Bouaziz, O., Brechet, Y., and Embury, J., 2008, “Heterogeneous and Architected Materials: A Possible Strategy for Design of Structural Materials,” *Adv. Eng. Mater.*, **10**(1–2), pp. 24–36.
- [34] Bollen, P., Quiévy, N., Huynen, I., Bailly, C., Detrembleur, C., Thomassin, J.-M., and Pardoën, T., 2013, “Multifunctional Architected Materials for Electromagnetic Absorption,” *Scr. Mater.*, **68**(1), pp. 50–54.
- [35] Ashby, M., 2013, “Designing Architected Materials,” *Scr. Mater.*, **68**(1), pp. 4–7.
- [36] Ashby, M., and Brechet, Y., 2003, “Designing Hybrid Materials,” *Acta Mater.*, **51**(19), pp. 5801–5821.
- [37] Griesshaber, E., Schmahl, W. W., Neuser, R., Pettke, T., Blüm, M., Mutterlose, J., and Brand, U., 2007, “Crystallographic Texture and Microstructure of Terebratulide Brachiopod Shell Calcite: An Optimized Materials Design With Hierarchical Architecture,” *Am. Mineral.*, **92**(5–6), pp. 722–734.
- [38] Bruchhaus, R., Honal, M., Symanczyk, R., and Kund, M., 2009, “Selection of Optimized Materials for CBRAM Based on HT-XRD and Electrical Test Results,” *J. Electrochem. Soc.*, **156**(9), pp. H729–H733.
- [39] Vetterl, O., Finger, F., Carius, R., Hapke, P., Houben, L., Kluth, O., Lambertz, A., Mück, A., Rech, B., and Wagner, H., 2000, “Intrinsic Microcrystalline Silicon: A New Material for Photovoltaics,” *Sol. Energy Mater. Sol. Cells*, **62**(1), pp. 97–108.
- [40] Zheludev, N. I., 2010, “The Road Ahead for Metamaterials,” *Science*, **328**(5978), pp. 582–583.
- [41] Ju, J., Summers, J. D., Ziegert, J., and Fadel, G., 2009, “Design of Honeycomb Meta-Materials for High Shear Flexure,” *ASME Paper No. DETC2009-87730*.

- [42] Engheta, N., and Ziolkowski, R. W., 2006, *Metamaterials: Physics and Engineering Explorations*, Wiley, Hoboken, NJ.
- [43] Del Vescovo, D., and Giorgio, I., 2014, "Dynamic Problems for Metamaterials: Review of Existing Models and Ideas for Further Research," *Int. J. Eng. Sci.*, **80**(SI), pp. 153–172.
- [44] Milton, G., and Seppecher, P., 2012, "A Metamaterial Having a Frequency Dependent Elasticity Tensor and a Zero Effective Mass Density," *Phys. Status Solidi (B)*, **249**(7), pp. 1412–1414.
- [45] Kang, I., Heung, Y. Y., Kim, J. H., Lee, J. W., Gollapudi, R., Subramaniam, S., Narasimhadevara, S., Hurd, D., Kirikera, G. R., Shanov, V., Schulz, M. J., Shi, D., Boerio, J., Mall, S., and Ruggles-Wren, M., 2006, "Introduction to Carbon Nanotube and Nanofiber Smart Materials," *Composites, Part B*, **37**(6), pp. 382–394.
- [46] Wang, Z. L., 1998, *Functional and Smart Materials*, Wiley Online Library, Hoboken, NJ.
- [47] Giurgiutiu, V., 2000, "Review of Smart-Materials Actuation Solutions for Aeroelastic and Vibration Control," *J. Intell. Mater. Syst. Struct.*, **11**(7), pp. 525–544.
- [48] Song, Y., Wei, W., and Qu, X., 2011, "Colorimetric Biosensing Using Smart Materials," *Adv. Mater.*, **23**(37), pp. 4215–4236.
- [49] Chopra, I., 2002, "Review of State of Art of Smart Structures and Integrated Systems," *AIAA J.*, **40**(11), pp. 2145–2187.
- [50] Vermeerey, F., Liu, W. K., and Moran, B., 2007, "Multi-Scale Micromorphic Theory for Hierarchical Materials," *J. Mech. Phys. Solids*, **55**(12), pp. 2603–2651.
- [51] Nicot, F., Darve, F., and Group, R., 2005, "A Multi-Scale Approach to Granular Materials," *Mech. Mater.*, **37**(9), pp. 980–1006.
- [52] Bentz, D., 2000, "Influence of Silica Fume on Diffusivity in Cement-Based Materials: II. Multi-Scale Modeling of Concrete Diffusivity," *Cem. Concr. Res.*, **30**(7), pp. 1121–1129.
- [53] Fast, T., Niezgodza, S. R., and Kalidindi, S. R., 2011, "A New Framework for Computationally Efficient Structure–Structure Evolution Linkages to Facilitate High-Fidelity Scale Bridging in Multi-Scale Materials Models," *Acta Mater.*, **59**(2), pp. 699–707.
- [54] Hao, S., Moran, B., Liu, W. K., and Olson, G. B., 2003, "A Hierarchical Multi-Physics Model for Design of High Toughness Steels," *J. Comput. Aided Mater. Des.*, **10**(2), pp. 99–142.
- [55] de Borst, R., 2008, "Challenges in Computational Materials Science: Multiple Scales, Multi-Physics and Evolving Discontinuities," *Comput. Mater. Sci.*, **43**(1), pp. 1–15.
- [56] Hamilton, R., MacKenzie, D., and Li, H., 2010, "Multi-Physics Simulation of Friction Stir Welding Process," *Eng. Comput.*, **27**(8), pp. 967–985.
- [57] Eremeyev, V., and Pietraszkiewicz, W., 2009, "Phase Transitions in Thermoelastic and Thermoelastoplastic Shells," *Arch. Mech.*, **61**(1), pp. 41–67.
- [58] Eremeyev, V., and Pietraszkiewicz, W., 2011, "Thermomechanics of Shells Undergoing Phase Transition," *J. Mech. Phys. Solids*, **59**(7), pp. 1395–1412.
- [59] Pietraszkiewicz, W., Eremeyev, V., and Konopińska, V., 2007, "Extended Non-Linear Relations of Elastic Shells Undergoing Phase Transitions," *Z. Angew. Math. Mech.*, **87**(2), pp. 150–159.
- [60] Piccardo, G., and Solari, G., 2000, "3D Wind-Excited Response of Slender Structures: Closed-Form Solution," *J. Struct. Eng.*, **126**(8), pp. 936–943.
- [61] Piccardo, G., 1993, "A Methodology for the Study of Coupled Aeroelastic Phenomena," *J. Wind Eng. Ind. Aerodyn.*, **48**(2), pp. 241–252.
- [62] de Villoria, R. G., Yamamoto, N., Miravete, A., and Wardle, B. L., 2011, "Multi-Physics Damage Sensing in Nano-Engineered Structural Composites," *Nanotechnology*, **22**(18), p. 185502.
- [63] Alessandrini, S., Andreus, U., dell'Isola, F., and Porfiri, M., 2004, "Piezo-Electromechanical (PEM) Kirchhoff–Love Plates," *Eur. J. Mech. A*, **23**(4), pp. 689–702.
- [64] Placidi, L., and Hutter, K., 2006, "Thermodynamics of Polycrystalline Materials Treated by the Theory of Mixtures With Continuous Diversity," *Continuum Mech. Thermodyn.*, **17**(6), pp. 409–451.
- [65] Andreus, U., and Porfiri, M., 2007, "Effect of Electrical Uncertainties on Resonant Piezoelectric Shunting," *J. Intell. Mater. Syst. Struct.*, **18**(5), pp. 477–485.
- [66] Kim, D.-H., Song, J., Choi, W. M., Kim, H.-S., Kim, R.-H., Liu, Z., Huang, Y. Y., Hwang, K.-C., Zhang, Y.-w., and Rogers, J. A., 2008, "Materials and Noncoplanar Mesh Designs for Integrated Circuits With Linear Elastic Responses to Extreme Mechanical Deformations," *Proc. Natl. Acad. Sci.*, **105**(48), pp. 18675–18680.
- [67] Mannsfeld, S. C., Tee, B. C., Stoltenberg, R. M., Chen, C. V. H., Barman, S., Muir, B. V., Sokolov, A. N., Reese, C., and Bao, Z., 2010, "Highly Sensitive Flexible Pressure Sensors With Microstructured Rubber Dielectric Layers," *Nat. Mater.*, **9**(10), pp. 859–864.
- [68] Maurini, C., Pouget, J., and dell'Isola, F., 2004, "On a Model of Layered Piezoelectric Beams Including Transverse Stress Effect," *Int. J. Solids Struct.*, **41**(16), pp. 4473–4502.
- [69] Lakes, R., 1993, "Advances in Negative Poisson's Ratio Materials," *Adv. Mater.*, **5**(4), pp. 293–296.
- [70] Lakes, R., and Drugan, W., 2002, "Dramatically Stiffer Elastic Composite Materials Due to a Negative Stiffness Phase?" *J. Mech. Phys. Solids*, **50**(5), pp. 979–1009.
- [71] Jaglinski, T., Kochmann, D., Stone, D., and Lakes, R., 2007, "Composite Materials With Viscoelastic Stiffness Greater Than Diamond," *Science*, **315**(5812), pp. 620–622.
- [72] Bertoldi, K., Reis, P. M., Willshaw, S., and Mullin, T., 2010, "Negative Poisson's Ratio Behavior Induced by an Elastic Instability," *Adv. Mat.*, **22**(3), pp. 361–366.
- [73] Kashdan, L., Conner Seepersad, C., Haberman, M., and Wilson, P. S., 2012, "Design, Fabrication, and Evaluation of Negative Stiffness Elements Using SLS," *Rapid Prototyping J.*, **18**(3), pp. 194–200.
- [74] Milton, G. W., 2002, "The Theory of Composites," *Cambridge Monographs on Applied and Computational Mathematics*, Cambridge University Press, Cambridge, UK.
- [75] Nikopour, H., and Selvadurai, A., 2013, "Torsion of a Layered Composite Strip," *Compos. Struct.*, **95**, pp. 1–4.
- [76] Nikopour, H., and Selvadurai, A., 2014, "Concentrated Loading of a Fibre-Reinforced Composite Plate: Experimental and Computational Modeling of Boundary Fixity," *Composites, Part B*, **60**, pp. 297–305.
- [77] Placidi, L., and Hutter, K., 2005, "An Anisotropic Flow Law for Incompressible Polycrystalline Materials," *Z. Angew. Math. Phys.*, **57**(1), pp. 160–181.
- [78] Selvadurai, A., and Nikopour, H., 2012, "Transverse Elasticity of a Unidirectionally Reinforced Composite With an Irregular Fibre Arrangement: Experiments, Theory and Computations," *Compos. Struct.*, **94**(6), pp. 1973–1981.
- [79] Arnold, C. B., Serra, P., and Piqué, A., 2007, "Laser Direct-Write Techniques for Printing of Complex Materials," *MRS Bull.*, **32**(1), pp. 23–31.
- [80] Pershin, Y. V., and Di Ventra, M., 2011, "Memory Effects in Complex Materials and Nanoscale Systems," *Adv. Phys.*, **60**(2), pp. 145–227.
- [81] Proffen, T., Billinge, S., Egami, T., and Louca, D., 2003, "Structural Analysis of Complex Materials Using the Atomic Pair Distribution Function—A Practical Guide," *Z. Kristallogr./Int. J. Struct. Phys. Chem. Aspects Cryst. Mater.*, **218**(2), pp. 132–143.
- [82] Grillo, A., Federico, S., and Wittum, G., 2012, "Growth, Mass Transfer, and Remodeling in Fiber-Reinforced, Multi-Constituent Materials," *Int. J. Nonlinear Mech.*, **47**(2), pp. 388–401.
- [83] Grillo, A., Federico, S., Wittum, G., Imatani, S., Giaquinta, G., and Mićunović, M. V., 2009, "Evolution of a Fibre-Reinforced Growing Mixture," *Nuovo Cimento C*, **32C**(1), pp. 97–119.
- [84] Grillo, A., and Wittum, G., 2010, "Growth and Mass Transfer in Multi-Constituent Biological Materials," *AIP Conf. Proc.*, **1281**(1), pp. 355–358.
- [85] Seddik, H., Greve, R., Zwinger, T., and Placidi, L., 2011, "A Full Stokes Ice Flow Model for the Vicinity of Dome Fuji, Antarctica, With Induced Anisotropy and Fabric Evolution," *Cryosphere*, **5**(2), pp. 495–508.
- [86] Porubov, A. V., Aero, E. L., and Andrievsky, B., 2010, "Dynamic Properties of Essentially Nonlinear Generalized Continua," *Mechanics of Generalized Continua*, Springer, New York, pp. 161–168.
- [87] Forest, S., 1998, "Mechanics of Generalized Continua: Construction by Homogenization," *J. Phys. IV*, **8**(PR4), pp. PR4–PR39.
- [88] Maugin, G. A., and Metrikine, A. V., 2010, "Mechanics of Generalized Continua," *Advances in Mechanics and Mathematics*, Vol. 21, Springer, New York.
- [89] Tekoğlu, C., and Onck, P. R., 2008, "Size Effects in Two-Dimensional Voronoi Foams: A Comparison Between Generalized Continua and Discrete Models," *J. Mech. Phys. Solids*, **56**(12), pp. 3541–3564.
- [90] Forest, S., and Trinh, D. K., 2011, "Generalized Continua and Non-Homogeneous Boundary Conditions in Homogenisation Methods," *ZAMM*, **91**(2), pp. 90–109.
- [91] Boutin, C., Hans, S., and Chesnais, C., 2010, "Generalized Beams and Continua. Dynamics of Reticulated Structures," *Mechanics of Generalized Continua*, Springer, New York, pp. 131–141.
- [92] Feyel, F., 2003, "A Multilevel Finite Element Method (FE 2) to Describe the Response of Highly Non-Linear Structures Using Generalized Continua," *Comput. Methods Appl. Mech. Eng.*, **192**(28), pp. 3233–3244.
- [93] Forest, S., and Sievert, R., 2003, "Elastoviscoplastic Constitutive Frameworks for Generalized Continua," *Acta Mechanica* **160**(1–2), pp. 71–111.
- [94] Green, A., and Naghdi, P., 1995, "A Unified Procedure for Construction of Theories of Deformable Media. II. Generalized Continua," *Proc. R. Soc. London A*, **448**(1934), pp. 357–377.
- [95] Eringen, A. C., 1965, "Theory of Micropolar Fluids," DTIC Document, Technical Report No. 27.
- [96] Eringen, A. C., and Suhubi, E., 1964, "Nonlinear Theory of Simple Micro-Elastic Solids," *Int. J. Eng. Sci.*, **2**(2), pp. 189–203.
- [97] Eringen, A. C., 1999, "Theory of Micropolar Elasticity," *Microcontinuum Field Theories*, Springer, New York, pp. 101–248.
- [98] Mindlin, R. D., 1964, "Micro-Structure in Linear Elasticity," *Arch. Ration. Mech. Anal.*, **16**(1), pp. 51–78.
- [99] Eringen, A. C., 2012, *Microcontinuum Field Theories: I. Foundations and Solids*, Springer Science & Business Media, New York.
- [100] Neff, P., Ghiba, I.-D., Madeo, A., Placidi, L., and Rosi, G., 2013, "A Unifying Perspective: The Relaxed Linear Micromorphic Continuum," *Continuum Mech. Thermodyn.*, **26**(5), pp. 639–681.
- [101] Neff, P., 2004, "On Material Constants for Micromorphic Continua," Trends in Applications of Mathematics to Mechanics, XIVth International Symposium on Trends in Applications of Mathematics to Mechanics (STAMM'2004), Seeheim, Germany, Aug. 22–28, pp. 337–348.
- [102] Misra, A., and Singh, V., 2013, "Micromechanical Model for Viscoelastic Materials Undergoing Damage," *Continuum Mech. Thermodyn.*, **25**(2), pp. 1–16.
- [103] Misra, A., and Yang, Y., 2010, "Micromechanical Model for Cohesive Materials Based Upon Pseudo-Granular Structure," *Int. J. Solids Struct.*, **47**(21), pp. 2970–2981.
- [104] Contraffatto, L., Cuomo, M., and Fazio, F., 2012, "An Enriched Finite Element for Crack Opening and Rebar Slip in Reinforced Concrete Members," *Int. J. Fract.*, **178**(1–2), pp. 33–50.
- [105] Scerrato, D., Giorgio, I., Della Corte, A., Madeo, A., and Limam, A., 2015, "A Micro-Structural Model for Dissipation Phenomena in the Concrete," *Int. J. Numer. Anal. Methods Geomech.*, **39**(18), pp. 2037–2052.

- [106] Scerrato, D., Giorgio, I., Madeo, A., Limam, A., and Darve, F., 2014, "A Simple Non-Linear Model for Internal Friction in Modified Concrete," *Int. J. Eng. Sci.*, **80**(SD), pp. 136–152.
- [107] Boutin, C., 1996, "Microstructural Effects in Elastic Composites," *Int. J. Solids Struct.*, **33**(7), pp. 1023–1051.
- [108] Eringen, A. C., 1968, *Mechanics of Micromorphic Continua*, Springer, Berlin.
- [109] Bréchet, Y., 2000, *Microstructures, Mechanical Properties and Processes*, Wiley-VCH, Weinheim, Germany.
- [110] Leismann, T., and Mahnken, R., 2015, "Comparison of Micromorphic, Micropolar and Microstrain Continua," *Book of Abstracts-Extract*, 86th Annual Meeting of the International Association of Applied Mathematics and Mechanics (GAMM 2015), Lecce, Italy, Mar. 23–27, Università del Salento, Lecce, Italy, p. 58.
- [111] Kim, D., Brunski, J., and Nicoletta, D., 2005, "Microstrain Fields for Cortical Bone in Uniaxial Tension: Optical Analysis Method," *Proc. Inst. Mech. Eng., Part H*, **219**(2), pp. 119–128.
- [112] Yang, Y., and Misra, A., 2012, "Micromechanics Based Second Gradient Continuum Theory for Shear Band Modeling in Cohesive Granular Materials Following Damage Elasticity," *Int. J. Solids Struct.*, **49**(18), pp. 2500–2514.
- [113] Yang, Y., Ching, W., and Misra, A., 2011, "Higher-Order Continuum Theory Applied to Fracture Simulation of Nanoscale Intergranular Glassy Film," *J. Nanomech. Micromech.*, **1**(2), pp. 60–73.
- [114] Seppecher, P., 2002, "Second-Gradient Theory: Application to Cahn–Hilliard Fluids," *Continuum Thermoelasticity*, Springer, New York, pp. 379–388.
- [115] Alibert, J.-J., Seppecher, P., and dell'Isola, F., 2003, "Truss Modular Beams With Deformation Energy Depending on Higher Displacement Gradients," *Math. Mech. Solids*, **8**(1), pp. 51–73.
- [116] Neff, P., Chelmiński, K., and Alber, H.-D., 2009, "Notes on Strain Gradient Plasticity: Finite Strain Covariant Modelling and Global Existence in the Infinitesimal Rate-Independent Case," *Math. Models Methods Appl. Sci.*, **19**(2), pp. 307–346.
- [117] Placidi, L., Rosi, G., Giorgio, I., and Madeo, A., 2014, "Reflection and Transmission of Plane Waves at Surfaces Carrying Material Properties and Embedded in Second-Gradient Materials," *Math. Mech. Solids*, **19**(5), pp. 555–578.
- [118] Askes, H., Suiker, A., and Sluys, L., 2002, "A Classification of Higher-Order Strain-Gradient Models—Linear Analysis," *Arch. Appl. Mech.*, **72**(2–3), pp. 171–188.
- [119] Rinaldi, A., and Placidi, L., 2013, "A Microscale Second Gradient Approximation of the Damage Parameter of Quasi-Brittle Heterogeneous Lattices," *Z. Angew. Math. Mech./J. Appl. Math. Mech.*, **94**(10), pp. 862–877.
- [120] Iordache, M.-M., and Willam, K., 1998, "Localized Failure Analysis in Elastoplastic Cosserat Continua," *Comput. Methods Appl. Mech. Eng.*, **151**(3), pp. 559–586.
- [121] Perić, D., Yu, J., and Owen, D., 1994, "On Error Estimates and Adaptivity in Elastoplastic Solids: Applications to the Numerical Simulation of Strain Localization in Classical and Cosserat Continua," *Int. J. Numer. Methods Eng.*, **37**(8), pp. 1351–1379.
- [122] Ehlers, W., Ramm, E., Diebels, S., and dAddetta, G., 2003, "From Particle Ensembles to Cosserat Continua: Homogenization of Contact Forces Towards Stresses and Couple Stresses," *Int. J. Solids Struct.*, **40**(24), pp. 6681–6702.
- [123] Neuber, H., 1966, "On the General Solution of Linear-Elastic Problems in Isotropic and Anisotropic Cosserat Continua," *Applied Mechanics*, Springer, Berlin, pp. 153–158.
- [124] Dietsche, A., and Willam, K., 1997, "Boundary Effects in Elasto-Plastic Cosserat Continua," *Int. J. Solids Struct.*, **34**(7), pp. 877–893.
- [125] Ieşan, D., 2007, "A Theory of Thermoelastic Composites Modelled as Interacting Cosserat Continua," *J. Therm. Stresses*, **30**(12), pp. 1269–1289.
- [126] Pietraszkiewicz, W., and Eremeyev, V., 2009, "On Vectorially Parameterized Natural Strain Measures of the Non-Linear Cosserat Continuum," *Int. J. Solids Struct.*, **46**(11), pp. 2477–2480.
- [127] Altenbach, J., Altenbach, H., and Eremeyev, V. A., 2010, "On Generalized Cosserat-Type Theories of Plates and Shells: A Short Review and Bibliography," *Arch. Appl. Mech.*, **80**(1), pp. 73–92.
- [128] Steinmann, P., and Stein, E., 1997, "A Unifying Treatise of Variational Principles for Two Types of Micropolar Continua," *Acta Mech.*, **121**(1–4), pp. 215–232.
- [129] Eremeyev, V. A., and Pietraszkiewicz, W., "Material Symmetry Group and Constitutive Equations of Micropolar Anisotropic Elastic Solids," *Math. Mech. Solids*, epub.
- [130] Eremeyev, V. A., and Pietraszkiewicz, W., 2012, "Material Symmetry Group of the Non-Linear Polar-Elastic Continuum," *Int. J. Solids Struct.*, **49**(14), pp. 1993–2005.
- [131] Pietraszkiewicz, W., and Eremeyev, V., 2009, "On Natural Strain Measures of the Non-Linear Micropolar Continuum," *Int. J. Solids Struct.*, **46**(3), pp. 774–787.
- [132] Jänicke, R., Diebels, S., Sehlhorst, H.-G., and Düster, A., 2009, "Two-Scale Modelling of Micromorphic Continua," *Continuum Mech. Thermodyn.*, **21**(4), pp. 297–315.
- [133] Forest, S., and Sievert, R., 2006, "Nonlinear Microstrain Theories," *Int. J. Solids Struct.*, **43**(24), pp. 7224–7245.
- [134] dell'Isola, F., Andreas, U., and Placidi, L., 2014, "At the Origins and in the Vanguard of Peridynamics, Non-Local and Higher-Gradient Continuum Mechanics: An Underestimated and Still Topical Contribution of Gabrio Piola," *Math. Mech. Solids*, **20**(8), pp. 887–928.
- [135] Carcaterra, A., dell'Isola, F., Esposito, R., and Pulvirenti, M., 2015, "Macroscopic Description of Microscopically Strongly Inhomogeneous Systems: A Mathematical Basis for the Synthesis of Higher Gradients Metamaterials," *Arch. Ration. Mech. Anal.*, **218**(3), pp. 1239–1262.
- [136] Alibert, J. J., and Corte, A. D., 2015, "Second-Gradient Continua as Homogenized Limit of Pantographic Microstructured Plates: A Rigorous Proof," *Z. Angew. Math. Phys.*, **66**(5), pp. 2855–2870.
- [137] Giorgio, I., Galantucci, L., Della Corte, A., and Del Vescovo, D., 2015, "Piezo-Electromechanical Smart Materials With Distributed Arrays of Piezoelectric Transducers: Current and Upcoming Applications," *Int. J. Appl. Electromagn. Mech.*, **47**(4), pp. 1051–1084.
- [138] Trinh, D. K., Janicke, R., Auffray, N., Diebels, S., and Forest, S., 2012, "Evaluation of Generalized Continuum Substitution Models for Heterogeneous Materials," *Int. J. Multiscale Comput. Eng.*, **10**(6), pp. 527–549.
- [139] Ashby, M. F., and Cebon, D., 1993, "Materials Selection in Mechanical Design," *J. Phys. IV*, **3**(C7), pp. C7-1–C7-9.
- [140] Elanchezian, C., and Sundar, G. S., 2007, *Computer Aided Manufacturing*, Firewall Media, New Delhi, India.
- [141] Auffray, N., dell'Isola, F., Eremeyev, V., Madeo, A., and Rosi, G., 2015, "Analytical Continuum Mechanics à la Hamilton–Piola Least Action Principle for Second Gradient Continua and Capillary Fluids," *Math. Mech. Solids*, **20**(4), pp. 375–417.
- [142] Milton, G. W., and Willis, J. R., 2007, "On Modifications of Newton's Second Law and Linear Continuum Elastodynamics," *Proc. R. Soc. London A*, **463**(2079), pp. 855–880.
- [143] Metropolis, N., 1987, "The Beginning of the Monte Carlo Method," *Los Alamos Sci., Special Issue*, pp. 125–130.
- [144] Happ, H. H., and Kron, G., 1973, *Gabriel Kron and Systems Theory*, Union College Press, Schenectady, NY.
- [145] Zienkiewicz, O. C., Taylor, R. L., Zienkiewicz, O. C., and Taylor, R. L., 1977, *The Finite Element Method*, Vol. 3, McGraw-Hill, London, UK.
- [146] Greco, L., Impollonia, N., and Cuomo, M., 2014, "A Procedure for the Static Analysis of Cable Structures Following Elastic Catenary Theory," *Int. J. Solids Struct.*, **51**(7), pp. 1521–1533.
- [147] Greco, L., and Cuomo, M., 2012, "On the Force Density Method for Slack Cable Nets," *Int. J. Solids Struct.*, **49**(13), pp. 1526–1540.
- [148] Garusi, E., Tralli, A., and Cazzani, A., 2004, "An Unsymmetric Stress Formulation for Reissner–Mindlin Plates: A Simple and Locking-Free Rectangular Element," *Int. J. Comput. Eng. Sci.*, **5**(3), pp. 589–618.
- [149] Reccia, E., Cazzani, A., and Cecchi, A., 2012, "FEM–DEM Modeling for Out-of-Plane Loaded Masonry Panels: A Limit Analysis Approach," *Open Civil Eng. J.*, **6**(1), pp. 231–238.
- [150] Greco, L., and Cuomo, M., 2014, "Consistent Tangent Operator for an Exact Kirchhoff Rod Model," *Continuum Mech. Thermodyn.*, **27**(4–5), pp. 861–877.
- [151] Carassale, L., and Piccardo, G., 2010, "Non-Linear Discrete Models for the Stochastic Analysis of Cables in Turbulent Wind," *Int. J. Nonlinear Mech.*, **45**(3), pp. 219–231.
- [152] Javili, A., and Steinmann, P., 2009, "A Finite Element Framework for Continua With Boundary Energies. Part I: The Two-Dimensional Case," *Comput. Meth. Appl. Mech. Eng.*, **198**(27), pp. 2198–2208.
- [153] Javili, A., and Steinmann, P., 2010, "A Finite Element Framework for Continua With Boundary Energies. Part II: The Three-Dimensional Case," *Comput. Methods Appl. Mech. Eng.*, **199**(9), pp. 755–765.
- [154] Turco, E., and Caracciolo, P., 2000, "Elasto-Plastic Analysis of Kirchhoff Plates by High Simplicity Finite Elements," *Comput. Methods Appl. Mech. Eng.*, **190**(5–7), pp. 691–706.
- [155] Ciancio, D., Carol, I., and Cuomo, M., 2007, "Crack Opening Conditions at 'Corner Nodes' in FE Analysis With Cracking Along Mesh Lines," *Eng. Fracture Mech.*, **74**(13), pp. 1963–1982.
- [156] Ciancio, D., Carol, I., and Cuomo, M., 2006, "On Inter-Element Forces in the FEM-Displacement Formulation, and Implications for Stress Recovery," *Int. J. Numer. Methods Eng.*, **66**(3), pp. 502–528.
- [157] Hughes, T. J., Cottrell, J. A., and Bazilevs, Y., 2005, "Isogeometric Analysis: CAD, Finite Elements, NURBS, Exact Geometry and Mesh Refinement," *Comput. Methods Appl. Mech. Eng.*, **194**(39), pp. 4135–4195.
- [158] Cazzani, A., Malagù, M., and Turco, E., "Isogeometric Analysis of Plane-Curved Beams," *Math. Mech. Solids*, epub.
- [159] Greco, L., and Cuomo, M., 2013, "B-Spline Interpolation of Kirchhoff–Love Space Rods," *Comput. Methods Appl. Mech. Eng.*, **256**, pp. 251–269.
- [160] Greco, L., and Cuomo, M., 2014, "An Implicit G1 Multi Patch B-Spline Interpolation for Kirchhoff–Love Space Rod," *Comput. Methods Appl. Mech. Eng.*, **269**, pp. 173–197.
- [161] Cazzani, A., Malagù, M., and Turco, E., 2014, "Isogeometric Analysis: A Powerful Numerical Tool for the Elastic Analysis of Historical Masonry Arches," *Continuum Mech. Thermodyn.*, epub.
- [162] Cazzani, A., Malagù, M., Turco, E., and Stochino, F., "Constitutive Models for Strongly Curved Beams in the Frame of Isogeometric Analysis," *Math. Mech. Solids*, epub.
- [163] Cuomo, M., Contrafatto, L., and Greco, L., 2014, "A Variational Model Based on Isogeometric Interpolation for the Analysis of Cracked Bodies," *Int. J. Eng. Sci.*, **80**(SD), pp. 173–188.
- [164] De Luycker, E., Benson, D., Belytschko, T., Bazilevs, Y., and Hsu, M., 2011, "X-FEM in Isogeometric Analysis for Linear Fracture Mechanics," *Int. J. Numer. Methods Eng.*, **87**(6), pp. 541–565.
- [165] Allen, M. P., 2004, "Introduction to Molecular Dynamics Simulation," *Comput. Soft Matter*, **23**, pp. 1–28.
- [166] Tinsley Oden, J., Prudhomme, S., Romkes, A., and Bauman, P. T., 2006, "Multiscale Modeling of Physical Phenomena: Adaptive Control of Models," *SIAM J. Sci. Comput.*, **28**(6), pp. 2359–2389.
- [167] Piola, G., 2014, *The Complete Works of Gabrio Piola: Commented English Translation*, Vol. 38, Springer, Cham, Switzerland.

- [168] Silling, S. A., Epton, M., Weckner, O., Xu, J., and Askari, E., 2007, "Peridynamic States and Constitutive Modeling," *J. Elasticity*, **88**(2), pp. 151–184.
- [169] Silling, S., and Lehoucq, R., 2010, "Peridynamic Theory of Solid Mechanics," *Adv. Appl. Mech.*, **44**(1), pp. 73–166.
- [170] Askari, E., Bobaru, F., Lehoucq, R., Parks, M., Silling, S., and Weckner, O., 2008, "Peridynamics for Multiscale Materials Modeling," *J. Phys.: Conf. Ser.*, **125**(1), p. 012078.
- [171] Silling, S. A., and Askari, E., 2005, "A Meshfree Method Based on the Peridynamic Model of Solid Mechanics," *Comput. Struct.*, **83**(17), pp. 1526–1535.
- [172] Parks, M. L., Lehoucq, R. B., Plimpton, S. J., and Silling, S. A., 2008, "Implementing Peridynamics Within a Molecular Dynamics Code," *Comput. Phys. Commun.*, **179**(11), pp. 777–783.
- [173] Leyendecker, S., Ober-Blöbaum, S., Marsden, J. E., and Ortiz, M., 2010, "Discrete Mechanics and Optimal Control for Constrained Systems," *Optim. Control Appl. Methods*, **31**(6), pp. 505–528.
- [174] Ferretti, M., Madeo, A., dell'Isola, F., and Boisse, P., 2014, "Modeling the Onset of Shear Boundary Layers in Fibrous Composite Reinforcements by Second-Gradient Theory," *Z. Angew. Math. Phys.*, **65**(3), pp. 587–612.
- [175] Andreaus, U., dell'Isola, F., and Porfiri, M., 2004, "Piezoelectric Passive Distributed Controllers for Beam Flexural Vibrations," *J. Vib. Control*, **10**(5), pp. 625–659.
- [176] Maurini, C., Pouget, J., and dell'Isola, F., 2006, "Extension of the Euler–Bernoulli Model of Piezoelectric Laminates to Include 3D Effects Via a Mixed Approach," *Comput. Struct.*, **84**(22), pp. 1438–1458.
- [177] dell'Isola, F., Maurini, C., and Porfiri, M., 2004, "Passive Damping of Beam Vibrations Through Distributed Electric Networks and Piezoelectric Transducers: Prototype Design and Experimental Validation," *Smart Mater. Struct.*, **13**(2), p. 299.
- [178] Gantzounis, G., Serra-Garcia, M., Homma, K., Mendoza, J., and Daraio, C., 2013, "Granular Metamaterials for Vibration Mitigation," *J. Appl. Phys.*, **114**(9), p. 093514.
- [179] Alessandrini, S., Andreaus, U., dell'Isola, F., and Porfiri, M., 2005, "A Passive Electric Controller for Multimodal Vibrations of Thin Plates," *Comput. Struct.*, **83**(15), pp. 1236–1250.
- [180] Bailey, T., and Ubbard, J. E., 1985, "Distributed Piezoelectric-Polymer Active Vibration Control of a Cantilever Beam," *J. Guid. Control Dyn.*, **8**(5), pp. 605–611.
- [181] Behrens, S., Fleming, A. J., and Moheimi, S. O. R., 2003, "A Broadband Controller for Shunt Piezoelectric Damping of Structural Vibration," *Smart Mater. Struct.*, **12**(1), p. 18.
- [182] Corr, L. R., and Clark, W. W., 2003, "A Novel Semi-Active Multi-Modal Vibration Control Law for a Piezoceramic Actuator," *ASME J. Vib. Acoust.*, **125**(2), pp. 214–222.
- [183] Dimitriadis, E. K., Fuller, C. R., and Rogers, C. A., 1991, "Piezoelectric Actuators for Distributed Vibration Excitation of Thin Plates," *ASME J. Vib. Acoust.*, **113**(1), pp. 100–107.
- [184] Hollkamp, J. J., 1994, "Multimodal Passive Vibration Suppression With Piezoelectric Materials and Resonant Shunts," *J. Intell. Mater. Syst. Struct.*, **5**(1), pp. 49–57.
- [185] Lallart, M., Lefeuvre, É., Richard, C., and Guyomar, D., 2008, "Self-Powered Circuit for Broadband, Multimodal Piezoelectric Vibration Control," *Sens. Actuators A*, **143**(2), pp. 377–382.
- [186] Pipkin, A., 1981, "Plane Traction Problems for Inextensible Networks," *Q. J. Mech. Appl. Math.*, **34**(4), pp. 415–429.
- [187] Rivlin, R., 1997, "Plane Strain of a Net Formed by Inextensible Cords," *Collected Papers of RS Rivlin*, Springer, New York, pp. 511–534.
- [188] D'Agostino, M. V., Giorgio, I., Greco, L., Madeo, A., and Boisse, P., 2015, "Continuum and Discrete Models for Structures Including (Quasi-) Inextensible Elasticae With a View to the Design and Modeling of Composite Reinforcements," *Int. J. Solids Struct.*, **59**, pp. 1–17.
- [189] dell'Isola, F., D'Agostino, M. V., Madeo, A., Boisse, P., and Steigmann, D., "Minimization of Shear Energy in Two Dimensional Continua With Two Orthogonal Families of Inextensible Fibers: The Case of Standard Bias Extension Test," *J. Elasticity*, epub.
- [190] dell'Isola, F., Giorgio, I., and Andreaus, U., 2015, "Elastic Pantographic 2D Lattices: A Numerical Analysis on Static Response and Wave Propagation," *Proc. Est. Acad. Sci.*, **64**(3), pp. 219–225.
- [191] Descamps, B., 2014, *Computational Design of Lightweight Structures: Form Finding and Optimization*, Wiley, Weinheim, Germany.
- [192] Dell'Isola, F., Della Corte, A., Greco, L., and Luongo, A., "Plane Bias Extension Test for a Continuum With Two Inextensible Families of Fibers: A Variational Treatment With Lagrange Multipliers and a Perturbation Solution," *Int. J. Solids Struct.* (in press).
- [193] dell'Isola, F., and Steigmann, D., 2015, "A Two-Dimensional Gradient-Elasticity Theory for Woven Fabrics," *J. Elasticity*, **118**(1), pp. 113–125.
- [194] Hamila, N., and Boisse, P., 2013, "Tension Locking in Finite-Element Analyses of Textile Composite Reinforcement Deformation," *C. R. Méc.*, **341**(6), pp. 508–519.
- [195] Hamila, N., and Boisse, P., 2013, "Locking in Simulation of Composite Reinforcement Deformations. Analysis and Treatment," *Composites, Part A*, **53**, pp. 109–117.
- [196] Federico, S., 2010, "On the Linear Elasticity of Porous Materials," *Int. J. Mech. Sci.*, **52**(2), pp. 175–182.
- [197] Hollister, S. J., 2005, "Porous Scaffold Design for Tissue Engineering," *Nat. Mater.*, **4**(7), pp. 518–524.
- [198] Serra, F., Vishnubhatla, K. C., Buscaglia, M., Cerbino, R., Osellame, R., Cerullo, G., and Bellini, T., 2011, "Topological Defects of Nematic Liquid Crystals Confined in Porous Networks," *Soft Matter*, **7**(22), pp. 10945–10950.
- [199] Araki, T., Buscaglia, M., Bellini, T., and Tanaka, H., 2011, "Memory and Topological Frustration in Nematic Liquid Crystals Confined in Porous Materials," *Nat. Mater.*, **10**(4), pp. 303–309.
- [200] Andreaus, U., and Colloca, M., 2009, "Prediction of Micromotion Initiation of an Implanted Femur Under Physiological Loads and Constraints Using the Finite Element Method," *Proc. Inst. Mech. Eng., Part H*, **223**, pp. 589–605.
- [201] Andreaus, U., Colloca, M., and Iacoviello, D., 2013, *Modeling of Trabecular Architecture as Result of an Optimal Control Procedure* (Lecture Notes in Computational Vision and Biomechanics), Vol. 4, Springer, Dordrecht.
- [202] Andreaus, U., Colloca, M., Iacoviello, D., and Pignataro, M., 2011, "Optimal-Tuning PID Control of Adaptive Materials for Structural Efficiency," *Struct. Multidiscip. Optim.*, **43**(1), pp. 43–59.
- [203] Andreaus, U., Giorgio, I., and Lekszycki, T., 2014, "A 2-D Continuum Model of a Mixture of Bone Tissue and Bio-Resorbable Material for Simulating Mass Density Redistribution Under Load Slowly Variable in Time," *Z. Angew. Math. Mech./J. Appl. Math. Mech.*, **94**(12), pp. 978–1000.
- [204] Park, J.-G., Ye, Q., Topp, E. M., Lee, C. H., Kostoryz, E. L., Misra, A., and Spencer, P., 2009, "Dynamic Mechanical Analysis and Esterase Degradation of Dentin Adhesives Containing a Branched Methacrylate," *J. Biomed. Mater. Res., Part B*, **91**(1), pp. 61–70.
- [205] Andreaus, U., Giorgio, I., and Madeo, A., 2014, "Modeling of the Interaction Between Bone Tissue and Resorbable Biomaterial as Linear Elastic Materials With Voids," *Z. Angew. Math. Phys.*, **66**(1), pp. 209–237.
- [206] Ganghoffer, J.-F., 2012, "A Contribution to the Mechanics and Thermodynamics of Surface Growth. Application to Bone External Remodeling," *Int. J. Eng. Sci.*, **50**(1), pp. 166–191.
- [207] Giorgio, I., Andreaus, U., and Madeo, A., 2014, "The Influence of Different Loads on the Remodeling Process of a Bone and Bio-Resorbable Material Mixture With Voids," *Continuum Mech. Thermodyn.*, epub.
- [208] Laurent, C., Durville, D., Vaquette, C., Rahouadj, R., and Ganghoffer, J., 2013, "Computer-Aided Tissue Engineering: Application to the Case of Anterior Cruciate Ligament Repair," *Biomech. Cells Tissues*, **9**(1), pp. 1–44.
- [209] Laurent, C., Durville, D., Mainard, D., Ganghoffer, J.-F., and Rahouadj, R., 2012, "Designing a New Scaffold for Anterior Cruciate Ligament Tissue Engineering," *J. Mech. Behav. Biomed. Mater.*, **12**(1), pp. 184–196.
- [210] Laurent, C., Durville, D., Wang, X., Ganghoffer, J.-F., and Rahouadj, R., 2010, "Designing a New Scaffold for Anterior Cruciate Ligament Tissue Engineering," *Comput. Methods Biomech. Biomed. Eng.*, **13**(S1), pp. 87–88.
- [211] Misra, A., Spencer, P., Marangos, O., Wang, Y., and Katz, J. L., 2005, "Parametric Study of the Effect of Phase Anisotropy on the Micromechanical Behaviour of Dentin–Adhesive Interfaces," *J. R. Soc. Interface*, **2**(3), pp. 145–157.
- [212] Spencer, P., Ye, Q., Park, J., Topp, E. M., Misra, A., Marangos, O., Wang, Y., Bohaty, B. S., Singh, V., Sene, F., Eslick, J., Camarda, K., and Katz, J. L., 2010, "Adhesive/Dentin Interface: The Weak Link in the Composite Restoration," *Ann. Biomed. Eng.*, **38**(6), pp. 1989–2003.
- [213] Steigmann, D. J., and dell'Isola, D., "Mechanical Response of Fabric Sheets to Three-Dimensional Bending, Twisting, and Stretching," *Acta Mech. Sin.*, **31**(3), pp. 373–382.
- [214] Ye, Q., Spencer, P., Wang, Y., and Misra, A., 2007, "Relationship of Solvent to the Photopolymerization Process, Properties, and Structure in Model Dentin Adhesives," *J. Biomed. Mater. Res., Part A*, **80**(2), pp. 342–350.
- [215] Hu, L., Pasta, M., Mantia, F. L., Cui, L., Jeong, S., Deshazer, H. D., Choi, J. W., Han, S. M., and Cui, Y., 2010, "Stretchable, Porous, and Conductive Energy Textiles," *Nano Lett.*, **10**(2), pp. 708–714.
- [216] Piccardo, G., Ranzani, G., and Luongo, A., 2014, "A Complete Dynamic Approach to the Generalized Beam Theory Cross-Section Analysis Including Extension and Shear Modes," *Math. Mech. Solids*, **19**(8), pp. 900–924.
- [217] Piccardo, G., and Tubino, F., 2012, "Dynamic Response of Euler–Bernoulli Beams to Resonant Harmonic Moving Loads," *Struct. Eng. Mech.*, **44**(5), pp. 681–704.
- [218] Luongo, A., Zulli, D., and Piccardo, G., 2007, "A Linear Curved-Beam Model for the Analysis of Galloping in Suspended Cables," *J. Mech. Mater. Struct.*, **2**(4), pp. 675–694.
- [219] Altenbach, H., Birsan, M., and Eremeyev, V. A., 2012, "On a Thermodynamic Theory of Rods With Two Temperature Fields," *Acta Mech.*, **223**(8), pp. 1583–1596.
- [220] Luongo, A., and Piccardo, G., 1998, "Non-Linear Galloping of Sagged Cables in 1:2 Internal Resonance," *J. Sound Vib.*, **214**(5), pp. 915–940.
- [221] Luongo, A., Zulli, D., and Piccardo, G., 2008, "Analytical and Numerical Approaches to Nonlinear Galloping of Internally Resonant Suspended Cables," *J. Sound Vib.*, **315**(3), pp. 375–393.
- [222] Luongo, A., Rega, G., and Vestroni, F., 1984, "Planar Non-Linear Free Vibrations of an Elastic Cable," *Int. J. Nonlinear Mech.*, **19**(1), pp. 39–52.
- [223] Luongo, A., 1996, "Perturbation Methods for Nonlinear Autonomous Discrete-Time Dynamical Systems," *Nonlinear Dyn.*, **10**(4), pp. 317–331.
- [224] Liu, W. K., Park, H. S., Qian, D., Karpov, E. G., Kadowaki, H., and Wagner, G. J., 2006, "Bridging Scale Methods for Nanomechanics and Materials," *Comput. Methods Appl. Mech. Eng.*, **195**(13), pp. 1407–1421.
- [225] Miehe, C., Schröder, J., and Schotte, J., 1999, "Computational Homogenization Analysis in Finite Plasticity Simulation of Texture Development in Polycrystalline Materials," *Comput. Methods Appl. Mech. Eng.*, **171**(3), pp. 387–418.

- [226] Brun, M., Lopez-Pamies, O., and Castaneda, P. P., 2007, "Homogenization Estimates for Fiber-Reinforced Elastomers With Periodic Microstructures," *Int. J. Solids Struct.*, **44**(18), pp. 5953–5979.
- [227] Milton, G., 1986, "Modelling the Properties of Composites by Laminates," *Homogenization and Effective Moduli of Materials and Media*, Springer, New York, pp. 150–174.
- [228] Dos Reis, F., and Ganghoffer, J., 2012, "Equivalent Mechanical Properties of Auxetic Lattices From Discrete Homogenization," *Comput. Mater. Sci.*, **51**(1), pp. 314–321.
- [229] Dos Reis, F., and Ganghoffer, J.-F., 2011, "Construction of Micropolar Continua From the Homogenization of Repetitive Planar Lattices," *Mechanics of Generalized Continua*, Springer, New York, pp. 193–217.
- [230] Ladeveze, P., and Nouy, A., 2003, "On a Multiscale Computational Strategy With Time and Space Homogenization for Structural Mechanics," *Comput. Methods Appl. Mech. Eng.*, **192**(28), pp. 3061–3087.
- [231] Federico, S., Grillo, A., and Herzog, W., 2004, "A Transversely Isotropic Composite With a Statistical Distribution of Spheroidal Inclusions: A Geometrical Approach to Overall Properties," *J. Mech. Phys. Solids*, **52**(10), pp. 2309–2327.
- [232] Goda, I., Assidi, M., Belouettar, S., and Ganghoffer, J., 2012, "A Micropolar Anisotropic Constitutive Model of Cancellous Bone From Discrete Homogenization," *J. Mech. Behav. Biomed. Mater.*, **16**, pp. 87–108.
- [233] Ebinger, T., Steeb, H., and Diebels, S., 2005, "Modeling Macroscopic Extended Continua With the Aid of Numerical Homogenization Schemes," *Comput. Mater. Sci.*, **32**(3), pp. 337–347.
- [234] Ober-Blöbaum, S., Junge, O., and Marsden, J. E., 2011, "Discrete Mechanics and Optimal Control: An Analysis," *ESAIM: Control Optim. Calculus Var.*, **17**(2), pp. 322–352.
- [235] Luongo, A., Rega, G., and Vestroni, F., 1986, "On Nonlinear Dynamics of Planar Shear Inextensible Beams," *ASME J. Appl. Mech.*, **53**(3), pp. 619–624.
- [236] Birsan, M., Altenbach, H., Sadowski, T., Eremeyev, V., and Pietras, D., 2012, "Deformation Analysis of Functionally Graded Beams by the Direct Approach," *Composites, Part B*, **43**(3), pp. 1315–1328.
- [237] Mei, C. C., and Vemescu, B., 2010, *Homogenization Methods for Multiscale Mechanics*, World Scientific, Singapore.
- [238] Madeo, A., Neff, P., Ghiba, I.-D., Placidi, L., and Rosi, G., 2013, "Wave Propagation in Relaxed Micromorphic Continua: Modeling Metamaterials With Frequency Band-Gaps," *Continuum Mech. Thermodyn.*, **27**(4), pp. 551–570.
- [239] Berezovski, A., Giorgio, I., and Della Corte, A., 2015, "Interfaces in Micromorphic Materials: Wave Transmission and Reflection With Numerical Simulations," *Math. Mech. Solids*, epub.
- [240] Madeo, A., Della Corte, A., Greco, L., and Neff, P., "Wave Propagation in Pantographic 2D Lattices With Internal Discontinuities," *Proc. Est. Acad. Sci.*, epub.
- [241] Seppecher, P., Alibert, J.-J., and dell'Isola, F., 2011, "Linear Elastic Trusses Leading to Continua With Exotic Mechanical Interactions," *J. Phys.: Conf. Ser.*, **319**(1), p. 012018.
- [242] Giorgio, I., Culla, A., and Del Vescovo, D., 2009, "Multimode Vibration Control Using Several Piezoelectric Transducers Shunted With a Multiterminal Network," *Arch. Appl. Mech.*, **79**(9), pp. 859–879.
- [243] Moheimani, S. O. R., 2003, "A Survey of Recent Innovations in Vibration Damping and Control Using Shunted Piezoelectric Transducers," *IEEE Trans. Control Syst. Technol.*, **11**(4), pp. 482–494.
- [244] Porfiri, M., dell'Isola, F., and Mascioli, F., 2004, "Circuit Analog of a Beam and Its Application to Multimodal Vibration Damping, Using Piezoelectric Transducers," *Int. J. Circuit Theory Appl.*, **32**(4), pp. 167–198.
- [245] Eremeyev, V., Freidin, A., and Sharipova, L., 2003, "Nonuniqueness and Stability in Problems of Equilibrium of Elastic Two-Phase Bodies," *Dokl. Phys.*, **48**(7), pp. 359–363.
- [246] Eremeyev, V., Freidin, A., and Sharipova, L., 2007, "The Stability of the Equilibrium of Two-Phase Elastic Solids," *J. Appl. Math. Mech.*, **71**(1), pp. 61–84.
- [247] Rizzi, N., Varano, V., and Gabriele, S., 2013, "Initial Postbuckling Behavior of Thin-Walled Frames Under Mode Interaction," *Thin-Walled Struct.*, **68**, pp. 124–134.
- [248] Rizzi, N., and Varano, V., 2011, "On the Postbuckling Analysis of Thin-Walled Frames," 13th International Conference On Civil, Structural And Environmental Engineering Computing (CC2011), Chania, Crete, Greece, Sept. 6-9, Paper No. 43.
- [249] Rizzi, N., and Varano, V., 2011, "The Effects of Warping on the Postbuckling Behaviour of Thin-Walled Structures," *Thin-Walled Struct.*, **49**(9), pp. 1091–1097.
- [250] Pignataro, M., Ruta, G., Rizzi, N., and Varano, V., 2010, "Effects of Warping Constraints and Lateral Restraint on the Buckling of Thin-Walled Frames," *ASME Paper No. IMECE2009-12254*.
- [251] Pignataro, M., Rizzi, N., Ruta, G., and Varano, V., 2009, "The Effects of Warping Constraints on the Buckling of Thin-Walled Structures," *J. Mech. Mater. Struct.*, **4**(10), pp. 1711–1727.
- [252] Ruta, G., Varano, V., Pignataro, M., and Rizzi, N., 2008, "A Beam Model for the Flexural-Torsional Buckling of Thin-Walled Members With Some Applications," *Thin-Walled Struct.*, **46**(7–9), pp. 816–822.
- [253] Pignataro, M., Rizzi, N., and Luongo, A., 1991, *Stability, Bifurcation, and Postcritical Behaviour of Elastic Structures*, Elsevier, Amsterdam.
- [254] Luongo, A., 2001, "Mode Localization in Dynamics and Buckling of Linear Imperfect Continuous Structures," *Nonlinear Dyn.*, **25**(1–3), pp. 133–156.
- [255] Luongo, A., and Piccardo, G., 2005, "Linear Instability Mechanisms for Coupled Translational Galloping," *J. Sound Vib.*, **288**(4), pp. 1027–1047.
- [256] Luongo, A., and Zulli, D., 2012, "Dynamic Instability of Inclined Cables Under Combined Wind Flow and Support Motion," *Nonlinear Dyn.*, **67**(1), pp. 71–87.
- [257] Luongo, A., and Zulli, D., 2014, "Aeroelastic Instability Analysis of NES-Controlled Systems Via a Mixed Multiple Scale/Harmonic Balance Method," *J. Vib. Control*, **20**(13), pp. 1985–1998.
- [258] Luongo, A., 2010, "A Unified Perturbation Approach to Static/Dynamic Coupled Instabilities of Nonlinear Structures," *Thin-Walled Struct.*, **48**(10), pp. 744–751.
- [259] Di Egidio, A., Luongo, A., and Paolone, A., 2007, "Linear and Non-Linear Interactions Between Static and Dynamic Bifurcations of Damped Planar Beams," *Int. J. Nonlinear Mech.*, **42**(1), pp. 88–98.
- [260] Vestroni, F., Luongo, A., and Pasca, M., 1995, "Stability and Control of Transversal Oscillations of a Tethered Satellite System," *Appl. Math. Comput.*, **70**(2), pp. 343–360.
- [261] Knight, J., Page, T., and Chandler, H., 1991, "Thermal Instability of the Microstructure and Surface Mechanical Properties of Hydrogenated Amorphous Carbon Films," *Surf. Coat. Technol.*, **49**(1), pp. 519–529.
- [262] Ma, E., 2003, "Nanocrystalline Materials: Controlling Plastic Instability," *Nat. Mater.*, **2**(1), pp. 7–8.
- [263] Konkova, T., Mironov, S., Korznikov, A., and Semiatin, S., 2010, "Microstructure Instability in Cryogenically Deformed Copper," *Scr. Mater.*, **63**(9), pp. 921–924.
- [264] Zhu, H., Maruyama, K., Seo, D., and Au, P., 2006, "Effect of Initial Microstructure on Microstructural Instability and Creep Resistance of XD TiAl Alloys," *Metall. Mater. Trans. A*, **37**(10), pp. 3149–3159.
- [265] Lipson, H., and Kurman, M., 2013, *Fabricated: The New World of 3D Printing*, Wiley, Weinheim, Germany.
- [266] Hockaday, L., Kang, K., Colangelo, N., Cheung, P., Duan, B., Malone, E., Wu, J., Girardi, L., Bonassar, L., Lipson, H., Chu, C. C., and Butcher, J. T., 2012, "Rapid 3D Printing of Anatomically Accurate and Mechanically Heterogeneous Aortic Valve Hydrogel Scaffolds," *Biofabrication*, **4**(3), p. 035005.
- [267] Greiner, A., and Wendorff, J. H., 2007, "Electrospinning: A Fascinating Method for the Preparation of Ultrathin Fibers," *Angew. Chem. Int. Ed.*, **46**(30), pp. 5670–5703.
- [268] Sill, T. J., and von Recum, H. A., 2008, "Electrospinning: Applications in Drug Delivery and Tissue Engineering," *Biomaterials*, **29**(13), pp. 1989–2006.
- [269] Bhardwaj, N., and Kundu, S. C., 2010, "Electrospinning: A Fascinating Fiber Fabrication Technique," *Biotechnol. Adv.*, **28**(3), pp. 325–347.
- [270] Di Camillo, D., Fasano, V., Ruggieri, F., Santucci, S., Lozzi, L., Camoseo, A., and Pisignano, D., 2013, "Near-Field Electrospinning of Conjugated Polymer Light-Emitting Nanofibers," *Nanoscale*, **5**, pp. 11637–11642.
- [271] Di Camillo, D., Ruggieri, F., Santucci, S., and Lozzi, L., 2012, "N-Doped TiO₂ Nanofibers Deposited by Electrospinning," *J. Phys. Chem. C*, **116**(34), pp. 18427–18431.
- [272] Dell'Erba, R., dell'Isola, F., and Rotoli, G., 1999, "The Influence of the Curvature Dependence of the Surface Tension on the Geometry of Electrically Charged Menisci," *Continuum Mech. Thermodyn.*, **11**(2), pp. 89–105.
- [273] Agarwal, S., Wendorff, J. H., and Greiner, A., 2009, "Progress in the Field of Electrospinning for Tissue Engineering Applications," *Adv. Mater.*, **21**(32–33), pp. 3343–3351.
- [274] Beachley, V., Kasyanov, V., Nagy-Mehesz, A., Norris, R., Ozolanta, I., Kalejs, M., Stradins, P., Baptista, L., da Silva, K., Grainjero, J., Wen, X., and Mironov, V., 2014, "The Fusion of Tissue Spheroids Attached to Pre-Stretched Electrospun Polyurethane Scaffolds," *J. Tissue Eng.*, **5**, p. 2041731414556561.
- [275] Yasuda, H., and Yang, J., 2015, "Reentrant Origami-Based Metamaterials With Negative Poisson's Ratio and Bistability," *Phys. Rev. Lett.*, **114**(18), p. 185502.
- [276] Boutin, C., and Becot, F. X., 2015, "Theory and Experiments on Poro-Acoustics With Inner Resonators," *Wave Motion*, **54**, pp. 76–99.
- [277] Boutin, L. D. M. C., Schwan, "Depolarization of Mechanical Waves by Anisotropic Metasurface," *J. Appl. Phys.*, **117**(6), p. 064902.
- [278] Boutin, C., and Auriault, J., 1993, "Rayleigh Scattering in Elastic Composite Materials," *Int. J. Eng. Sci.*, **31**(12), pp. 1669–1689.
- [279] Boutin, C., Rallu, A., and Hans, S., 2012, "Large Scale Modulation of High Frequency Acoustic Waves in Periodic Porous Media," *J. Acoust. Soc. Am.*, **132**(6), pp. 3622–3636.
- [280] Boutin, C., Royer, P., and Auriault, J., 1998, "Acoustic Absorption of Porous Surfacing With Dual Porosity," *Int. J. Solids Struct.*, **35**(34), pp. 4709–4737.
- [281] Chesnais, C., Hans, S., and Boutin, C., 2007, "Wave Propagation and Diffraction in Discrete Structures: Effect of Anisotropy and Internal Resonance," *PAMM*, **7**(1), p. 1090.
- [282] Fokin, V., Ambati, M., Sun, C., and Zhang, X., 2007, "Method for Retrieving Effective Properties of Locally Resonant Acoustic Metamaterials," *Phys. Rev. B*, **76**(14), p. 144302.
- [283] Wang, P., Casadei, F., Shan, S., Weaver, J. C., and Bertoldi, K., 2014, "Harnessing Buckling to Design Tunable Locally Resonant Acoustic Metamaterials," *Phys. Rev. Lett.*, **113**(1), p. 014301.
- [284] Altenbach, H., Eremeyev, V. A., and Morozov, N. F., 2013, "Mechanical Properties of Materials Considering Surface Effects," IUTAM Symposium on Surface Effects in the Mechanics of Nanomaterials and Heterostructures, Beijing, Aug. 8–12, pp. 105–115.
- [285] Nesterenko, V., Daraio, C., Herbold, E., and Jin, S., 2005, "Anomalous Wave Reflection at the Interface of Two Strongly Nonlinear Granular Media," *Phys. Rev. Lett.*, **95**(15), p. 158702.

- [286] Eremeyev, V. A., 2015, "On Effective Properties of Materials at the Nano- and Microscales Considering Surface Effects," *Acta Mech.*, epub.
- [287] Cuenot, S., Frétyng, C., Demoustier-Champagne, S., and Nysten, B., 2004, "Surface Tension Effect on the Mechanical Properties of Nanomaterials Measured by Atomic Force Microscopy," *Phys. Rev. B*, **69**(16), p. 165410.
- [288] Chen, C., Shi, Y., Zhang, Y., Zhu, J., and Yan, Y., 2006, "Size Dependence of Young's Modulus in ZnO Nanowires," *Phys. Rev. Lett.*, **96**(7), p. 075505.
- [289] Liu, X., Luo, J., and Zhu, J., 2006, "Size Effect on the Crystal Structure of Silver Nanowires," *Nano Lett.*, **6**(3), pp. 408–412.
- [290] Jing, G. Y., Duan, H. L., Sun, X. M., Zhang, Z. S., Xu, J., Li, Y. D., Wang, J. X., and Yu, D. P., 2006, "Surface Effects on Elastic Properties of Silver Nanowires: Contact Atomic-Force Microscopy," *Phys. Rev. B*, **73**(23), p. 235409.
- [291] He, J., and Lilley, C. M., 2008, "Surface Effect on the Elastic Behavior of Static Bending Nanowires," *Nano Lett.*, **8**(7), pp. 1798–1802.
- [292] Greer, J. R., and De Hosson, J. T. M., 2011, "Plasticity in Small-Sized Metallic Systems: Intrinsic Versus Extrinsic Size Effect," *Prog. Mater. Sci.*, **56**(6), pp. 654–724.
- [293] Greer, J. R., and Nix, W. D., 2005, "Size Dependence of Mechanical Properties of Gold at the Sub-Micron Scale," *Appl. Phys. A*, **80**(8), pp. 1625–1629.
- [294] Özgür, Ü., Alivov, Y. I., Liu, C., Teke, A., Reshchikov, M., Doğan, S., Avrutin, V., Cho, S.-J., and Morkoc, H., 2005, "A Comprehensive Review of ZnO Materials and Devices," *J. Appl. Phys.*, **98**(4), p. 041301.
- [295] Bhushan, B., ed., 2007, *Handbook Springer of Nanotechnology*, Springer, Berlin.
- [296] Melechko, A. V., Merkulov, V. I., McKnight, T. E., Guillorn, M., Klein, K. L., Lowndes, D. H., and Simpson, M. L., 2005, "Vertically Aligned Carbon Nanofibers and Related Structures: Controlled Synthesis and Directed Assembly," *J. Appl. Phys.*, **97**(4), p. 041301.
- [297] Grimm, S., Giesa, R., Sklarek, K., Langner, A., Gosele, U., Schmidt, H.-W., and Steinhardt, M., 2008, "Nondestructive Replication of Self-Ordered Nanoporous Alumina Membranes Via Cross-Linked Polyacrylate Nanofiber Arrays," *Nano Lett.*, **8**(7), pp. 1954–1959.
- [298] Ma, X., Liu, A., Xu, H., Li, G., Hu, M., and Wu, G., 2008, "A Large-Scale-Oriented ZnO Rod Array Grown on a Glass Substrate Via an In Situ Deposition Method and Its Photoconductivity," *Mater. Res. Bull.*, **43**(8), pp. 2272–2277.
- [299] Tan, L. K., Kumar, M. K., An, W. W., and Gao, H., 2010, "Transparent, Well-Aligned TiO₂ Nanotube Arrays With Controllable Dimensions on Glass Substrates for Photocatalytic Applications," *ACS Appl. Mater. Interfaces*, **2**(2), pp. 498–503.
- [300] Hutchens, S. B., Needleman, A., and Greer, J. R., 2011, "Analysis of Uniaxial Compression of Vertically Aligned Carbon Nanotubes," *J. Mech. Phys. Solids*, **59**(10), pp. 2227–2237.
- [301] Spinelli, P., Verschuren, M., and Polman, A., 2012, "Broadband Omnidirectional Antireflection Coating Based on Subwavelength Surface Mie Resonators," *Nat. Commun.*, **3**, p. 692.
- [302] Naumenko, K., and Eremeyev, V. A., 2014, "A Layer-Wise Theory for Laminated Glass and Photovoltaic Panels," *Compos. Struct.*, **112**, pp. 283–291.
- [303] Kang, X., Zi, W.-W., Xu, Z.-G., and Zhang, H.-L., 2007, "Controlling the Micro/Nanostructure of Self-Cleaning Polymer Coating," *Appl. Surf. Sci.*, **253**(22), pp. 8830–8834.
- [304] Rios, P., Dodiuk, H., Kenig, S., McCarthy, S., and Dotan, A., 2007, "Transparent Ultra-Hydrophobic Surfaces," *J. Adhes. Sci. Technol.*, **21**(5–6), pp. 399–408.
- [305] Sanjay, S. L., Annaso, B. G., Chavan, S. M., and Rajiv, S. V., 2012, "Recent Progress in Preparation of Superhydrophobic Surfaces: A Review," *J. Surf. Eng. Mater. Adv. Technol.*, **2**(2), pp. 76–94.
- [306] Dastjerdi, R., and Montazer, M., 2010, "A Review on the Application of Inorganic Nano-Structured Materials in the Modification of Textiles: Focus on Anti-Microbial Properties," *Colloids Surf. B*, **79**(1), pp. 5–18.
- [307] Contreras, C. B., Chagas, G., Strumia, M. C., and Weibel, D. E., 2014, "Permanent Superhydrophobic Polypropylene Nanocomposite Coatings by a Simple One-Step Dipping Process," *Appl. Surf. Sci.*, **307**, pp. 234–240.
- [308] Tian, X., Yi, L., Meng, X., Xu, K., Jiang, T., and Lai, D., 2014, "Superhydrophobic Surfaces of Electrospun Block Copolymer Fibers With Low Content of Fluorosilicones," *Appl. Surf. Sci.*, **307**, pp. 566–575.
- [309] Heinonen, S., Huttunen-Saarivirta, E., Nikkanen, J.-P., Raulio, M., Priha, O., Laakso, J., Storgårds, E., and Levänen, E., 2014, "Antibacterial Properties and Chemical Stability of Superhydrophobic Silver-Containing Surface Produced by Sol-Gel Route," *Colloids Surf. A*, **453**, pp. 149–161.
- [310] Escobar, A. M., and Llorca-Isern, N., 2014, "Superhydrophobic Coating Deposited Directly on Aluminum," *Appl. Surf. Sci.*, **305**, pp. 774–782.
- [311] Li, J., Zheng, W., Zeng, W., Zhang, D., and Peng, X., 2014, "Structure, Properties and Application of a Novel Low-Glossed Waterborne Polyurethane," *Appl. Surf. Sci.*, **307**, pp. 255–262.
- [312] Ganesh, V. A., Raut, H. K., Nair, A. S., and Ramakrishna, S., 2011, "A Review on Self-Cleaning Coatings," *J. Mater. Chem.*, **21**(41), pp. 16304–16322.
- [313] Liu, K., and Jiang, L., 2012, "Bio-Inspired Self-Cleaning Surfaces," *Annu. Rev. Mater. Res.*, **42**, pp. 231–263.
- [314] Longley, W. R., and Name, R. G. V., eds., 1928, *The Collected Works of J. Willard Gibbs, PH.D., LL.D. I Thermodynamics*, Longmans, New York.
- [315] Rowlinson, J. S., and Widom, B., 2003, *Molecular Theory of Capillarity*, Dover, New York.
- [316] de Gennes, P. G., Brochard-Wyart, F., and Quéré, D., 2004, *Capillarity and Wetting Phenomena: Drops, Bubbles, Pearls, Waves*, Springer, New York.
- [317] Gurtin, M. E., and Murdoch, A. I., 1975, "A Continuum Theory of Elastic Material Surfaces," *Arch. Ration. Mech. Anal.*, **57**(4), pp. 291–323.
- [318] Gurtin, M. E., and Murdoch, A. I., 1975, "Addenda to Our Paper. A Continuum Theory of Elastic Material Surfaces," *Arch. Ration. Mech. Anal.*, **59**(4), pp. 389–390.
- [319] Duan, H. L., Wang, J., and Karihaloo, B. L., 2008, "Theory of Elasticity at the Nanoscale," *Adv. Appl. Mech.*, **42**, pp. 1–68.
- [320] Wang, J., Huang, Z., Duan, H., Yu, S., Feng, X., Wang, G., Zhang, W., and Wang, T., 2011, "Surface Stress Effect in Mechanics of Nanostructured Materials," *Acta Mech. Solida Sin.*, **24**(1), pp. 52–82.
- [321] Javili, A., McBride, A., and Steinmann, P., 2012, "Thermomechanics of Solids With Lower-Dimensional Energetics: On the Importance of Surface, Interface, and Curve Structures at the Nanoscale. A Unifying Review," *ASME Appl. Mech. Rev.*, **65**, p. 010802.
- [322] Wang, J., Duan, H. L., Huang, Z. P., and Karihaloo, B. L., 2006, "A Scaling Law for Properties of Nano-Structured Materials," *Proc. R. Soc. A*, **462**(2069), pp. 1355–1363.
- [323] Steigmann, D. J., and Ogden, R. W., 1999, "Elastic Surface-Substrate Interactions," *Proc. R. Soc. A*, **455**(1982), pp. 437–474.
- [324] Javili, A., and Steinmann, P., 2010, "On Thermomechanical Solids With Boundary Structures," *Int. J. Solids Struct.*, **47**(24), pp. 3245–3253.
- [325] Povstenko, Y., 2013, "Mathematical Modeling of Phenomena Caused by Surface Stresses in Solids," *Surface Effects in Solid Mechanics*, H. Altenbach and N. F. Morozov, eds., Springer, Berlin, pp. 135–153.
- [326] Rubin, M., and Benveniste, Y., 2004, "A Cosserat Shell Model for Interphases in Elastic Media," *J. Mech. Phys. Solids*, **52**(5), pp. 1023–1052.
- [327] Kim, C. I., Schiavone, P., and Ru, C.-Q., 2011, "Effect of Surface Elasticity on an Interface Crack in Plane Deformations," *Proc. R. Soc. A*, **467**(2136), pp. 3530–3549.
- [328] Kim, C., Ru, C., and Schiavone, P., 2013, "A Clarification of the Role of Crack-Tip Conditions in Linear Elasticity With Surface Effects," *Math. Mech. Solids*, **18**(1), pp. 59–66.
- [329] Schiavone, P., and Ru, C.-Q., 2009, "Solvability of Boundary Value Problems in a Theory of Plane-Strain Elasticity With Boundary Reinforcement," *Int. J. Eng. Sci.*, **47**(11), pp. 1331–1338.
- [330] Javili, A., McBride, A., Steinmann, P., and Reddy, B., 2012, "Relationships Between the Admissible Range of Surface Material Parameters and Stability of Linearly Elastic Bodies," *Philos. Mag.*, **92**(28–30), pp. 3540–3563.
- [331] Guo, J. G., and Zhao, Y. P., 2005, "The Size-Dependent Elastic Properties of Nanofilms With Surface Effects," *J. Appl. Phys.*, **98**(7), p. 074306.
- [332] Wang, Z. Q., Zhao, Y.-P., and Huang, Z.-P., 2010, "The Effects of Surface Tension on the Elastic Properties of Nano Structures," *Int. J. Eng. Sci.*, **48**(2), pp. 140–150.
- [333] Eremeyev, V. A., Altenbach, H., and Morozov, N. F., 2009, "The Influence of Surface Tension on the Effective Stiffness of Nanosize Plates," *Dokl. Phys.*, **54**(2), pp. 98–100.
- [334] Altenbach, H., Eremeyev, V. A., and Morozov, N. F., 2012, "Surface Viscoelasticity and Effective Properties of Thin-Walled Structures at the Nanoscale," *Int. J. Eng. Sci.*, **59**(S1), pp. 83–89.
- [335] Altenbach, H., and Eremeyev, V. A., 2011, "On the Shell Theory on the Nanoscale With Surface Stresses," *Int. J. Eng. Sci.*, **49**(12), pp. 1294–1301.
- [336] Lagowski, J., Gatos, H. C., and Sproles, E. S., 1975, "Surface Stress and Normal Mode of Vibration of Thin Crystals: GaAs," *Appl. Phys. Lett.*, **26**(9), pp. 493–495.
- [337] Gurtin, M. E., Markenscoff, X., and Thurston, R. N., 1976, "Effect of Surface Stress on Natural Frequency of Thin Crystals," *Appl. Phys. Lett.*, **29**(9), pp. 529–530.
- [338] Wang, G.-F., and Feng, X.-Q., 2007, "Effects of Surface Elasticity and Residual Surface Tension on the Natural Frequency of Microbeams," *Appl. Phys. Lett.*, **90**(23), p. 231904.
- [339] Kampshoff, E., Hahn, E., and Kern, K., 1994, "Correlation Between Surface Stress and the Vibrational Shift of CO Chemisorbed on Cu Surfaces," *Phys. Rev. Lett.*, **73**(5), pp. 704–707.
- [340] Wang, G. F., and Feng, X. Q., 2010, "Effect of Surface Stresses on the Vibration and Buckling of Piezoelectric Nanowires," *EPL*, **91**(5), p. 56007.
- [341] Huang, Z., and Wang, J., 2006, "A Theory of Hyperelasticity of Multi-Phase Media With Surface/Interface Energy Effect," *Acta Mech.*, **182**(3), pp. 195–210.
- [342] Huang, Z., and Sun, L., 2007, "Size-Dependent Effective Properties of a Heterogeneous Material With Interface Energy Effect: From Finite Deformation Theory to Infinitesimal Strain Analysis," *Acta Mech.*, **190**(1), pp. 151–163.
- [343] Zhu, H. X., Wang, J. X., and Karihaloo, B. L., 2009, "Effects of Surface and Initial Stresses on the Bending Stiffness of Trilayer Plates and Nanofilms," *J. Mech. Mater. Struct.*, **4**(3), pp. 589–604.
- [344] Huang, Z., and Wang, J., 2012, "Micromechanics of Nanocomposites With Interface Energy Effect," *Handbook on Micromechanics and Nanomechanics*, S. Li and X.-L. Gao, eds., Pan Stanford Publishing, Stanford, CA, pp. 303–348.
- [345] Javili, A., and Steinmann, P., 2009, "A Finite Element Framework for Continua With Boundary Energetics. Part I: The Two-Dimensional Case," *Comput. Methods Appl. Mech. Eng.*, **198**(27–29), pp. 2198–2208.
- [346] Javili, A., and Steinmann, P., 2011, "A Finite Element Framework for Continua With Boundary Energetics. Part III: The Thermomechanical Case," *Comput. Methods Appl. Mech. Eng.*, **200**(21), pp. 1963–1977.
- [347] Javili, A., McBride, A., and Steinmann, P., 2012, "Numerical Modelling of Thermomechanical Solids With Mechanically Energetic (Generalised) Kapitza Interfaces," *Comput. Mater. Sci.*, **65**, pp. 542–551.

- [348] Arroyo, M., and Belytschko, T., 2002, "An Atomistic-Based Finite Deformation Membrane for Single Layer Crystalline Films," *J. Mech. Phys. Solids*, **50**(9), pp. 1941–1977.
- [349] Sfyris, D., Sfyris, G., and Galiotis, C., 2014, "Curvature Dependent Surface Energy for a Free Standing Monolayer Graphene: Some Closed Form Solutions of the Non-Linear Theory," *Int. J. Nonlinear Mech.*, **67**, pp. 186–197.
- [350] Miller, R. E., and Shenoy, V. B., 2000, "Size-Dependent Elastic Properties of Nanosized Structural Elements," *Nanotechnology*, **11**(3), p. 139.
- [351] Shenoy, V. B., 2005, "Atomistic Calculations of Elastic Properties of Metallic FCC Crystal Surfaces," *Phys. Rev. B*, **71**(9), p. 094104.
- [352] Ibach, H., 1997, "The Role of Surface Stress in Reconstruction, Epitaxial Growth and Stabilization of Mesoscopic Structures," *Surf. Sci. Rep.*, **29**(5), pp. 195–263.
- [353] De Gennes, P. G., 1981, "Some Effects of Long Range Forces on Interfacial Phenomena," *J. Phys. Lett.*, **42**(16), pp. 377–379.
- [354] Sepecher, P., 1996, *Les Fluides de Cahn-Hilliard*, Mémoire D'habilitation à Diriger des Recherches, Université du Sud Toulon, La Garde, France.
- [355] dell'Isola, F., and Sepecher, P., 1997, "Edge Contact Forces and Quasi-Balanced Power," *Meccanica*, **32**(1), pp. 33–52.
- [356] dell'Isola, F., and Sepecher, P., 1995, "The Relationship Between Edge Contact Forces, Double Forces and Interstitial Working Allowed by the Principle of Virtual Power," *C. R. Acad. Sci. Sér. II*, **321**(8), pp. 303–308.
- [357] dell'Isola, F., Lekszycki, T., Pawlikowski, M., Grygoruk, R., and Greco, L., 2015, "Designing a Light Fabric Metamaterial Being Highly Macroscopically Tough Under Directional Extension: First Experimental Evidence," *Z. Angew. Math. Phys.*, **66**(6), pp. 3473–3498.
- [358] Giorgio, I., Grygoruk, R., dell'Isola, F., and Steigmann, D. J., 2015, "Pattern Formation in the Three-Dimensional Deformations of Fibered Sheets," *Mech. Res. Commun.*, **69**, pp. 164–171.
- [359] G. L. B. A. C. M. dell'Isola, F., "Second Gradient Shear Energies for Pantomorphic 2D Plates: Numerical Simulations Towards Explanation of Experimental Evidence," (in preparation).
- [360] Ball, J. M., 1976, "Convexity Conditions and Existence Theorems in Nonlinear Elasticity," *Arch. Ration. Mech. Anal.*, **63**(4), pp. 337–403.
- [361] Kim, D.-H., Lu, N., Ma, R., Kim, Y.-S., Kim, R.-H., Wang, S., Wu, J., Won, S. M., Tao, H., Islam, A., Yu, K. J., Kim, T.-i., Chowdhury, R., Ying, M., Xu, L., Li, M., Chung, H.-J., Keum, H., McCormick, M., Liu, P., Zhang, Y.-W., Omenetto, F. G., Huang, Y., Coleman, T., and Rogers, J. A., 2011, "Epidermal Electronics," *Science*, **333**(6044), pp. 838–843.
- [362] Arumugam, V., Naresh, M., and Sanjeevi, R., 1994, "Effect of Strain Rate on the Fracture Behaviour of Skin," *J. Biosci.*, **19**(3), pp. 307–313.
- [363] Elsner, P., Berardesca, E., and Wilhelm, K.-P., 2001, *Bioengineering of the Skin: Skin Biomechanics*, Vol. 5, Taylor & Francis, New York.
- [364] Geerlings, M., Van Breemen, L., Peters, G., Ackermans, P., Baaijens, F., and Oomens, C., 2011, "in vitro Indentation to Determine the Mechanical Properties of Epidermis," *J. Biomech.*, **44**(6), pp. 1176–1181.
- [365] Goriely, A., Destrade, M., and Amar, M. B., 2006, "Instabilities in Elastomers and in Soft Tissues," *Q. J. Mech. Appl. Math.*, **59**(4), pp. 615–630.
- [366] Lacour, S. P., Jones, J., Wagner, S., Li, T., and Suo, Z., 2005, "Stretchable Interconnects for Elastic Electronic Surfaces," *Proc. IEEE*, **93**(8), pp. 1459–1467.
- [367] Pailler-Mattei, C., Bec, S., and Zahouani, H., 2008, "in vivo Measurements of the Elastic Mechanical Properties of Human Skin by Indentation Tests," *Med. Eng. Phys.*, **30**(5), pp. 599–606.
- [368] Sekitani, T., Noguchi, Y., Hata, K., Fukushima, T., Aida, T., and Someya, T., 2008, "A Rubberlike Stretchable Active Matrix Using Elastic Conductors," *Science*, **321**(5895), pp. 1468–1472.
- [369] Rey, T., Le Cam, J.-B., Chagnon, G., Favier, D., Rebouah, M., Razan, F., Robin, E., Didier, P., Heller, L., Faure, S., and Janouchova, K., 2014, "An Original Architected NiTi Silicone Rubber Structure for Biomedical Applications," *Mater. Sci. Eng. C*, **45**, pp. 184–190.
- [370] Galilei, G., 1894, *Opere: Edizione Nazionale sotto gli Auspicii di Sua Maestà il re d'Italia*, Vol. 6, Barbèra, Florence, Italy.
- [371] Drake, S., 1957, *Discoveries and Opinions of Galileo*, Doubleday, New York.
- [372] Cannone, M., and Friedlander, S., 2003, "Navier: Blow-Up and Collapse," *Not. AMS*, **50**(1), pp. 7–13.
- [373] Picon, A., 1988, "Navier and the Introduction of Suspension Bridges in France," *Construction History*, **4**, pp. 21–34.

Chapter 1

Second-gradient continua as homogenized limit of
pantographic microstructured plates: a rigorous
proof



Second-gradient continua as homogenized limit of pantographic microstructured plates: a rigorous proof

Jean-Jacques Alibert and Alessandro Della Corte

Abstract. Since the works by Gabrio Piola, it has been debated the relevance of higher-gradient continuum models in mechanics. Some authors even questioned the logical consistency of higher-gradient theories, and the applicability of generalized continuum theories seems still open. The present paper considers a pantographic plate constituted by Euler beams suitably interconnected and proves that Piola’s heuristic homogenization method does produce an approximating continuum in which deformation energy depends only on second gradients of displacements. The Γ -convergence argument presented herein shows indeed that Piola’s conjecture can be rigorously proven in a Banach space whose norm is physically dictated by energetic considerations.

Mathematics Subject Classification. 74Q05 · 28A33 · 35B27.

Keywords. Continuum mechanics, Second-gradient continua, Homogenization, Γ -convergence, Pantographic structures, Elasticity, Microstructure.

1. Introduction

In the present work, we want to provide a rigorous proof for a theoretical problem which clearly links two (practically) relevant topics in today’s mechanics: n -th gradient theory and homogenization procedures from discrete to continuous models. The link between the two subjects can be briefly described as follows.

In the classical works by Mindlin, Toupin and Germain (see, e.g., [1–5]), n -th gradient theory has been definitely proven to be a logically consistent formal framework, and since then, it has been intensively employed in studying (among other things) the behavior of elastic microstructured materials (for interesting applications of this kind, the reader can see, e.g., [6–14]; for a general theoretical framework in which is discussed the link between n -th gradient models and the variational formulation, see [15]). It has been already shown, in particular, that boundary conditions for second- and higher-gradient materials are not those usually considered. These novel conditions describe ‘real’ mechanical actions which, in the continuum mechanics framework, cannot be interpreted either as density of forces or torques. Discrete systems with suitable continuous limit can give a natural microscopic interpretation for these new (at least in a higher sense, as they were first described in the works of Gabrio Piola, see [16]) contact actions.

Discrete systems, in turn, can entail very rich behaviors. In many cases, it is possible to ‘outline’ a continuous limit for a given discrete model by simply substituting, in a suitable way, finite differences with differential operators, but obtaining explicitly and rigorously the continuous limit from a given discrete elastic model is at the moment, in general, a challenge. This challenge can be guided by what has been recognized (in [17]) to be a major contribution by Gabrio Piola to mechanical science. Indeed, Piola, in building homogenized models of discrete microstructures (or microsystems), conjectured the existence of regular fields whose value in a given set of lagrangian nodes supplies the finite set of lagrangian parameters needed to characterize the kinematics of the microsystem. This conjecture cannot be proven (yet) in a general setting. However, in particular cases, once the microstructure has been chosen and the continuous

limit has been conjectured (à la Piola), one can try to rigorously prove the convergence of the discrete model to the continuum one.

Linear and nonlinear elasticity nontrivial problems, even when involving a very rich bifurcation scenario, can be studied by means of direct methods which consider integro-differential equations without employing any a priori discretization (as done, e.g., in [18]). However, when dealing with problems of the type above described, it is natural to try to exploit the intrinsic multiscale nature of the problem identifying a suitable convergence method of the discrete model to a continuum one. One of the main theoretical tools employed for this purpose is of course Γ -convergence (for a general introduction, the reader can refer to, e.g., [19], and for methods similar to those employed in the present paper [20]). The aim of the present paper is indeed to provide a rigorous proof of the convergence of the considered discrete model, suitable for the description of a pantographic microstructured plates, to a continuous model, establishing the Γ -convergence of a sequence of discrete measure energy functionals to a continuous limit; thus, inserting what in our opinion is a little but crucial piece in a more general puzzle.

Hopefully, thus, providing an example of a generalized continuum (purely second gradient) which is rigorously proven to be the homogenized limit of a simple elastic discrete model may influence the status itself of higher-order continua, which in today's mechanics is still controversial.

The paper is organized as follows. In Sect. 2, the basic definitions employed are given. In Sects. 3 and 4, the continuous and discrete models (respectively) are described. In Sect. 5, the convergence of the discrete model to the continuous one is proven; the proof is divided in three subsections accounting for (respectively) equicoercivity, upper-bound inequality and lower-bound inequality; this last subsection is further divided in three steps, and some further definitions and Lemmas employed in this subsection are provided in the following Sect. 6. Finally, some conclusions are drawn in Sect. 7.

2. Γ -convergence of measure functionals

Let K be a compact set in \mathbb{R}^d , $C(K)$ the space of continuous functions provided with the uniform norm $\|\varphi\|_{C(K)} := \sup\{|\varphi(x)| : x \in K\}$, and $M(K)$ the set of bounded Borel measures on K provided with the norm

$$\int_K |\mu| = \|\mu\|_{M(K)} := \sup \{ \langle \mu, \varphi \rangle : \varphi \in C(K), \|\varphi\|_{C(K)} \leq 1 \}.$$

For every integer n , let (F_n) and F be functionals on $M(K)$ with values in $\mathbb{R} \cup \{+\infty\}$. We say that the sequence F_n Γ -converges to F if the following three properties are satisfied.

(i) *Equicoercivity*

There are an integer N and a function $f : [0, +\infty] \rightarrow \mathbb{R}$ such that $\lim_{t \rightarrow +\infty} f(t) = +\infty$ and

$$F_n(\mu) \geq f(\|\mu\|_{M(K)})$$

$\forall n \geq N, \forall \mu \in M(K)$.

(ii) *Upper-bound inequality*

$\forall \mu \in M(K)$, there is a sequence (μ_n) in $M(K)$, converging to μ in the weak topology of the dual, for which

$$\limsup_n F_n(\mu) \leq F(\mu).$$

(iii) *Lower-bound inequality*

$\forall \mu \in M(K)$, $\forall (\mu_n)$ in $M(K)$, converging to μ in the weak topology of the dual,

$$\liminf_n F_n(\mu) \geq F(\mu).$$

3. Continuous model

Let us put $\Omega :=]0, 1[\times]0, 1[$ and $K := [0, 1] \times [0, 1]$. Let $M^2(K) \subset M(K)$ be the set of absolutely continuous measures, with respect to Lebesgue measure, whose density with respect to Lebesgue measure is an element of the usual Sobolev space $H^2(\Omega)$. Every $\mu \in M^2(K)$ can be written in a unique way as $\mu = u dx$, with $u \in H^2(\Omega)$. Let us define the functional E on $M(K)$ by:

$$E(\mu) := \begin{cases} \sum_{m=1}^2 \int_{\Omega} (\partial_m^2 u)^2 dx & \text{if } \mu = u dx \in M^2(K) \\ +\infty & \text{otherwise} \end{cases}$$

Let a, b be two real numbers such that $0 \leq a < b \leq 1$, and $M^{2,\Sigma}(K)$ the subset of $\mu = u dx \in M^2(K)$ such that

$$u = \partial_1 u = 0 \quad \text{in } \Sigma := \{0\} \times [a, b]$$

Let us define the functional E^Σ on $M(K)$ by:

$$E^\Sigma(\mu) := \begin{cases} 0 & \text{if } \mu = u dx \in M^{2,\Sigma}(K) \\ +\infty & \text{otherwise} \end{cases}$$

4. Discrete model

$\forall x \in \mathbb{R}^2$, let δ_x be the Dirac measure concentrated at x , and ν_n the measure on \mathbb{R}^2 defined by

$$\nu_n := \sum_{i,j} \delta_{(\frac{i}{n}, \frac{j}{n})}$$

where the sum is extended to every $(i, j) \in \mathbb{Z}^2$. Let us put $e_1 := (1, 0)$ and $e_2 = (0, 1)$. For $m \in \{1, 2\}$ and for every function u , we put

$$\begin{aligned} \partial_{n,m}^+ u(x) &:= n \left(u \left(x + \frac{1}{n} e_m \right) - u(x) \right), \\ \partial_{n,m}^- u(x) &:= n \left(u(x) - u \left(x - \frac{1}{n} e_m \right) \right). \end{aligned}$$

The four operators defined above commute. Composing them, we obtain a list of second-order operators. From this list, we will select the two operators $\partial_{n,m}^2 := \partial_{n,m}^- \partial_{n,m}^+$, *i.e.*:

$$\partial_{n,m}^2 u(x) = n^2 \left(u \left(x + \frac{1}{n} e_m \right) - 2u(x) + u \left(x - \frac{1}{n} e_m \right) \right).$$

The operator $\partial_{n,m}^2$ transforms a function defined ν_n -almost everywhere in K in a function defined ν_n -almost everywhere in $K_{n,m}$, with

$$K_{n,1} := \left[\frac{1}{n}, \frac{n-1}{n} \right] \times [0, 1] \quad \text{and} \quad K_{n,2} := [0, 1] \times \left[\frac{1}{n}, \frac{n-1}{n} \right].$$

Let $M_n(K)$ be the subset of $M(K)$ of absolutely continuous measures with respect to ν_n . Every $\mu \in M_n(K)$ can be written in a unique way as $\mu = u(\nu_n/n^2)$, where u is a function defined ν_n -almost everywhere in K . We define the functionals E_n on $M(K)$ by:

$$E_n(\mu) := \begin{cases} \sum_{m=1}^2 \int_{K_{n,m}} (\partial_{n,m}^2 u)^2 \frac{d\nu_n}{n^2} & \text{if } \mu = u(\nu_n/n^2) \in M_n(K) \\ +\infty & \text{otherwise} \end{cases}$$

We observe that if $u(\nu_n/n^2) \in M_n(K)$, then

$$\int_{K_{n,1}} (\partial_{n,1}^2 u)^2 \frac{d\nu_n}{n^2} = n^2 \sum_{i=1}^{n-1} \sum_{j=0}^n \left(u\left(\frac{i+1}{n}, \frac{j}{n}\right) - 2u\left(\frac{i}{n}, \frac{j}{n}\right) + u\left(\frac{i-1}{n}, \frac{j}{n}\right) \right)^2.$$

$$\int_{K_{n,2}} (\partial_{n,2}^2 u)^2 \frac{d\nu_n}{n^2} = n^2 \sum_{i=0}^n \sum_{j=1}^{n-1} \left(u\left(\frac{i}{n}, \frac{j+1}{n}\right) - 2u\left(\frac{i}{n}, \frac{j}{n}\right) + u\left(\frac{i}{n}, \frac{j-1}{n}\right) \right)^2.$$

Let $M_n^\Sigma(K)$ be the subset of $u(\nu_n/n^2) \in M_n(K)$ such that

$$u = \partial_{n,1}^+ u = 0 \quad \nu_n - \text{almost everywhere in } \Sigma$$

Let us define the functional E_n^Σ on $M(K)$ by:

$$E_n^\Sigma(\mu) := \begin{cases} 0 & \text{if } \mu = u(\nu_n/n^2) \in M_n^\Sigma(K) \\ +\infty & \text{otherwise} \end{cases}$$

The two models presented above represent the natural mathematical formulation of a pantographic structure in which two families of equally spaced flexural Euler beams, with standard energy density, are interconnected by ideal hinges; the stiffness parameters are assumed to be equal to 1.

The considered structure has been chosen to play, for its simplicity, the role of a model case. It can be of course generalized in various ways, including the introduction of multi-physics properties (some references that can suggest some interesting possibilities are [21–25]), and more complicated beam models (see below the Sect. 7).

It should be noted that the physical system that we wanted to model is a mixed continuous–discrete one (since it is constituted by continuous one-dimensional beams with discrete pivots). For our mathematical formulation, we chose to discretize the expression of the energy of every beam, by means of an integration with respect to a measure which is concentrated on points, thus obtaining a purely discrete model.

5. Convergence of the discrete model to the continuous one

Our main result is the following:

Theorem 1. *The sequence of functionals $(E_n + E_n^\Sigma)$ Γ -converges to the functional $E + E^\Sigma$ in $M(K)$.*

The proof is divided into three parts.

5.1. Proof of equicoercivity

Lemma 1. *There are an integer N and a function $f : [0, +\infty] \rightarrow \mathbb{R}$ such that $\lim_{t \rightarrow +\infty} f(t) = +\infty$ and that*

$$E_n(\mu) + E_n^\Sigma(\mu) \geq f(\|\mu\|_{M(K)})$$

$\forall n \geq N, \forall \mu \in M(K)$.

Proof. Since the functional E_n^Σ has value $+\infty$ in the complement of $M_n^\Sigma(K)$, it is sufficient to prove the inequality for $\mu \in M_n^\Sigma(K)$.

Let us put $\mu := u(\nu_n/n^2) \in M_n^\Sigma(K)$. For every real number t , we define $(t)^+ := \max\{0, t\}$. Direct calculation shows that for every function v defined ν_n -almost everywhere in K the following equality holds:

$$v\left(\frac{i}{n}, \frac{j}{n}\right) = v\left(\frac{0}{n}, \frac{j}{n}\right) + \frac{i}{n} \partial_{n,1}^+ v\left(\frac{0}{n}, \frac{j}{n}\right) + \frac{1}{n} \sum_{k=1}^{n-1} \left(\frac{i-k}{n}\right)^+ \partial_{n,1}^2 v\left(\frac{k}{n}, \frac{j}{n}\right) \tag{1}$$

Summing over all pairs (i, j) such that $0 \leq i \leq n$ and $na \leq j \leq nb$ and using the Cauchy–Schwarz inequality, we get

$$\int_{[0,1] \times [a,b]} (u(x))^2 \frac{\nu_n(dx)}{n^2} \leq \int_{K_{n,1}} (\partial_{n,1}^2 u(x))^2 \frac{\nu_n(dx)}{n^2}. \tag{2}$$

Let us choose a function $\varphi \in C^\infty(\mathbb{R})$ whose support is contained in $[a, b]$ and satisfying $\varphi > 0$ in $]a, b[$. For every n such that $n(b - a) > 2$, we put

$$\varphi_n(t) := \frac{\varphi(t)}{\frac{1}{n} \sum_{k=0}^n \varphi\left(\frac{k}{n}\right)} \quad \text{and} \quad C_n := \max_{t \in [a,b]} \varphi_n(t) + \max_{t \in [a,b]} |\varphi'_n(t)|.$$

Finally, we put $v := \partial_{n,2}^+ u$ (which implies $\partial_{n,2}^- v = \partial_{n,2}^2 u$). Using the Jensen inequality, we thus get

$$\begin{aligned} \left(u\left(\frac{i}{n}, \frac{j}{n}\right)\right)^2 &\leq 2 \left(\frac{1}{n} \sum_{k=0}^n u\left(\frac{i}{n}, \frac{k}{n}\right) \varphi_n\left(\frac{k}{n}\right)\right)^2 + \frac{2}{n} \sum_{k=0}^n \left(u\left(\frac{i}{n}, \frac{j}{n}\right) - u\left(\frac{i}{n}, \frac{k}{n}\right)\right)^2 \varphi_n\left(\frac{k}{n}\right) \\ &\leq 2 \left(\frac{1}{n} \sum_{k=0}^n u\left(\frac{i}{n}, \frac{k}{n}\right) \varphi_n\left(\frac{k}{n}\right)\right)^2 + \frac{2}{n} \sum_{\ell=0}^{n-1} \left(\partial_{n,2}^+ u\left(\frac{i}{n}, \frac{\ell}{n}\right)\right)^2 \\ &= 2 \left(\frac{1}{n} \sum_{k=0}^n u\left(\frac{i}{n}, \frac{k}{n}\right) \varphi_n\left(\frac{k}{n}\right)\right)^2 + \frac{2}{n} \sum_{\ell=0}^{n-1} \left(v\left(\frac{i}{n}, \frac{\ell}{n}\right)\right)^2 \\ &\leq \frac{2C_n}{n} \sum_{k=0}^n \left(u\left(\frac{i}{n}, \frac{k}{n}\right)\right)^2 1_{[a,b]}\left(\frac{k}{n}\right) + \frac{2}{n} \sum_{\ell=0}^{n-1} \left(v\left(\frac{i}{n}, \frac{\ell}{n}\right)\right)^2 \end{aligned}$$

and

$$\begin{aligned} \left(v\left(\frac{i}{n}, \frac{\ell}{n}\right)\right)^2 &\leq 2 \left(\frac{1}{n} \sum_{k=0}^{n-1} v\left(\frac{i}{n}, \frac{k}{n}\right) \varphi_n\left(\frac{k}{n}\right)\right)^2 + \frac{2}{n} \sum_{k=0}^{n-1} \left(v\left(\frac{i}{n}, \frac{\ell}{n}\right) - v\left(\frac{i}{n}, \frac{k}{n}\right)\right)^2 \varphi_n\left(\frac{k}{n}\right) \\ &\leq 2 \left(\frac{1}{n} \sum_{k=0}^{n-1} v\left(\frac{i}{n}, \frac{k}{n}\right) \varphi_n\left(\frac{k}{n}\right)\right)^2 + \frac{2}{n} \sum_{k=1}^{n-1} \left(\partial_{n,2}^- v\left(\frac{i}{n}, \frac{k}{n}\right)\right)^2 \\ &= 2 \left(\sum_{k=1}^n u\left(\frac{i}{n}, \frac{k}{n}\right) (\varphi_n\left(\frac{k}{n}\right) - \varphi_n\left(\frac{k-1}{n}\right))\right)^2 + \frac{2}{n} \sum_{k=1}^{n-1} \left(\partial_{n,2}^2 u\left(\frac{i}{n}, \frac{k}{n}\right)\right)^2 \\ &\leq \frac{2C_n^2}{n} \sum_{k=1}^n \left(u\left(\frac{i}{n}, \frac{k}{n}\right)\right)^2 1_{[a,b]}\left(\frac{k}{n}\right) + \frac{2}{n} \sum_{k=1}^{n-1} \left(\partial_{n,2}^2 u\left(\frac{i}{n}, \frac{k}{n}\right)\right)^2 \end{aligned}$$

the previous equality resulting from a discrete integration by parts.

Finally, we have

$$\left(u\left(\frac{i}{n}, \frac{j}{n}\right)\right)^2 \leq \frac{2C_n + 4C_n^2}{n} \sum_{k=0}^n \left(u\left(\frac{i}{n}, \frac{k}{n}\right)\right)^2 1_{[a,b]}\left(\frac{k}{n}\right) + \frac{4}{n} \sum_{k=1}^{n-1} \left(\partial_{n,2}^2 u\left(\frac{i}{n}, \frac{k}{n}\right)\right)^2.$$

Summing on $(i, j) \in \{0, 1, \dots, n\} \times \{0, 1, \dots, n\}$ and using (2), we get

$$\int_K (u(x))^2 \frac{\nu_n(dx)}{n^2} \leq (4C_n + 8C_n^2) \int_{K_{n,1}} (\partial_{n,1}^2 u(x))^2 \frac{\nu_n(dx)}{n^2} + 8 \int_{K_{n,2}} (\partial_{n,2}^2 u(x))^2 \frac{\nu_n(dx)}{n^2}.$$

Since

$$\lim_n C_n = \frac{\max_{t \in [a,b]} \varphi(t) + \max_{t \in [a,b]} |\varphi'(t)|}{\int_a^b \varphi(t) dt} > 0$$

there is an integer N and a real number $C > 0$ such that for all $n \geq N$ and all $\mu = u(\nu_n/n^2) \in M_n^\Sigma(K)$,

$$E_n(\mu) \geq C \int_K (u(x))^2 \frac{\nu_n(dx)}{n^2} \tag{3}$$

Using the Cauchy–Schwarz inequality, we can say that for all $n \geq N$ and all $\mu \in M(K)$,

$$E_n(\mu) + E_n^\Sigma(\mu) \geq C \left(\frac{N}{N+1} \right)^2 \|\mu\|_{M(K)}^2 \tag{4}$$

□

5.2. Proof of the upper-bound inequality

Lemma 2. *Let us consider $\mu \in M(K)$. Exists a sequence (μ_n) which converges to μ in $M(K)$ equipped with its weak topology $*$ and which satisfies*

$$E(\mu) + E^\Sigma(\mu) \geq \limsup_n (E_n(\mu_n) + E_n^\Sigma(\mu_n)).$$

Proof. Since the functional E^Σ has value $+\infty$ in the complement of $M^{2,\Sigma}(K)$, it is sufficient to prove the inequality for $\mu = udx \in M^{2,\Sigma}(K)$. The function u can be extended by a function of class $H_0^2(\mathbb{R}^2 \setminus \Sigma)$ which can be approximated by a sequence of functions of class $C_c^\infty(\mathbb{R}^2 \setminus \Sigma)$ with respect to the usual $H^2(\mathbb{R}^2)$ norm. Therefore, it is sufficient to prove the upper-bound inequality for $\mu = udx$ with $u \in C_c^\infty(\mathbb{R}^2 \setminus \Sigma)$.

Let us put $\mu = udx$ with $u \in C_c^\infty(\mathbb{R}^2 \setminus \Sigma)$ and $\mu_n := u(\nu_n/n^2)$. Firstly, for all $\varphi \in C(K)$,

$$\langle \mu, \varphi \rangle = \int_\Omega \varphi(x)u(x)dx = \lim_n \int_\Omega \varphi(x)u(x) \frac{\nu_n(dx)}{n^2} = \lim_n \langle \mu_n, \varphi \rangle$$

and on the other hand, $\mu_n \in M_n^\Sigma(K)$ for sufficiently large values of n , so

$$\begin{aligned} \limsup_n (E_n(\mu_n) + E_n^\Sigma(\mu_n)) &= \limsup_n \sum_{m=1}^2 \int_{K_{n,m}} (\partial_{n,m}^2 u(x))^2 \frac{\nu_n(dx)}{n^2} \\ &= \limsup_n \sum_{m=1}^2 \int_{K_{n,m}} (\partial_m^2 u(x))^2 \frac{\nu_n(dx)}{n^2} \\ &= \sum_{m=1}^2 \int_\Omega (\partial_m^2 u)^2 dx \\ &= E(\mu) + E^\Sigma(\mu). \end{aligned}$$

□

5.3. Proof of the lower-bound inequality

Lemma 3. *Let us consider $\mu \in M(K)$. Every sequence (μ_n) which converges to μ in $M(K)$ equipped with its weak topology $*$ verifies*

$$E(\mu) + E^\Sigma(\mu) \leq \liminf_n (E_n(\mu_n) + E_n^\Sigma(\mu_n)).$$

The proof of this Lemma is more delicate than the previous ones. The definition of the operators $T_{n,m}$, $I_{n,m}^2$ and $I_{n,m}^{2,*}$ as well as the lemmas used in the following proof can be found in Sect. 6.

Proof. Let us consider $\mu \in M(K)$ and a sequence (μ_n) which converges to μ in $M(K)$ equipped with its weak topology $*$. Without losing generality, one can assume

$$M := \sup_n (E_n(\mu_n) + E_n^\Sigma(\mu_n)) < +\infty \tag{5}$$

which implies $\mu_n = u_n(\nu_n/n^2) \in M_n^\Sigma(K)$ for all n .

STEP 1: μ does not charge the boundary of Ω .

Let be $\varepsilon \in]0, 1/2[$ and $\partial_\varepsilon\Omega$ the set of points of K whose distance from $\partial\Omega$ is strictly less than ε . Then, using the inclusion $\partial\Omega \subset \partial_\varepsilon\Omega$ and the weak lower semicontinuity of the total variation on $\partial_\varepsilon\Omega$, the Cauchy–Schwarz inequality and the inequalities (3) and (5) lead to

$$\begin{aligned} \left(\int_{\partial\Omega} |\mu| \right)^2 &\leq \liminf_n \left(\int_{\partial_\varepsilon\Omega} |\mu_n| \right)^2 \\ &= \liminf_n \left(\int_{\partial_\varepsilon\Omega} |u_n(x)| \frac{\nu_n(dx)}{n^2} \right)^2 \\ &\leq \liminf_n \frac{\nu_n(\partial_\varepsilon\Omega)}{n^2} \int_K (u_n(x))^2 \frac{\nu_n(dx)}{n^2} \\ &\leq (4\varepsilon - 4\varepsilon^2) \liminf_n \int_K (u_n(x))^2 \frac{\nu_n(dx)}{n^2} \\ &\leq (4\varepsilon - 4\varepsilon^2) \liminf_n \frac{E_n(\mu_n)}{C} \\ &\leq \frac{4M}{C} \varepsilon. \end{aligned}$$

STEP 2: $\mu \in M^2(K)$ and $E(\mu) \leq \liminf_n (E_n(\mu_n) + E_n^\Sigma(\mu_n))$.

Let be $\varphi \in C_c^\infty(\Omega)$. Using the Lemma 4 of the following paragraph and the Cauchy–Schwarz inequality, one gets

$$\begin{aligned} \langle \mu, \partial_m^2 \varphi \rangle^2 &= \lim_n \langle \mu_n, \partial_m^2 \varphi \rangle^2 \\ &= \lim_n \left(\int_K (\partial_m^2 \varphi)(u_n) \frac{d\nu_n}{n^2} \right)^2 \\ &= \lim_n \left(\int_K (\partial_m^2 \varphi)(T_{n,m}u_n + I_{n,m}^2 \partial_{n,m}^2 u_n) \frac{d\nu_n}{n^2} \right)^2 \\ &= \lim_n \left(\int_K (\partial_m^2 \varphi)(I_{n,m}^2 \partial_{n,m}^2 u_n) \frac{d\nu_n}{n^2} \right)^2 \end{aligned}$$

$$\begin{aligned}
 &= \lim_n \left(\int_{K_{n,m}} (I_{n,m}^{2,*} \partial_m^2 \varphi) (\partial_{n,m}^2 u_n) \frac{d\nu_n}{n^2} \right)^2 \\
 &\leq \liminf_n \left(\left(\int_{K_{n,m}} (\partial_{n,m}^2 u_n)^2 \frac{d\nu_n}{n^2} \right) \left(\int_{K_{n,m}} (I_{n,m}^{2,*} \partial_m^2 \varphi)^2 \frac{d\nu_n}{n^2} \right) \right) \\
 &\leq \left(\liminf_n \int_{K_{n,m}} (\partial_{n,m}^2 u_n)^2 \frac{d\nu_n}{n^2} \right) \int_{\Omega} (\varphi(x))^2 dx.
 \end{aligned}$$

Taking into account the Step 1, the Lemma 5 of the following paragraph implies that $\mu \in M^2(K)$ and $E(\mu) \leq \liminf_n (E_n(\mu_n) + E_n^\Sigma(\mu_n))$.

STEP 3: μ satisfies the Dirichlet condition $E^\Sigma(\mu) = 0$.

Let be $\varphi \in C_c^\infty(]0, 1[\times]a, b[)$. Using the Cauchy–Schwarz inequality and the Lemma 6 from the following paragraph, one gets

$$\begin{aligned}
 \left(\int_{]0,1[\times]a,b[} \frac{u(x)}{x_1} \varphi(x) dx \right)^2 &= \lim_n \left(\int_{]0,1[\times]a,b[} \frac{u_n(x)}{x_1} \varphi(x) \frac{\nu_n(dx)}{n^2} \right)^2 \\
 &\leq \liminf_n \left(\int_{]0,1[\times]a,b[} \left(\frac{u_n(x)}{x_1} \right)^2 \frac{\nu_n(dx)}{n^2} \right) \left(\int_{]0,1[\times]a,b[} (\varphi(x))^2 \frac{\nu_n(dx)}{n^2} \right) \\
 &\leq 4^4 M \int_{]0,1[\times]a,b[} (\varphi(x))^2 dx.
 \end{aligned}$$

where by x_1 we indicate the first component of the vector x . This implies that the function $x \mapsto \frac{u(x)}{x_1}$ is of class $L^2(]0, 1[\times]a, b[)$, and thus, the function u vanishes (in the sense of traces) over $\Sigma := \{0\} \times [a, b]$. Defining $\psi(x) = \varphi(x)/x_1$, we have

$$\begin{aligned}
 \left(\int_{]0,1[\times]a,b[} \frac{\partial_1 u(x)}{x_1} \varphi(x) dx \right)^2 &= \left(\int_{]0,1[\times]a,b[} u(x) \partial_1 \psi(x) dx \right)^2 \\
 &= \lim_n \left(\int_{]0,1[\times]a,b[} u_n(x) \partial_1 \psi(x) \frac{\nu_n(dx)}{n^2} \right)^2 \\
 &= \lim_n \left(\int_{]0,1[\times]a,b[} u_n(x) \partial_{n,1}^- \psi(x) \frac{\nu_n(dx)}{n^2} \right)^2 \\
 &= \lim_n \left(\int_{]0,1[\times]a,b[} \partial_{n,1}^+ u_n(x) \psi(x) \frac{\nu_n(dx)}{n^2} \right)^2
 \end{aligned}$$

$$\begin{aligned}
 &= \lim_n \left(\int_{]0,1[\times]a,b[} \frac{\partial_{n,1}^+ u_n(x)}{x_1} \varphi(x) \frac{\nu_n(dx)}{n^2} \right)^2 \\
 &\leq \liminf_n \left(\int_{]0,1[\times]a,b[} \left(\frac{\partial_{n,1}^+ u_n(x)}{x_1} \right)^2 \frac{\nu_n(dx)}{n^2} \right) \left(\int_{]0,1[\times]a,b[} (\varphi(x))^2 \frac{\nu_n(dx)}{n^2} \right) \\
 &\leq 4^2 M \int_{]0,1[\times]a,b[} (\varphi(x))^2 dx
 \end{aligned}$$

This implies that the function $x \mapsto \frac{\partial_1 u(x)}{x_1}$ is of class $L^2(]0,1[\times]a,b[)$, and thus, the function $\partial_1 u$ vanishes (in the sense of traces) over $\Sigma := \{0\} \times [a, b]$. So in conclusion, $E^\Sigma(\mu) = 0$. \square

6. Definitions and lemmas used in Section 5.3

Definition 1. Given a function u defined ν_n -almost everywhere in K , let us define the two functions $T_{n,1}u$ and $T_{n,2}u$ ν_n -almost everywhere in K by:

$$\begin{aligned}
 T_{n,1}u\left(\frac{i}{n}, \frac{j}{n}\right) &:= u\left(\frac{0}{n}, \frac{j}{n}\right) + \frac{i}{n} \partial_{n,1}^+ u\left(\frac{0}{n}, \frac{j}{n}\right), \\
 T_{n,2}u\left(\frac{i}{n}, \frac{j}{n}\right) &:= u\left(\frac{i}{n}, \frac{0}{n}\right) + \frac{j}{n} \partial_{n,2}^+ u\left(\frac{i}{n}, \frac{0}{n}\right).
 \end{aligned}$$

Definition 2. Given two functions v_1 and v_2 defined ν_n -almost everywhere, respectively, in $K_{n,1}$ and $K_{n,2}$, let us define the two functions $I_{n,1}^2 v_1$ and $I_{n,2}^2 v_2$ ν_n -almost everywhere in K by:

$$\begin{aligned}
 I_{n,1}^2 v_1\left(\frac{i}{n}, \frac{j}{n}\right) &:= \frac{1}{n} \sum_{k=1}^{n-1} \left(\frac{i}{n} - \frac{k}{n}\right)^+ v_1\left(\frac{k}{n}, \frac{j}{n}\right), \\
 I_{n,2}^2 v_2\left(\frac{i}{n}, \frac{j}{n}\right) &:= \frac{1}{n} \sum_{\ell=1}^{n-1} \left(\frac{j}{n} - \frac{\ell}{n}\right)^+ v_2\left(\frac{i}{n}, \frac{\ell}{n}\right).
 \end{aligned}$$

Definition 3. Given a function u defined ν_n -almost everywhere in K , let us define the two functions $I_{n,1}^{2,*}u$ and $I_{n,2}^{2,*}u$ ν_n -almost everywhere, respectively, in $K_{n,1}$ and in $K_{n,2}$ by:

$$\begin{aligned}
 I_{n,1}^{2,*}u\left(\frac{k}{n}, \frac{j}{n}\right) &:= \frac{1}{n} \sum_{i=2}^n \left(\frac{i}{n} - \frac{k}{n}\right)^+ u\left(\frac{i}{n}, \frac{j}{n}\right), \\
 I_{n,2}^{2,*}u\left(\frac{i}{n}, \frac{\ell}{n}\right) &:= \frac{1}{n} \sum_{j=2}^n \left(\frac{j}{n} - \frac{\ell}{n}\right)^+ u\left(\frac{i}{n}, \frac{j}{n}\right).
 \end{aligned}$$

Lemma 4. For every function u defined ν_n -almost everywhere in K and every $m \in \{1, 2\}$,

$$u = T_{n,m}u + I_{n,m}^2 \partial_{n,m}^2 u \quad \nu_n\text{-almost everywhere in } K. \tag{6}$$

For every sequence (μ_n) in $M(K)$ such that $\sup_n (E_n(\mu_n) + E_n^\Sigma(\mu_n)) < +\infty$, every $m \in \{1, 2\}$ and every $\varphi \in C_c^\infty(\Omega)$,

$$\sup_n \int_K (T_{n,m}u_n(x))^2 \frac{\nu_n(dx)}{n^2} < +\infty, \tag{7}$$

$$\lim_n \int_K (\partial_m^2 \varphi(x)) (T_{n,m}u_n(x)) \frac{\nu_n(dx)}{n^2} = 0 \tag{8}$$

For every function u defined ν_n -almost everywhere in K , every $m \in \{1, 2\}$ and every function v defined ν_n -almost everywhere in $K_{n,m}$

$$\int_K (u(x))(I_{n,m}^2 v(x)) \frac{\nu_n(dx)}{n^2} = \int_{K_{n,m}} (I_{n,m}^{2,*} u(x))(v(x)) \frac{\nu_n(dx)}{n^2}. \tag{9}$$

For every function $\varphi \in C_c^\infty(\Omega)$ and every $m \in \{1, 2\}$,

$$\lim_n \int_{K_{n,m}} (I_{n,m}^{2,*} \partial_m^2 \varphi(x))^2 \frac{\nu_n(dx)}{n^2} = \int_\Omega (\varphi(x))^2 dx. \tag{10}$$

Proof. Let u be a function defined ν_n -almost everywhere in K . Direct calculation shows that

$$\begin{aligned} u\left(\frac{i}{n}, \frac{j}{n}\right) &= u\left(\frac{0}{n}, \frac{j}{n}\right) + \frac{i}{n} \partial_{n,1}^+ u\left(\frac{0}{n}, \frac{j}{n}\right) + \frac{1}{n} \sum_{k=1}^{n-1} \left(\frac{i-k}{n}\right)^+ \partial_{n,1}^2 u\left(\frac{k}{n}, \frac{j}{n}\right), \\ u\left(\frac{i}{n}, \frac{j}{n}\right) &= u\left(\frac{i}{n}, \frac{0}{n}\right) + \frac{j}{n} \partial_{n,1}^+ u\left(\frac{i}{n}, \frac{0}{n}\right) + \frac{1}{n} \sum_{\ell=1}^{n-1} \left(\frac{j-\ell}{n}\right)^+ \partial_{n,2}^2 u\left(\frac{i}{n}, \frac{\ell}{n}\right), \end{aligned}$$

which exactly corresponds to (6).

Let be (μ_n) in $M(K)$ such that $\sup_n (E_n(\mu_n) + E_n^\Sigma(\mu_n)) < +\infty$. Let be $\varphi \in C_c^\infty(\Omega)$ and $m \in \{1, 2\}$. Then, $\mu_n = u_n(\nu_n/n^2) \in M_n^\Sigma(K)$. Using (6) and the Jensen inequality, one gets

$$\begin{aligned} \int_K (T_{n,m} u_n(x))^2 \frac{\nu_n(dx)}{n^2} &= \int_K (u_n(x) - I_{n,m}^2 \partial_{n,m}^2 u_n(x))^2 \frac{\nu_n(dx)}{n^2} \\ &\leq 2 \int_K (u_n(x))^2 \frac{\nu_n(dx)}{n^2} + 2 \int_K (I_{n,m}^2 \partial_{n,m}^2 u_n(x))^2 \frac{\nu_n(dx)}{n^2} \\ &\leq 2 \int_K (u_n(x))^2 \frac{\nu_n(dx)}{n^2} + 4 \int_K (\partial_{n,m}^2 u_n(x))^2 \frac{\nu_n(dx)}{n^2} \end{aligned}$$

and, recalling (3), one deduces (7).

Let be $\varphi \in C_c^\infty(\Omega)$. Let us put $M := \sup_{n,m} \int_K (T_{n,m} u(x))^2 \frac{\nu_n(dx)}{n^2} < +\infty$. For every n and $m \in \{1, 2\}$,

$$\partial_{n,m}^2 T_{n,m} u_n = 0 \quad \text{almost everywhere in } K_{n,m}.$$

Since the support of φ is contained in a compact in Ω , using a discrete integration by parts, one deduces that exists an N such that, for every $n \geq N$, the support of φ is contained in $K_{n,m}$ and

$$\int_{K_{n,m}} (\partial_{n,m}^2 \varphi(x))(T_{n,m} u_n(x)) \frac{\nu_n(dx)}{n^2} = 0,$$

Therefore, using the Cauchy–Schwarz inequality, one gets

$$\begin{aligned} &\left(\int_K (\partial_m^2 \varphi(x))(T_{n,m} u_n(x)) \frac{\nu_n(dx)}{n^2} \right)^2 \\ &= \left(\int_{K_{n,m}} (\partial_m^2 \varphi(x) - \partial_{n,m}^2 \varphi(x))(T_{n,m} u_n(x)) \frac{\nu_n(dx)}{n^2} \right)^2 \end{aligned}$$

$$\begin{aligned} &\leq M \int_{K_{n,m}} (\partial_m^2 \varphi(x) - \partial_{n,m}^2 \varphi(x))^2 \frac{\nu_n(dx)}{n^2} \\ &\leq M \max\{(\partial_m^2 \varphi(x) - \partial_{n,m}^2 \varphi(x))^2 : x \in \mathbb{R}^2\} \end{aligned}$$

which implies (8).

Let u be a function defined ν_n -almost everywhere in K and v a function defined ν_n -almost everywhere in $K_{n,1}$. Then,

$$\begin{aligned} \int_K u(x) (I_{n,1}^2 v(x)) \frac{\nu_n(dx)}{n^2} &= \frac{1}{n^2} \sum_{i=0}^n \sum_{j=0}^n I_{n,1}^2 v\left(\frac{i}{n}, \frac{j}{n}\right) u\left(\frac{i}{n}, \frac{j}{n}\right) \\ &= \frac{1}{n^2} \sum_{i=0}^n \sum_{j=0}^n \left(\frac{1}{n^2} \sum_{k=1}^{n-1} (i-k)^+ v\left(\frac{k}{n}, \frac{j}{n}\right) \right) u\left(\frac{i}{n}, \frac{j}{n}\right) \\ &= \frac{1}{n^2} \sum_{k=1}^{n-1} \sum_{j=0}^n \left(\frac{1}{n^2} \sum_{i=0}^n (i-k)^+ u\left(\frac{i}{n}, \frac{j}{n}\right) \right) v\left(\frac{k}{n}, \frac{j}{n}\right) \\ &= \frac{1}{n^2} \sum_{k=1}^{n-1} \sum_{j=0}^n \left(\frac{1}{n^2} \sum_{i=2}^n (i-k)^+ u\left(\frac{i}{n}, \frac{j}{n}\right) \right) v\left(\frac{k}{n}, \frac{j}{n}\right) \\ &= \frac{1}{n^2} \sum_{k=1}^{n-1} \sum_{j=0}^n I_{n,1}^{2,*} u\left(\frac{k}{n}, \frac{j}{n}\right) v\left(\frac{k}{n}, \frac{j}{n}\right) \\ &= \int_{K_{n,1}} (I_{n,1}^{2,*} u(x)) v(x) \frac{\nu_n(dx)}{n^2}. \end{aligned}$$

Similar calculation holds for $m = 2$ which completes the proof of (9).

Finally, direct calculation shows that $I_{n,m}^{2,*} \partial_{n,m}^2 \varphi = \varphi$ ν_n -almost everywhere in $K_{n,m}$, which implies (10). □

Let us call $H^{-1}(\Omega)$ the topological dual of the usual Sobolev space $H_0^1(\Omega)$. We recall (see, for instance, in [26]) that if Ω is a limited open set with Lipschitzian boundary, then every distribution over Ω whose first-order partial derivatives are of class $H^{-1}(\Omega)$ is necessarily a distribution of class $L^2(\Omega)$. We will use this result to prove the following lemma.

Lemma 5. *Let be $\mu \in M(K)$ and C_1, C_2 two strictly positive real numbers. If for every $\varphi \in C_c^\infty(\Omega)$ and every $m \in \{1, 2\}$*

$$\langle \mu, \partial_m^2 \varphi \rangle \leq C_i \|\varphi\|_{L^2(\Omega)} \tag{11}$$

then there is a unique $(\mu_{\partial\Omega}, u) \in M(\overline{\Omega}) \times H^2(\Omega)$ satisfying

$$\int_{\Omega} |\mu_{\partial\Omega}| = 0 \quad \text{and} \quad \mu = \mu_{\partial\Omega} + u dx.$$

Proof. The measure μ admits a unique decomposition in the form of $\mu = \mu_{\partial\Omega} + \mu_\Omega$, where the measure $\mu_{\partial\Omega}$ is concentrated over $\partial\Omega$ and the measure μ_Ω is concentrated over Ω . It follows from (11) that there is $(u_1, u_2) \in L^2(\Omega)^2$ such that $\|u_m\|_{L^2(\Omega)} \leq C_m$ and for every $\varphi \in C_c^\infty(\Omega)$,

$$\langle \mu_\Omega, \partial_m^2 \varphi \rangle = \int_{\Omega} \varphi(x) u_m(x) dx.$$

Therefore,

$$\begin{aligned} \langle \mu_\Omega, \partial_1 \partial_2 (\partial_1 \varphi) \rangle &= \langle \mu_\Omega, \partial_1^2 (\partial_2 \varphi) \rangle = \int_\Omega \partial_2 \varphi(x) u_1(x) \, dx \\ \langle \mu_\Omega, \partial_1 \partial_2 (\partial_2 \varphi) \rangle &= \langle \mu_\Omega, \partial_2^2 (\partial_1 \varphi) \rangle = \int_\Omega \partial_1 \varphi(x) u_2(x) \, dx. \end{aligned}$$

It follows from the Cauchy–Schwarz inequality that all first-order partial derivatives of the distribution $\partial_1 \partial_2 \mu_\Omega$ are of class $H^{-1}(\Omega)$ and thus $\partial_1 \partial_2 \mu_\Omega$, for the previously recalled theorem, is of class $L^2(\Omega)$. Therefore, all second-order partial derivatives of μ_Ω are of class $L^2(\Omega)$, and thus, there is $u \in H^2(\Omega)$ such that $\mu_\Omega = u \, dx$. \square

This result will be used to show that finite energy displacements of the limit model satisfy a Dirichlet condition homogeneous over Σ .

Lemma 6. *Let be $n \geq 3$ and u a function defined ν_n -almost everywhere in K which satisfies the homogeneous Dirichlet condition $u(\nu_n/n^2) \in M_n^\Sigma(K)$. Then,*

$$\begin{aligned} \int_{[\frac{1}{n}, \frac{n-1}{n}] \times [a, b]} \left(\frac{\partial_{n,1}^+ u(x)}{x_1} \right)^2 \frac{d\nu_n(x)}{n^2} &\leq 4^2 \int_{[\frac{1}{n}, \frac{n-1}{n}] \times [a, b]} (\partial_{n,1}^2 u)^2 \frac{d\nu_n}{n^2}, \\ \int_{[\frac{1}{n}, 1] \times [a, b]} \left(\frac{u(x)}{x_1} \right)^2 \frac{d\nu_n(x)}{n^2} &\leq 4^4 \int_{[\frac{1}{n}, \frac{n-1}{n}] \times [a, b]} (\partial_{n,1}^2 u)^2 \frac{d\nu_n}{n^2}. \end{aligned}$$

Proof. Let $(v_i)_{0 \leq i \leq n} \in \mathbb{R}^{n+1}$ be such that $v_0 = 0$. Direct calculation (corresponding to a discrete integration by parts) shows

$$\sum_{i=1}^n \frac{v_i}{i} (v_i - v_{i-1}) + \sum_{i=1}^{n-1} \frac{v_i}{i+1} (v_{i+1} - v_i) = \sum_{i=1}^n \frac{(v_i)^2}{i(i+1)} + \left(1 - \frac{1}{n+1}\right) \frac{(v_n)^2}{n}$$

This equality and the Cauchy–Schwarz inequality imply

$$\begin{aligned} \left(\sum_{i=1}^n \left(\frac{v_i}{i} \right)^2 \right)^2 &\leq 4 \left(\sum_{i=1}^n \frac{(v_i)^2}{i(i+1)} \right)^2 \\ &\leq 4 \left(\sum_{i=1}^n \frac{v_i}{i} (v_i - v_{i-1}) + \sum_{i=1}^{n-1} \frac{v_i}{i+1} (v_{i+1} - v_i) \right)^2 \\ &\leq 4^2 \sum_{i=1}^n \left(\frac{v_i}{i} \right)^2 \sum_{i=1}^n (v_i - v_{i-1})^2 \end{aligned}$$

and therefore

$$\sum_{i=1}^n \left(\frac{v_i}{i} \right)^2 \leq 4^2 \sum_{i=1}^n (v_i - v_{i-1})^2. \tag{12}$$

Let u be a function defined ν_n -almost everywhere in K which satisfies the homogeneous Dirichlet condition $u(\nu_n/n^2) \in M_n^\Sigma(K)$. It follows from (12) that for every j such that $\frac{j}{n} \in [a, b]$

$$\sum_{i=1}^{n-1} \left(\frac{\partial_{n,1}^+ u(\frac{i}{n}, \frac{j}{n})}{i} \right)^2 \leq \frac{4^2}{n^2} \sum_{i=1}^{n-1} (\partial_{n,1}^2 u(\frac{i}{n}, \frac{j}{n}))^2,$$

and

$$\begin{aligned}
 \sum_{i=1}^n \left(\frac{u(\frac{i}{n}, \frac{j}{n})}{i} \right)^2 &\leq \frac{4^2}{n^2} \sum_{i=1}^n (\partial_{n,1}^- u(\frac{i}{n}, \frac{j}{n}))^2 \\
 &= \frac{4^2}{n^2} \sum_{i=1}^{n-1} (\partial_{n,1}^+ u(\frac{i}{n}, \frac{j}{n}))^2 \\
 &\leq 4^2 \sum_{i=1}^{n-1} \left(\frac{\partial_{n,1}^+ u(\frac{i}{n}, \frac{j}{n})}{i} \right)^2 \\
 &\leq \frac{4^4}{n^2} \sum_{i=1}^{n-1} (\partial_{n,1}^2 u(\frac{i}{n}, \frac{j}{n}))^2.
 \end{aligned}$$

The proof is completed summing over all j such that $\frac{j}{n} \in [a, b]$. \square

7. Conclusions

Nontrivial continuum models are needed for describing complex systems, and the literature in the field is huge, including applications to biomechanics (and in particular bone modeling, see, e.g., [27–29]), as well as to the designing of metamaterials (see, e.g., [30–35]) and in general to the study of a very wide and diverse set of multi-physics systems (see, e.g., [36–38]) whose study is by now within the possibilities of modern computational tools and thus theoretically even more relevant than in the past. The focus on these subjects has very practical reasons, as it entails the possibility to have qualitative and simplified analysis and predictions of the physical behavior of the systems under investigations. This is indeed the ultimate motivation for the study of homogenized problems, which have become by now a classic topic in the mechanical modeling of a very large set of phenomena, including biological ones (see, e.g., [39–41]). It could be disputed the true need for introducing such continuous and approximated models, but we think that it is reasonable to just *empirically* accept that sound and relevant information about discrete systems can be obtained from their homogenized limit. In this flow of thought and research, it is of course relevant to establish when a given discrete system has to be described by means of higher-gradient continuum models in the homogenized limit.

Despite a good deal of efforts in studying higher-gradient theories, in particular in connection with discrete systems (see, e.g., [42–52]), no general method or technique is available yet for characterizing the discrete microstructures which must be modeled in the homogenized limit by means of generalized continua. It is now clear, however, that some microstructures cannot be treated in a continuum limit without introducing higher-gradient continua.

The considered pantographic microstructure, although often ignored in engineering practice, is still well-known and used in some historical engineering devices. Its judicious use in periodic microstructures (as proposed in [53]) produces naturally a model which cannot be framed in the standard scheme developed by Navier and Cauchy. The rigorous proof which we presented here firmly bases Piola's conjecture and the aforementioned heuristic considerations. Of course, the analysis performed here is relative to the statics of the system, while when dealing with the dynamics very complex problems can easily arise. Addressing them is in our opinion one of the crucial challenges for the near future, and in this connection, the notable results exposed in [54] could be very useful. Finally, if the starting discrete structure is not constituted by simple Euler beams but involves some more complex beam models (a general reference on the subject can be, e.g., [55]), one can conjecture that the relative homogenized limit is not a purely second-gradient continuum anymore, but instead a microstructured continuum is called for. This is a very natural generalization, since it is well-known that higher-gradient continua can be always modeled by means of microstructured theories and represents one of the most active research fields in today's

mechanics (see, e.g., [56–59]). The investigation of such kind of complex systems can benefit from the use of suitable numerical simulations (for a numerical analysis of a structure very close to the one studied in the present work, see [60]). Very difficult numerical problems can arise when considering structures with this kind of peculiar geometry. A set of numerical tools has been elaborated to take care of this kind of problems, among which an important role is played by suitably employed isogeometric FEM (the reader is referred, e.g., to [61–65]). Particularly delicate is the case in which one has unilateral constraints connected to the inextensibility of the beams; this can be numerically addressed using Lagrangian Multipliers Methods, as performed in ([66, 67]). The simultaneous employment of a renewed mechanical approach via n -th gradient theories, of rigorous mathematical methods and of suitable numerical simulations promises to disclose new very promising paths in the next future for the given line of investigation.

References

1. Germain, P.: La méthode des puissances virtuelles en mécanique des milieux continus. Première partie. Théorie du second gradient. *J. Méc.* **12**, 235–274 (1973)
2. Germain, P.: The method of virtual power in continuum mechanics. Part 2: microstructure. *SIAM J. Appl. Math.* **25**, 556–575 (1973)
3. Mindlin, R.D.: Second gradient of strain and surface tension in linear elasticity. *Int. J. Solids Struct.* **1**(4), 417–438 (1965)
4. Toupin, R.A.: Elastic materials with couple-stresses. *Arch. Ration. Mech. Anal.* **11**(1), 385–414 (1962)
5. Toupin, R.A.: Theories of elasticity with couple-stress. *Arch. Ration. Mech. Anal.* **17**(2), 85–112 (1964)
6. dell’Isola, F., Seppecher, P., Madeo, A.: How contact interactions may depend on the shape of Cauchy cuts in n -th gradient continua: approach á la D’Alembert. *Z. Angew. Math. Phys. (ZAMP)* **63**(6), 1119–1141 (2012)
7. dell’Isola, F., Seppecher, P., Madeo, A.: Beyond Euler-Cauchy continua: the structure of contact actions in n -th gradient generalized continua: a generalization of the Cauchy tetrahedron argument. In: *Variational Models and Methods in Solid and Fluid Mechanics CISM Courses and Lectures*, vol. 535, pp. 17–106 (2012)
8. Seppecher, P., Alibert, J.-J., dell’Isola, F.: Linear elastic trusses leading to continua with exotic mechanical interactions. *J. Phys. Conf. Ser.* **319**(1), 012018 (2011)
9. Aifantis, E.C.: On the role of gradients in the localization of deformation and fracture. *Int. J. Eng. Sci.* **30**(10), 1279–1299 (1992)
10. Aifantis, E.C.: Strain gradient interpretation of size effects. *Int. J. Fract.* **95**(1–4), 299–314 (1999)
11. Altenbach, H., Eremeyev, V.A., Lebedev, L.P.: On the existence of solution in the linear elasticity with surface stresses. *J. Appl. Math. Mech./Z. Angew. Math. Mech. (ZAMM)* **90**(3), 231–240 (2010)
12. Auffray, N., dell’Isola, F., Eremeyev, V.A., Madeo, A., Rosi, G.: Analytical continuum mechanics á la Hamilton–Piola least action principle for second gradient continua and capillary fluids. *Math. Mech. Solids* (2013). doi:[10.1177/1081286513497616](https://doi.org/10.1177/1081286513497616)
13. Javili, A., dell’Isola, F., Steinmann, P.: Geometrically nonlinear higher-gradient elasticity with energetic boundaries. *J. Mech. Phys. Solids* **61**(12), 2381–2401 (2013)
14. dell’Isola, F., Steigmann, D.: A two-dimensional gradient-elasticity theory for woven fabrics. *J. Elast.* **118**(1), 113–125 (2015)
15. dell’Isola, F., Placidi, L.: Variational principles are a powerful tool also for formulating field theories. In: *Variational Models and Methods in Solid and Fluid Mechanics CISM Courses and Lectures*, vol. 535, pp. 1–15 (2012)
16. Piola, G.: Sull’applicazione de’ principj della meccanica analitica del Lagrange ai principali problemi. Memoria di Gabrio Piola presentata al concorso del premio e coronata dall’I.R. Istituto di Scienze, ecc. nella solennita del giorno 4 ottobre 1824, Milano, Imp. Regia stamperia, 1825. In: dell’Isola, F., Maier, G., Perego, U., Andreaus, U., Esposito, R., Forest, S. (eds.) *The Complete Works of Gabrio Piola*, vol. I. Springer, Berlin (2014)
17. dell’Isola, F., Andreaus, U., Placidi, L.: At the origins and in the vanguard of peridynamics, non-local and higher-gradient continuum mechanics: an underestimated and still topical contribution of Gabrio Piola. *Math. Mech. Solids* (2014). doi:[10.1177/1081286513509811](https://doi.org/10.1177/1081286513509811)
18. Di Egidio, A., Luongo, A., Paolone, A.: Linear and non-linear interactions between static and dynamic bifurcations of damped planar beams. *Int. J. Non-Linear Mech.* **42**(1), 88–98 (2007)
19. Braides, A.: Γ -convergence for beginners. In: *Oxford Lecture Series in Mathematics and Its Applications*, Band 22. Oxford University Press, Oxford (2002)
20. Braides, A., Solci, M., Vitali, E.: A derivation of linear elastic energies from pair-interaction atomistic systems. *Netw. Heterog. Medias* **2**, 551–567 (2007)
21. Maurini, C., Pouget, J., dell’Isola, F.: On a model of layered piezoelectric beams including transverse stress effect. *Int. J. Solids Struct.* **41**(16–17), 4473–4502 (2004)

22. dell'Isola, F., Maurini, C., Porfiri, M.: Passive damping of beam vibrations through distributed electric networks and piezoelectric transducers: Prototype design and experimental validation. *Smart Mater. Struct.* **13**(2), 299–308 (2004)
23. Porfiri, M., dell'Isola, F., Frattale Mascioli, F.M.: Circuit analog of a beam and its application to multimodal vibration damping, using piezoelectric transducers. *Int. J. Circuit Theory Appl.* **32**(4), 167–198 (2004)
24. Andreaus, U., dell'Isola, F., Porfiri, M.: Piezoelectric passive distributed controllers for beam flexural vibrations. *J. Vib. Control* **10**(5), 625 (2004)
25. Porfiri, M., dell'Isola, F.: Multimodal beam vibration damping exploiting PZT transducers and passive distributed circuits. *J. Phys. IV Fr.* **115**(1), 323–330 (2004)
26. Temam, R.: *Navier-Stokes Equations Theory and Numerical Analysis*. North-Holland, Amsterdam (1977)
27. Madeo, A., Lekszycki, T., dell'Isola, F.: A continuum model for the bio-mechanical interactions between living tissue and bio-resorbable graft after bone reconstructive surgery. *Comptes Rendus Méc.* **339**(10), 625–640 (2011)
28. Lekszycki, T., dell'Isola, F.: A mixture model with evolving mass densities for describing synthesis and resorption phenomena in bones reconstructed with bio-resorbable materials. *J. Appl. Math. Mech./Z. Angew. Math. Mech. (ZAMM)* **92**(6), 426–444 (2012)
29. Andreaus, U., Giorgio, I., Madeo, A.: Modeling of the interaction between bone tissue and resorbable biomaterial as linear elastic materials with voids. *J. Appl. Math. Phys. (ZAMP)* (2014). doi:[10.1007/s00033-014-0403-z](https://doi.org/10.1007/s00033-014-0403-z)
30. Placidi, L., Rosi, G., Giorgio, I., Madeo, A.: Reflection and transmission of plane waves at surfaces carrying material properties and embedded in second-gradient materials. *Math. Mech. Solids* **19**(5), 555–578 (2014)
31. Madeo, A., dell'Isola, F., Darve, F.: A continuum model for deformable, second gradient porous media partially saturated with compressible fluids. *J. Mech. Phys. Solids* **61**, 2196–2211 (2013)
32. dell'Isola, F., Madeo, A., Seppecher, P.: Boundary conditions at fluid-permeable interfaces in porous media: A variational approach. *Int. J. Solids Struct.* **46**(17), 3150–3164 (2009)
33. Ferretti, M., Madeo, A., dell'Isola, F., Boisse, P.: Modelling the onset of shear boundary layers in fibrous composite reinforcements by second gradient theory. *Z. Angew. Math. Phys. (ZAMP)* **65**(3), 587–612 (2014)
34. Sciarra, G., dell'Isola, F., Hutter, K.: A solid-fluid mixture model allowing for solid dilatation under external pressure. *Contin. Mech. Thermodyn.* **13**(5), 287–306 (2001)
35. Del Vescovo, D., Giorgio, I.: Dynamic problems for metamaterials: review of existing models and ideas for further research. *Int. J. Eng. Sci.* **80**, 153–172 (2014)
36. Steinmann, P., Elizondo, A., Sunyk, R.: Studies of validity of the Cauchy–Born rule by direct comparison of continuum and atomistic modelling. *Model. Simul. Mater. Sci. Eng.* **15**, S271–S281 (2007)
37. Sciarra, G., dell'Isola, F., Coussy, O.: Second gradient poromechanics. *Int. J. Solids Struct.* **44**(20), 6607–6629 (2007)
38. Scerrato, D., Giorgio, I., Madeo, A., Limam, A., Darve, F.: A simple non-linear model for internal friction in modified concrete. *Int. J. Eng. Sci.* **80**, 136–152 (2014)
39. Goda, I., Assidi, M., Belouettar, S., Ganghoffer, J.F.: A micropolar anisotropic constitutive model of cancellous bone from discrete homogenization. *J. Mech. Behav. Biomed. Mater.* **16**, 87–108 (2012)
40. Dos Reis, F., Ganghoffer, J.F.: Equivalent mechanical properties of auxetic lattices from discrete homogenization. *Comput. Mater. Sci.* **51**, 314–321 (2012)
41. Assidi, M., Dos Reis, F., Ganghoffer, J.F.: Equivalent mechanical properties of biological membranes from lattice homogenization. *J. Mech. Behav. Biomed. Mater.* **4**(8), 1833–1845 (2011)
42. Haseganu, E.M., Steigmann, D.J.: Equilibrium analysis of finitely deformed elastic networks. *Comput. Mech.* **17**, 359–373 (1996)
43. Pideri, C., Seppecher, P.: A second gradient material resulting from the homogenization of an heterogeneous linear elastic medium. *Contin. Mech. Thermodyn.* **9**, 241–257 (1997)
44. dell'Isola, F., Seppecher, P.: The relationship between edge contact forces, double force and interstitial working allowed by the principle of virtual power. *Comptes Rendus Acad. Sci. Sér. IIb* **321**, 303–308 (1995)
45. dell'Isola, F., Rosa, L., Woźniak, C.: Dynamics of solids with micro periodic nonconnected fluid inclusions. *Arch. Appl. Mech.* **67**(4), 215–228 (1997)
46. dell'Isola, F., Rosa, L., Woźniak, C.: A micro-structured continuum modelling compacting fluid-saturated grounds: The effects of pore-size scale parameter. *Acta Mech.* **127**(1–4), 165–182 (1998)
47. dell'Isola, F., Guarascio, M., Hutter, K.A.: Variational approach for the deformation of a saturated porous solid. A second-gradient theory extending Terzaghi's effective stress principle. *Arch. Appl. Mech.* **70**, 323–337 (2000)
48. dell'Isola, F., Madeo, A., Placidi, L.: Linear plane wave propagation and normal transmission and reflection at discontinuity surfaces in second gradient 3D continua. *Z. Angew. Math. Mech. (ZAMM)* **92**(1), 52–71 (2012)
49. dell'Isola, F., Sciarra, G., Vidoli, S.: Generalized Hooke's law for isotropic second gradient materials. *Proc. R. Soc. Lon. Ser. A Math. Phys. Eng. Sci.* **465**, 2177–2196 (2009)
50. Yang, Y., Ching, W.Y., Misra, A.: Higher-order continuum theory applied to fracture simulation of nano-scale intergranular glassy film. *Journal of Nanomechanics and Micromechanics* **1**, 60–71 (2011)
51. Yang, Y., Misra, A.: Higher-order stress–strain theory for damage modeling implemented in an element-free Galerkin formulation. *Comput. Model. Eng. Sci.* **64**, 1–36 (2010)

52. Yang, Y., Misra, A.: Micromechanics based second gradient continuum theory for shear band modeling in cohesive granular materials following damage elasticity. *Int. J. Solids Struct.* **49**, 2500–2514 (2012)
53. Alibert, J.J., Seppecher, P., dell’Isola, F.: Truss modular beams with deformation energy depending on higher displacement gradients. *Math. Mech. Solids* **8**, 51–73 (2003)
54. Sestieri, A., Carcaterra, A.: Space average and wave interference in vibration conductivity. *J. Sound Vib.* **263**(3), 475–491 (2003)
55. Piccardo, G., Ranzi, G., Luongo, A.: A complete dynamic approach to the Generalized Beam Theory cross-section analysis including extension and shear modes. *Math. Mech. Solids* (2013). doi:[10.1177/1081286513493107](https://doi.org/10.1177/1081286513493107)
56. dell’Isola, F., Batra, R.C.: Saint-Venant’s Problem for Porous Linear Elastic Materials. *J. Elast.* **47**(1), 73–81 (1997)
57. Placidi, L., dell’Isola, F., Ianiro, N., Sciarra, G.: Variational formulation of pre-stressed solid-fluid mixture theory, with an application to wave phenomena. *Eur. J. Mech. A Solids* **27**(4), 582–606 (2008)
58. Sciarra, G., dell’Isola, F., Ianiro, N., Madeo, A.: A variational deduction of second gradient poroelasticity part I: General theory. *J. Mech. Mater. Struct.* **3**(3), 507–526 (2008)
59. Madeo, A., dell’Isola, F., Ianiro, N., Sciarra, G.: A variational deduction of second gradient poroelasticity II: An application to the consolidation problem. *J. Mech. Mater. Struct.* **3**(4), 607–625 (2008)
60. dell’Isola, F., Giorgio, I., Andreaus, U.: Elastic pantographic 2D lattices: a numerical analysis on static response and wave propagation. *Proc. Est. Acad. Sci. Eng.* (2015), in press
61. Garusi, E., Tralli, A., Cazzani, A.: An unsymmetric stress formulation for Reissner-Mindlin plates: A simple and locking-free rectangular element. *Int. J. Comput. Eng. Sci.* **5**(3), 589–618 (2004)
62. Cazzani, A., Malagù, M., Turco, E.: Isogeometric analysis of plane-curved beams. *Math. Mech. Solids* (2014). doi:[10.1177/1081286514531265](https://doi.org/10.1177/1081286514531265)
63. Cazzani, A., Ruge, P.: Numerical aspects of coupling strongly frequency-dependent soil-foundation models with structural finite elements in the time-domain. *Soil Dyn. Earthq. Eng.* **37**, 56–72 (2012)
64. Cuomo, M., Contrafatto, L.: Stress rate formulation for elastoplastic models with internal variables based on augmented Lagrangian regularisation. *Int. J. Solids Struct.* **37**(29), 3935–3964 (2000)
65. Dos Reis, F., Ganghoffer, J.F.: Discrete homogenization of architected materials: Implementation of the method in a simulation tool for the systematic prediction of their effective elastic properties. *Tech. Mech.* **30**, 85–109 (2010)
66. Cuomo, M., Ventura, G.: Complementary energy approach to contact problems based on consistent augmented Lagrangian formulation. *Math. Comput. Model.* **28**(4), 185–204 (1998)
67. Cuomo, M., Contrafatto, L., Greco, L.: A variational model based on isogeometric interpolation for the analysis of cracked bodies. *Int. J. Eng. Sci.* **80**, 173–188 (2014)

Jean-Jacques Alibert
 IMATH
 Université du Sud Toulon-Var
 Bâtiment U
 BP 20132-83957
 La Garde Cedex
 France
 e-mail: alibert@univ-tln.fr

Alessandro Della Corte
 Doctoral School in Theoretical and Applied Mechanics
 University La Sapienza
 Rome
 Italy
 e-mail: alessandro.dellacorte@uniroma1.it

(Received: March 2, 2015; revised: March 30, 2015)

Chapter 2

Extensional Elastica in large deformation as Γ -limit
of a discrete 1D mechanical system



Extensional *Elastica* in large deformation as Γ -limit of a discrete 1D mechanical system

Jean-Jacques Alibert, Alessandro Della Corte[✉], Ivan Giorgio[✉] and Antonio Battista[✉]

Abstract. The present paper deals with the rigorous homogenization of a discrete system consisting of extensible rods linked by rotational springs. Specifically, a Γ -convergence result is proven for a sequence of discrete measure functionals E_n , describing the energy of the discrete system, toward the continuous energy functional for the extensible Euler beam model (*Elastica*) in large deformation regime. A relative compactness result for the sequence E_n is also proven. Moreover, numerical results are shown on the deformed shape and on the total energy of the system when the number of elements of the discrete system increases. The numerical convergence of the energy to a definite value is shown in two cases. The results provide rigorous justification of a very commonly used algorithm for the discretization of the extensible Euler beam, namely Hencky-type beam model.

Mathematics Subject Classification. 74Q05, 28A33, 35B27.

Keywords. Solid mechanics, Extensible Euler beam, Large deformation, Γ -convergence, Hencky-type beam model.

1. Introduction

In [1], a rigorous Γ -convergence result was established for a discrete system consisting of rigid bars and rotational springs toward Euler's inextensible *Elastica* in large deformation. The present paper aims at generalizing the result including in the energy a contribution due to the extensional deformation of the *Elastica*. Another generalization will concern the inclusion in the energy of possible material nonlinearities (under standard assumptions of convexity, lower semicontinuity and sufficiently rapid divergence at infinity). In this way, the model is applicable to a much larger class of real-world phenomena. Of course, the related mathematical problems are significantly more complex, requiring new ideas.

Technically speaking, the main aim of the paper is to establish a Γ -convergence result for the functional describing the energy of a discrete mechanical system consisting of extensional and rotational springs, respectively modeled as two- and three-points interactions at the microscale. The sequence of functionals which will be proven to Γ -converge to the continuum energy model is not obtained (as it is fairly common) by means of interpolation of the discrete kinematical descriptors with piecewise suitably regular functions. Instead, a sequence of (Radon) measure functionals is introduced and used to prove the Γ -convergence result. We prefer this approach so as to circumscribe as much as possible the role of arbitrariness, which is always an issue when selecting *ad hoc* interpolating functions. Moreover, a relative compactness property of the sequence of discrete functionals is proven, which ensures that it is enough to control the norm of the measure employed for the description of the current configuration of the discrete model in order to control the corresponding deformation energy.

The significance of the result herein obtained is twofold. First of all, the problem of the homogenization of (possibly very complex) micro- and nanostructures is today very relevant in theoretical and applied mechanics, and much effort is devoted to various heuristic or asymptotic homogenization methods (see, e.g., [2–8] for examples involving generalized continua). This emphasizes the need for rigorous results, and indeed the rigorous homogenization here proven provides a sound basis which numerical investigations of extensible *Elasticae* can be based on; in fact, this is particularly important since Hencky-type beam

models are already employed by several numerical codes (see [9]; for some recent applications see [10–12]). Moreover, including the large deformation regime in the homogenization result offers many more prospects of applying it to real problems of structural mechanics (see for instance [13]) and is especially significant in view of application to the design of metamaterials (see, e.g., [14]), i.e., materials, typically endowed with a microstructure, displaying behaviors which are not found in natural materials ([15–18]). The possibility to consider large deformations of the microstructure while retaining meaningful numerical simulations based on discretized systems can enrich markedly the class of behaviors which can be designed and investigated. Among the case studies covered by this kind of generalizations, particularly promising for their mechanical characteristics are fibrous microstructured systems in which the fibers undergo large deformations ([19–24]).

The paper is organized as follows: in Sect. 2, the notion of Γ -convergence of measure functionals and of relative compactness of a sequence of functionals is recalled; in Sects. 3 and 4, micro- and macro-models (respectively) for an extensible beam in large deformation are introduced; in Sect. 5, the main convergence result is proven; in Sect. 6, some numerical results are presented and in Sect. 7, some conclusions are drawn and further research directions are outlined.

2. Γ -convergence of measure functionals

Let $(C[0, 1])^d$ be the space of vector-valued continuous functions on $[0, 1]$ endowed with the uniform norm $\|\varphi\|_\infty := \sup\{\|\varphi(t)\| : t \in [0, 1]\}$ and $(\mathcal{M}[0, 1])^d$ the set of vector-valued bounded measures on $[0, 1]$ endowed with the norm

$$\|\mu\|_{\mathcal{M}} := \sup\{\langle \mu, \varphi \rangle : \varphi \in (C[0, 1])^d, \|\varphi\|_\infty = 1\}$$

where $\langle \cdot, \cdot \rangle$ stands for the duality bracket between $(\mathcal{M}[0, 1])^d$ and $(C[0, 1])^d$. We write simply $\mu_n \rightharpoonup \mu$ to specify that a sequence (μ_n) of vector-valued bounded measures converges to a vector-valued bounded measure μ . Recall that if a sequence of vector-valued bounded measures (μ_n) satisfies $\sup_n \|\mu_n\|_{\mathcal{M}} < +\infty$, then there exists a vector-valued bounded measure μ and a subsequence (n_k) such that $\mu_{n_k} \rightharpoonup \mu$. Let (F_n) and F be functionals on $(\mathcal{M}[0, 1])^d$ with values in $\mathbb{R} \cup \{+\infty\}$. We say that F_n Γ -converges to F if the following two properties are satisfied (for an introduction to Γ -convergence see [25]):

- (a) *Upper bound inequality.* For every $\mu \in (\mathcal{M}([0, 1])^d)$, there exists a sequence (μ_n) in $(\mathcal{M}[0, 1])^d$ such that

$$\mu_n \rightharpoonup \mu \quad \text{and} \quad \limsup_{n \rightarrow \infty} F_n(\mu_n) \leq F(\mu).$$

- (b) *Lower bound inequality.* For every $\mu \in (\mathcal{M}[0, 1])^d$ and every sequence (μ_n) in $(\mathcal{M}[0, 1])^d$,

$$\mu_n \rightharpoonup \mu \quad \implies \quad \liminf_{n \rightarrow \infty} F_n(\mu_n) \geq F(\mu).$$

We also define the following property for the sequence F_n :

- (c) *Relative compactness.* For every sequence (μ_n) in $(\mathcal{M}[0, 1])^d$

$$\sup_n F_n(\mu_n) < +\infty \quad \implies \quad \sup_n \|\mu_n\|_{\mathcal{M}} < +\infty.$$

3. Micro-model for beams in large deformation

3.1. Discrete configurations and operators

Let δ_t denote the Dirac measure at the point $t \in [0, 1]$. The discrete micro-system is described by means of measures valued $\frac{1}{n}$ placed at the points $\frac{i}{n}$ where $i = 0, 1, \dots, n$. Therefore, it will be described by the

positive Radon measure¹ on $[0, 1]$:

$$\bar{\nu}_n := \frac{1}{n} \sum_{i=0}^n \delta_{\frac{i}{n}} \quad (1)$$

The current configuration will be described by a vector bounded measure μ on $[0, 1]$ of the form $\mu(dt) := u(t)\bar{\nu}_n(dt)$ where the placement function $u : [0, 1] \rightarrow \mathbf{R}^2$ is defined $\bar{\nu}_n$ —almost everywhere, i.e., at the points $\frac{i}{n}$ where $i = 0, 1, \dots, n$. Herein, we will use the following notations.

$$\nu_n^+ := \frac{1}{n} \sum_{i=0}^{n-1} \delta_{\frac{i}{n}} \quad \nu_n^- := \frac{1}{n} \sum_{i=1}^n \delta_{\frac{i}{n}} \quad (2)$$

$$D_n^+ u(t) := n(u(t + \frac{1}{n}) - u(t)) \quad D_n^- u(t) := n(u(t) - u(t - \frac{1}{n})) \quad (3)$$

$$\nu_n := \frac{1}{n} \sum_{i=1}^{n-1} \delta_{\frac{i}{n}} \quad (4)$$

$$D_n^2 u := n(D_n^+ u - D_n^- u) \quad (5)$$

$$T_n(u) := n \left(\frac{D_n^+ u}{\|D_n^+ u\|} - \frac{D_n^- u}{\|D_n^- u\|} \right) \quad (6)$$

Note that:

- if u is a placement function then $D_n^+ u$ is defined ν_n^+ —almost everywhere, and $D_n^- u$ is defined ν_n^- —almost everywhere;
- if u is a placement function then $D_n^2 u$ is defined ν_n —almost everywhere;
- if u is a placement function and $D_n^+ u \neq 0$ ν_n^+ —almost everywhere, then $T_n(u)$ is defined ν_n —almost everywhere;
- clearly, T_n is a nonlinear operator.

3.2. Deformation energy associated with two points interactions

A generic pair of adjacent masses is connected by a spring whose deformation energy depends on the distance between their current positions and must be equal to zero if the distance is equal to $\frac{1}{n}$. The micro-Lagrangian discrete system having its configuration specified by the bounded measure $\mu(dt) = u(t)\bar{\nu}_n(dt)$ has a deformation energy given by

$$E_n^{(2)}(\mu) := \frac{1}{n} \sum_{i=0}^{n-1} f(n\|u(\frac{i+1}{n}) - u(\frac{i}{n})\|) = \int f(\|D_n^+ u(t)\|) \nu_n^+(dt) \quad (7)$$

where the integrand f is a function from \mathbb{R} into $[0, +\infty]$ such that $f(t) = +\infty$ if $t \leq 0$, $f(t) > 0$ if $t \neq 1$ and $f(1) = 0$. The beam is said to be inextensible when the integrand f is defined by (this case is studied in [1]):

¹We recall that a Radon measure is a measure defined on the σ -algebra of Borel sets of a (Hausdorff) topological space which is locally finite and such that, for every Borel set S , $m(S)$ is the supremum of $m(K)$ over the compact subsets of S (see [26]).

$$f(\rho) = \begin{cases} 0 & \text{if } \rho = 1 \\ +\infty & \text{otherwise} \end{cases} \quad (8)$$

In this case $E_n^{(2)}(\mu) \in \{0, +\infty\}$ and $E_n^{(2)}(\mu) = 0$ if and only if $\mu(dt) = u(t)\bar{\nu}_n(dt)$ with

$$\|D_n^+ u\| = 1 \quad \nu_n^+ \text{—almost everywhere.}$$

3.3. Deformation energy associated with three-points interactions

At each node $\frac{i}{n}$, a rotational spring is placed, whose deformation energy depends on the angle $\theta_n u(\frac{i}{n}) \in (-\pi, +\pi)$ formed by the vectors $u(\frac{i+1}{n}) - u(\frac{i}{n})$ and $u(\frac{i}{n}) - u(\frac{i-1}{n})$ and must be equal to zero if the angle is 0. Following [27], the micro-Lagrangian discrete system having its configuration specified by the above bounded measure $\mu(dt) = u(t)\bar{\nu}_n(dt)$ has a deformation energy given by

$$E_n^{(3)}(\mu) := \frac{1}{n} \sum_{i=1}^{n-1} n^2 (1 - \cos \theta_n u(\frac{i}{n})).$$

A direct computation gives

$$E_n^{(3)}(\mu) = \int \frac{\|T_n(u)(t)\|^2}{2} \nu_n(dt).$$

Recall that this energy is well defined if and only if $D_n^+ u \neq 0$ ν_n^+ —almost everywhere. This is the case when $E_n^{(2)}(\mu) < +\infty$ because the integrand f is assumed to be equal to $+\infty$ for nonpositive real numbers. In this paper, we consider the more general deformation energy of the form

$$E_n^{(3)}(\mu) := \int g(\|T_n(u)(t)\|) \nu_n(dt) \quad (9)$$

where the integrand g is a function from $[0, +\infty)$ into $[0, +\infty]$ such that $g(0) = 0$ and $g(r) > 0$ if $r \neq 0$. If the beam is assumed to be inextensible and $E_n^{(2)}(\mu) < +\infty$ then one has

$$E_n^{(3)}(\mu) = \int g(\|D_n^2 u(t)\|) \nu_n(dt).$$

3.4. Energy functional associated to a left-hand side clamped beam

Let $(\mathcal{M}_n[0, 1])^d$ denote the set of those vector bounded measures of the form $\mu(dt) = u(t)\bar{\nu}_n(dt)$ and such that

$$E_n^{(2)}(\mu) < +\infty \quad E_n^{(3)}(\mu) < +\infty \quad u(0) = 0 \quad D_n^+ u(0) = e_1 \quad (10)$$

where e_1 denotes the first vector of the canonical base of \mathbb{R}^d . In the micro-model, the total deformation energy is seen as a functional E_n defined on $(\mathcal{M}[0, 1])^d$ by

$$E_n(\mu) := \begin{cases} E_n^{(2)}(\mu) + E_n^{(3)}(\mu) & \text{if } \mu \in (\mathcal{M}_n[0, 1])^d \\ +\infty & \text{otherwise} \end{cases} \quad (11)$$

4. Macro model for nonlinear beams and main result

4.1. Energy functional associated to a left-hand side clamped beam

Let $L^1(0, 1)$ be the usual Lebesgue space and $W^{1,1}(0, 1)$ be the Sobolev space of those functions $v \in L^1(0, 1)$ with distributional derivative in $L^1(0, 1)$. According to the embedding $W^{1,1}(0, 1) \longrightarrow C[0, 1]$,

any function in $W^{1,1}(0,1)$ will be assumed to be continuous on $[0,1]$. Let $(\mathcal{M}_\infty[0,1])^d$ be the set of those vector-valued bounded measures on $[0,1]$ of the form

$$\mu(dt) = u(t)dt$$

and such that there exists $(\rho, v) \in L^1(0,1) \times (W^{1,1}(0,1))^d$ with

$$(P_1) \quad \int_0^1 f(\rho(t)) dt < +\infty$$

$$(P_2) \quad \int_0^1 g(\|v'(t)\|) dt < +\infty \quad \|v(t)\| = 1 \text{ for every } t \in [0,1] \quad v(0) = e_1$$

$$(P_3) \quad u(t) = \int_0^t v(s)\rho(s) ds \text{ for every } t \in [0,1]$$

Since $f(\rho) = +\infty$ for $\rho \leq 0$, property (P_1) implies that ρ is positive almost everywhere on $(0,1)$. As a consequence, properties (P_2) and (P_3) imply that the pair (ρ, v) is unique when it exists, i.e.

$$\rho = \rho_u := \|u'\| \quad \text{and} \quad v = v_u := \frac{u'}{\|u'\|} \quad (12)$$

The total energy functional (associated to the macro model) is defined by setting

$$E(\mu) := \begin{cases} \int_0^1 f(\rho_u(t)) dt + \int_0^1 g(\|v'_u(t)\|) dt & \text{if } \mu(dt) = u(t)dt \in (\mathcal{M}_\infty[0,1])^d \\ +\infty & \text{otherwise} \end{cases} \quad (13)$$

4.2. Main result and example

In this section, the integrands $f : \mathbb{R} \rightarrow [0, +\infty]$ and $g : [0, +\infty) \rightarrow [0, +\infty]$ are assumed to satisfy the following properties

- (H_1) f is convex and lower semicontinuous on \mathbb{R} ,
- (H_2) $f(\rho) = +\infty$ for every $\rho \leq 0$ and $\lim_{\rho \rightarrow +\infty} \frac{f(\rho)}{\rho} = +\infty$,
- (H_3) $f(1) = 0$ and $f(\rho) > 0$ for every $\rho \neq 1$,
- (H_4) g is convex and lower semicontinuous on $[0, +\infty)$,
- (H_5) $\lim_{r \rightarrow +\infty} \frac{g(r)}{r} = +\infty$,
- (H_6) $\lim_{r \rightarrow 0^+} g(r) = g(0) = 0$ and $g(r) > 0$ for every $r > 0$.

We remark that these properties are able to describe a very wide class of elastic constitutive relations, and in particular can account for the behavior of polyamide in elastic regime, used for 3D-printing the fibrous systems mentioned in the Introduction.

Theorem 1. *If the properties $(H_1) \dots (H_6)$ hold, then the sequence (E_n) Γ -converges to the functional E . Moreover the sequence (E_n) has the relative compactness property.*

The above result may be used when the beam is assumed to be inextensible (namely if the integrand f is defined by (8)) and the integrand is given by $g(r) := r^2/2$. In this particular case, the limit energy functional is given by

$$E(\mu) := \begin{cases} \frac{1}{2} \int_0^1 \|u''(t)\|^2 dt & \text{if } \mu(dt) = u(t)dt \in (\mathcal{M}_\infty[0, 1])^d \\ +\infty & \text{otherwise} \end{cases}$$

where $(\mathcal{M}_\infty[0, 1])^d$ denotes the set of those vector-valued bounded measures on $[0, 1]$ of the form $\mu(dt) = u(t)dt$ such that u belongs to the usual Sobolev space $(H^2(0, 1))^d$ and $\|u'(t)\| = 1$ for every $t \in [0, 1]$ (see [1]).

5. Proof of the main theorem

Before proving Theorem 1, we need some preliminary results.

5.1. Approximations results

Let (μ_n) be a sequence with bounded energy which means that $\mu_n(dt) = u_n(t)\bar{\nu}_n(dt) \in (\mathcal{M}_n[0, 1])^d$ and there exists a positive real number M such that

$$\int f(\|D_n^+ u_n(t)\|) \nu_n^+(dt) + \int g(\|T_n(u_n)(t)\|) \nu_n(dt) \leq M \tag{14}$$

for every n . Let us define an approximating sequence $(\bar{\mu}_n)$ of vector-valued bounded measures by setting $\bar{\mu}_n(dt) = \bar{u}_n(t)dt$ and

$$\begin{aligned} \rho_n(t) &:= \sum_{i=0}^{n-1} \|D_n^+ u_n(\frac{i}{n})\| \delta_t((\frac{i}{n}, \frac{i+1}{n})) \\ v_n(0) &:= e_1 \quad v'_n(t) := \sum_{i=1}^{n-1} T_n(u_n)(\frac{i}{n}) \delta_t((\frac{i}{n} - \frac{1}{2n}, \frac{i}{n} + \frac{1}{2n})) \\ \bar{u}_n(t) &:= \int_0^t v_n(s) \rho_n(s) ds \end{aligned}$$

Note that $\|v_n(t)\|$ is not necessarily equal to 1, and therefore in general $\bar{\mu}_n \notin (\mathcal{M}_\infty[0, 1])^d$. The following result will be used to establish the lower bound inequality.

Lemma 1. *If (μ_n) is a sequence with bounded energy, then the approximating sequence $(\bar{\mu}_n)$ defined above satisfies the following properties.*

$$\begin{aligned} E_n(\mu_n) &= \int_0^1 f(\rho_n(t)) dt + \int_0^1 g(\|v'_n(t)\|) dt \quad \text{for every } n, \\ \lim_{n \rightarrow \infty} \|v_n(t)\| &= 1 \quad \text{for every } t \in [0, 1], \\ \bar{\mu}_n - \mu_n &\rightharpoonup 0. \end{aligned}$$

Proof. For any positive integer n ,

$$\begin{aligned}
E_n(\mu_n) &= \int f(\|D_n^+ u_n(t)\|) \nu_n^+(dt) + \int g(\|T_n(u_n)(t)\|) \nu_n(dt) \\
&= \frac{1}{n} \sum_{i=0}^{n-1} f(\|D_n u_n(\frac{i}{n})\|) + \frac{1}{n} \sum_{i=1}^{n-1} g(\|T_n(u_n)(\frac{i}{n})\|) \\
&= \sum_{i=0}^{n-1} \int_{\frac{i}{n}}^{\frac{i+1}{n}} f(\rho_n(t)) dt + \sum_{i=1}^{n-1} \int_{\frac{i}{n} - \frac{1}{2n}}^{\frac{i}{n} + \frac{1}{2n}} g(\|v'_n(t)\|) dt \\
&= \int_0^1 f(\rho_n(t)) dt + \int_0^1 g(\|v'_n(t)\|) dt
\end{aligned}$$

As a consequence, one has

$$\sup_n \int_0^1 g(\|v'_n(t)\|) dt < +\infty$$

Then, using (H_4) , (H_5) , (H_6) we obtain (for this result, we refer to [28] proposition 3, page 40) that the sequence (v'_n) is equi-integrable which implies that:

$$\text{The sequence } (v_n) \text{ is equi-continuous on } [0, 1]. \quad (15)$$

On the other hand, for any $i = 0, 1, \dots, n-1$ one has

$$\begin{aligned}
v_n(\frac{i}{n} + \frac{1}{2n}) &= v_n(0) + \int_0^{\frac{i}{n} + \frac{1}{2n}} v'_n(t) dt \\
&= e_1 + \sum_{k=1}^i \int_{\frac{k}{n} - \frac{1}{2n}}^{\frac{k}{n} + \frac{1}{2n}} T_n(u_n)(t) dt \\
&= e_1 + \frac{1}{n} \sum_{k=1}^i T_n(u_n)(\frac{k}{n}) \\
&= e_1 + \frac{1}{n} \sum_{k=1}^i D_n^- \left(\frac{D_n^+ u_n}{\|D_n^+ u_n\|} \right) (\frac{k}{n}) \\
&= \frac{D_n^+ u_n(\frac{i}{n})}{\|D_n^+ u_n(\frac{i}{n})\|}
\end{aligned}$$

Therefore

$$\|v_n(\frac{i}{n} + \frac{1}{2n})\| = 1 \quad \text{for } i = 0, 1, \dots, n-1. \quad (16)$$

Together with (15), this implies that $\lim_{n \rightarrow \infty} \|v_n(t)\| = 1$ for every $t \in [0, 1]$.

Let $\varphi \in (C[0, 1])^d$ and $\psi \in (C^1[0, 1])^d$ such that $\psi' = \varphi$ and $\psi(1) = 0$. Let us define

$$\begin{aligned}\varepsilon_1\left(\frac{1}{n}\right) &:= \sum_{i=0}^{n-1} \|D_n^+ u_n\left(\frac{i}{n}\right)\| \int_{\frac{i}{n}}^{\frac{i+1}{n}} \psi(t) \cdot \left(v_n\left(\frac{i}{n} + \frac{1}{2n}\right) - v_n(t)\right) dt \\ \varepsilon_2\left(\frac{1}{n}\right) &:= \varepsilon_1\left(\frac{1}{n}\right) + \frac{1}{n} \sum_{i=0}^{n-1} D_n^+ u_n\left(\frac{i}{n}\right) \cdot \left(\psi\left(\frac{i}{n}\right) - n \int_{\frac{i}{n}}^{\frac{i+1}{n}} \psi(t) dt\right) \\ \varepsilon_3\left(\frac{1}{n}\right) &:= \varepsilon_2\left(\frac{1}{n}\right) + \frac{1}{n} \sum_{i=1}^n u_n\left(\frac{i}{n}\right) \cdot \left(D_n^- \psi\left(\frac{i}{n}\right) - \psi'\left(\frac{i}{n}\right)\right)\end{aligned}$$

Since the sequence $(E_n(\mu_n))$ is bounded, one has

$$\sup_n \int f(\|D_n^+ u_n(t)\|) \nu_n^+(dt) < +\infty.$$

Then using (H_1) , (H_2) and the condition $u_n(0) = 0$, we obtain

$$\sup_n \int \|D_n^+ u_n(t)\| \nu_n^+(dt) < +\infty \quad \text{and} \quad \sup_n \int \|u_n\| \bar{\nu}_n(dt) < +\infty.$$

Together with (15), the above bounds imply that the sequences $\varepsilon_1(\frac{1}{n})$, $\varepsilon_2(\frac{1}{n})$, $\varepsilon_3(\frac{1}{n})$ tend to zero as n tends to ∞ . For any positive integer n , one has

$$\begin{aligned}\langle \bar{\mu}_n, \varphi \rangle &= \langle \bar{\mu}_n, \psi' \rangle = - \int_0^1 \psi(t) \cdot v_n(t) \bar{\rho}_n(t) dt \\ &= - \sum_{i=0}^{n-1} \|D_n^+ u_n\left(\frac{i}{n}\right)\| \int_{\frac{i}{n}}^{\frac{i+1}{n}} \psi(t) \cdot v_n(t) dt \\ &= - \sum_{i=0}^{n-1} \|D_n^+ u_n\left(\frac{i}{n}\right)\| \int_{\frac{i}{n}}^{\frac{i+1}{n}} \psi(t) \cdot v_n\left(\frac{i}{n} + \frac{1}{2n}\right) dt + \varepsilon_1\left(\frac{1}{n}\right) \\ &= - \frac{1}{n} \sum_{i=0}^{n-1} D_n^+ u_n\left(\frac{i}{n}\right) \cdot n \int_{\frac{i}{n}}^{\frac{i+1}{n}} \psi(t) dt + \varepsilon_1\left(\frac{1}{n}\right) \\ &= - \frac{1}{n} \sum_{i=0}^{n-1} D_n^+ u_n\left(\frac{i}{n}\right) \cdot \psi\left(\frac{i}{n}\right) + \varepsilon_2\left(\frac{1}{n}\right) \\ &= \frac{1}{n} \sum_{i=1}^n u_n\left(\frac{i}{n}\right) \cdot D_n^- \psi\left(\frac{i}{n}\right) + \varepsilon_2\left(\frac{1}{n}\right) \\ &= \frac{1}{n} \sum_{i=1}^n u_n\left(\frac{i}{n}\right) \cdot \psi'\left(\frac{i}{n}\right) + \varepsilon_3\left(\frac{1}{n}\right) \\ &= \langle \mu_n, \varphi \rangle + \varepsilon_3\left(\frac{1}{n}\right)\end{aligned}$$

The proof is complete. □

Let $\mu(dt) = u(t)dt \in (\mathcal{M}_\infty[0, 1])^d$. Recall that $\rho_u := \|u'\|$ and $v_u := u'/\|u'\|$. Let us define an approximating sequence (μ_n) of vector-valued bounded measures by setting $\mu_n(dt) = u_n(t)\bar{\nu}_n(dt)$ and

$$u_n(0) := 0$$

$$D_n^+(\tfrac{i}{n}) := \left(n \int_{\frac{i}{n}}^{\frac{i+1}{n}} \rho_u(t) dt \right) v_u(\tfrac{i}{n}) \quad \text{for } i = 0, 1, \dots, n-1.$$

The following result will be used to establish the upper bound inequality.

Lemma 2. *If $\mu \in (\mathcal{M}_\infty[0, 1])^d$, then the approximating sequence (μ_n) defined above satisfies the following property*

$$\mu_n - \mu \rightarrow 0.$$

Proof. Let $\varphi \in (C[0, 1])^d$ and define

$$\varepsilon_1(\tfrac{1}{n}) := \frac{1}{n} \sum_{i=1}^n \varphi(\tfrac{i}{n}) \cdot \left(\sum_{k=0}^{i-1} \int_{\frac{k}{n}}^{\frac{k+1}{n}} (v_u(\tfrac{k}{n}) - v_u(t)) \rho_u(t) dt \right),$$

$$\varepsilon_2(\tfrac{1}{n}) := \varepsilon_1(\tfrac{1}{n}) + \int \varphi(t) \cdot u(t) \bar{\nu}_n(dt) - \int_0^1 \varphi(t) \cdot u(t) dt.$$

Since the function v_u is continuous on $[0, 1]$ and the function ρ_u is integrable on $[0, 1]$, one has $\lim_{n \rightarrow \infty} \varepsilon_1(\frac{1}{n}) = 0$. Riemann's theorem implies $\lim_{n \rightarrow \infty} \varepsilon_2(\frac{1}{n}) = 0$. For any integer n , the following holds

$$\begin{aligned} \langle \mu_n, \varphi \rangle &:= \int \varphi(t) \cdot u_n(t) \bar{\nu}_n(dt) \\ &= \frac{1}{n} \sum_{i=1}^n \varphi(\tfrac{i}{n}) \cdot \left(\frac{1}{n} \sum_{k=0}^{i-1} D_n^+ u_n(\tfrac{k}{n}) \right) \\ &= \frac{1}{n} \sum_{i=1}^n \varphi(\tfrac{i}{n}) \cdot \left(\sum_{k=0}^{i-1} \int_{\frac{k}{n}}^{\frac{k+1}{n}} v_u(\tfrac{k}{n}) \rho_u(t) dt \right) \\ &= \frac{1}{n} \sum_{i=1}^n \varphi(\tfrac{i}{n}) \cdot \left(\sum_{k=0}^{i-1} \int_{\frac{k}{n}}^{\frac{k+1}{n}} v_u(t) \rho_u(t) dt \right) + \varepsilon_1(\tfrac{1}{n}) \\ &= \frac{1}{n} \sum_{i=1}^n \varphi(\tfrac{i}{n}) \cdot \left(\int_0^{\frac{i}{n}} v_u(t) \rho_u(t) dt \right) + \varepsilon_1(\tfrac{1}{n}) \\ &= \int \varphi(t) \cdot u(t) \bar{\nu}_n(dt) + \varepsilon_1(\tfrac{1}{n}) \\ &= \int_0^1 \varphi(t) \cdot u(t) dt + \varepsilon_2(\tfrac{1}{n}) := \langle \mu, \varphi \rangle + \varepsilon_2(\tfrac{1}{n}), \end{aligned}$$

which completes the proof. □

5.2. The proof of Theorem 4.1

We divide this proof in three steps.

Step 1. (*Relative compactness*). Since f is convex, $f(1) = 0$ and $f(\rho) > 0$ for every $\rho \neq 1$, it is easily seen that there exists $b \in \mathbb{R}$ and $a > 0$ such that $f(\rho) \geq b + a\rho$. Hence, for any $\mu(dt) = u(t)\bar{\nu}_n(dt) \in (\mathcal{M}_n[0, 1])^d$.

$$\begin{aligned} E_n(\mu) &\geq \int f(\|D_n^+ u(t)\|) \nu_n^+(dt) \\ &\geq b + a \int \|D_n^+ u(t)\| \nu_n^+(dt) \\ &\geq b + a \int \|u(t)\| \bar{\nu}_n(dt) = b + a \|\mu\|_{\mathcal{M}} \end{aligned}$$

Hence, for any sequence (μ_n) in $(\mathcal{M}[0, 1])^d$

$$\sup_n E_n(\mu_n) < +\infty \implies \sup_n \|\mu_n\|_{\mathcal{M}} < +\infty.$$

Step 2. (*Upper bound inequality*). Let $\mu(dt) = u(t)dt \in (\mathcal{M}_\infty[0, 1])^d$ and (μ_n) the approximating sequence used in Lemma 2. Note that

$$\begin{aligned} \|D_n^+ u_n(\tfrac{i}{n})\| &= n \int_{\frac{i}{n}}^{\frac{i+1}{n}} \rho(t) dt \quad \text{for } i = 0, 1, \dots, n-1, \\ T_n(u_n)(\tfrac{i}{n}) &= n \int_{\frac{i-1}{n}}^{\frac{i}{n}} v'(t) dt \quad \text{for } i = 1, \dots, n-1. \end{aligned}$$

Using Jensen inequality (recall that g and f are convex), we obtain

$$\begin{aligned} \limsup_{n \rightarrow \infty} \int g(\|T_n(u_n)(t)\|) \nu_n(dt) &= \limsup_{n \rightarrow \infty} \frac{1}{n} \sum_{i=1}^{n-1} g\left(\left\|n \int_{\frac{i-1}{n}}^{\frac{i}{n}} v'(t) dt\right\|\right) \\ &\leq \limsup_{n \rightarrow \infty} \frac{1}{n} \sum_{i=1}^{n-1} n \int_{\frac{i-1}{n}}^{\frac{i}{n}} g(\|v'(t)\|) dt \\ &\leq \int_0^1 g(\|v'(t)\|) dt \end{aligned} \tag{17}$$

and

$$\begin{aligned} \limsup_{n \rightarrow \infty} \int f(\|D_n^+ u_n(t)\|) \nu_n^+(dt) &= \limsup_{n \rightarrow \infty} \frac{1}{n} \sum_{i=0}^{n-1} f\left(n \int_{\frac{i}{n}}^{\frac{i+1}{n}} \rho(t) dt\right) \\ &\leq \limsup_{n \rightarrow \infty} \frac{1}{n} \sum_{i=0}^{n-1} n \int_{\frac{i}{n}}^{\frac{i+1}{n}} f(\rho(t)) dt \end{aligned}$$

$$= \int_0^1 f(\rho(t))dt \tag{18}$$

Therefore one has $\limsup_{n \rightarrow \infty} E_n(\mu_n) \leq E(\mu)$ and Lemma 2 gives us $\mu_n \rightharpoonup \mu$.

Step 3. (*Lower bound inequality*). Let $\mu, \mu_n \in (\mathcal{M}[0, 1])^d$ such that $\mu_n \rightharpoonup \mu$. Without loss of generality, we may assume that $\mu_n(dt) = u_n(t)\bar{\nu}_n(dt) \in (\mathcal{M}_n[0, 1])^d$ and there exists a nonnegative real number M such that

$$\lim_{n \rightarrow \infty} E_n(\mu_n) = M.$$

If $(\bar{\mu}_n), (\bar{u}_n), (\rho_n), (v_n)$ denote the sequences associated to (μ_n) defined before Lemma 1, one has

$$\bar{u}_n(t)dt = \bar{\mu}_n(dt) \rightharpoonup \mu(dt) \quad \text{and} \quad \lim_{n \rightarrow \infty} \int_0^1 f(\rho_n(t)) dt + \int_0^1 g(\|v'_n(t)\|) dt = M$$

Reasoning as in the proof of Lemma 1, it is easily seen that the following hold

- (ρ_n) is bounded in $L^1(0, 1)$ -norm and equi-integrable on $[0, 1]$,
- (v'_n) is bounded in $L^1(0, 1)$ -norm and equi-integrable on $[0, 1]$,
- (v_n) is uniformly bounded and equi-continuous on $[0, 1]$.

As a consequence, there exist $(\rho, v) \in L^1(0, 1) \times (W^{1,1}(0, 1))^d$ and some subsequence (not relabeled) such that

$$\begin{aligned} \rho_n(t)dt &\rightharpoonup \rho(t)dt, \\ v'_n(t)dt &\rightharpoonup v'(t)dt, \\ v_n &\text{converges to } v \text{ uniformly on } [0, 1], \end{aligned}$$

Using assumptions $(H_1), (H_3), (H_4), (H_5)$, we first obtain

$$\liminf_{n \rightarrow \infty} \int_0^1 f(\rho_n(t)) dt + \liminf_{n \rightarrow \infty} \int_0^1 g(\|v'_n(t)\|) dt \geq \int_0^1 f(\rho(t)) dt + \int_0^1 g(\|v'(t)\|) dt$$

Using Lemma 1, we obtain $\|v(t)\| = 1$ for every $t \in [0, 1]$ and $v(0) = e_1$. We also have $v_n(t)\rho_n(t)dt \rightharpoonup v(t)\rho(t)dt$. Since $\bar{u}'_n = \rho_n v_n$ and $u_n(0) = 0$, we deduce that

$$\mu(dt) = u(t)dt \quad \text{where} \quad u(t) := \int_0^t v(t)\rho(t)dt \quad \text{for every } t \in [0, 1].$$

As a consequence

$$\int_0^1 f(\rho(t)) dt + \int_0^1 g(\|v'(t)\|) dt = E(\mu)$$

and the proof of the main theorem is complete.

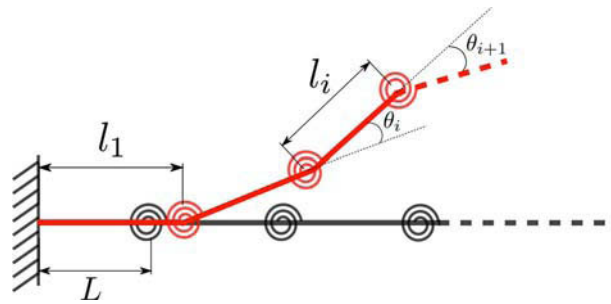


FIG. 1. Scheme of the discrete system approximating a continuous extensible Euler beam

6. Numerical results

In this section, we want to provide some simple numerical results, showing the convergence of the discrete model described by the functional E_n to the continuous one described by the functional E , as we proved in the previous section.

Specifically, let us again consider a system of n identical extensible rods linked by means of rotational springs, as shown in Fig. 1. We will call θ_i ($i = 1, \dots, n-1$) the angles between the (i) th and the $(i+1)$ th rod, and θ_0 the angle that the first rod forms with the horizontal axis; the angles θ_i are all zero in the reference unstressed configuration. We will call u_i and w_i the component of the displacement of the i th node which is, respectively, orthogonal or parallel to the initial reference configuration of the system. The boundary conditions are those of a clamp on the left extremum, with the clamp direction parallel to the reference configuration, i.e. $u_0 = w_0 = 0$ and $\theta_0 = 0$.

We considered two energy models:

1. A case without material nonlinearities, in which the functions $f(x)$ and $g(x)$ before introduced are, respectively, $\frac{x^2}{2}$ and the identity;
2. A case in which $f(x) := k_1 \frac{x^2}{2} + k_2 \frac{x^4}{4}$ (while g is again the identity).

In all the cases we consider, the total energy of the system can be therefore written as:

$$W_n = \sum_{i=0}^{i=n-1} \left[k_1^n \frac{|L - l_i|^2}{2} + k_2^n \frac{|L - l_i|^4}{4} + k_3^n (1 - \cos \theta_i) \right] - bu_i - pw_i \quad (19)$$

Here L is the original (unstressed) length of the rods and l_i is the current length of the i th rod, b and p represent, respectively, the transversal and axial components of the dead load in the reference configuration applied in the nodes.

We initially set $b = 1$ and $p = 0$, i.e., we introduced a unitary dead load applied at the nodes which is orthogonal to the reference configuration. In the first case (purely quadratic energy), the chosen value for the axial stiffness is $k_1^n = n(2 \times 10^5)$ ($k_2^n = 0$), while the value for the bending stiffness is $k_3^n = n(1 \times 10^{-1})$. In the second case, we set for simplicity $k_1^n = 0$, while $k_2^n = n(4 \times 10^5)$.

The numerical procedure for minimizing the total energy was the simplex search method of Lagarias (see [29]).

In Fig. 2, we show the corresponding deformed shape of the Hencky-type beam with $n = 10, 20$ and 100 . The results in Fig. 3 show that, both in case of quadratic and quartic energy, the discrete energy is rapidly converging toward a very definite value when the number of elements n increases. In particular, already between $n = 50$ and $n = 100$ there is no appreciable difference in the total energy of the system. This is in agreement with the previous mathematical results.

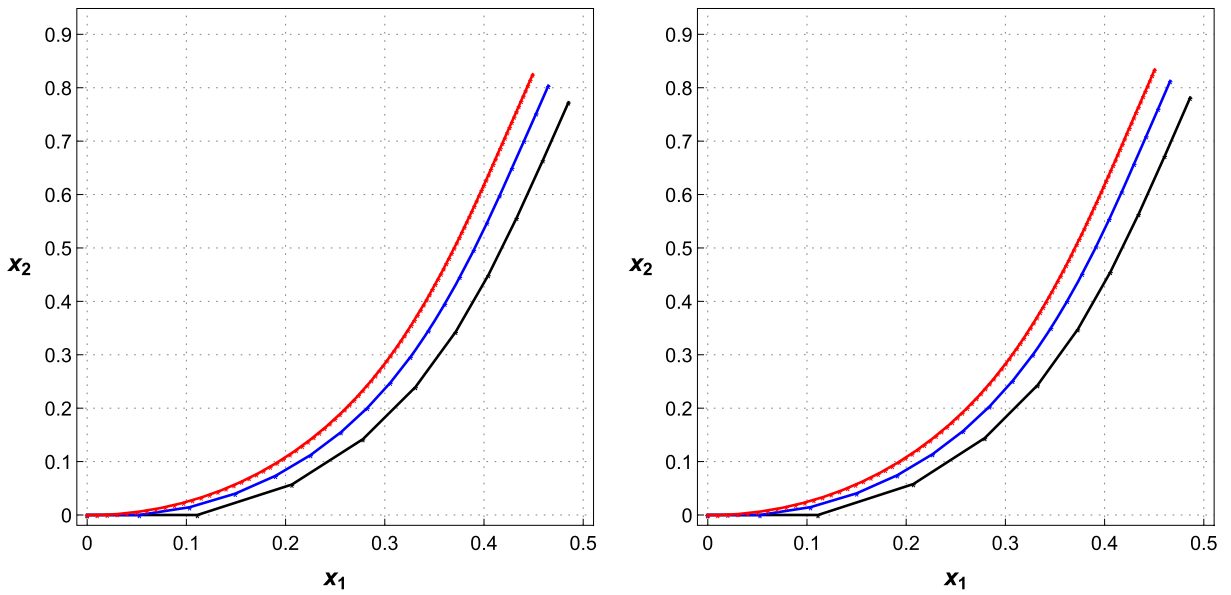


FIG. 2. Simulation of a Hencky-type discrete beam model under transverse distributed load. *Left* deformed configurations for discrete systems with $n = 10, 20$ and 100 in case of purely quadratic extensional energy. *Right* the same for a quartic extensional energy model

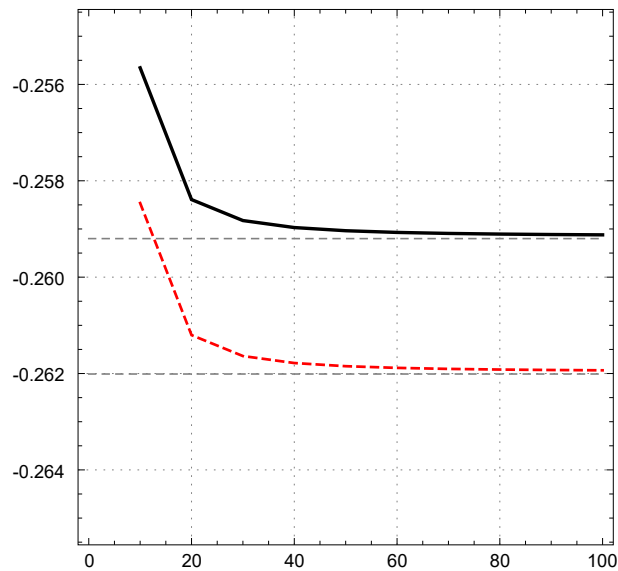


FIG. 3. Plot of the total energy of the system versus the number n of elements in case of quadratic (*dashed line*) or quartic (*solid line*) extensional energy with a transverse distributed load. The energy clearly converges to a definite value as n increases. The two *thin lines* represent the numerically evaluated asymptotic values of the energy for the two cases

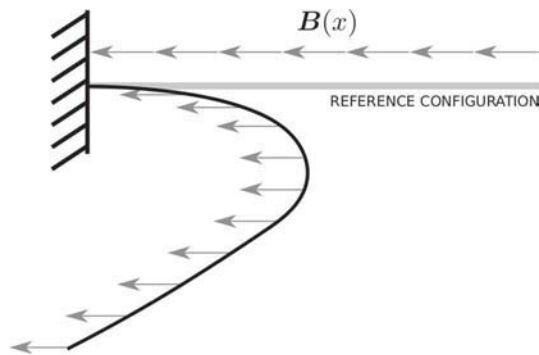


FIG. 4. Graphical representation of the buckling simulated below with a Hencky-type discrete beam model

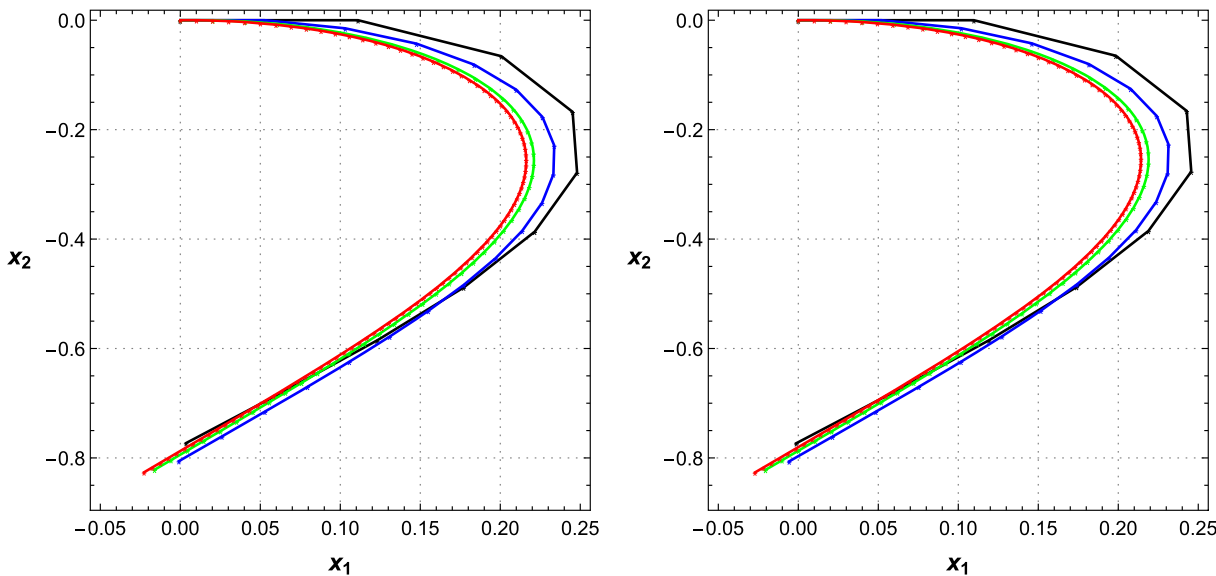


FIG. 5. Simulation of a Hencky-type discrete beam model under axial distributed compressive load. *Left* deformed configurations for discrete systems with $n = 10, 20$ and 100 in case of purely quadratic extensional energy. *Right* the same for a quartic extensional energy model

Then we studied a case in which *local* minima of the total energy are involved, namely a classic buckling problem for a clamped beam with a distributed (compressive) load parallel to the reference configuration (a graphical representation is given in Fig. 4). In this case, we thus set $p = 0.7$ and $b = 0$, while for the stiffnesses we used the same sets of values as before. Also in this case the discrete model converges to a well definite limit configuration when the number of elements diverges. The two panels in Fig. 5 correspond to the deformed shape with a quadratic (left) and quartic (right) energy model. The energy versus number of nodes n plot is shown in Fig. 6.

Finally, we want to compare the discrete energy as a function of n with an exponential function. Applying least squares method to the discrete energies found in case of quadratic energy and transverse load (with n ranging from 3 to 100), we find the curve $ae^{bx} + c$, with $a = 0.84$, $b = -0.75$ and $c = -0.26$. The result, together with a plot of the corresponding rate of convergence, is graphically represented in Fig. 7. Of course a rigorous estimate of the error of convergence would require, in addition to the estimate

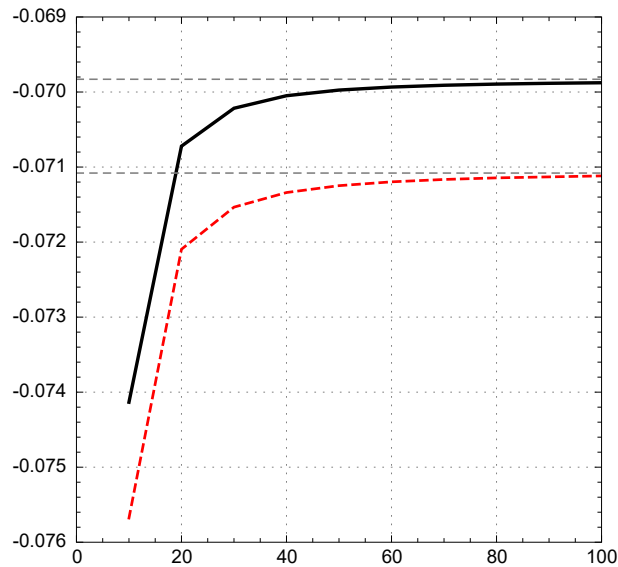


FIG. 6. Plot of the total energy of the system versus the number n of elements in case of quadratic (*dashed line*) or quartic (*solid line*) extensional energy with an axial distributed compressive load. The energy clearly converges to a definite value as n increases. The two *thin lines* represent the numerically evaluated asymptotic values of the energy for the two cases

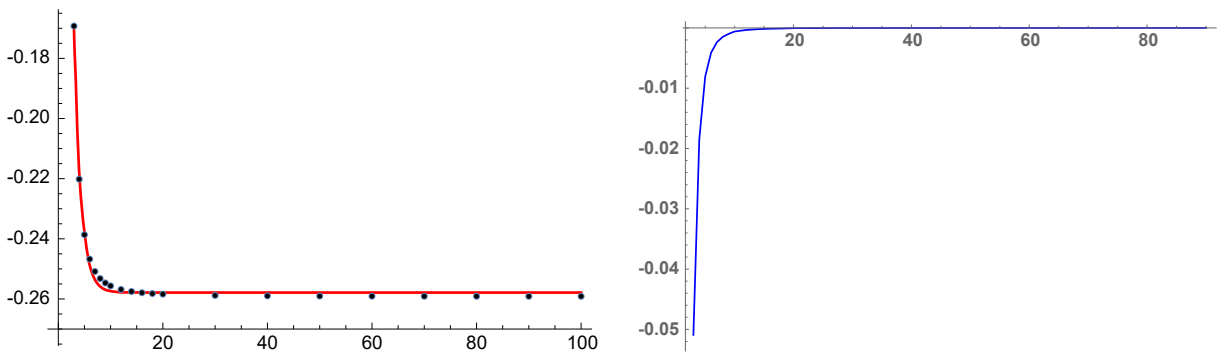


FIG. 7. *Left* comparison of the discrete energy (quadratic case) with the curve $ae^{bx} + c$, where $a = 0.84$, $b = -0.75$ and $c = -0.26$. The number of nodes n ranges from 3 to 100. *Right* plot of the corresponding rate of convergence

of the error due to the discretization itself, an estimate of how sharp is the employed version of the Jensen inequality (for instance in Eqs. 17 and 18) [30].

7. Conclusions

In this paper, we proved the Γ -convergence of a discrete system consisting of rigid bars and rotational springs toward Euler’s inextensible *Elastica* in large deformation. The result has been established including possible material nonlinearities involving convex, lower semicontinuous and sufficiently fast diverging at infinity dependence of the energy density on the extensional and bending deformation measures.

Further progresses along the lines here followed may involve the generalization of the result to Timoshenko beams (see [31,32] for a rational review on the subject and [33] for an application to curved

reference configurations), and also to more complex beam models, such as those usually gathered under the label of *Generalized Beam Theory* (GBT) [34–38] or to functionally graded beams [39, 40]. Moreover, a particularly interesting direction is the one concerning higher order continua, i.e., material models in which the deformation energy depends on second and higher gradients of the displacement (classical references on the topic are [41, 42]; see also [43–48] for theoretical investigations, and [22, 49, 50] for numerical results; a recent review is [51]). Indeed, the result of [52] (proof of the Γ -convergence of a discrete truss system to a second gradient model) can be generalized to cases in which the microstructure is also capable of storing extensional energy, thus covering a wider class of real-world truss systems. We also notice that higher order models are in turn a particular case of micromorphic models, in which additional kinematical descriptors are introduced (a standard reference is [53], see also [54–60] for interesting applications). As it was shown for the case of fibrous systems cited in the introduction, in this case the microstructure can often be described by Euler beam models.

Of course the results established herein only concern static problems. Addressing convergence problems in dynamic cases (see for instance [61] for a case concerning a 1D second gradient model) is in general more complicated, but can lead to a rigorous mathematical formulation for the numerical study of a class of interesting dynamic problems involving instabilities of various kinds [62–64].

References

- [1] Alibert, J.-J., Della Corte, A., Seppecher, P: Convergence of Hencky-type discrete beam model to Euler inextensible elastica in large deformation: Rigorous proof. In: *Mathematical Modelling in Solid Mechanics*. Springer Nature Singapore PTE. LTD. (2017)
- [2] Reda, H., Rahali, Y., Ganghoffer, J.-F., Lakiss, H.: Analysis of dispersive waves in repetitive lattices based on homogenized second-gradient continuum models. *Compos. Struct.* **152**, 712–728 (2016)
- [3] Reda, H., Rahali, Y., Ganghoffer, J.F., Lakiss, H.: Nonlinear dynamical analysis of 3D textiles based on second order gradient homogenized media. *Compos. Struct.* **154**, 538–555 (2016)
- [4] Reda, H., Rahali, Y., Ganghoffer, J.-F., Lakiss, H.: Wave propagation in 3D viscoelastic auxetic and textile materials by homogenized continuum micropolar models. *Compos. Struct.* **141**, 328–345 (2016)
- [5] Reda, H., Goda, I., Ganghoffer, J.F., L’Hostis, G., Lakiss, H.: Dynamical analysis of homogenized second gradient anisotropic media for textile composite structures and analysis of size effects. *Compos. Struct.* **161**, 540–551 (2017)
- [6] Yang, Y., Misra, A.: Higher-order stress–strain theory for damage modeling implemented in an element-free Galerkin formulation. *Comput. Model. Eng. Sci.* **64**(1), 1–36 (2010)
- [7] Yang, Y., Misra, A.: Micromechanics based second gradient continuum theory for shear band modeling in cohesive granular materials following damage elasticity. *Int. J. Solids Struct.* **49**(18), 2500–2514 (2012)
- [8] Misra, A., Poorolhjouy, P.: Identification of higher-order elastic constants for grain assemblies based upon granular micromechanics. *Math. Mech. Complex Syst.* **3**(3), 285–308 (2015)
- [9] Hencky H.: *Über die angenäherte Lösung von Stabilitätsproblemen im Raum mittels der elastischen Gelenkkette*. PhD thesis, Engelmann (1921)
- [10] Emilio, T., dell’Isola, F., Cazzani, A., Rizzi, N.L.: Hencky-type discrete model for pantographic structures: numerical comparison with second gradient continuum models. *Z. Angew. Math. Phys.* **67**(4), 1–28 (2016)
- [11] Wang, C.M., Zhang, Hui, Gao, R.P., Duan, W.H., Challamel, N.: Hencky bar-chain model for buckling and vibration of beams with elastic end restraints. *Int. J. Struct. Stab. Dyn.* **15**(07), 1540007 (2015)
- [12] Zhang, H., Wang, C.M., Challamel, N.: Buckling and vibration of Hencky bar-chain with internal elastic springs. *Int. J. Mech. Sci.* **119**, 383–395 (2016)
- [13] Fertis, D.G.: *Nonlinear Structural Engineering*. Springer, Berlin (2006)
- [14] Milton, G.W.: Adaptable nonlinear bimode metamaterials using rigid bars, pivots, and actuators. *J. Mech. Phys. Solids* **61**(7), 1561–1568 (2013)
- [15] Del Vescovo, D., Giorgio, I.: Dynamic problems for metamaterials: review of existing models and ideas for further research. *Int. J. Eng. Sci.* **80**, 153–172 (2014)
- [16] dell’Isola, F., Bucci, S., Battista, A.: Against the fragmentation of knowledge: the power of multidisciplinary research for the design of metamaterials. In: *Advanced Methods of Continuum Mechanics for Materials and Structures*, pp. 523–545. Springer (2016)
- [17] dell’Isola, F., Steigmann, D., Della Corte, A.: Synthesis of fibrous complex structures: designing microstructure to deliver targeted macroscale response. *Appl. Mech. Rev.* **67**(6), 060804 (2015)

- [18] Davydov, D., Javili, A., Steinmann, P.: On molecular statics and surface-enhanced continuum modeling of nano-structures. *Comput. Mater. Sci.* **69**, 510–519 (2013)
- [19] Giorgio, I., Della Corte, A., dell’Isola, F.: Buckling modes in pantographic lattices. *Comptes Rendus Mecanique* **344**(7), 487–501 (2016)
- [20] dell’Isola, F., Steigmann, D.: A two-dimensional gradient-elasticity theory for woven fabrics. *J. Elast.* **118**(1), 113–125 (2015)
- [21] dell’Isola, F., Giorgio, I., Andreaus, U.: Elastic pantographic 2D lattices: a numerical analysis on the static response and wave propagation. *Proc. Estonian Acad. Sci.* **64**(3), 219 (2015)
- [22] Cuomo, M., dell’Isola, F., Leopoldo, G.: Simplified analysis of a generalized bias test for fabrics with two families of inextensible fibres. *Z. Angew. Math. Phys.* **67**(3), 1–23 (2016)
- [23] Steigmann, D.J., Pipkin, A.C.: Equilibrium of elastic nets. *Philos. Trans. R. Soc. Lond. A Math. Phys. Eng. Sci.* **335**(1639), 419–454 (1991)
- [24] Steigmann, J.: On the nonlinear mechanics of discrete networks. *Arch. Appl. Mech.* **67**(5), 303–319 (1997)
- [25] Braides, A.: *Gamma-Convergence for Beginners*, vol. 22. Clarendon Press, Oxford (2002)
- [26] Schwartz, L.: *Radon Measures on Arbitrary Topological Spaces and Cylindrical Measures*, vol. 6. Oxford University Press, Oxford (1973)
- [27] dell’Isola, F., Giorgio, I., Pawlikowski, M., Rizzi, N.L.: Large deformations of planar extensible beams and pantographic lattices: heuristic homogenization, experimental and numerical examples of equilibrium. In: *Proceedings of the Royal Society A*, vol. 472, p. 20150790. The Royal Society (2016)
- [28] Giaquinta, M., Modica, G., Soucek, J.: *Cartesian Currents in the Calculus of Variations, Modern Surveys in Mathematics*, vol. 37. Springer, Berlin (1998)
- [29] Lagarias, J.C., Reeds, J.A., Wright, M.H., Wright, P.E.: Convergence properties of the Nelder–Mead simplex method in low dimensions. *SIAM J. Optim.* **9**(1), 112–147 (1998)
- [30] Costarelli, D., Spigler, R.: How sharp is the Jensen inequality? *J. Inequal. Appl.* **2015**(1), 69 (2015)
- [31] Cazzani, A., Stochino, F., Turco, E.: On the whole spectrum of Timoshenko beams. Part I: a theoretical revisit. *Z. Angew. Math. Phys.* **67**(2), 1–30 (2016)
- [32] Cazzani, A., Stochino, F., Turco, E.: On the whole spectrum of Timoshenko beams. Part II further applications. *Z. Angew. Math. Phys.* **67**(25), 1–21 (2016)
- [33] Cazzani, A., Malagù, M., Turco, E.: Isogeometric analysis of plane-curved beams. *Math. Mech. Solids* **21**(5), 562–577 (2016)
- [34] Piccardo, G., Ranzi, G., Luongo, A.: A complete dynamic approach to the generalized beam theory cross-section analysis including extension and shear modes. *Math. Mech. Solids* **19**(8), 900–924 (2014)
- [35] Piccardo, G., Ranzi, G., Luongo, A.: A direct approach for the evaluation of the conventional modes within the GBT formulation. *Thin-Walled Struct.* **74**, 133–145 (2014)
- [36] Taig, G., Ranzi, G., Dias-da Costa, D., Piccardo, G., Luongo, A.: A GBT model for the analysis of composite steel–concrete beams with partial shear interaction. In: *Structures*, vol. 4, pp. 27–37. Elsevier (2015)
- [37] Taig, G., Ranzi, G., Luongo, A.: GBT pre-buckling and buckling analyses of thin-walled members under axial and transverse loads. *Contin. Mech. Thermodyn.* **28**(1–2), 41–66 (2016)
- [38] Piccardo, G., Ferrarotti, A., Luongo, A.: Nonlinear generalized beam theory for open thin-walled members. *Math. Mech. Solids*. (2016). doi:[10.1177/1081286516649990](https://doi.org/10.1177/1081286516649990)
- [39] Birsan, M., Altenbach, H., Sadowski, T., Eremeyev, V.A., Pietras, D.: Deformation analysis of functionally graded beams by the direct approach. *Compos. Part B Eng.* **43**(3), 1315–1328 (2012)
- [40] Altenbach, H., Birsan, M., Eremeyev, V.A.: On a thermodynamic theory of rods with two temperature fields. *Acta Mech.* **223**(8), 1583–1596 (2012)
- [41] Eringen, A.C.: *Nonlocal Continuum Field Theories*. Springer, Berlin (2002)
- [42] Mindlin, R.D.: Micro-structure in linear elasticity. *Arch. Ration. Mech. Anal.* **16**(1), 51–78 (1964)
- [43] dell’Isola, F., Seppecher, P.: The relationship between edge contact forces, double forces and interstitial working allowed by the principle of virtual power. In: *Comptes Rendus de l’Académie des Sciences. Série IIb, Mécanique, Physique, Astronomie*, p. 7. (1995)
- [44] dell’Isola, F., Seppecher, P., Madeo, A.: Beyond Euler–Cauchy continua: the structure of contact actions in n-th gradient generalized continua: a generalization of the Cauchy tetrahedron argument. In: *Variational Models and Methods in Solid and Fluid Mechanics*, pp. 17–106. Springer (2011)
- [45] dell’Isola, F., Madeo, A., Seppecher, P.: Cauchy tetrahedron argument applied to higher contact interactions. *Arch. Ration. Mech. Anal.* **219**(3), 1305–1341 (2016)
- [46] Placidi, L., Andreaus, U., Giorgio, I.: Identification of two-dimensional pantographic structure via a linear D4 orthotropic second gradient elastic model. *J. Eng. Math.* (2016). doi:[10.1007/s10665-016-9856-8](https://doi.org/10.1007/s10665-016-9856-8)
- [47] Javili, A., dell’Isola, F., Steinmann, P.: Geometrically nonlinear higher-gradient elasticity with energetic boundaries. *J. Mech. Phys. Solids* **61**(12), 2381–2401 (2013)

- [48] Placidi, L.: A variational approach for a nonlinear one-dimensional damage-elasto-plastic second-gradient continuum model. *Contin. Mech. Thermodyn.* **28**(1–2), 119–137 (2016)
- [49] Placidi, L., Greco, L., Bucci, S., Turco, E., Rizzi, N.L.: A second gradient formulation for a 2D fabric sheet with inextensible fibres. *Z. Angew. Math. Phys.* **67**(5), 114 (2016)
- [50] dell’Isola, F., Cuomo, M., Greco, L., Della Corte, A.: Bias extension test for pantographic sheets: numerical simulations based on second gradient shear energies. *J. Eng. Math.* pp. 1–31 (2016). doi:[10.1007/s10665-016-9865-7](https://doi.org/10.1007/s10665-016-9865-7)
- [51] Placidi, L., Barchiesi, E., Turco, E., Rizzi, N.L.: A review on 2D models for the description of pantographic fabrics. *Z. Angew. Math. Phys.* **67**(5), 121 (2016)
- [52] Alibert, J.-J., Della Corte, A.: Second-gradient continua as homogenized limit of pantographic microstructured plates: a rigorous proof. *Z. Angew. Math. Phys.* **66**(5), 2855–2870 (2015)
- [53] Eringen, A.C.: Mechanics of micromorphic continua. In: *Mechanics of Generalized Continua*, pp. 18–35. Springer, Berlin (1968)
- [54] Placidi, L., Faria, S.H., Hutter, K.: On the role of grain growth, recrystallization and polygonization in a continuum theory for anisotropic ice sheets. *Ann. Glaciol.* **39**(1), 49–52 (2004)
- [55] Placidi, L., Hutter, K., Faria, S.H.: A critical review of the mechanics of polycrystalline polar ice. *GAMM-Mitteilungen* **29**(1), 80–117 (2006)
- [56] Placidi, L., Greve, R., Seddik, H., Faria, S.H.: Continuum-mechanical, anisotropic flow model for polar ice masses, based on an anisotropic flow enhancement factor. *Contin. Mech. Thermodyn.* **22**(3), 221–237 (2010)
- [57] Misra, A., Poorsolhjouy, P.: Granular micromechanics based micromorphic model predicts frequency band gaps. *Contin. Mech. Thermodyn.* **28**(1–2), 215–234 (2016)
- [58] Forest, S.: Micromorphic approach for gradient elasticity, viscoplasticity, and damage. *J. Eng. Mech.* **135**(3), 117–131 (2009)
- [59] Altenbach, J., Altenbach, H., Eremeyev, V.A.: On generalized cosserat-type theories of plates and shells: a short review and bibliography. *Arch. Appl. Mech.* **80**(1), 73–92 (2010)
- [60] Seddik, H., Greve, R., Placidi, L., Hamann, I., Gagliardini, O.: Application of a continuum-mechanical model for the flow of anisotropic polar ice to the EDML core, Antarctica. *J. Glaciol.* **54**(187), 631–642 (2008)
- [61] Carcaterra, A., dell’Isola, F., Esposito, R., Pulvirenti, M.: Macroscopic description of microscopically strongly inhomogeneous systems: a mathematical basis for the synthesis of higher gradients metamaterials. *Arch. Ration. Mech. Anal.* **218**(3), 1239–1262 (2015)
- [62] Luongo, A., D’Annibale, F.: A paradigmatic minimal system to explain the Ziegler paradox. *Contin. Mech. Thermodyn.* **27**(1–2), 211–222 (2015)
- [63] Luongo, A., D’Annibale, F.: Double zero bifurcation of non-linear viscoelastic beams under conservative and non-conservative loads. *Int. J. Non-Linear Mech.* **55**, 128–139 (2013)
- [64] Luongo, A., Piccardo, G.: Linear instability mechanisms for coupled translational galloping. *J. Sound Vib.* **288**(4), 1027–1047 (2005)

Jean-Jacques Alibert
 IMATH
 Université de Toulon
 Toulon
 France

Alessandro Della Corte and Ivan Giorgio
 DIMA
 Sapienza University of Rome
 Rome
 Italy

Alessandro Della Corte, Ivan Giorgio and Antonio Battista
 M&MoCS
 University of L’Aquila
 L’Aquila
 Italy
 e-mail: antoniobattista1986@gmail.com

Antonio Battista
Laboratoire des Sciences de l'Ingénieur pour l'Environnement
Université de La Rochelle
La Rochelle
France

(Received: February 3, 2017; revised: February 17, 2017)

Chapter 3

Plane bias extension test for a continuum with two inextensible families of fibers: A variational treatment with Lagrange multipliers and a perturbation solution

Plane Bias Extension Test for a continuum with two inextensible families of fibers:
a variational treatment with Lagrange Multipliers and a Perturbation Solution

Francesco dell'Isola*, Alessandro Della Corte[†], Leopoldo Greco[‡] and Angelo Luongo[§]

February 22, 2017

Abstract

In the present paper, a system constituted by two families of nearly inextensible fibers is studied. The interest towards this kind of structures, which can be suitably modeled by 2D continua with inextensible curves, comes from both theoretical and applicative motivations. Indeed, the advantageous weight/strength ratio and the particularly safe behavior in fractures make them attractive in many engineering fields, while the mechanical properties displayed by them are theoretically interesting and still not well understood in full generality. We focused on dead-loading traction boundary-value problems assuming particular forms for the deformation energy associated to every node of the structure. The main result of the paper consists in the determination of the nonlinear integral equations describing fibers directions for a specific class of deformation energies. A perturbative analysis of a particular solution is also performed, and some physical justification for one of the considered forms for the energy density are provided in the Appendix.

*Department of Structural and Geotechnical Engineering, University La Sapienza of Rome (Italy).

[†]Doctoral School in Theoretical and Applied Mechanics, University La Sapienza of Rome - email: alessandro.dellacorte@uniroma1.it Phone: +393479421586 (corresponding author).

[‡]International Research Center on Mathematics and Mechanics of Complex Systems (M&MoCS), University of L'Aquila (Italy).

[§]International Research Center on Mathematics and Mechanics of Complex Systems (M&MoCS), University of L'Aquila (Italy).

KEYWORDS: Inextensible fibers; Generalized continua; Variational treatment; Perturbation analysis

1 Introduction

The conceptual framework of this paper coincides with the one set in the pioneering works by Pipkin and Rivlin, in particular in [1,2]. We introduce a bidimensional continuum B whose placement is always plane. This continuum models finite and plane deformations of sheets or nets formed by two intersecting families of fibers orthogonal in the reference configuration. The intersection point of two initially orthogonal fibers is always the same material particle, which is identified with a material particle of the introduced 2D continuum. The fibers are assumed to be inextensible and the network resists shearing: this is modeled by a deformation energy which depends (only) on the shear angle between the fibers. The equilibrium configurations are characterized via the condition of stationarity of total energy.

The growing interest in such systems stems both from theoretical and technological fields. From a theoretical point of view a deep understanding of the mechanics of such systems can need the further development of an exhaustive and coherent theory of generalized continua. It is well known in fact that by means of suitable homogenization procedure one can recover, from a system similar to the one considered in this paper, higher gradient continuum models (the reader interested is referred to [3–10]). It is important to notice that higher continuum theories can be contextualized in the widest field of micromorphic continua (a general coverage of the field can be found e.g. in [11–24]). From a technological point of view such systems are finding very wide applications in different fields (see e.g. [25–32]), including biomedical applications (see for instance [33–40]).

In dead-loading traction boundary-value problems, the vectors representing the directions of the fibers of our system satisfy a pair of coupled integral equations, which are highly nonlinear. The main result of the paper consists in the determination of such equations for a specific class of

deformation energies. The model considered in the present paper is exposed and studied in detail in [41]. In the first section we provide a condensed exposition of the formalism there introduced and of the basic properties of the system, together with a suitable set of boundary conditions that define what is called a *standard bias test*. In the same section inextensibility and some symmetries of the system are taken into account in order to define a set of constraints and conditions that, in the framework of the principle of stationary action, will bring to the mentioned equations. To the stability of the solution of these equations are devoted sections 3 and 4, in which a perturbative analysis near a homogeneous constant solution is performed. Finally it is shown how the class of energies we consider can be suitable for describing a particular 3D-printed sample.

2 A variational deduction of equilibrium conditions

For the considered mechanical system the most suitable postulation process is to be framed in the Lagrangian Continuum Analytical Mechanics (see [42–44]). The concept of balance of force itself, in the present context, becomes even more difficult to grasp than usual.¹

The main difficulty to be confronted with concerns the need to take into account (in the considered mathematical model) the inextensibility of all material lines belonging to two families of parallel curves. These families are a natural choice for a reference system in the Lagrangian configuration of B . In the fundamental paper by J. Ball ([45]) it is clearly stated that

<<Note, however, that the constraint of inextensibility [...] is not included [in the presented treatment]. It seems possible, therefore, that solutions do not in general exist for boundary-value problems of inextensible elasticity, and that a higher order theory is required to make such constraints well behaved.>>.

¹As a brief historical remark, we simply want to recall that in the *Traité de Dynamique* by D’Alembert one finds the following (very impressive) statement:

I have proscribed completely the forces relative to the bodies in motion, entities obscure and metaphysical, which are capable only to throw darkness on a Science which is clear by itself.

We therefore attack the problem as follows: we characterize the kinematics of considered continuum by finding a suitable set (the space of configurations) which specifies all admissible states. Since it does not seem that we have available (for safely proceeding in our treatment) any general and sound mathematical result, after having characterized the kinematics of the system, we simply choose a set of deformation energies and look for the minimum in the set of placements verifying some precise boundary (kinematical) conditions.

Besides the inextensibility, another feature of the mechanical system we want to investigate can cause difficulties. The modeling of elastic systems with an intrinsically mixed continuous-discrete nature, like the one herein considered, can indeed involve hard mathematical problems. We will try to outline the key difficulties along the path of achieving a more advanced (generalized) continuum theory in the following sections; however, the classical mathematical tools developed for the mathematical description of elasticity are still of course very useful, and in this regard useful references are [46–48].

2.1 Geometry of Standard Bias Test. Placements.

Let us consider the set of material particles of the considered continuum B included in the Lagrangian space $\mathcal{E}_{\mathcal{L}}$. We introduce an orthonormal system (\mathcal{O}, X_1, X_2) in $\mathcal{E}_{\mathcal{L}}$ to label material particles. In every configuration each material particle is placed, by a map \mathbf{r} , into positions belonging to the Eulerian space \mathcal{E} :

$$B \xrightarrow{\mathbf{r}} \mathbf{r}(B) \subseteq \mathcal{E}.$$

In this paper, we assume that B is a rectangle whose sides have length l and L , described by the following conditions:

$$B = \left\{ (X_1, X_2) \in \mathcal{E}_{\mathcal{L}} : X_1 \in [0, L], X_2 \in \left[-\frac{l}{2}, \frac{l}{2} \right] \right\}.$$

We explicitly observe that the length ratio plays a relevant role. In this paper we will limit ourselves to the case of standard bias test, i.e. $L = 3l$.

The continuum body B is intended as a suitable homogeneous limit for a mechanical system composed by two (nearly-)inextensible families of fibers which form a uniform orthogonal net intersecting the perimeter of B with an angle of $\pi/4$. In order to take into account the material properties related to inextensibility, it is useful to introduce an adapted orthogonal reference system, $(\mathcal{O}, \xi_1, \xi_2)$, which is oriented according to the directions of the inextensible fibers and which uses dimensionless space coordinates. This is done by means of the following definitions:

$$\xi_1 := \frac{1}{l}(X_1 - X_2) + \frac{1}{2}, \quad \xi_2 := \frac{1}{l}(X_1 + X_2) + \frac{1}{2}. \quad (1)$$

This secondly introduced reference system will be called *fiber reference* and the two directions ξ_1, ξ_2 *fiber directions*. Clearly it will be useful to represent all deformation measures in $(\mathcal{O}, \xi_1, \xi_2)$, since ξ_1, ξ_2 represent the orthotropic directions of the material. We can use the coordinates (ξ_1, ξ_2) to label a generic material particle of B and we will indicate with $\mathbf{D}_1(\xi_1, \xi_2)$ and $\mathbf{D}_2(\xi_1, \xi_2)$ the unit vectors tangent to the two families of fibers in the reference configuration at point (ξ_1, ξ_2) .

2.2 Inextensibility and consequent representation of admissible placements

Let $\gamma \subset B$ be a rectifiable curve whose length is l : we say that γ is inextensible for an admissible placement \mathbf{r} of B if for every arc α of γ we have that $\mathbf{r}(\alpha)$ has the same length as α . To formulate this condition for every curve with support belonging to the reference configuration C^* , it is necessary that the considered placement maps rectifiable curves into rectifiable curves. It seems that the space of all placements verifying such condition is the most suitable one for describing the kinematics of continua with inextensible curves. While it is quite easily seen that continuous functions of Bounded Variation (from $D \subset \mathbb{R}^2$ taking values in \mathbb{R}^2) have the aforementioned property, it is harder to prove that the inverse implication holds, and in the present work this is merely suggested as a reasonable

conjecture.

The previous considerations indicate that the regularity requirements for the set of admissible placements must be consistent with inextensibility constraint. However in the present work, having in mind the results by Rivlin [2], we will simply assume that the placement field \mathbf{r} is piecewise twice continuously differentiable in B . If we indicate with \mathbf{F} the gradient of \mathbf{r} in the points where it is defined we get obviously that

$$\mathbf{d}_1 = \mathbf{F} \cdot \mathbf{D}_1, \quad \mathbf{d}_2 = \mathbf{F} \cdot \mathbf{D}_2. \quad (2)$$

where the two vectors \mathbf{d}_1 and \mathbf{d}_2 represent the directions of the fibers in the current configuration.

Under Rivlin's regularity requirements the inextensibility of the fibers implies that the considered admissible placements have a rather particular form. Indeed the inextensibility constraint implies that a placement field of class C^1 in the neighborhood of a material particle P must verify the following conditions in P :

$$\|\mathbf{F} \cdot \mathbf{D}_1\|^2 = \|\mathbf{d}_1\|^2 = \|\mathbf{F} \cdot \mathbf{D}_2\|^2 = \|\mathbf{d}_2\|^2 = 1. \quad (3)$$

Moreover, when $\mathbf{r} \in C^2(\Delta)$, where Δ is an open simply linearly connected subset of B , the inextensibility of the fibers implies that it is possible to decompose the placement field in the following manner (see [2]): there exist two vector fields $\mathbf{r}_1^{(\Delta)}(\xi_1)$ and $\mathbf{r}_2^{(\Delta)}(\xi_2)$ respectively defined on the projection of Δ on the fiber axes ξ_1 and ξ_2 such that

$$\mathbf{r}_{(\Delta)}(\xi_1, \xi_2) = \mathbf{r}_1^{(\Delta)}(\xi_1) + \mathbf{r}_2^{(\Delta)}(\xi_2). \quad (4)$$

We can represent these two vector fields in the basis $(\mathbf{D}_1, \mathbf{D}_2)$ as follows:

$$\begin{cases} \mathbf{r}_1^{(\Delta)}(\xi_1) = \mu_1^{(\Delta)}(\xi_1) \mathbf{D}_1 + \nu_1^{(\Delta)}(\xi_1) \mathbf{D}_2 \\ \mathbf{r}_2^{(\Delta)}(\xi_2) = \nu_2^{(\Delta)}(\xi_2) \mathbf{D}_1 + \mu_2^{(\Delta)}(\xi_2) \mathbf{D}_2, \end{cases} \quad (5)$$

being $\mu_1^{(\Delta)}, \mu_2^{(\Delta)}, \nu_1^{(\Delta)}, \nu_2^{(\Delta)}$ suitably regular scalar functions on the projections of Δ on the fiber axes ξ_1 and ξ_2 .

If we indicate with $I_{1\Delta}$ the projection of Δ on the axis ξ_1 and with $I_{2\Delta}$ the projection of Δ on the axis ξ_2 , we have

$$\|\mathbf{F} \cdot \mathbf{D}_1\|^2 = 1 \Rightarrow \left(\mu_{1,1}^{(\Delta)}\right)^2 + \left(\nu_{1,1}^{(\Delta)}\right)^2 = 1 \quad (6)$$

$$\Rightarrow \exists \vartheta_1(\xi_1) : (\forall \xi_1 \in I_{1\Delta}) \mathbf{F} \cdot \mathbf{D}_1 = \cos(\vartheta_1(\xi_1)) \mathbf{D}_1 + \sin(\vartheta_1(\xi_1)) \mathbf{D}_2$$

$$\|\mathbf{F} \cdot \mathbf{D}_2\|^2 = 1 \Rightarrow \left(\mu_{2,2}^{(\Delta)}\right)^2 + \left(\nu_{2,2}^{(\Delta)}\right)^2 = 1 \quad (7)$$

$$\Rightarrow \exists \vartheta_2(\xi_2) : (\forall \xi_2 \in I_{2\Delta}) \mathbf{F} \cdot \mathbf{D}_2 = \sin(\vartheta_2(\xi_2)) \mathbf{D}_1 + \cos(\vartheta_2(\xi_2)) \mathbf{D}_2$$

Roughly speaking, the previous equations clearly means that on any subdomain Δ whose points can be connected with segments parallel to ξ axes, the whole displacement field is known in terms of only two real functions of one real variable. Indeed once, for instance, the functions $\mu_1^{(\Delta)}$ and $\mu_2^{(\Delta)}$ are chosen then the functions $\nu_1^{(\Delta)}$ and $\nu_2^{(\Delta)}$ are simply obtained via integration in terms of the functions $\mu_1^{(\Delta)}$ and $\mu_2^{(\Delta)}$ plus some integration constants (to be determined via suitable boundary

conditions).

2.3 Imposed boundary conditions

The two segments Σ_1 and Σ_2 characterized respectively by the conditions

$$X_1 = 0, X_2 \in \left[-\frac{l}{2}, \frac{l}{2}\right]; X_1 = L, X_2 \in \left[-\frac{l}{2}, \frac{l}{2}\right]$$

are described, in the [former](#) reference, by the following corresponding ones:

$$\Sigma_1 := \{(\xi_1, \xi_2) \in B : \xi_1 \in [0, 1], \xi_2 = 1 - \xi_1\}, \quad (8)$$

$$\Sigma_2 := \{(\xi_1, \xi_2) \in B : \xi_1 \in [3, 4], \xi_2 = 7 - \xi_1\}. \quad (9)$$

In this paper, we impose the following boundary conditions on the two subsets Σ_1 and Σ_2 of the boundary of B :

1. vanishing displacement of the side Σ_1 ,
2. imposed displacement $\mathbf{u}_0 = u_0 \frac{(\mathbf{D}_1 + \mathbf{D}_2)}{\|(\mathbf{D}_1 + \mathbf{D}_2)\|}$ of the side Σ_2 .

As already remarked in [\[1, 2\]](#) because of inextensibility the boundary conditions determine the placement field not only at the boundary but also in some regions inside the continuum at which they are applied. Depending on the geometry of the body and on the nature of applied boundary conditions one can distinguish different regions in considered body each of which is affected in a specific way

by the applied boundary conditions. This can be done in our case by defining the following lines:

$$\begin{aligned}
S_1 &:= \{(\xi_1, \xi_2) \in B : \xi_1 \in [0, 2], \xi_2 = 1\}, & S_2 &:= \{(\xi_1, \xi_2) \in B : \xi_1 = 1, \xi_2 \in [0, 2]\}, \\
S_3 &:= \{(\xi_1, \xi_2) \in B : \xi_1 \in [1, 3], \xi_2 = 2\}, & S_4 &:= \{(\xi_1, \xi_2) \in B : \xi_1 = 2, \xi_2 \in [1, 3]\} \\
S_5 &:= \{(\xi_1, \xi_2) \in B : \xi_1 \in [2, 4], \xi_2 = 3\}, & S_6 &:= \{(\xi_1, \xi_2) \in B : \xi_1 = 3, \xi_2 \in [2, 4]\}.
\end{aligned} \tag{10}$$

It is necessary to consider the projections of these lines on the fiber axes: we indicate with π_1 and π_2 the projection maps respectively on ξ_1 and ξ_2 and introduce the following notations:

$$I_{10} := \pi_1(\Sigma_1) = [0, 1] \quad I_{13} := \pi_1(\Sigma_2) = [3, 4] \tag{11}$$

$$I_{20} := \pi_1(\Sigma_1) = [0, 1] \quad I_{23} := \pi_1(\Sigma_2) = [3, 4]. \tag{12}$$

$$I_1 := \pi_1(B), \quad I_2 := \pi_2(B). \tag{13}$$

$$I_{11} := [\pi_1(S_2), \pi_1(S_4)] = [1, 2], \quad I_{12} := [\pi_1(S_4), \pi_1(S_6)] = [2, 3] \tag{14}$$

$$I_{21} := [\pi_2(S_1), \pi_2(S_3)] = [1, 2] \quad I_{23} := [\pi_2(S_3), \pi_2(S_5)] = [2, 3]. \tag{15}$$

As a consequence, a natural covering of the two intervals I_1 and I_2 , by means of intervals whose intersections reduce to single points, can be introduced (for simplicity we will call it simply a partition):

$$I_1 = I_{10} \cup I_{11} \cup I_{12} \cup I_{13} \quad I_2 = I_{20} \cup I_{21} \cup I_{22} \cup I_{23} \quad (16)$$

Obviously this partition of the intervals I_1 and I_2 naturally induces a covering of B by means of the regions Δ_{ij} , whose intersections reduce to curves, defined as follows (also in this case we will simply refer to this covering as a partition):

$$\Delta_{ij} := (I_{1i} \times I_{2j}) \cap B, \quad B = \bigcup_{i,j=1}^3 \Delta_{ij}. \quad (17)$$

The partition of B is graphically represented in Fig. 1.

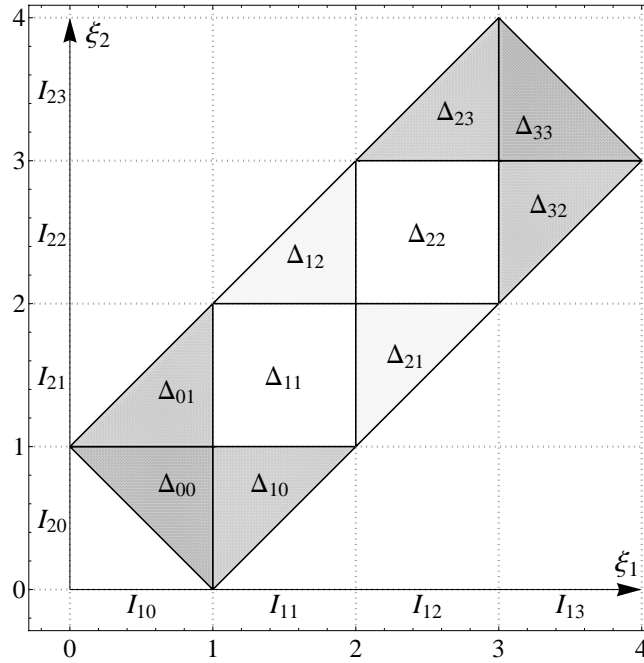


Figure 1: Partition of B in Δ_{ij} regions.

We can therefore assume that the placement field is twice continuously differentiable in the interior of any Δ_{ij} . If we indicate with $\mathbf{r}^{(i,j)}(\xi_1, \xi_2)$ the restriction of \mathbf{r} to the region Δ_{ij} , recalling (4) we have

$$\mathbf{r}^{(i,j)}(\xi_1, \xi_2) = \mathbf{r}_1^{(i)}(\xi_1) + \mathbf{r}_2^{(j)}(\xi_2). \quad (18)$$

Because of the the global continuity condition of \mathbf{r} , we are allowed to identify the vector fields $\mathbf{r}_1^{(i)}(\xi_1)$ and $\mathbf{r}_2^{(j)}(\xi_2)$ along straight lines included in B .

So, if we consider two regions Δ_{ij} and Δ_{hk} with $i = h$ or $j = k$, then we have respectively that $\mathbf{r}_1^{(i)}(\xi_1) = \mathbf{r}_1^{(h)}(\xi_1)$, $\mathbf{r}_2^{(j)}(\xi_2) = \mathbf{r}_2^{(k)}(\xi_2)$. This property allows us to define the continuous scalar fields μ_1 and μ_2 in the entire intervals I_1 and I_2 respectively. These two scalar functions will belong to $C^1[1, 3]$.

2.4 Placement field in Δ_{00} and Δ_{33} and integral conditions implied by boundary conditions

The chosen boundary conditions on Σ_1 and Σ_2 , imply that \mathbf{r} is the identity on Δ_{00} and a translation in Δ_{33} (for the proof the reader is referred to [41]).

In Δ_{00} we have that

$$\mathbf{r}(\xi_1, \xi_2) = \xi_1 \mathbf{D}_1 + \xi_2 \mathbf{D}_2 \quad (19)$$

while in Δ_{33} we get:

$$\mathbf{r}(\xi_1, \xi_2) = (\xi_1 + u_{01}) \mathbf{D}_1 + (\xi_2 + u_{02}) \mathbf{D}_2 \quad (20)$$

The continuity conditions in $P_i = (1, 1)$ and $P_f = (3, 3)$ of the placement field can be written as

(see [41]):

$$\begin{cases} \mu_1(3) + \int_1^3 \sin(\vartheta_2(\eta)) d\eta = 3 + u_0 \\ \mu_2(3) + \int_1^3 \sin(\vartheta_1(\eta)) d\eta = 3 + u_0 \end{cases} \quad (21)$$

This condition imposes the continuity of the translation imposed to Δ_{33} with the displacement of the contiguous domains. Once one recalls that ($i = 1, 2$)

$$\frac{d\mu_i(\xi_i)}{d\xi_i} - \cos(\vartheta_i(\xi_i)) = 0, \quad \mu_i(1) = 1, \quad (22)$$

it is easy to express the found integral conditions exclusively in terms of the fields $\vartheta_i(\xi_i)$ as follows

$$\begin{cases} \int_1^3 (\cos(\vartheta_1(\eta)) + \sin(\vartheta_2(\eta))) d\eta = 2 + u_{01} \\ \int_1^3 (\cos(\vartheta_2(\eta)) + \sin(\vartheta_1(\eta))) d\eta = 2 + u_{02} \end{cases} \quad (23)$$

This form will be useful when looking for the equilibrium shapes of considered body.

A remark can be done regarding the interface separating the undeformed triangles Δ_{00} and Δ_{33} from the other regions. In the simple model here considered, indeed, there exists an a priori determinable and geometrically constant interface between regions with different deformation. Since this fact is closely related to the particular set of boundary conditions imposed, one can easily understand that such a priori determination is not possible anymore whether more general and complex conditions are chosen. The theoretical treatment of the problems related to this fact can be rather difficult; a set of useful tools has been developed (also in connection with phase transitions) in [49–52].

2.5 Symmetric placements

In this section we will consider placement fields verifying some specific symmetry conditions.

2.5.1 Placement fields symmetric with respect to the X_1 axis.

This means that, given a point P of coordinates (ξ, η) and his symmetric P_s having coordinates (η, ξ) , the following conditions hold:

$$\begin{cases} \mathbf{d}_1(P) \cdot D_1 = \mathbf{d}_2(P_s) \cdot D_2 \\ \mathbf{d}_1(P) \cdot D_2 = \mathbf{d}_2(P_s) \cdot D_1 \end{cases} \implies \begin{cases} \mu_{1,1}(\xi) = \mu_{2,2}(\xi) \\ \nu_{1,1}(\xi) = \nu_{2,2}(\xi) \end{cases} \quad (24)$$

Considering the symmetry of boundary conditions and the first equality in (24) we derive directly the following identities:

$$\mu(\xi) := \mu_1(\xi) = \mu_2(\xi) \quad \vartheta(\xi) := \vartheta_1(\xi) = \vartheta_2(\xi) \quad \forall \xi \in [0, 4]. \quad (25)$$

Therefore, considering the relation between μ and ν , the kinematics of the problem is completely described by means of an unique field.

It is easily verified that a similar conclusion can be obtained replacing this type of symmetry with the invariance for a reflection with respect to the X_1 axis.

2.5.2 The space of configurations for 2D continua with two families of inextensible fibers in symmetric plane motion

If we assume the hypothesis of symmetry described in 2.5.1, the placement of B is completely determined by one scalar field $\mu(\xi)$ only, defined in the real interval $[0, 4]$. Because of the considered boundary conditions, recalling (19) and (20), μ has to be determined only in the interval $I = [1, 3]$.

Thanks to (21) we have also the conditions

$$\mu(1) = 1, \quad \mu(3) + \int_1^3 \sin(\vartheta(\eta)) d\eta = 3 + u_0, \quad (26)$$

or equivalently the conditions

$$\mu(1) = 1, \quad \int_1^3 (\cos(\vartheta(\eta)) + \sin(\vartheta(\eta))) d\eta = 2 + u_0. \quad (27)$$

The space of (admissible) configurations for 2D continua with two families of inextensible fibers (having everywhere orthogonal tangent vectors in the reference configuration) in plane motion is given by the set of pairs of fields (μ, ϑ) the first of which is piecewise C^2 and the second of which is piecewise C^1 with possible discontinuities in the point $\xi = 2$ which, together with the conditions (27), verify the local condition

$$\frac{d\mu(\xi)}{d\xi} - \cos(\vartheta(\xi)) = 0 \quad \forall \xi \in [1, 3]. \quad (28)$$

2.6 Euler-Lagrange equilibrium condition for a class of factorisable energies

The equilibrium configuration will be given by means of two pairs of fields (μ_i, ϑ_i) defined in the interval $[1, 3]$ which verify the conditions (23), (22), respectively two and one times continuously differentiable in the set $[1, 3] - \{2\}$, which minimize the deformation energy functional. Because of the definitions of the fields ϑ_i and the definitions (2), (3) and because of the requirement of objectivity, the density of deformation energy W , in the case of first gradient continua, must be a function of the shear angle $\gamma = \vartheta_1 + \vartheta_2$. As discussed in [10] when second gradient deformation energies will be needed then the deformation energy must be assumed to depend also on $\nabla\gamma$.

2.6.1 Some examples of deformation energy density.

We may find several physically reasonable constitutive assumptions for the deformation energy density. In the present paper we will consider the following ones

$$W_1(\gamma) = \frac{k}{2} (\sin\gamma)^2 = \frac{k}{2} (\cos\vartheta_1 \sin\vartheta_2 + \sin\vartheta_1 \cos\vartheta_2)^2 = \frac{k}{2} (\mathbf{d}_1 \cdot \mathbf{d}_2)^2 \quad (29)$$

$$W_2(\gamma) = \sum_{i=1}^N k_i (\vartheta_1 + \vartheta_2)^{2i} \quad (30)$$

These examples suggest that an interesting class to be considered is the one in which the function W can be represented as the sum of products of two functions each depending only on one of the ϑ_i . The determination of corresponding Euler-Lagrange conditions will be made easier by considering that both fields ϑ_i depend only on the variable ξ_i .

In the following, we will mainly focus on the energy W_1 , which our experimental work has shown as a particularly relevant case (a related article is in preparation).

2.6.2 Factorizable energy densities and corresponding Euler-Lagrange conditions

In this paper we will consider deformation energy densities having the following structure

$$W(\vartheta_1 + \vartheta_2) = \sum_{\alpha=1}^M l_1^\alpha(\vartheta_1) l_2^\alpha(\vartheta_2) \quad (31)$$

In the previous subsection some examples of factorizable energies which are also objective were given.

The deformation energy functional is therefore given by

$$\mathcal{E}^{\mathcal{D}\mathcal{E}\mathcal{F}} = \int_B \sum_{\alpha=1}^M l_1^\alpha(\vartheta_1) l_2^\alpha(\vartheta_2) \quad (32)$$

We start by calculating its first variation relative to the variations $(\delta\mu_1, \delta\vartheta_1)$.

To this aim we start by remarking that the region B can be represented as follows

$$B = \bigcup_{\xi_1 \in [0,4]} [\xi_2^-(\xi_1), \xi_2^+(\xi_1)]$$

where the functions ξ_2^\pm have as graph two curves whose union forms the perimeter of B and are defined as follows

$$\begin{cases} \xi_1 \in [0, 1] & \xi_2^-(\xi_1) := 1 - \xi_1 \\ \xi_1 \in [1, 4] & \xi_2^-(\xi_1) := \xi_1 - 1 \\ \xi_1 \in [0, 3] & \xi_2^+(\xi_1) := \xi_1 + 1 \\ \xi_1 \in [3, 4] & \xi_2^+(\xi_1) := 7 - \xi_1. \end{cases}$$

By applying Fubini's Theorem we get that the energy functional can be represented in a form which is more suitable for calculating its variation with respect to the variations $(\delta\mu_1, \delta\vartheta_1)$. Indeed it can be transformed as follows

$$\mathcal{E}^{\mathcal{D}\mathcal{E}\mathcal{F}} = \int_0^4 d\xi_1 \sum_{\alpha=1}^M \left(l_1(\vartheta_1) \int_{\xi_2^-(\xi_1)}^{\xi_2^+(\xi_1)} l_2(\vartheta_2(\xi_2)) d\xi_2 \right). \quad (33)$$

Further calculation will become easier if we introduce the integral operator defined as follows:

$$\mathcal{A}_2[f(\xi)](\eta) := \int_{\xi_2^-(\eta)}^{\xi_2^+(\eta)} f(\xi) d\xi.$$

Among the introduced constraints two are of local nature (see (22)), while two others are of integral nature (see (23)). Therefore the functional whose stationarity conditions will supply the searched equilibrium conditions is the following one (remark that the integration interval is now $[1, 3]$)

as in the intervals $[0, 1]$ and $[3, 4]$ the fields (μ_1, ϑ_1) are fixed by the imposed boundary conditions)

$$\begin{aligned} \mathcal{E}^{\mathcal{T}\mathcal{O}\mathcal{T}} = & \int_1^3 \sum_{\alpha=1}^M \mathcal{A}_2 [l_2^\alpha(\vartheta_2)](\xi_1) (l_1^\alpha(\vartheta_1(\xi_1))) d\xi_1 + \\ & \int_1^3 \left(\lambda_1 \left(\frac{d\mu_1(\xi_1)}{d\xi_1} - \cos(\vartheta_1(\xi_1)) \right) \right) d\xi_1 + \\ & \int_1^3 \left(\lambda_2 \left(\frac{d\mu_2(\xi_2)}{d\xi_2} - \cos\vartheta_2(\xi_2) \right) \right) d\xi_2 + \\ & \Lambda_1 \left(\mu_1(3) + \int_1^3 \sin(\vartheta_2(\eta)) d\eta - 3 - u_{01} \right) + \\ & \Lambda_2 \left(\mu_2(3) + \int_1^3 \sin(\vartheta_1(\eta)) d\eta - 3 - u_{02} \right) +, \end{aligned}$$

where we introduced the global Lagrange multipliers Λ_i ($i = 1, 2$) and the fields of Lagrange multipliers λ_i each depending only on the variable ξ_i .

By denoting with δ_1 the first variation of functional to be minimized with respect to the variations $(\delta\mu_1, \delta\vartheta_1)$ while keeping (μ_2, ϑ_2) fixed, we get

$$\begin{aligned} \delta_1 \mathcal{E}^{\mathcal{D}\mathcal{E}\mathcal{F}} = & \int_1^3 \left(\sum_{\alpha=1}^M \frac{\partial l_1^\alpha}{\partial \vartheta_1} \mathcal{A}_2 [l_2^\alpha(\vartheta_2)] + \Lambda_2 \cos(\vartheta_1) + \lambda_1 \sin(\vartheta_1) \right) \delta\vartheta_1 d\xi_1 + \\ & \int_1^3 \left(-\frac{d\lambda_1(\xi_1)}{d\xi_1} \right) \delta\mu_1 d\xi_1 + (\lambda_1(3) + \Lambda_1) \delta\mu_1(3) = 0. \end{aligned} \quad (34)$$

We can obtain similar results interchanging the role of indexes 1 and 2². Because of the arbitrariness of the variations $(\delta\mu_1, \delta\vartheta_1)$, we get the following Euler-Lagrange conditions:

$$\frac{d\lambda_i(\xi_1)}{d\xi_1} = 0; \quad \Lambda_i = -\lambda_i(3) \quad (i = 1, 2) \quad (35)$$

$$\sum_{\alpha=1}^M \frac{\partial l_1^\alpha}{\partial \vartheta_1} \mathcal{A}_2 [l_2^\alpha(\vartheta_2)] + \Lambda_2 \cos(\vartheta_1) - \Lambda_1 \sin(\vartheta_1) = 0 \quad (36)$$

$$\sum_{\alpha=1}^M \frac{\partial l_2^\alpha}{\partial \vartheta_2} \mathcal{A}_1 [l_1^\alpha(\vartheta_1)] + \Lambda_1 \cos(\vartheta_2) - \Lambda_2 \sin(\vartheta_2) = 0 \quad (37)$$

²This means we can apply Fubini's theorem interchanging the role of variables and express the deformation energy also as $\mathcal{E}^{\mathcal{D}\mathcal{E}\mathcal{F}} = \int_0^4 d\xi_2 \sum_{\alpha=1}^M \left(l_2(\vartheta_2) \int_{\xi_1^-(\xi_2)}^{\xi_1^+(\xi_2)} l_1(\vartheta_1(\xi_1)) d\xi_1 \right)$.

The Lagrange multipliers A_i ($i = 1, 2$) will be determined by means of the integral conditions (27).

2.6.3 Euler-Lagrange condition for the energy W_1

The factorization of the energy W_1 is easily obtained via trigonometric identities

$$\sin^2(\vartheta_1 + \vartheta_2) = \sin^2\theta_1\cos^2\theta_2 + \cos^2\theta_1\sin^2\theta_2 + \frac{\sqrt{2}}{2}\sin 2\theta_1\frac{\sqrt{2}}{2}\sin 2\theta_2$$

The equation (36) becomes

$$\begin{aligned} \sin(2\vartheta_1)\mathcal{A}_2 [\cos^2(\vartheta_2)] - \sin(2\vartheta_1)\mathcal{A}_2 [\sin^2(\vartheta_2)] + \sqrt{2}\cos(2\vartheta_1)\mathcal{A}_2 \left[\frac{\sqrt{2}}{2}\sin(2\vartheta_2) \right] \\ + \Lambda_2\cos(\vartheta_1) - \Lambda_1\sin(\vartheta_1) = 0 \end{aligned} \quad (38)$$

which when recalling the first between equalities (22) becomes (when assuming that both ϑ_i belong to the interval $[0, \frac{\pi}{4}]$),

$$\begin{aligned} 2\frac{d\mu_1}{d\xi_1}\sqrt{1 - \left(\frac{d\mu_1}{d\xi_1}\right)^2}\mathcal{A}_2 \left[\left(\frac{d\mu_2}{d\xi_2}\right)^2 \right] - 2\frac{d\mu_1}{d\xi_1}\sqrt{1 - \left(\frac{d\mu_1}{d\xi_1}\right)^2}\mathcal{A}_2 \left[1 - \left(\frac{d\mu_2}{d\xi_2}\right)^2 \right] + \\ + \sqrt{2} \left(2\left(\frac{d\mu_1}{d\xi_1}\right)^2 - 1 \right) \mathcal{A}_2 \left[\sqrt{2}\left(\frac{d\mu_2}{d\xi_2}\right)\sqrt{1 - \left(\frac{d\mu_2}{d\xi_2}\right)^2} \right] + \Lambda_2\frac{d\mu_1}{d\xi_1} - \Lambda_1\sqrt{1 - \left(\frac{d\mu_1}{d\xi_1}\right)^2} = 0 \end{aligned} \quad (39)$$

When the symmetry conditions are accepted, we have that $\Lambda_1 = \Lambda_2 =: \Lambda$, $\mathcal{A}_1 = \mathcal{A}_2 =: \mathcal{A}$, and

the last condition becomes the following integral relation for the eld $\frac{d\mu}{d\xi}$

$$\begin{aligned}
& 2\frac{d\mu}{d\xi}\sqrt{1-\left(\frac{d\mu}{d\xi}\right)^2}\mathcal{A}\left[\left(\frac{d\mu}{d\xi}\right)^2\right]-2\frac{d\mu}{d\xi}\sqrt{1-\left(\frac{d\mu}{d\xi}\right)^2}\mathcal{A}\left[1-\left(\frac{d\mu}{d\xi}\right)^2\right]+ \\
& +\sqrt{2}\left(2\left(\frac{d\mu}{d\xi}\right)^2-1\right)\mathcal{A}\left[\sqrt{2}\left(\frac{d\mu}{d\xi}\right)\sqrt{1-\left(\frac{d\mu}{d\xi}\right)^2}\right]+\Lambda\frac{d\mu}{d\xi}-\Lambda\sqrt{1-\left(\frac{d\mu}{d\xi}\right)^2}=0
\end{aligned} \tag{40}$$

which will be studied later.

2.6.4 Euler-Lagrange condition for the energy $(\vartheta_1 + \vartheta_2)^2$

The factorization of considered energy is easily obtained as follows

$$(\vartheta_1 + \vartheta_2)^2 = (\vartheta_1)^2 + (\vartheta_2)^2 + \sqrt{2}\vartheta_1\sqrt{2}\vartheta_2$$

so that the 36 becomes, in the considered instance,

$$2\vartheta_1\mathcal{A}_2[1] + \sqrt{2}\mathcal{A}_2[\sqrt{2}\vartheta_2] + \Lambda_2\cos(\vartheta_1) - \Lambda_1\sin(\vartheta_1) = 0$$

which, when the symmetry conditions are accepted, become

$$2\vartheta\mathcal{A}[1] + \sqrt{2}\mathcal{A}[\sqrt{2}\vartheta] + \Lambda(\cos(\vartheta) - \sin(\vartheta)) = 0.$$

The reader will easily note that this Euler-Lagrange condition excludes that the eld ϑ can be constant in the interval $[1, 3]$.

3 Problem formulation for symmetric solutions

Once we recall the symmetry conditions given in 2.5.1, the problem is governed by field equations of the following form (the derivation of which is performed in [41]):

$$\begin{aligned} \frac{1 - 2x'(s)^2}{2\sqrt{1 - x'(s)^2}} a_1(s) - x'(s) b_1(s) + \Lambda \left(1 - \frac{x'(s)}{\sqrt{1 - x'(s)^2}} \right) &= 0 & s \in [1, 2] \\ \frac{1 - 2x'(s)^2}{2\sqrt{1 - x'(s)^2}} a_2(s) - x'(s) b_2(s) + \Lambda \left(1 - \frac{x'(s)}{\sqrt{1 - x'(s)^2}} \right) &= 0 & s \in [2, 3] \end{aligned} \quad (41)$$

sided by the constraint equation:

$$x(3) + \int_1^3 \sqrt{1 - x'(s)^2} ds = 3 - u \quad (42)$$

together with the boundary condition:

$$x(1) = 1 \quad (43)$$

In Eqs (41), Λ is a Lagrangian multiplier, u the control parameter, and:

$$\begin{aligned} a_i(s) &:= \int_{\alpha_i(s)}^{\beta_i(s)} x'(t) \sqrt{1 - x'(t)^2} dt, & b_i(s) &:= 1 - \int_{\alpha_i(s)}^{\beta_i(s)} (1 - x'(t)^2) dt \\ (\alpha_1(s), \beta_1(s)) &= (1, s + 1), & (\alpha_2, \beta_2) &= (s - 1, 3) \end{aligned} \quad (44)$$

Note that Eqs (41) are coupled by the integral terms. Namely, when s belong to the left (right) interval, the integrals are extended to this whole interval and a part of the right (left) interval.

Therefore, the integrals can be more conveniently broken as follows:

$$\begin{aligned}\int_1^{s+1} (\cdot) dt &= \int_1^2 (\cdot) dt + \int_2^{s+1} (\cdot) dt & s \in [1, 2] \\ \int_{s-1}^3 (\cdot) dt &= \int_{s-1}^2 (\cdot) dt + \int_2^3 (\cdot) dt & s \in [2, 3]\end{aligned}\tag{45}$$

It can be shown (see the Appendix) that the problem admits solutions $y(s) := x'(s)$ which are symmetric with respect to the midpoint $s = 2$, i.e. $y(2 - \xi) = y(2 + \xi)$. Exploiting the symmetry property, we can write:

$$\begin{aligned}\mathcal{I}[\cdot] &:= \int_1^{s+1} (\cdot) dt = \int_1^2 (\cdot) dt - \int_2^{3-s} (\cdot) dt \\ \int_1^3 (\cdot) ds &= 2 \int_1^2 (\cdot) ds & s \in [1, 2]\end{aligned}\tag{46}$$

In conclusion, the problem is recast in the form of an integral-algebraic equation in the unknowns $y(s), \Lambda$, namely:

$$\begin{aligned}\mathcal{I} \left[y(t) \sqrt{1 - y(t)^2} \right] \frac{1 - 2y(s)^2}{2\sqrt{1 - y(s)}} - \left(1 - \mathcal{I} \left[1 - y(t)^2 \right] \right) y(s) \\ + \Lambda \left(1 - \frac{y(s)}{\sqrt{1 - y(s)}} \right) &= 0 & s \in [1, 2] \\ 1 + 2 \int_1^2 y(s) ds + 2 \int_1^2 \sqrt{1 - y(s)^2} ds &= 3 - u\end{aligned}\tag{47}$$

where use has been made of Eq (43). Once the problem has been solved, the original variable is found by integration:

$$x(s) = 1 + \int_1^s y(t) dt\tag{48}$$

The shear strain ϑ is successively recovered using (22).

4 Critical solution

A simple inspection of Eq (47-a) reveals that $y = y_c = \text{const}$ are, in principle, solutions, representing homogeneous states of strain for the system. However, since the problem is nonlinear, the number, values and character (real or complex) of the the constant solutions are unknown. We denote by a subscript c all the quantities associated with the constant solution, namely (y_c, Λ_c, u_c) , and refer to it as the critical solution, since it possibly occurs at critical values of the control parameter.

By substituting the ansatz in Eq (47-a), and performing the integrations, we find:

$$\frac{1}{2}y_c(1 - 2y_c^2)s - y_c(1 - s(1 - y_c^2)) + \Lambda_c\left(1 - \frac{y_c}{\sqrt{1 - y_c}}\right) = 0 \quad (49)$$

By requiring that it is satisfied for any s , two algebraic equations are derived:

$$\begin{aligned} 2y_c^3 - \frac{3}{2}y_c &= 0 \\ \Lambda_c\left(1 - \frac{y_c}{\sqrt{1 - y_c}}\right) - y_c &= 0 \end{aligned} \quad (50)$$

They admit the unique non-trivial solution in the real field:

$$y_c = \frac{\sqrt{3}}{2}, \quad \Lambda_c = \frac{\sqrt{3}}{2(1 - \sqrt{3})} \quad (51)$$

after having disregarded the opposite one for physical reasons.

With $y = y_c$ now known, Eq (47-b)) provides the critical value of the control parameter:

$$u_c = \sqrt{3} - 1 \approx 0.732051 \quad (52)$$

consistently with the numerical results.

Finally, coming back to the original variable, we have:

$$x(s) = 1 + \frac{\sqrt{3}}{2}(s - 1) \quad (53)$$

5 Perturbation solution

In this paper a numerical investigation of the solution in the neighborhood of the critical parameter u_c is provided via perturbation method (an explanatory application of which can be found in [53]). In the considered case the numerical problems are relatively easy. However, if one is interested in performing numerical investigations of 3D continua which model the real-world 3D-printed object graphically represented in Fig. 6, some sophisticated numerical methods would be required. In particular, a refined choice of the mesh is called for, capable to take into account all the peculiarities of the geometry and of kinematics of the object without leading to an explosion in terms of computational costs. Among them, a suitable version of isogeometric FE methods can be of use; the reader interested can see for example [54–68].

The previous analysis revealed that no other homogeneous solutions, in addition to the critical one, are admitted by the system. However, by means of a continuity argument, it should be clear that solutions close enough to the homogeneous state exist in a small neighborhood of the critical parameter u_c , which we want to investigate here.

First, the control parameter is written as:

$$u = u_c + \varepsilon u_1 \quad (54)$$

where u_1 the increment of u measured from the critical state, and $0 < \varepsilon \ll 1$ is a bookkeeping (perturbation) parameter (to be removed at the end of the procedure), which remember us that the increment is small with respect to u_c . Consistently, the unknowns are expanded in Taylor series of

ϵ , taking the critical state as the starting point :

$$\begin{aligned} y(s) &= y_c + \epsilon y_1(s) + \epsilon^2 y_2(s) + O(\epsilon^3) \\ \Lambda &= \Lambda_c + \epsilon \Lambda_1 + \epsilon^2 \Lambda_2 + O(\epsilon^3) \end{aligned} \quad (55)$$

where $y_i(s), \Lambda_i$ are unknown. By substituting Eqs (54), (55) into the problem equations (47) and expanding in series, the order-1 terms mutually cancel; by separately equating to zero the terms with the same power of ϵ , the following perturbation equations, at the ϵ - and ϵ^2 -order, are derived:

Order ϵ :

$$\begin{aligned} \mathcal{I}[y_1(s)] + \left(\frac{3\sqrt{3}+1}{\sqrt{3}-1} - 2s \right) y_1(s) + 2 \frac{\sqrt{3}-2}{\sqrt{3}-1} \Lambda_1 &= 0 \\ \int_1^2 y_1(s) ds &= \frac{1}{2(1-\sqrt{3})} u_1 \end{aligned} \quad (56)$$

Order ϵ^2 :

$$\begin{aligned} \mathcal{I}[y_2(s)] + \left(\frac{3\sqrt{3}+1}{\sqrt{3}-1} - 2s \right) y_2(s) + 2 \frac{\sqrt{3}-2}{\sqrt{3}-1} \Lambda_2 &= \\ = \frac{\sqrt{3}-3}{\sqrt{3}-1} \mathcal{I}[y_1^2(s)] + \frac{2\sqrt{3}-6}{\sqrt{3}-1} y_1(s) \mathcal{I}[y_1(s)] + 8\Lambda_1 y_1(s) - \frac{36+6(\sqrt{3}-3)s}{\sqrt{3}-1} y_1^2(s) & \quad (57) \\ \int_1^2 y_2(s) ds &= \frac{4}{1-\sqrt{3}} \int_1^2 y_1^2(s) ds \end{aligned}$$

For any given u_1 , Eqs (56) and (57) must be solved in sequence to find first- and second-order quantities of the series (55).

5.1 First-order solution

If we try the solution $y_1 = \text{const}$ in equations (56), we find that this constant can only be zero, according to the fact that the unique constant solution of the nonlinear problem is y_c .

Equation (56-a) can be transformed, by performing simple variable substitutions, in a Forward Differential Equation with variable coefficients. Setting:

$$\zeta(s+1) := \int_1^{s+1} y_1(t) dt, \quad \alpha(s) := -\frac{1}{\frac{3\sqrt{3}+1}{\sqrt{3}-1} - 2s}, \quad \beta(s) := -2\frac{\sqrt{3}-2}{\sqrt{3}-1}\Lambda_1\alpha(s) \quad (58)$$

equation (56) indeed becomes:

$$\frac{d\zeta(s)}{ds} = \alpha(s)\zeta(s+1) + \beta(s) \quad (59)$$

For numerical evaluation we will start directly from equations (56), and will search a solution in the form of a truncated series of powers of the independent variable s , namely:

$$y_1(s) = \sum_{k=0}^n A_k s^k \quad (60)$$

where A_k are unknown coefficients, and n is the degree of the approximating polynomial. By substituting the power series in Eqs (56-a,b), and separately equating to zero the coefficients of s^k , with $k = 0, 1, \dots, n$ (i.e. ignoring the residuals of higher degrees), a linear algebraic system of $n+2$

equations in the unknown $A_0, A_1, \dots, A_n, \Lambda_1$ is derived, having the following form:

$$\begin{bmatrix} c_{00} & c_{01} & \dots & c_{0,n-2} & c_{0,n-1} & c_{0n} & c_{0\Lambda} \\ c_{10} & c_{11} & \dots & c_{1,n-2} & c_{1,n-1} & c_{1n} & 0 \\ 0 & c_{21} & \dots & c_{2,n-2} & c_{2,n-1} & c_{2n} & 0 \\ \dots & \dots & \dots & \dots & \dots & \dots & 0 \\ 0 & 0 & \dots & c_{n-1,n-2} & c_{n-1,n-1} & c_{n-1,n} & 0 \\ 0 & 0 & \dots & 0 & c_{n,n-1} & c_{nn} & 0 \\ b_0 & b_1 & \dots & b_{n-2} & b_{n-1} & b_n & 0 \end{bmatrix} \begin{pmatrix} A_0 \\ A_1 \\ \dots \\ A_{n-2} \\ A_{n-1} \\ A_n \\ \Lambda_1 \end{pmatrix} = \begin{pmatrix} 0 \\ 0 \\ 0 \\ 0 \\ 0 \\ 0 \\ u_1 \end{pmatrix} \quad (61)$$

where the b s and c s are numerical coefficients. The almost-triangular structure of the matrix of coefficients permits, by backward substitution, to get a closed-form solution for any n . By solving Eqs (61) for increasing n s, the solutions reported in Table 1 are found, where $\hat{A}_k := A_k/u_1$ and similar. There, the residual R_{n+1} is the value assumed by coefficient of the $n + 1$ -th power of s , when the series truncated at the n -th term is substituted in it. It is seen that the coefficients of the series converge fast, and that the residual goes rapidly to zero.

n	$\hat{\Lambda}_1$	\hat{A}_0	\hat{A}_1	\hat{A}_2	\hat{A}_3	\hat{R}_{n+1}
0	-7.897114	-0.683013				0.683013
1	-6.816709	-0.589569	-0.062295			0.093443
2	-6.612251	-0.571886	-0.059431	-0.009419		0.015699
3	-6.562494	-0.567583	-0.058844	-0.009073	-0.001597	0.002796

Below we give the exact expressions for the $y_1(s)$ and for the Lagrangian multipliers Λ_1 by truncating the series respectively at $n = 0, 1, 2, 3$, for the first order perturbation approximation.

Case $n = 0$:

$$y_1(s) = \left[-\frac{(1 + \sqrt{3})}{4} \right] u_1 \quad (62)$$

$$\Lambda_1 = -\frac{(16 + 9\sqrt{3})}{4} \quad (63)$$

Case $n = 1$:

$$y_1(s) = \left[-\frac{2(7 + 6\sqrt{3})}{59} - \frac{(3 + 11\sqrt{3})}{354} s \right] u_1 \quad (64)$$

$$\Lambda_1 = -\frac{(203 + 115\sqrt{3})}{59} \quad (65)$$

Case $n = 2$:

$$y_1(s) = \left[-\frac{3(1053 + 851\sqrt{3})}{13256} - \frac{24 + 43\sqrt{3}}{1657} s - \frac{3(35\sqrt{3} - 19)}{13256} s^2 \right] u_1 \quad (66)$$

$$\Lambda_1 = -\frac{3(14727 + 8366\sqrt{3})}{13256} \quad (67)$$

Case $n = 3$:

$$y_1(s) = \left[-\frac{994993 + 783681\sqrt{3}}{4144537} - \frac{66049 + 102673\sqrt{3}}{4144537} s + \right. \\ \left. - \frac{12(2050\sqrt{3} - 417)}{4144537} s^2 - \frac{5(2189\sqrt{3} - 2467)}{4144537} s^3 \right] u_1 \quad (68)$$

$$\Lambda_1 = -\frac{13701112 + 7792721\sqrt{3}}{4144537} \quad (69)$$

For the sake of completeness it is show the convergence plots of the principal coefficients with the increasing of n

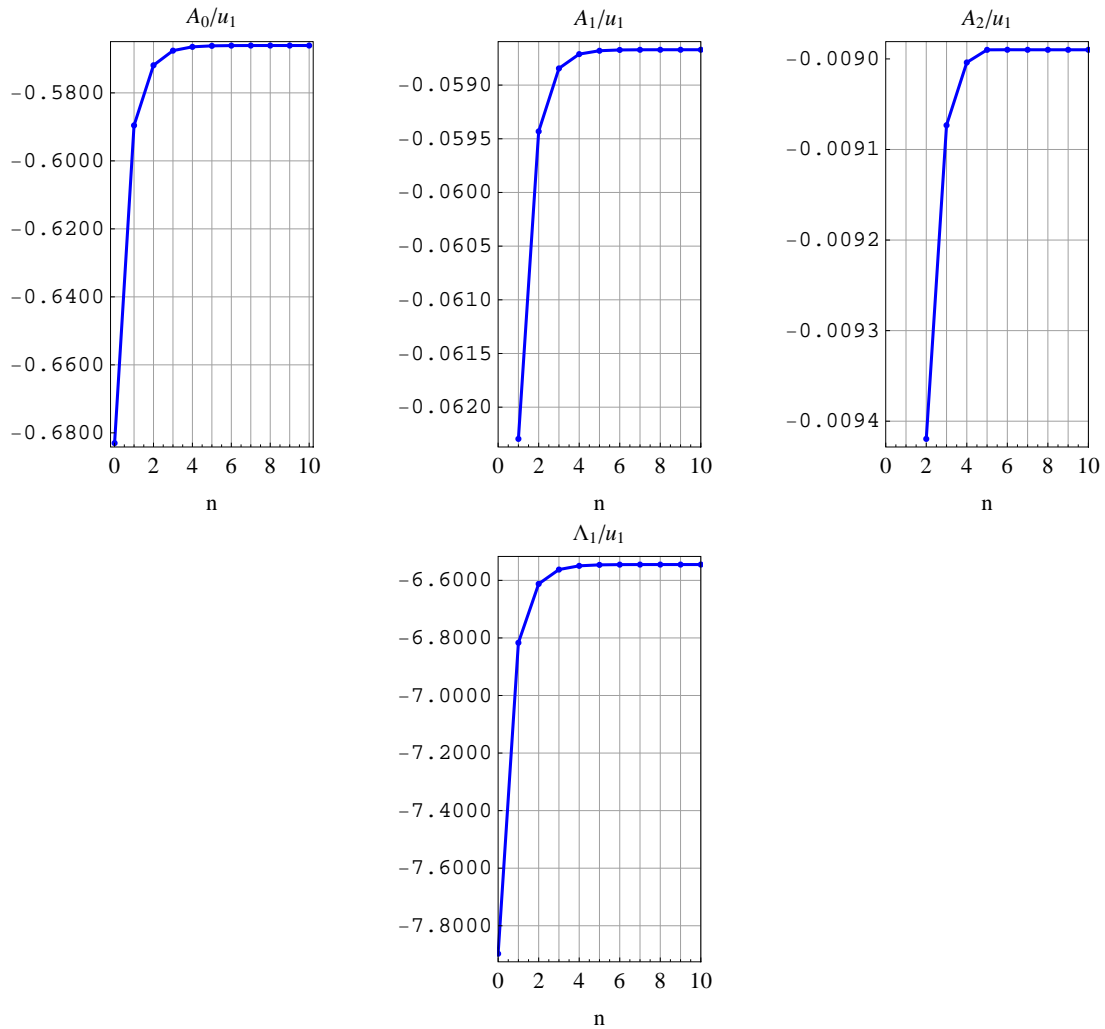


Figure 2: Convergence behavior of the coefficients \hat{A}_0 , \hat{A}_1 , \hat{A}_2 and $\hat{\Lambda}_1$ for the first order perturbation approximation.

5.2 Second-order solution

In the equations (57) the first-order quantities $y_1(s)$ and Λ_1 are known. They can be transformed in FDE in a similar way as done before, and here are solved again in power series, by taking:

$$y_2(s) = \sum_{k=0}^n B_k s^k \quad (70)$$

where B_k are unknown coefficients. By proceeding as before, a linear algebraic system in the unknown is obtained, in which the matrix is the same than Eq (61), but the known terms are much more involved.

n	$\hat{\Lambda}_2$	\hat{B}_0	\hat{B}_1	\hat{B}_2	\hat{B}_3	\hat{R}_{n+1}
0	-45.163774	-1.366025				0.125
1	-38.234434	-1.411087	0.029140			-0.130869
2	-37.373062	-1.447710	0.009535	0.027427		-0.051697
3	-37.281122	-1.466172	0.004268	0.024249	0.008545	-0.014475

By summarizing, the second-order solution (with ε reabsorbed) reads:

$$y(s) = y_c + \sum_{k=0}^n \left[\hat{A}_k (u - u_c) + \hat{B}_k (u - u_c)^2 \right] s^k \quad (71)$$

$$\Lambda = \Lambda_c + \hat{\Lambda}_1 (u - u_c) + \hat{\Lambda}_2 (u - u_c)^2$$

The original variable, consequently is:

$$x(s) = 1 + y_c (s - 1) + \sum_{k=0}^n \frac{1}{k+1} \left[\hat{A}_k (u - u_c) + \hat{B}_k (u - u_c)^2 \right] (s^{k+1} - 1) \quad (72)$$

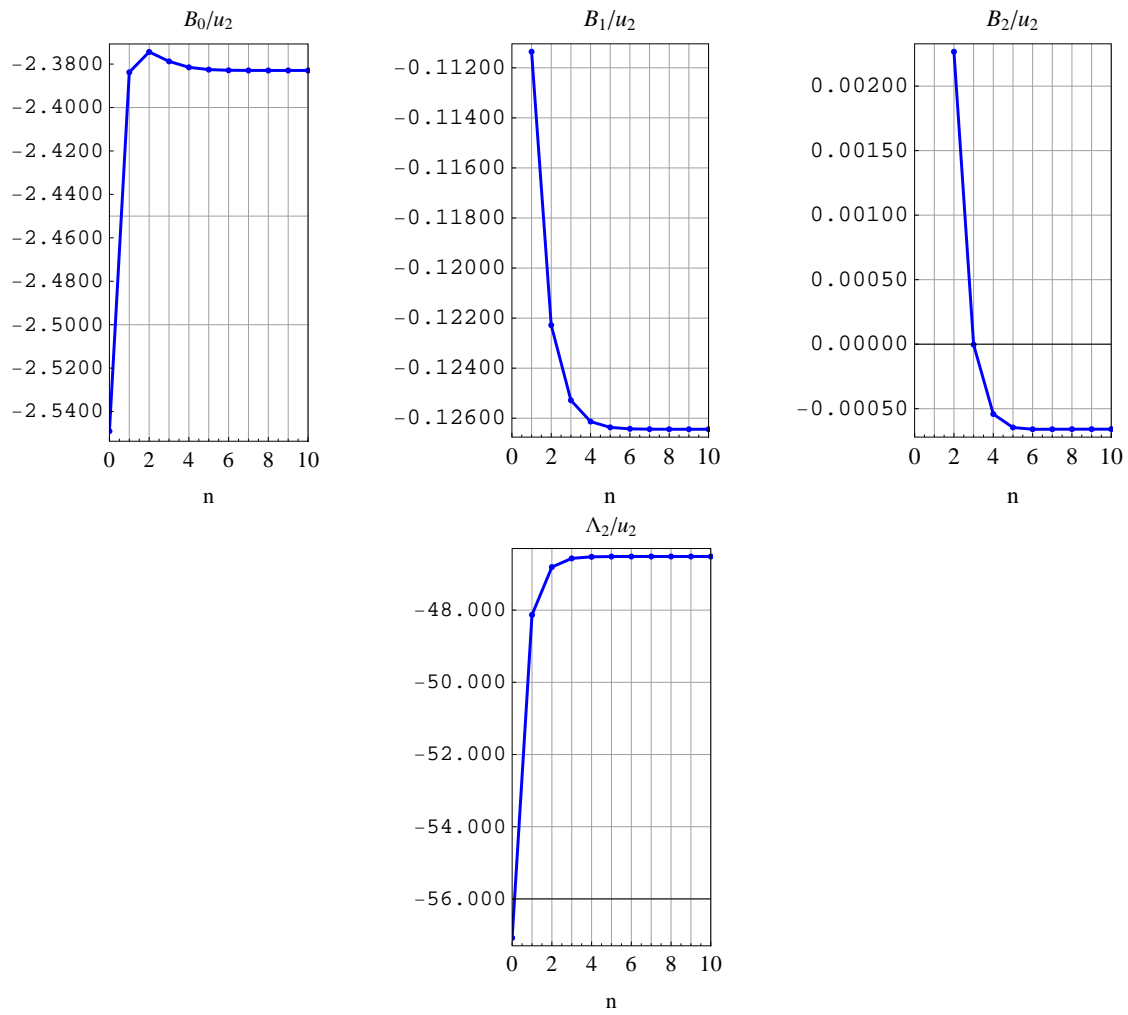


Figure 3: Convergence behavior of the coefficients \hat{B}_0 , \hat{B}_1 , \hat{B}_2 and $\hat{\Lambda}_2$ for the second order perturbation approximation.

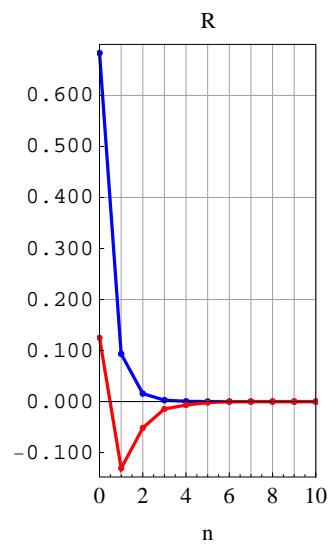


Figure 4: Convergence of the residual for the first (blue line) and second (red line) perturbation approximation.

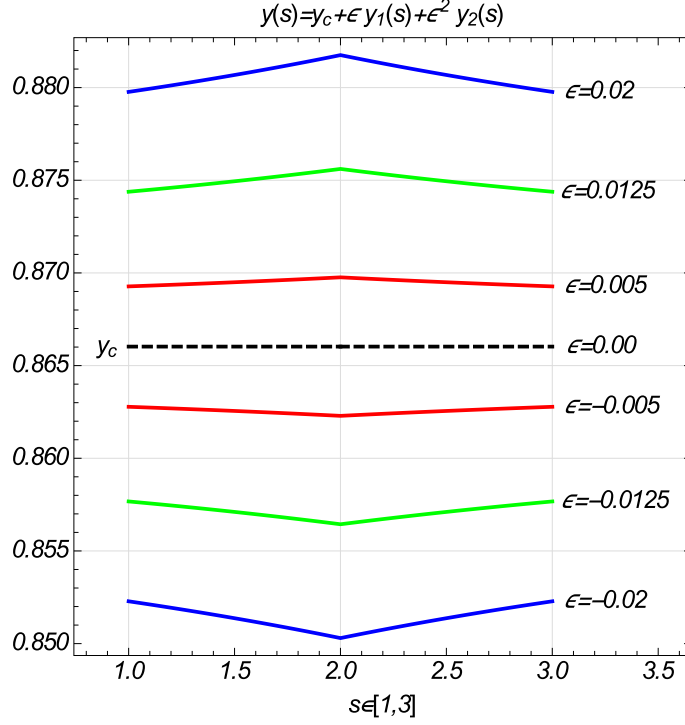


Figure 5: Solution $y(s)$ for $s \in [1, 3]$ for different values of ϵ in a neighborhood of the critical solution.

We observe that, since all the \hat{A} 's coefficient are negative, $y(s) \simeq y_c + y_1(s) < y_c \forall s$ when $u - u_c > 0$ (supercritical range) and $y(s) \simeq y_c + y_1(s) < y_c \forall s$ when $u - u_c < 0$ (subcritical range). Moreover, $y'(s) < 0 \forall s$ in the supercritical range and $y'(s) > 0 \forall s$ in the subcritical range, this enabling a change of concavity of $y(s)$ passing through the critical state. Second-order terms $y_2(s)$ are always negative, but, being of higher order, do not change the qualitative behaviour described.

In Fig 5 the solution $y(s)$ is plotted (up to second order) for a set of values of ϵ .

6 Appendix: Nonlinear torsion extension of a circular cylinder

In this appendix we present a simple analysis for the assumption of a particular deformation energy associated to every node of the considered model, namely deformation energy density W_2 defined in

equation (30). We assume that the structure is made of two families of parallel and equally spaced beams overlapping, with the connection between the beams of the two families being realized by means of circular cylinders (see Fig. 6). The shear deformation energy of B is then related to the torsion of the cylinders; since we need to consider large deformations, the torsion, because of Poynting effect, is in general coupled with an elongation.

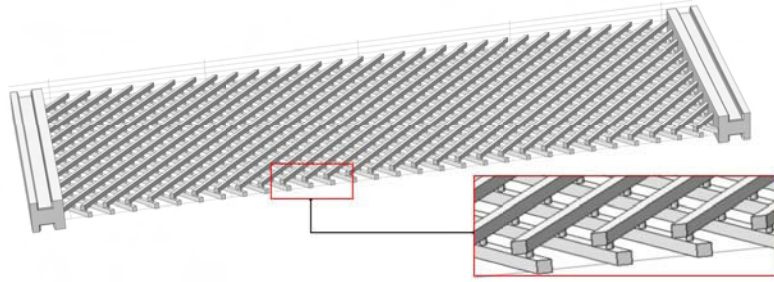


Figure 6: 3D view of a possible physical realization of B , with a zoom showing the cylindric pivots.

We consider a cylinder subjected to a combined elongation-twisting deformation (with respect to z axis). During the considered deformation the circular cross section remains undeformed. The aim of this section consists in deducing a 1D constitutive law from the 3D case by means of standard Saint Venant assumptions. Although the proposed model is satisfactory for a 3D system such that of Fig. 6 below, a generalization to micro- and nano-scale systems may require taking into account the important effects arising from a large ratio between surface and volume. Effects of this kind are becoming increasingly relevant from a theoretical and practical point of view because of the novel possibilities in micro- and nano-engineering; for useful references, the reader can see e.g. [69–71].

6.1 Kinematic model

We assume that the cross section remains plane during the deformation process, i.e. the warping of the cross section is neglected. The displacement consists in an arbitrary rotation, $\theta(z)$, around the centroid z and in a translation $w(z)$ along the z axis independent of x and y coordinates on the

cross section:

$$\begin{aligned}
u &= x (\cos \theta (z) - 1) - y \sin \theta (z) \\
v &= x \sin \theta (z) + y (\cos \theta (z) - 1) \\
w &= w(z)
\end{aligned} \tag{73}$$

in which u, v are the orthogonal components in the cross section plane. The strain gradient deformation tensor associated to (73) is given by

$$\mathbf{F} = \begin{pmatrix} \cos(\vartheta) & -\sin(\vartheta) & \vartheta'(-x \sin(\vartheta) - y \cos(\vartheta)) \\ \sin(\vartheta) & \cos(\vartheta) & \vartheta'(x \cos(\vartheta) - y \sin(\vartheta)) \\ 0 & 0 & w'(z) + 1 \end{pmatrix} \tag{74}$$

The Green-Lagrange tensor, $2 \mathbf{E} = \mathbf{F}^T \mathbf{F} - \mathbf{I}$, associated to the displacement (73), is:

$$\{\mathbf{E}\}_{ij} = \begin{pmatrix} 0 & 0 & -\frac{y}{2}\vartheta' \\ 0 & 0 & \frac{x}{2}\vartheta' \\ -\frac{y}{2}\vartheta' & \frac{x}{2}\vartheta' & w' + \frac{1}{2}(w')^2 + \frac{r^2}{2}(\vartheta')^2 \end{pmatrix} \tag{75}$$

where $r^2 = x^2 + y^2$. The only non vanishing terms are:

$$\begin{aligned}
\varepsilon_z &:= w' + \frac{1}{2}(w')^2 + \frac{(r \theta')^2}{2}, \\
\gamma &:= \sqrt{\gamma_{xz}^2 + \gamma_{yz}^2} = r\theta'.
\end{aligned} \tag{76}$$

6.2 Elastic energy and constitutive equations

By assuming a linear elastic material, the potential energy for the considered model reduces to

$$U = \int_0^l dz \int_A \frac{1}{2} (E\varepsilon_z^2 + G\gamma^2) dA \quad (77)$$

where A is the cross section area. By substituting (76), and integrating with respect to A , we obtain:

$$U = \int_0^l \left\{ \frac{EA}{2}(w')^2 + \frac{EA}{2}(w')^3 + \frac{EA}{8}(w')^4 + \frac{EJ}{2}w'(\theta')^2 + \frac{EJ}{4}(w')^2(\theta')^2 + \frac{EH}{8}(\theta')^4 + \frac{GJ}{2}(\theta')^2 \right\} dz \quad (78)$$

where:

$$J := \int_A r^2 dA, \quad H := \int_A r^4 dA. \quad (79)$$

Let $w' = \varepsilon$ and $\theta' = \kappa$. The density of the energy for the 1D model becomes then:

$$\phi(\varepsilon, \kappa) = \frac{EA}{2}\varepsilon^2 + \frac{EA}{2}\varepsilon^3 + \frac{EA}{8}\varepsilon^4 + \frac{EJ}{2}\varepsilon\kappa^2 + \frac{EJ}{4}\varepsilon^2\kappa^2 + \frac{EH}{8}\kappa^4 + \frac{GJ}{2}\kappa^2, \quad (80)$$

so that the constitutive equation are given by:

$$N = \partial_\varepsilon \phi(\varepsilon, \kappa), \quad M = \partial_\kappa \phi(\varepsilon, \kappa), \quad (81)$$

in which N and M are the the axial stress and the twisting moment respectively. The non linear

coupled constitutive equations for the reduced 1D theory are given by:

$$\begin{aligned} N(\varepsilon, \kappa) &= EA\varepsilon + \frac{3EA}{2}\varepsilon^2 + \frac{EA}{2}\varepsilon^3 + \frac{EJ}{2}\kappa^2 + \frac{EJ}{2}\varepsilon\kappa^2, \\ M(\varepsilon, \kappa) &= GJ\kappa + \frac{EH}{2}\kappa^3 + EJ\varepsilon\kappa + \frac{EJ}{2}\varepsilon^2\kappa. \end{aligned} \quad (82)$$

6.3 Condensation of the constitutive equations

If there is no axial stress, we can assume $N(z) = 0$ to define the $\varepsilon = \varepsilon(\kappa)$ and finally one has $M = M(\kappa)$, i.e. exists a local axial deformation on the generic fiber that globally produces $N = 0$. But the condition, $N = 0$, is not solvable in an easy analytical way, so we assume for the ε the subsequent even power series expansion:

$$\varepsilon = \sum_{i=2,4,6} c_i \kappa^i \quad (83)$$

in this way the elongation is independent on the sign of the torsion. Substituting in the equation of $N = 0$ by means of the polynomial identity principle we get a linear set of equations defining the coefficients c_i . In this way, considering only the first three terms of the series (83), we have:

$$\varepsilon = -\frac{1}{2} \frac{EJ}{EA} \kappa^2 - \frac{1}{8} \left(\frac{EJ}{EA} \right)^2 \kappa^4 - \frac{1}{16} \left(\frac{EJ}{EA} \right)^3 \kappa^6 + \dots \quad (84)$$

so that, the twisting moment is $M(\varepsilon, \kappa) = M(\kappa)$:

$$M = GJ\kappa + \frac{1}{2} \left(EH - \frac{(EJ)^2}{EA} \right) \kappa^3 + \frac{5}{128} \frac{(EJ)^5}{(EA)^4} \kappa^9 + \dots \quad (85)$$

in which only odd powers of κ are present, and then the sign of $M(\kappa)$ changes according to the sign of the κ deformation component. It is easily verified that the related deformation energy is of the polynomial form W_2 above considered. As already mentioned, experimental results are indicating the alternative form W_1 as a reasonable assumption. The fact that basic assumptions lead to the

form W_2 is interesting and suggests that probably a more refined reduction procedure has to be considered in order to better capture the peculiarities of the mechanics of the system.

7 Conclusions

The considered mechanical system entails rich prospects of theoretical and application-oriented developments, as it can be generalized in many possible directions:

- More general geometry, e.g. non orthogonal or non rectilinear fibers.
- More general kinematics, e.g. non symmetrical/non uniform boundary conditions, non planar placements, non planar reference (unstressed) configuration.
- More general beam model, e.g. non exactly inextensible and shear deformable beams (on generalized beam theory the reader can see e.g. [72–75])
- More general forms for the deformation energy.
- Multiphysics systems, e.g. beams displaying piezo- electro electric effects (for general references see [76, 77]).
- Investigation of dynamical effects due to inertia, and in particular wave propagation. In this connection, one can observe that peculiar geometry and kinematics like the ones considered can entail the onset of various kinds of instabilities (see e.g. [78, 79]).

Besides these possible generalizations, some delicate theoretical questions, touched in the present paper (in particular concerning the most suitable function space in which one has to settle), have to be more deeply addressed and rigorous results have to be provided. Moreover, numerical investigations, as already observed, have to be widened and results related to 2D and 3D modeling have to be systematically compared. Finally, the development of new experimental results is also crucial

in this line of investigation. The joint effort of researchers from many areas is therefore called for to achieve substantial progresses on this topic, as is always the case with rich and potentially fruitful subjects.

References

- [1] AC Pipkin. Plane traction problems for inextensible networks. *The Quarterly Journal of Mechanics and Applied Mathematics*, 34(4):415–429, 1981.
- [2] RS Rivlin. Plane strain of a net formed by inextensible cords. In *Collected Papers of RS Rivlin*, pages 511–534. Springer, 1997.
- [3] S. Forest. Mechanics of generalized continua: construction by homogenization. *Le Journal de Physique IV*, 8(PR4):Pr4–39, 1998.
- [4] L. Placidi, G. Rosi, I. Giorgio, and A. Madeo. Reflection and transmission of plane waves at surfaces carrying material properties and embedded in second-gradient materials. *Mathematics and Mechanics of Solids*, 19(5):555–578, 2014.
- [5] Patrizio Neff, Krzysztof Chmiński, and Hans-Dieter Alber. Notes on strain gradient plasticity: finite strain covariant modelling and global existence in the infinitesimal rate-independent case. *Mathematical Models and Methods in Applied Sciences*, 19(02):307–346, 2009.
- [6] J.-J. Alibert, P. Seppecher, and F. dell’Isola. Truss modular beams with deformation energy depending on higher displacement gradients. *Mathematics and Mechanics of Solids*, 8(1):51–73, 2003.
- [7] Francesco dell’Isola, Ugo Andreaus, and Luca Placidi. At the origins and in the vanguard of peridynamics, non-local and higher-gradient continuum mechanics: An underestimated and

- still topical contribution of Gabrio Piola. *Mathematics and Mechanics of Solids*, 20(8):887–928, 2014.
- [8] M. Assidi, B. Ben Boubaker, and J.F. Ganghoffer. Equivalent properties of monolayer fabric from mesoscopic modelling strategies. *International Journal of Solids and Structures*, 48(20):2920–2930, 2011.
- [9] F. Dos Reis and J.F. Ganghoffer. Equivalent mechanical properties of auxetic lattices from discrete homogenization. *Computational Materials Science*, 51:314–321, 2012.
- [10] Francesco Dell Isola and David Steigmann. A two-dimensional gradient-elasticity theory for woven fabrics. *Journal of Elasticity*, 118(1):113–125, 2015.
- [11] Johannes Altenbach, Holm Altenbach, and Victor A Eremeyev. On generalized cosserat-type theories of plates and shells: a short review and bibliography. *Archive of Applied Mechanics*, 80(1):73–92, 2010.
- [12] E. Garusi, A. Tralli, and A. Cazzani. An unsymmetric stress formulation for reissner-mindlin plates: A simple and locking-free rectangular element. *International Journal of Computational Engineering Science*, 5(3):589–618, 2004.
- [13] A. Rinaldi and L. Placidi. A microscale second gradient approximation of the damage parameter of quasi-brittle heterogeneous lattices. *ZAMM - Zeitschrift für Angewandte Mathematik und Mechanik/Journal of Applied Mathematics and Mechanics*, 2013.
- [14] S. Federico, A. Grillo, and W. Herzog. A transversely isotropic composite with a statistical distribution of spheroidal inclusions: a geometrical approach to overall properties. *Journal of the Mechanics and Physics of Solids*, 52(10):2309–2327, 2004. DOI: 10.1016/j.jmps.2004.03.010.
- [15] Patrizio Neff. On material constants for micromorphic continua. *Trends in Applications of Mathematics to Mechanics, STAMM Proceedings, Seeheim*, pages 337–348, 2004.

- [16] Claude Boutin. Microstructural effects in elastic composites. *International Journal of Solids and Structures*, 33(7):1023–1051, 1996.
- [17] S. Federico. On the linear elasticity of porous materials. *International Journal of Mechanical Sciences*, 52(2):175–182, 2010.
- [18] P. Neff, I.-D. Ghiba, A. Madeo, L. Placidi, and G. Rosi. A unifying perspective: the relaxed linear micromorphic continuum. *Continuum Mechanics and Thermodynamics*, pages 1–43, 2013.
- [19] L. Placidi and Hutter K. Thermodynamics of polycrystalline materials treated by the theory of mixtures with continuous diversity. *Continuum Mechanics and Thermodynamics*, 17:409–451, 2006.
- [20] J J Alibert and A Della Corte. Second-gradient continua as homogenized limit of pantographic microstructured plates: a rigorous proof. *Zeitschrift für angewandte Mathematik und Physik* DOI: 10.1007/s00033-015-0526-x, 66(5):2855–2870, 2015.
- [21] Patrizio Neff and Samuel Forest. A geometrically exact micromorphic model for elastic metallic foams accounting for a fine microstructure. modelling, existence of minimizers, identification of moduli and computational results. *Journal of Elasticity*, 87(2-3):239–276, 2007.
- [22] R. D. Mindlin. Micro-structure in linear elasticity. *Archive for Rational Mechanics and Analysis*, 16(1):51–78, 1964.
- [23] A. Misra and Y. Yang. Micromechanical model for cohesive materials based upon pseudo-granular structure. *International Journal of Solids and Structures*, 47:2970–2981, 2010.
- [24] Angela Madeo, Patrizio Neff, Ionel-Dumitrel Ghiba, Luca Placidi, and Giuseppe Rosi. Wave propagation in relaxed micromorphic continua: modeling metamaterials with frequency band-gaps. *Continuum Mechanics and Thermodynamics*, pages 1–20, 2013.

- [25] Manuel Ferretti, Angela Madeo, Francesco Dell Isola, and Philippe Boisse. Modeling the onset of shear boundary layers in fibrous composite reinforcements by second-gradient theory. *Zeitschrift für angewandte Mathematik und Physik*, 65(3):587–612, 2014.
- [26] Pierre Seppecher, Jean-Jacques Alibert, and Francesco Dell Isola. Linear elastic trusses leading to continua with exotic mechanical interactions. In *Journal of Physics: Conference Series*, volume 319, page 012018. IOP Publishing, 2011.
- [27] A. Grillo, S. Federico, G. Wittum, S. Imatani, G. Giacomini, and M. V. Miunovi. Evolution of a fibre-reinforced growing mixture. *Nuovo Cimento C*, 32C(1):97–119, 2009.
- [28] A. Grillo, G. Wittum, A. Tomic, and S. Federico. Remodelling in statistically oriented fibre-reinforced materials and biological tissues. *Mathematics and Mechanics of Solids*, 2014. DOI: 10.1177/1081286513515265.
- [29] A. Grillo, S. Federico, and G. Wittum. Growth, mass transfer, and remodeling in fibre-reinforced, multi-constituent materials. *International Journal of Non-Linear Mechanics*, 47(2):388–401, 2012.
- [30] Nahiene Hamila and Philippe Boisse. Locking in simulation of composite reinforcement deformations. analysis and treatment. *Composites Part A: Applied Science and Manufacturing*, 53:109–117, 2013.
- [31] A. Misra and V. Singh. Micromechanical model for viscoelastic-materials undergoing damage. *Continuum Mechanics and Thermodynamics*, 25:1–16, 2013.
- [32] Daria Scerrato, Ivan Giorgio, Angela Madeo, Ali Limam, and Félix Darve. A simple non-linear model for internal friction in modified concrete. *International Journal of Engineering Science*, 80:136–152, 2014.

- [33] C.P. Laurent, D. Durville, C. Vaquette, R. Rahouadj, and J.F. Ganghoffer. Computer-aided tissue engineering: Application to the case of anterior cruciate ligament repair. *Biomechanics of Cells and Tissues*, 9:1–44, 2013.
- [34] C.P. Laurent, D. Durville, D. Mainard, J-F. Ganghoffer, and R. Rahouadj. Designing a new scaffold for anterior cruciate ligament tissue engineering. *Journal of the mechanical behavior of biomedical materials*, 12:184–196, 2012.
- [35] C.P. Laurent, D. Durville, X. Wang, J-F. Ganghoffer, and R. Rahouadj. Designing a new scaffold for anterior cruciate ligament tissue engineering. *Computer Methods in Biomechanics and Biomedical Engineering*, 13(S1):87–88, 2010.
- [36] I. Goda, M. Assidi, S. Belouettar, and J.F. Ganghoffer. A micropolar anisotropic constitutive model of cancellous bone from discrete homogenization. *Journal of the Mechanical Behavior of Biomedical Materials*, 16:87–108, 2012.
- [37] S. J. Hollister. Porous scaffold design for tissue engineering. *Nature materials*, 4(7):518–524, 2005.
- [38] A. Grillo and G. Wittum. Growth and mass transfer in multi-constituent biological materials. *AIP Conference Proceedings*, 1281(1):355–358, 2010.
- [39] U. Andreaus, I. Giorgio, and T. Lekszycki. A 2-D continuum model of a mixture of bone tissue and bio-resorbable material for simulating mass density redistribution under load slowly variable in time. *ZAMM - Zeitschrift für Angewandte Mathematik und Mechanik / Journal of Applied Mathematics and Mechanics*, 94(12):978–1000, 2014.
- [40] I. Giorgio, U. Andreaus, and A. Madeo. The influence of different loads on the remodeling process of a bone and bio-resorbable material mixture with voids. *Continuum Mechanics and Thermodynamics*, 2014. DOI: 10.1007/s00161-014-0397-y.

- [41] F dell Isola, MV D Agostino, Madeo A, Boisse P, and Steigmann D. Minimization of shear energy in two dimensional continua with two orthogonal families of inextensible fibers: the case of standard bias extension test. *Journal of Elasticity*, 2015, DOI: 10.1007/s10659-015-9536-3.
- [42] Francesco dell Isola and Luca Placidi. Variational principles are a powerful tool also for formulating field theories. In *Variational Models and Methods in Solid and Fluid Mechanics*. Springer Science & Business Media, 2012.
- [43] L. Placidi. A variational approach for a nonlinear one-dimensional damage-elasto-plastic second-gradient continuum model. *Continuum Mechanics and Thermodynamics*, Published online 23 December 2014. DOI: 10.1007/s00161-014-0405-2.
- [44] L. Placidi. A variational approach for a nonlinear 1-dimensional second gradient continuum damage model. *Continuum Mechanics and Thermodynamics*, Published online 20 February 2014. DOI: 10.1007/s00161-014-0338-9.
- [45] John M Ball. Convexity conditions and existence theorems in nonlinear elasticity. *Archive for rational mechanics and Analysis*, 63(4):337–403, 1976.
- [46] Victor A Eremeyev and Leonid P Lebedev. Existence of weak solutions in elasticity. *Mathematics and Mechanics of Solids*, 18(2):204–217, 2013.
- [47] S. Federico. On the volumetric-distortional decomposition of deformation in elasticity. *Mathematics and Mechanics of Solids*, 15(6):672–690, 2010.
- [48] S. Federico, A. Grillo, and S. Imatani. The linear elasticity tensor of incompressible materials. *Mathematics and Mechanics of Solids*, Available online 2014-10-06. DOI: 10.1177/1081286514550576.
- [49] V.A. Yeremeyev, A.B. Freidin, and L.L. Sharipova. The stability of the equilibrium of two-phase elastic solids. *Journal of Applied Mathematics and Mechanics*, 71(1):61 – 84, 2007.

- [50] W. Pietraszkiewicz, V. Eremeyev, and V. Konopi ska. Extended non-linear relations of elastic shells undergoing phase transitions. *ZAMM - Zeitschrift für Angewandte Mathematik und Mechanik / Journal of Applied Mathematics and Mechanics*, 87(2):150–159, 2007.
- [51] V. A. Eremeyev and W. Pietraszkiewicz. Phase transitions in thermoelastic and thermoviscoelastic shells. *Archives of Mechanics*, 61(1):41–67, 2009.
- [52] V. A. Eremeyev and W. Pietraszkiewicz. Thermomechanics of shells undergoing phase transition. *Journal of the Mechanics and Physics of Solids*, 59(7):1395–1412, 2011.
- [53] A. Luongo. Perturbation methods for nonlinear autonomous discrete-time dynamical systems. *Nonlinear Dynamics*, 10(4):317–331, 1996.
- [54] E. Turco and P. Caracciolo. Elasto-plastic analysis of kirchhoff plates by high simplicity finite elements. *Computer Methods in Applied Mechanics and Engineering*, 190(5–7):691–706, 2000.
- [55] A. Cazzani, M. Malagù, and E. Turco. Isogeometric analysis of plane-curved beams. *Mathematics and Mechanics of Solids*, 2014. DOI: 10.1177/1081286514531265.
- [56] L. Greco, N. Impollonia, and M. Cuomo. A procedure for the static analysis of cable structures following elastic catenary theory. *International Journal of Solids and Structures*, 51(7):1521–1533, 2014.
- [57] Luigi Carassale and Giuseppe Piccardo. Non-linear discrete models for the stochastic analysis of cables in turbulent wind. *International Journal of Non-Linear Mechanics*, 45(3):219–231, 2010.
- [58] A. Cazzani and M. Rovati. Sensitivity analysis and optimum design of elastic-plastic structural systems. *Meccanica*, 26(2–3):173–178, 1991.

- [59] B. Descamps. *Computational Design of Lightweight Structures: Form Finding and Optimization*. John Wiley & Sons, 2014.
- [60] U. Andreaus and M. Colloca. Prediction of micromotion initiation of an implanted femur under physiological loads and constraints using the finite element method. *Proc Inst Mech Eng H*, 223(5):589–605, Jul 2009.
- [61] L. Greco and M. Cuomo. B-Spline interpolation of Kirchhoff-Love space rods. *Computer Methods in Applied Mechanics and Engineering*, 256(0):251–269, 2013.
- [62] L. Greco and M. Cuomo. An implicit G1 multi patch B-spline interpolation for Kirchhoff-Love space rod. *Computer Methods in Applied Mechanics and Engineering*, 269(0):173–197, 2014.
- [63] Ali Javili and Paul Steinmann. A finite element framework for continua with boundary energies. part i: The two-dimensional case. *Computer Methods in Applied Mechanics and Engineering*, 198(27):2198–2208, 2009.
- [64] A Javili and P Steinmann. A finite element framework for continua with boundary energies. part ii: The three-dimensional case. *Computer Methods in Applied Mechanics and Engineering*, 199(9):755–765, 2010.
- [65] Arkadi Berezovski, Ivan Giorgio, and Alessandro Della Corte. Interfaces in micromorphic materials: Wave transmission and reflection with numerical simulations. *Mathematics and Mechanics of Solids*, 2015, DOI: 10.1177/1081286515572244.
- [66] U. Andreaus, M. Colloca, and D. Iacoviello. *Modeling of Trabecular Architecture as Result of an Optimal Control Procedure*, volume 4 of *Lecture Notes in Computational Vision and Biomechanics*. Springer Netherlands, 2013.
- [67] U. Andreaus, M. Colloca, and D. Iacoviello. An optimal control procedure for bone adaptation under mechanical stimulus. *Control Engineering Practice*, 20(6):575–583, 2012.

- [68] U. Andreaus, M. Colloca, D. Iacoviello, and M. Pignataro. Optimal-tuning pid control of adaptive materials for structural efficiency. *Structural and Multidisciplinary Optimization*, 43(1):43–59, 2011.
- [69] VA Eremeyev. Nonlinear micropolar shells: theory and applications. *Shell structures: Theory and applications*, pages 11–18, 2005.
- [70] VA Eremeyev and NF Morozov. The effective stiffness of a nanoporous rod. In *Doklady Physics*, volume 55, pages 279–282. Springer, 2010.
- [71] Holm Altenbach, Victor A Eremeyev, and Nikita F Morozov. Mechanical properties of materials considering surface effects. In *IUTAM Symposium on Surface Effects in the Mechanics of Nanomaterials and Heterostructures*, pages 105–115. Springer, 2013.
- [72] Mircea Bîrsan, Holm Altenbach, Tomasz Sadowski, VA Eremeyev, and Daniel Pietras. Deformation analysis of functionally graded beams by the direct approach. *Composites Part B: Engineering*, 43(3):1315–1328, 2012.
- [73] Giuseppe Piccardo, Gianluca Ranzi, and Angelo Luongo. A complete dynamic approach to the generalized beam theory cross-section analysis including extension and shear modes. *Mathematics and Mechanics of Solids*, 19(8):900–924, 2014.
- [74] Giuseppe Piccardo and Federica Tubino. Dynamic response of euler-bernoulli beams to resonant harmonic moving loads. *Structural Engineering and Mechanics*, 44(5):681–704, 2012.
- [75] Claude Boutin, Stéphane Hans, and Céline Chesnais. Generalized beams and continua. dynamics of reticulated structures. In *Mechanics of Generalized Continua*, pages 131–141. Springer, 2010.

- [76] I. Giorgio, A. Culla, and D. Del Vescovo. Multimode vibration control using several piezoelectric transducers shunted with a multiterminal network. *Archive of Applied Mechanics*, 79(9):859–879, September 2009.
- [77] D. Del Vescovo and I. Giorgio. Dynamic problems for metamaterials: review of existing models and ideas for further research. *International Journal of Engineering Science*, 80:153–172, 2014.
- [78] A. Luongo, D. Zulli, and G. Piccardo. A linear curved-beam model for the analysis of galloping in suspended cables. *Journal of Mechanics of Materials and Structures*, 2(4):675–694, 2007.
- [79] Giuseppe Piccardo, Luisa Carlotta Pagnini, and Federica Tubino. Some research perspectives in galloping phenomena: critical conditions and post-critical behavior. *Continuum Mechanics and Thermodynamics*, 27(1-2):261–285, 2015.

Chapter 4

Experimental extension tests on polyamide
pantographic sheets

Experimental extension tests on polyamide pantographic sheets

1 Overview

In this Chapter it will be shown and discussed some experimental evidence concerning extension tests performed on pantographic sheets of the type introduced as a model case in Section 7 of the Introduction. The main aim of the experimental tests were:

- To show the advantages of these kind of structures, with particular focus on the behavior in fracture.
- To show the need of generalized continuum models for a convenient description of the behavior of pantographic structures.

The experiments have been performed thanks to the cooperation with the group headed by Prof. Tomasz Lekszycki, Warsaw University of Technology, Poland.

The experimental tests will be compared with numerical results obtained with a simple algorithm developed in [1] and [2].

2 Experimental tests

A 21 cm polyamide sample, whose geometry is represented schematically in Fig.1, has been manufactured by 3D-printing. The cross section of the fibers is a rectangle and the length of its sides are 1.6 mm (height) and 0.9 mm (width). The pivots are cylinders with height equal to 0.5 mm and a radius of 0.25 mm. The lattice step has been chosen small enough to make macroscopic effects (such as the presence of boundary layers) visible, but at the same time large enough to make the microstructure clearly observable. In potential applications, of course, a much smaller lattice step can be employed. A picture of the sample is visible in Fig.2, left.

The bottom short side of the sample has been clamped and the top short side has been connected rigidly to a hard device imposing a rigid translation orthogonal to the side in the extension direction.

Pictures have been taken at regular intervals with the imposed displacement ranging from 0 to 80 mm, which amounts to $\approx 38\%$ of the total length.

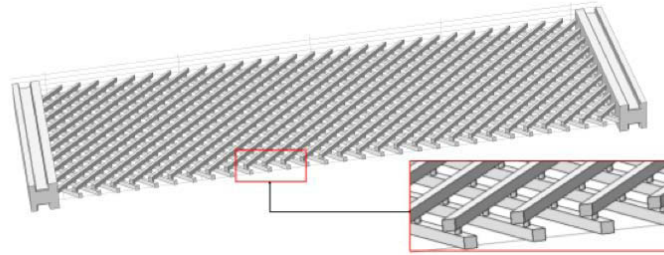


Figure 1: Scheme of the geometry of the 3D-printed sample.

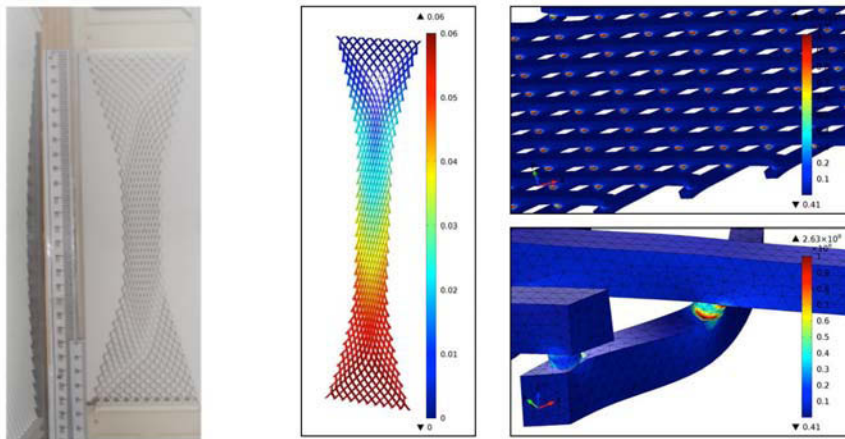


Figure 2: On the left: a 3D-printed polyamide sample of total length 21 cm (when undeformed). The picture represents a (moderately) deformed shape in which the two short sides of the sample are farther than in the undeformed configuration. Boundary layers, i.e. small zones in which the variation of the deformation is concentrated, are clearly visible. At the center: a possible (but computationally very expensive) numerical approach using a classical 3D Cauchy continuum discretized by finite elements with a mesh of $\approx 10^6$ elements; in color map the displacement is represented. On the right: two zooms showing the mesh; in color map the deformation energy density is represented. It can be seen that the deformation is concentrated in the pivots.

Looking at Fig.3, we can observe that, as it was shown in Chapter 3, two triangular regions close to the short sides remain rigid (because of inextensibility). As the test goes on (see Fig.4 and 5), we can see that fracture always arises close to the corners of the sample, as the fiber at the corner indeed

undergoes the sharpest axial stress. Once a fiber collapses, the maximum axial stress is then sustained by the following one in the lattice geometry, and so on: see for instance the sequence of fractures in panels h), i), j) and k) of Fig.5. This kind of behavior in fracture is very safe for two reasons:

1. The structure is resilient, i.e. the fracture does not occur abruptly but progressively. Moreover, the structure keeps resisting for long after the fracture has begun before the ultimate collapse.
2. Because of the particular geometry of the microstructure, the fracture zone is very well predictable.

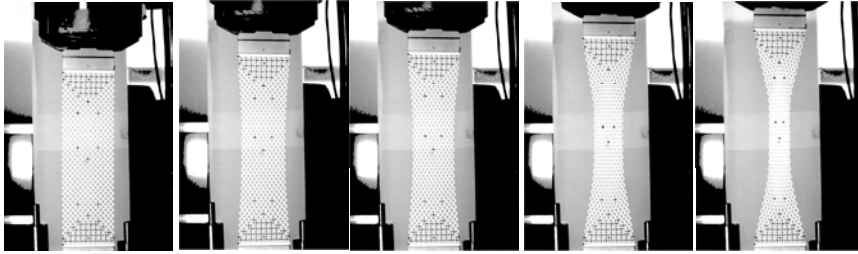


Figure 3: A standard extension test performed using a hard device. The bottom side of the sample is clamped, the top side undergoes a rigid translation upwards. As it was shown in Chapter 3, two triangular regions close to the short sides remain rigid. In this first part of the test, the pictures have been chosen wide enough to show the hard device.

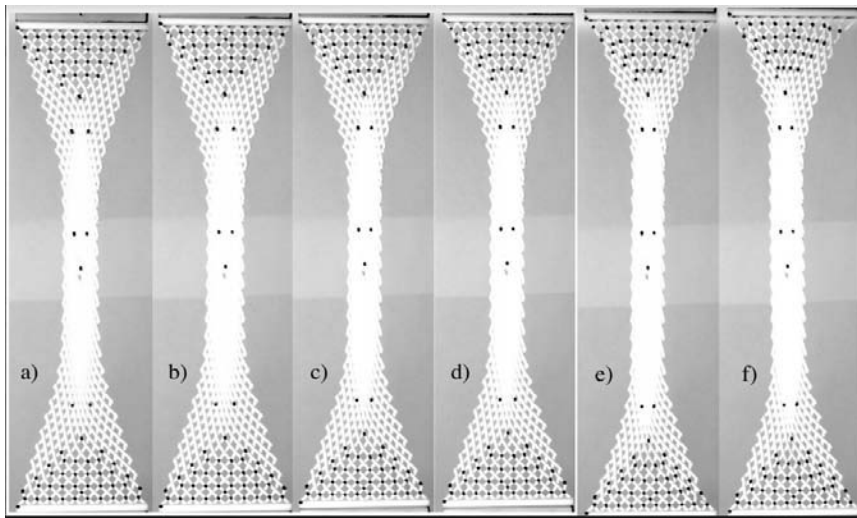


Figure 4: A standard extension test performed using a hard device - part 2. The bottom side of the sample is clamped, the top side undergoes a rigid translation upwards. In panel f) it is visible the beginning of fibers' fracture close to the top right corner.

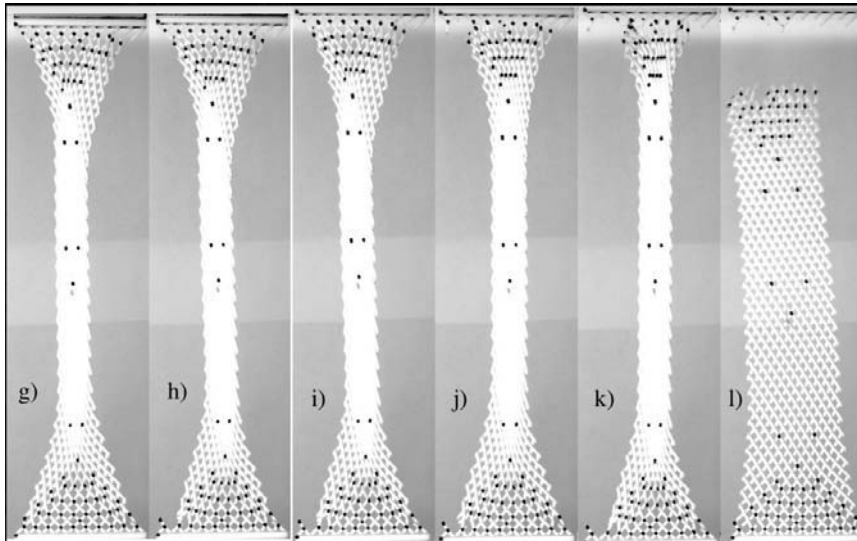


Figure 5: A standard extension test performed using a hard device - part 3. The bottom side of the sample is clamped, the top side undergoes a rigid translation upwards. Progressive fractures of fibers close to the corners (both at the top and at the bottom) are visible. In panel l) the final collapse of the pantographic structure is reached.

In Fig.6, the experimental force-displacement plot is shown. The points of the graph corresponding to the fractures of single fibers are clearly visible as local maxima of the curve. Estimating the area under the curve, it can be seen that the amount of energy between the beginning of the fracture (from 57 mm on) and the ultimate collapse and the energy corresponding to the elastic region (up to 57 mm) have the same order of magnitude. This depends again on the particular geometry of the object, and it means that the structure is capable of releasing potential energy for long, and very gradually, after the fracture starts.

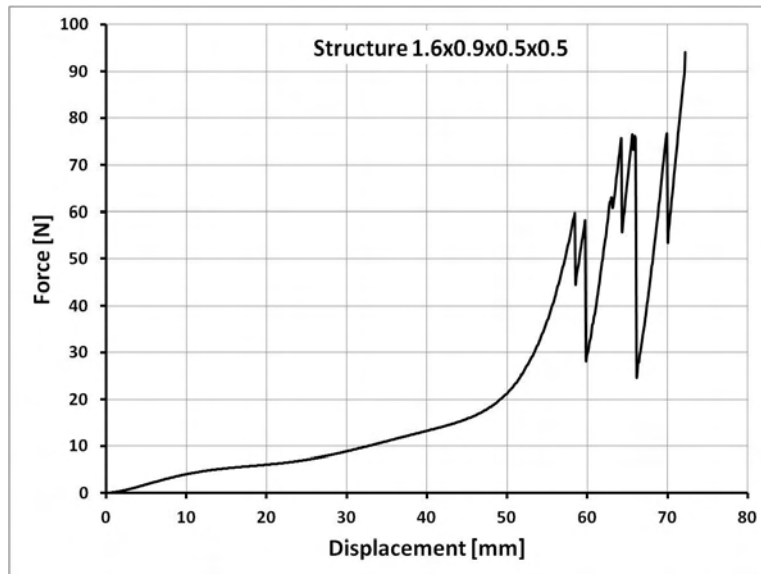


Figure 6: Force-displacement plot for the extension test shown in Fig.3, 4 and 5. In the figure the lengths of the sides of the cross-section of the fibers and the height and diameter of the cylindrical pivots are indicated (in mm). For further comments on the graph see the text.

In Fig.7 and 8, a different kind of extension test is shown. This time the hard device pulls vertically one corner of the structure (top left corner), while the bottom short side is clamped, and the pulled corner is free to rotate. The overall qualitative behavior in fracture is very similar to the previous test: again fractures occur close to the corners of the sample, and the structure displays significant resilience before the ultimate collapse. Force-displacement data from this experimental test will be compared with numerical simulations in the following section.

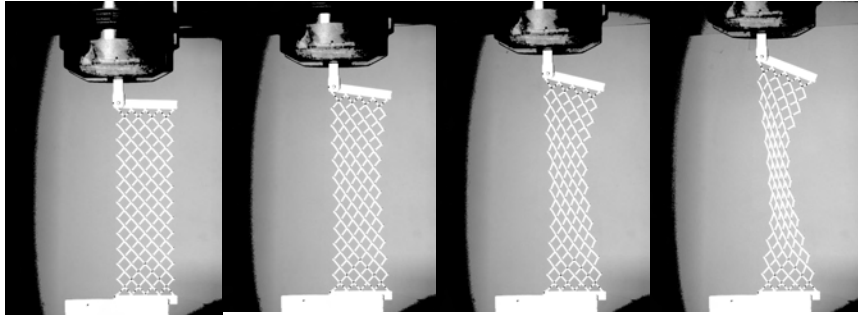


Figure 7: Another extension test in which the hard device pulls vertically one corner of the structure (top left corner), while the bottom short side is clamped. The pulled corner is free to rotate. The pictures show the first part of the test.

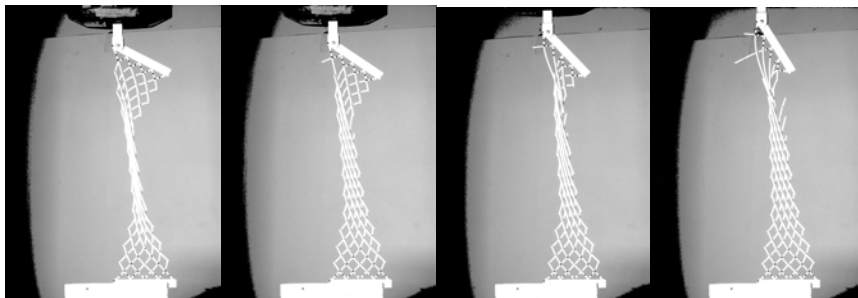


Figure 8: Another extension test in which the hard device pulls vertically one corner of the structure (top left corner), while the bottom short side is clamped. The pulled corner is free to rotate. The pictures show the second part of the test. Again, fracture arises at the corners of the sample.

3 Comparison with numerical results

A simple numerical algorithm has been introduced in [1] and in [2] is enhanced and employed for a comparison with the experimental data corresponding to the test shown in Fig.7 and 8. A quick sketch of the algorithm (in the version used in [2]) is the following.

The algorithm is based on the idea of modeling the fibers as extensible Euler beams, partitioned in such a way that each part corresponds to a portion between two adjacent pivots. The portions are subject to compatibility conditions ensuring continuity of displacements and rotations at the pivoted ends. The employed set of admissible test functions consists of fifth-order Hermite polynomials verifying the boundary data and the compatibility con-

ditions. An energy is introduced which takes into account the torsion of the pivots (shear deformation at the macro-level) and the elongation and bending of the fibers. The solution is obtained by minimizing (with the standard “NMinimize” function of the software *Mathematica*) the total energy in the set of admissible test functions. In Fig.9, the experimental data (grey dots) relative to the test shown in Fig.7 and 8 are compared to the previsions of the numerical algorithm (red dots). The blue line represents an interpolation curve for experimental data. The units are m (horizontal axis) and N (vertical axis). It can be seen that the numerical model is capable of well capturing the behavior of the experimental test, and therefore the comparison validates the employed numerical algorithm.

In Fig.10, a numerical simulation on the distribution of the various components of the total deformation energy is shown. It can be seen that the bending energy is not a negligible fraction of the total energy. This deformation energy is associated to the in-plane curvature of the fibers and, as it is well known (see for instance the Introduction, especially Section 7 and references therein), cannot be captured by a classical Cauchy continuum. Therefore, a second gradient continuum, in which the in-plane geometric curvature can be easily introduced in the energy, is called for in order to obtain a convenient homogenized model. This is well consistent with what we saw in Chapter 1, where a second gradient continuum has been obtained as Γ -limit of a sequence of lattice (truss-like) structures with progressively smaller lattice step. It is worth noting that the homogenized model is computationally much more efficient than a fully detailed 3D Cauchy model as the one employed for the simulation shown in Fig.2, center and right (this has been demonstrated in detail in [3]).

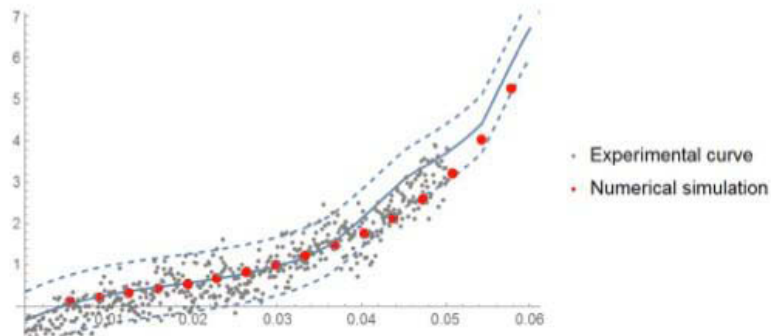


Figure 9: Comparison between experimental data (grey dots) relative to the test shown in Fig.7 and 8 and numerical simulations (red dots) ([2]). The blue line represents an interpolation curve for experimental data. The units are m (horizontal axis) and N (vertical axis). It can be seen that the numerical model is capable of well capturing the behavior of the experimental test.

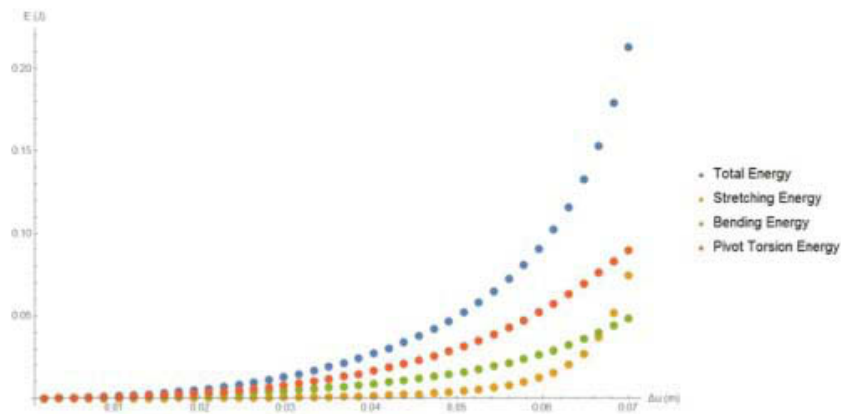


Figure 10: Distribution of the total deformation energy corresponding to the test shown in Fig.7 and 8 (numerical simulation). The bending energy is not a negligible fraction of the total energy, and therefore a second gradient continuum is needed for a convenient homogenized model.

Finally, it is interesting to address the problem theoretically at the meso-scale, i.e. to consider the pantographic structure not as a homogenized second gradient plate (macro-scale), nor as a 3D Cauchy continuum (micro-scale), but rather as a lattice of Euler beams. In this case, as already said, it is reasonable to describe mathematically the interaction between a single

fiber and the “external world” as a distributed load, and this approximation (exactly as in the case of the homogenized model) will be better and better as the lattice step decreases. Experimental evidence in extension tests shows that the fibers undergo large deformations even when the overall deformation is moderate: see for instance Fig.11, left. The deformation can be even larger when a shear test is performed (see Fig.11, right, experimental test described in [4]). In the literature there is of course a very large number of papers dealing with the large deformations of Euler’s *Elastica*, but they generally focus on the case of concentrated end load, while much less is available on the case of distributed load. This motivated the study done in the following Chapter 5, to which we address also for a bibliography on the problem.

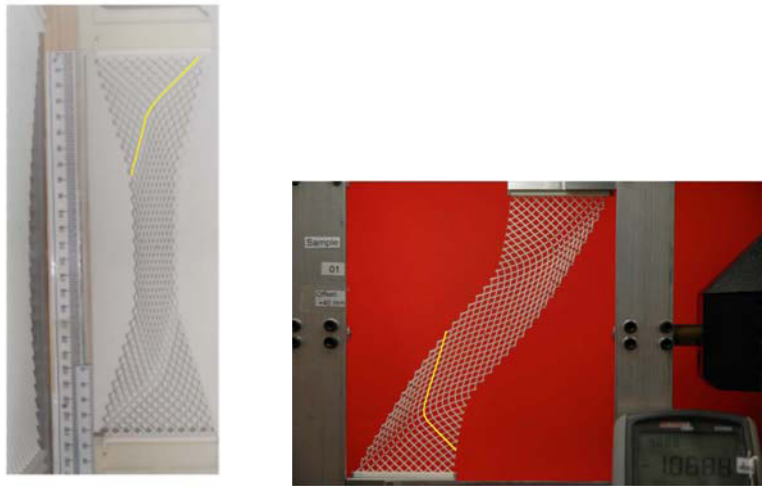


Figure 11: Single fibers undergo large deformations in standard extension test (left) as well as in a shear test (right). Two fibers have been highlighted in yellow to show the deformation. Notice in particular that the overall deformation in the left figure is quite moderate and still the highlighted fiber clearly undergoes geometrically nonlinear deformations (the test in the right picture has been described in [4]).

4 References

References

- [1] Andreaus U., Spagnuolo M., Lekszycki T., Eugster S, dell’Isola F. Geometrically nonlinear static analysis of planar pantographic structures, 2017. *Submitted*.

- [2] Andreaus U., Spagnuolo M., **Della Corte, A.** et al. Discrete geometrically nonlinear pantographic structures: numerics and experiments (2017) [*In preparation*].
- [3] dell'Isola, F., Cuomo, M., Greco, L., **Della Corte, A.** (2017). Bias extension test for pantographic sheets: numerical simulations based on second gradient shear energies. *Journal of Engineering Mathematics*, 103(1), 127-157.
- [4] Turco E., dell'Isola F., Rizzi N.L., Grygoruk R., Muller W.H. and Liebold C. Fiber rupture in sheared planar pantographic sheets: Numerical and experimental evidence, *Mechanics Research Communications*, vol. 76, 2016 (DOI: 10.1016/j.mechrescom.2016.07.007).

Chapter 5

Equilibria of a clamped Euler beam (*Elastica*) with distributed load: large deformations

**Equilibria of a clamped Euler beam (*Elastica*)
with distributed load: Large deformations**

Alessandro Della Corte

*International Research Center on the Mathematics and
Mechanics of Complex Systems M&MoCS, University of L'Aquila,
L'Aquila, Italy*

*Department of Mechanical and Aerospace Engineering,
Sapienza University of Rome, Rome, Italy
alessandro.dellacorte@uniroma1.it*

Francesco dell'Isola

*International Research Center on the Mathematics and
Mechanics of Complex Systems M&MoCS, University of L'Aquila,
L'Aquila, Italy*

*Department of Structural and Geotechnical Engineering,
Sapienza University of Rome, Rome, Italy
francesco.dellisola@uniroma1.it*

Raffaele Esposito* and Mario Pulvirenti†

*International Research Center on the Mathematics and
Mechanics of Complex Systems M&MoCS, University of L'Aquila,
L'Aquila, Italy*

**raff.esposito@gmail.com*

†pulviren@mat.uniroma1.it

Received 22 October 2016

Revised 18 February 2017

Accepted 14 March 2017

Published 12 June 2017

Communicated by N. Bellomo

We present some novel equilibrium shapes of a clamped Euler beam (*Elastica* from now on) under uniformly distributed dead load orthogonal to the straight reference configuration. We characterize the properties of the minimizers of total energy, determine the corresponding Euler–Lagrange conditions and prove, by means of direct methods of calculus of variations, the existence of curled local minimizers. Moreover, we prove some

†Corresponding author

sufficient conditions for stability and instability of solutions of the Euler–Lagrange, that can be applied to numerically found curled shapes.

Keywords: Clamped *Elastica*; uniformly distributed load; large deformations; equilibrium and stability.

AMS Subject Classification: 74B20, 74G25, 74G35, 74G55, 49JXX

1. Introduction

In this paper we consider the planar configurations of an inextensible *Elastica*¹² of length L , clamped at one of its ends, which is assumed to be the origin of the reference curvilinear abscissa s . The endpoint corresponding to $s = L$ is assumed to be free. Let us assume that \mathcal{E}^2 is the affine Euclidean plane including the placements of the *Elastica*. In \mathcal{E}^2 we introduce a coordinate system whose origin \mathcal{O} coincides with the reference placement of the clamped end of the *Elastica*, and whose basis $(\mathbf{D}_1, \mathbf{D}_2)$ is orthonormal. \mathbf{D}_1 is the tangent unit vector to the reference shape of the *Elastica* (assumed to be straight when undeformed) and coincides with the imposed clamping direction at the clamped end.

1.1. Some considerations on the history of the problem

The theory of large deformations of *Elasticae* was fully formulated by Euler already in 1744,¹² with the important contribution of the ideas of Daniel⁴ and James Bernoulli.⁵ One important tool for finding the equilibrium forms of *Elasticae* was developed by Lagrange,²² who formulated the stationarity condition for their total energy. The relative boundary value problems for the resulting ordinary differential equations have been since then extensively used for determining the equilibrium shapes. Without even trying to provide a complete bibliography, it is worth mentioning that large deformations of the *Elastica* have been studied by many other great scientists (including for instance Max Born in his Doctoral Thesis).⁷ Euler’s beam model, in the inextensible case considered herein, has been validated by means of rigorous derivation from 3D elasticity^{25,27} and systematically and thoroughly used in structural mechanics.

The theory of *Elastica*, indeed, still represents the basis for many more complex problems of structural mechanics (as for instance the behavior of the fibrous structures described in Refs. 30 and 28). In the literature we could not find rigorous results on the study of the whole set of equilibrium shapes and of their stability for an *Elastica* in large deformation under a uniformly distributed load. There were, however, some suggestive numerical results that deserved, in the opinion of the authors, greater attention than they received. Namely, in Refs. 14 and 29 some numerical results producing equilibrium shapes similar to the ones we will present later are shown; in these papers the solutions of the boundary value problem are obtained by means of a shooting technique. In the older paper, Ref. 18 some numerically evaluated stability results on shapes similar to those considered herein are

presented in case of concentrated end load. The cited papers appeared when the first effective numerical codes capable to deal with nonlinear boundary value problems became available. In subsequent investigations, while the numerical methods were more and more developed, the mechanical problems related to large deformations of beams, with the noticeable exception of problems with concentrated end load (see Ref. 3 for a rational bibliography on the problem), seem to have somewhat escaped rigorous treatment.

In the recent past, however, the awareness of the importance of large deformation problems in structural mechanics came back in both theoretical^{6,15,17,1} and computational²¹ directions, and this importance will probably increase whether further substantial progresses will be achieved, in particular since large deformations play a relevant role in topical research lines as the design of metamaterials.^{9,23,11,26} An interesting research stream in the design of novel metamaterials involved the so-called pantographic structures,^{31,34,10} which were first conceived in order to synthesize a particular class of generalized continua, i.e. those described by second gradient energy models.^{24,19} Exactly as in many other conceivable metamaterials, pantographic ones base their exotic behavior on the particular geometrical and mechanical micro-structure of beam lattices² and on the deformation energy localization allowed by the onset of large deformations in portion of beams located in some specific areas of the lattice structure. It is therefore clear that, if one is interested in designing and optimizing pantographic metamaterials, a reasonably complete knowledge of the behavior of beams in large deformations is needed. The authors were indeed pushed in the present research direction exactly pursuing the aforementioned aims.

1.2. Setting of the problem

The configurations of the system are curves

$$\chi : s \in [0, L] \rightarrow \chi(s) \in \mathcal{E}^2 = \chi_1(s)\mathbf{D}_1 + \chi_2(s)\mathbf{D}_2,$$

where \mathcal{E}^2 is the Euclidean plane including the placement of the *Elastica*. We assume that the reference configuration is given by

$$\chi_0 : s \in [0, L] \rightarrow \chi_0(s) = s\mathbf{D}_1 \in \mathcal{E}^2.$$

The considered *Elastica* is subject to an inextensibility constraint, so that placements verify the local condition (denoting with apexes differentiation with respect to the reference abscissa):

$$\chi'(s) \cdot \chi'(s) = 1 \quad \text{for all } s \in [0, L]. \quad (1.1)$$

The elastic energy of the inextensible *Elastica*, as originally assumed by Bernoulli and Euler, is given by the quadratic form

$$\frac{1}{2} \int_0^L k_M \chi''(s) \cdot \chi''(s) ds = \frac{1}{2} \int_0^L k_M \kappa^2(s) ds,$$

where k_M is the bending stiffness of the *Elastica* (we assume $k'_M(s) = 0$) and $\kappa(s)$ is the geometrical curvature of the actual shape of the *Elastica* (because of the inextensibility condition).

Finally we will suppose that the *Elastica* is subject to the uniformly distributed dead load (like gravitational force) given by $\mathbf{b}(s) = b\mathbf{D}_2$, with $b > 0$, whose associated energy is $-b \int_0^L \chi_2(s) ds$. Therefore the equilibria of the system are the stationary points of the energy functional

$$E(\chi(\cdot)) = \frac{1}{2} \int_0^L \chi''(s) \cdot \chi''(s) ds - b \int_0^L \chi_2(s) ds, \quad (1.2)$$

with the additional condition (1.1). The left boundary conditions are $\chi(0) = \mathcal{O}$ and $\chi'(0) = \mathbf{D}_1$, while the right boundary conditions (at $s = L$) are free.

In this paper we study the equilibrium configurations of the system, namely the stationary points of E .

We treat the constraint (1.1) by introducing a different configuration field verifying the inextensibility condition automatically. We define the angle θ , counted in the counter-clockwise sense by the position

$$\chi'(s) = \cos \theta(s) \mathbf{D}_1 + \sin \theta(s) \mathbf{D}_2. \quad (1.3)$$

Once the scalar field $\theta(s)$ is known, together with the clamping condition $\chi(0) = \mathcal{O}$, the placement $\chi(s)$ is uniquely determined by integration. The condition imposing the clamping direction is equivalent to $\theta(0) = 0$.

1.3. Description of the results

Once formulated the problem which consists in studying the stationary points of the energy functional expressed in terms of θ , we make use of the well-known direct method of calculus of variations. The existence of global and local minima of the energy functional is ensured by general theorems based on results first obtained by Tonelli.^{33,8}

A qualitative analysis of the shape of these stationary points is carried out by means of comparisons based on energy considerations.

In this way we find two branches of solutions, parametrized by the load parameter. The first, called “primary branch”, corresponds to global minima of the energy. The solutions, characterized by a positive rotation θ , look like equilibria of a trampoline under the action of a positive gravitational field (see Fig. 8 below).

Another branch of solutions, called “secondary branch” is a topological extension of a family of solution with a negative angle θ (see Fig. 15 below) rotating around the origin (clamping point), which are local minimizers of the energy. These solutions are possible only if the load is sufficiently large or, equivalently, the beam is sufficiently long.

Profiles of the primary and secondary branches are found also numerically by means of a shooting technique. This complements previous qualitative analysis by further quantitative information.

In order to establish a suitable stability chart of these solutions, we note that the primary branch is obviously stable since it is formed by global minima. As for the secondary branch, the situation is richer. Indeed, by establishing sufficient conditions for the stability/instability of the solutions of the Euler–Lagrange equations associated to our variational problem we are able to show that the secondary branch contains stable solutions and give sufficient conditions for the instability.

The paper is organized as follows: in Sec. 2 we reformulate the problem of equilibrium of *Elastica* under uniform load in terms of the rotation field of the cross-section. This allows for a Lagrangian characterization of *Elastica*'s space of configurations. In Sec. 3 we provide rigorous results on the characterization of the equilibrium shapes attaining global energy minima when the intensity of externally applied load varies. In Sec. 4, we prove the existence of a branch of stable equilibrium shapes exhibiting a curling around the clamped extremum. In Sec. 5, we provide some results on the stability and instability of stationary points verifying some particular properties. In Sec. 6, we apply these results to numerically found stationary points. In Sec. 7, we show that the ending part of the curled equilibrium shape coincides (up to a reflection) to the shape of the global minimizer for an *Elastica* of suitably reduced length.

2. Reformulation of the Problem and First Considerations

As already explained, in order to eliminate the constraint (1.1) it is convenient to introduce the new variable θ that is the angle (counted in the anti-clockwise sense) formed by the unitary tangent $\chi'(s)$ to the graph of the curve χ with the x -axis. In the new configuration field, the energy reads

$$E(\theta(\cdot)) = \frac{1}{2} \int_0^L |\theta'(s)|^2 ds - b \int_0^L (L-s) \sin \theta(s) ds. \quad (2.1)$$

Remark 1. Since $|\sin \theta| \leq 1$, it is immediate to see that $E(\theta) \geq -\frac{b}{2}$ for all admissible $\theta \in L^2([0, L])$. In particular, E is bounded from below.

A standard formal computation shows that the Euler–Lagrange conditions associated to the functional (2.1) are

$$\theta'' = -b(L-s) \cos \theta, \quad (2.2)$$

in the set of admissible functions verifying

$$\theta(0) = \theta'(L) = 0. \quad (2.3)$$

Note that, while the condition

$$\theta(0) = 0, \quad (2.4)$$

characterizes the admissible kinematics and is given by the problem, the condition at L is a consequence of imposing stationarity, and can be interpreted by saying that at the free end the curvature must vanish.

We remark that the boundary condition $\theta(0) = \pi$ would also describe a clamped beam. This boundary condition would give rise to solutions that are specular reflection of the solutions with boundary data (2.4). Therefore we will ignore them.

By obvious scaling properties of Eq. (2.2) we see that any solution of such an equation, for a given pair L and b , can be recovered by setting $L = 1$ rescaling $b \rightarrow bL^3$. Therefore from now on we shall assume $L = 1$ leaving b as the only parameter.

By (2.2) we easily obtain the following integral equation for the unknown field θ :

$$\theta(s) = b \int_0^s d\sigma \int_\sigma^1 (1 - \sigma') \cos \theta(\sigma') d\sigma'. \quad (2.5)$$

We define the nonlinear integral operator T as

$$[T\theta](s) = b \int_0^s d\sigma \int_\sigma^1 (1 - \sigma') \cos \theta(\sigma') d\sigma'. \quad (2.6)$$

The solutions to (2.2) with conditions (2.3) and (2.4) are all the fixed points of the map $\theta \rightarrow T(\theta)$.

Proposition 1. *Under the smallness assumption*

$$\frac{b}{6} < 1. \quad (2.7)$$

the solution of the problem (2.2)–(2.4) exists and is unique.

Proof. It is easy to check that under the condition (2.7), the operator T is a strict contraction and hence the proof follows by a standard application of the Banach fixed point theorem. \square

To understand the behavior of the solution obtained for small b , we compute the solution of the boundary value problem:

$$\begin{aligned} \theta'' &= -b(1 - s), \\ \theta(0) &= \theta'(1) = 0, \end{aligned}$$

which follows by setting $\cos \theta = 1$, which is a reasonable approximation when b is small. The result is

$$\theta(s) = \frac{-b}{6} [(1 - s)^3 - 1], \quad (2.8)$$

which means that θ is strictly positive, increasing and concave.

To go further, namely looking for solutions with a large b , we investigate the minima of the energy functional (2.1). We first observe that the energy has the form

$$E(\theta(\cdot)) = \int_0^1 ds \mathcal{L}(\theta', \theta, s), \quad (2.9)$$

where

$$\mathcal{L}(\theta', \theta, s) = \frac{1}{2}(\theta'^2 - b(1-s)\sin\theta). \quad (2.10)$$

We define E on the space

$$H_{0,1}^1 = \{\theta \in H^1[0,1] \mid \theta(0) = 0\}. \quad (2.11)$$

Note that

$$p \rightarrow \mathcal{L}(p, q, s)$$

is a continuous function which is convex and coercive for all q and s . Therefore, by a classical result in Calculus of Variations (see for instance Ref. 16, Sec. 3.2), we have a minimizer in $H_{0,1}^1$, not necessarily unique. Such a minimizer, say θ , is a solution of (2.2) in a weak form,^{16,13} for any value of b , namely

$$(\varphi', \theta') = b(\varphi, (1-s)\cos\theta), \quad (2.12)$$

for all $\varphi \in H_{0,1}^1$ vanishing at the extrema.

Lemma 1. *If θ is weak solution of Eq. (2.12), then it is in C^∞ and is a classical solution of (2.2). In particular, any stationary point of the energy is a classical solution of the problem (2.2), (2.3).*

Proof. Let us define $\Psi = T\theta$. Straightforward computation provides

$$\Psi'' = -b(1-s)\cos\theta(s), \quad (2.13)$$

and therefore, by Eq. (2.12), we get

$$(\varphi', \theta') = -(\varphi, \Psi'') = (\varphi', \Psi'),$$

so that

$$\theta = \Psi.$$

By definition of the operator T (see (2.6)), Ψ is in C^2 if θ is H^1 . Hence the previous equality tells us that θ is in C^2 as well, and applying the argument recursively one obtains that θ is in C^∞ . \square

3. The Primary Branch

In this and in the next section, we investigate some properties of stationary points of $E(\theta(\cdot))$ and in particular of its minimizers.

3.1. Qualitative properties of the minimizer

We start by proving some properties of the stationary points introduced in the previous section.

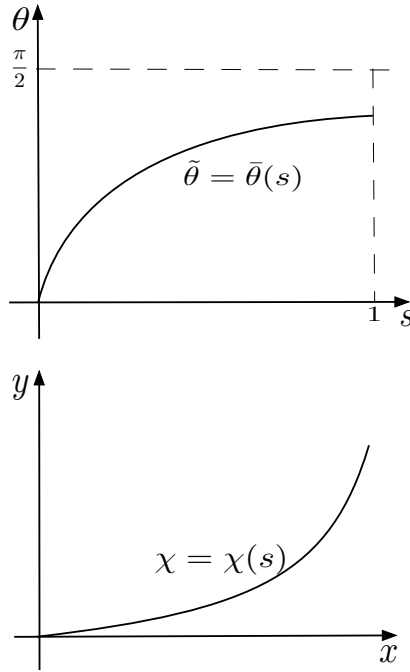


Fig. 1. θ -graph of the minimizer and corresponding shape of the beam.

Proposition 2. *For any $b > 0$ there exists a minimizer $\tilde{\theta} \in C^\infty[0, 1]$ of the energy E , strictly increasing and concave. Moreover $\tilde{\theta}(1) < \frac{\pi}{2}$.*

The statement of the above proposition is illustrated in Fig. 1.

Proof. Let $\tilde{\theta}$ be a minimizer of E . Then it is a solution of (2.12) and, because of Lemma 1, of (2.2).

We note that $\tilde{\theta}''(0) \leq 0$. Then $\tilde{\theta}(s)$ is concave for s sufficiently small and, by using the equation, $\tilde{\theta}$ must cross either $\pi/2$ or $-\pi/2$ to change its concavity.

We start by proving that $\tilde{\theta}$ is increasing in a sufficiently small right neighborhood of the origin. Supposing the contrary by contradiction, then $\tilde{\theta}$ starts to decrease. Since $\tilde{\theta}'(1) = 0$, $\tilde{\theta}$ must change concavity and this means it has to cross $-\pi/2$ in a point s_0 . Consider now the function $\xi \in H_{0,1}^1$ defined as

$$\xi(s) = -\tilde{\theta}(s) \quad \text{for } s \in (0, s_0), \quad \xi(s) = \frac{\pi}{2} \quad \text{for } s \geq s_0.$$

Then

$$E(\xi) < E(\tilde{\theta}).$$

Indeed:

$$\int_0^1 |\xi'(s)|^2 ds \leq \int_0^1 |\tilde{\theta}'(s)|^2 ds,$$

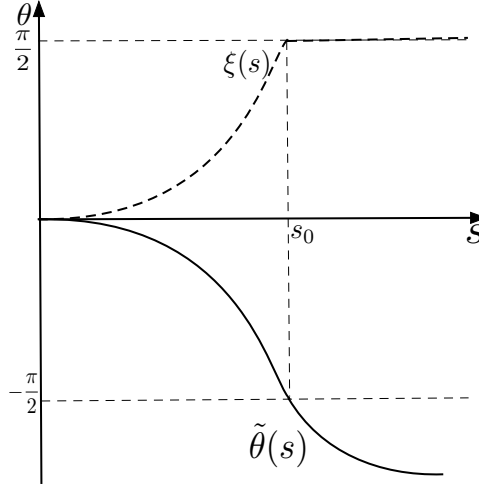


Fig. 2. $\tilde{\theta}$ continuous line; ξ dashed line.

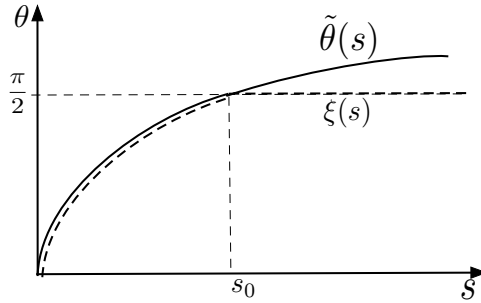


Fig. 3. $\tilde{\theta}$ continuous line; ξ dashed line.

and, as $\tilde{\theta} < 0$ and the function $\sin(\cdot)$ has the same sign of its argument in $(-\frac{\pi}{2})$, it follows

$$\int_0^1 (1-s) \sin \xi(s) ds > \int_0^1 (1-s) \sin \tilde{\theta}(s) ds.$$

The situation is represented in Fig. 2.

Next we observe that $\tilde{\theta}(s)$ cannot cross the axis $\theta(s) = \pi/2$ at a point s_0 (therefore changing concavity at that point) because the function (see Fig. 3):

$$\xi(s) = \tilde{\theta}(s) \quad \text{for } s \in (0, s_0), \quad \xi(s) = \frac{\pi}{2} \quad \text{for } s \geq s_0$$

is again energetically more convenient.

Suppose now that $\theta(s)$ has a maximum below $\pi/2$ after which it decreases to cross the axis $-\pi/2$. This change of concavity (at s_0) is necessary to satisfy the

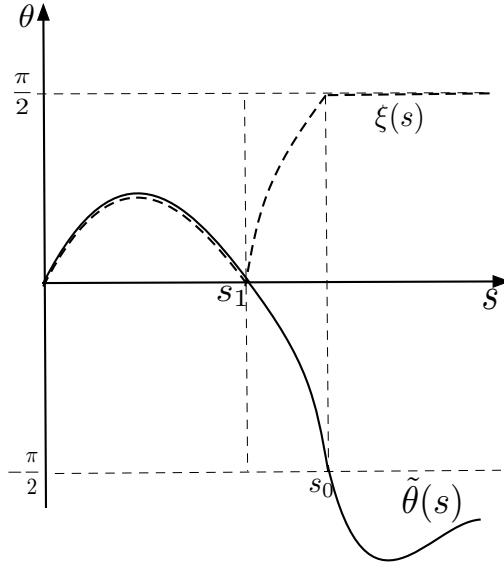


Fig. 4. $\tilde{\theta}$ continuous line; ξ dashed line.

condition $\tilde{\theta}'(1) = 0$. Consider now the function:

$$\begin{aligned} \xi(s) &= \tilde{\theta}(s) \quad \text{for } s \in (0, s_1), & \xi(s) &= -\tilde{\theta}(s) \quad \text{for } s \in (s_1, s_0), \\ \xi(s) &= \frac{\pi}{2} \quad \text{for } s \geq s_0, \end{aligned}$$

where s_1 is the first point in which $\tilde{\theta}$ vanishes. See Fig. 4. Then the same arguments as before show that the profile ξ is energetically more convenient.

It remains to exclude the case depicted in Fig. 5, namely when $\tilde{\theta}$ reaches the value $\pi/2$ at $s_0 < 1$ and then it proceeds constantly. However this situation is excluded.

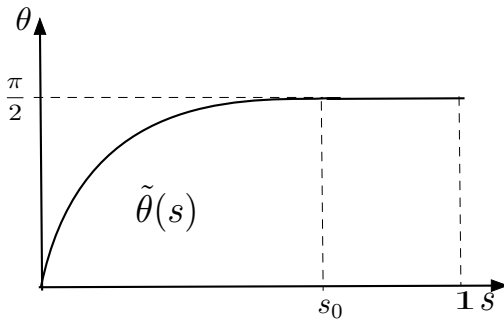


Fig. 5. $\tilde{\theta}$ reaches the value $\pi/2$ at $s_0 < 1$.

Suppose indeed that $\tilde{\theta}'(s) = 0$ for $s > s_0$ and $\tilde{\theta}$ is not constant for $s < s_0$. Consider now the Cauchy problem:

$$\theta'' = -b(1 - s) \cos \theta, \tag{3.1}$$

$$\theta(s_0) = \frac{\pi}{2}, \quad \theta'(s_0) = 0. \tag{3.2}$$

Then the solution $\theta = \frac{\pi}{2}$ is unique in a neighbor of s_0 , which contradicts the fact that $\tilde{\theta}$ is not constant in a left neighbor of s_0 . By a similar argument we show that $\tilde{\theta}(1) < \frac{\pi}{2}$. We already know that $\tilde{\theta}(1) \leq \frac{\pi}{2}$. By contradiction, suppose that $\theta(1) = \frac{\pi}{2}$ and look at the solution of the following problem:

$$\theta'' = -b(1 - s) \cos \theta, \tag{3.3}$$

$$\theta(1) = \frac{\pi}{2}, \quad \theta'(1) = 0. \tag{3.4}$$

The solution $\theta(s) = \frac{\pi}{2}$ is unique in a left neighbor of 1. Moreover we know that $\tilde{\theta} \neq \frac{\pi}{2}$ in a left neighbor of 1, and therefore it cannot be that $\tilde{\theta}(1) = \frac{\pi}{2}$. By the monotonicity of $\tilde{\theta}(\cdot)$ we also conclude that $\tilde{\theta}(s) < \frac{\pi}{2}$ for any $s \in [0, 1]$. Then, by Eq. (2.2) we also conclude that $\theta''(s) < 0$ for any $s \in [0, 1]$ and hence $\tilde{\theta}$ is strictly convex. This completes the proof of Proposition 1. \square

We now establish the uniqueness of the minimizer of the energy functional (1.2).

Proposition 3. *For any $b > 0$ let $\bar{\theta}$ be a solution to Eq. (2.2) with range contained in $[0, \frac{\pi}{2})$. Then $\bar{\theta} = \tilde{\theta}$. In particular there is a unique minimizer of $E(\theta(\cdot))$ and no other stationary points with range in $[0, \frac{\pi}{2})$.*

Proof. The set \mathcal{S} of functions θ defined on $[0, 1]$ and such that $0 \leq \theta(s) < \frac{\pi}{2}$ is a convex set. The second variation of functional (1.2) in θ is

$$\int_0^1 [(h')^2 + b(1 - s) \sin \theta(s) h^2] ds, \tag{3.5}$$

and it is clearly positive in \mathcal{S} as $\sin \theta \geq 0$. Suppose now that $\tilde{\theta} \neq \bar{\theta}$. Consider now the function:

$$E(\lambda) : \lambda \in [0, 1] \rightarrow E(\lambda \bar{\theta} + (1 - \lambda) \tilde{\theta}).$$

Since $\bar{\theta}$ solves (2.2) it is a stationary point of (1.2). However, the function $E(\lambda)$ is convex and has a minimum in 0. Therefore, it cannot have a stationary point in 1, which contradicts the hypothesis that $\tilde{\theta} \neq \bar{\theta}$. \square

We now want to study the topology of the set of solutions when b changes. To this aim let us begin with a standard definition.

Definition 1. Let us denote by $\theta_{\bar{b}}$ a solution of Eq. (2.2) with $b = \bar{b}$, $\theta(0) = 0$ and $\theta'(1) = 0$. Given an arbitrary $B > 0$, we say that the map $b \in [0, B] \rightarrow \theta_b \in H_{0,1}^1$ is a branch of solutions if it is continuous as a function of b .

We first establish the following:

Lemma 2. *Let θ_b denote the minimizer of the energy (expliciting the dependence on b). The function $b \rightarrow E_b(\theta_b)$ is decreasing.*

Proof. Let be $b_2 > b_1$. Then we have:

$$E_{b_2}(\theta_{b_2}) - E_{b_1}(\theta_{b_1}) = E_{b_2}(\theta_{b_2}) - E_{b_2}(\theta_{b_1}) + E_{b_2}(\theta_{b_1}) - E_{b_1}(\theta_{b_1}). \quad (3.6)$$

The last member is negative since θ_{b_2} is the minimizer of E_{b_2} (which makes negative the difference between the first two terms) and by direct substitution in (2.1) we have: $E_{b_2}(\theta_{b_1}) - E_{b_1}(\theta_{b_1}) = (b_1 - b_2) \int_0^1 (1-s) \sin \theta_{b_1} ds$, which is negative since $\sin \theta_{b_1}$ is positive. \square

Proposition 4. *The set of minimizers forms a branch of solutions.*

Proof. We start by showing that, if $b \rightarrow b_0$, then θ_b is a minimizing sequence for E_{b_0} . For every $\psi \in H_{0,1}^1$ one has:

$$E_b(\psi) - E_{b_0}(\psi) = (b - b_0) \int_0^1 (1-s) \sin \psi ds \leq |(b - b_0)| \int_0^1 (1-s) ds = \frac{1}{2} |b_0 - b|.$$

Therefore, recalling that θ_b minimizes E_b , it follows:

$$E_{b_0}(\psi) = E_b(\psi) + E_{b_0}(\psi) - E_b(\psi) \geq E_b(\theta_b) - \frac{1}{2} |b_0 - b| \quad (3.7)$$

$$= E_b(\theta_b) - E_{b_0}(\theta_b) + E_{b_0}(\theta_b) - \frac{1}{2} |b_0 - b| \quad (3.8)$$

$$\geq E_{b_0}(\theta_b) - |b_0 - b|.$$

As the result holds for every $\psi \in H_{0,1}^1$, this implies that

$$E_{b_0}(\theta_b) \leq E_{b_0}(\theta_{b_0}) + |b_0 - b|.$$

This immediately implies that θ_b is a minimizing sequence for E_{b_0} .

We recall that θ_{b_0} is a stationary point for E_{b_0} , and therefore the first Fréchet derivative of $E_{b_0}(\theta(\cdot))$ vanishes in $\theta = \theta_{b_0}$. This implies that, recalling the second variation of $E(\theta(\cdot))$ given in formula (3.5), we can write the difference $E_{b_0}(\theta_b) - E_{b_0}(\theta_{b_0})$ as:

$$E_{b_0}(\theta_b) - E_{b_0}(\theta_{b_0}) = \frac{1}{2} \|(\theta_b - \theta_{b_0})'\|_{L_{0,1}^2}^2 + \frac{1}{2} b_0 \int_0^1 ds (1-s) \sin \xi(s) (\theta_b - \theta_{b_0})^2,$$

where $\xi(s) = \alpha \theta_b(s) + (1-\alpha) \theta_{b_0}(s)$ for some $\alpha \in [0, 1]$. Since $\sin \xi \geq 0$ we obtain

$$\|(\theta_b - \theta_{b_0})'\|_{L_{0,1}^2}^2 \leq E_{b_0}(\theta_b) - E_{b_0}(\theta_{b_0}) \rightarrow 0, \quad (3.9)$$

as $b \rightarrow b_0$, which completes the proof. \square

Summarizing, we have found a branch of solutions which are minimizers of the energy. We call this branch *primary*. The next proposition excludes that such a

branch bifurcates for some b_0 with the occurrence of a new branch of solutions of (2.2) or, in other words, the primary branch $b \rightarrow \theta_b^p$ cannot generate any other branch of solutions.

Proposition 5. *It does not exist b_0 in which a new branch of solutions arises from the primary branch.*

Proof. Let us consider a value $b = b_0$ such that at b_0 a new branch of solutions arises. Let θ_b be a branch of solutions and denote by θ_b^p the primary one. Then computing the first and second variations of the energy we find, for a given H^1 function h satisfying the boundary conditions $h(0) = 0$,

$$\frac{d^2}{d\lambda^2} E_b(\theta_b + \lambda h)|_{\lambda=0} = \int |h'|^2 + b \int (1-s)h^2 \sin \theta_b > 0. \quad (3.10)$$

The previous inequality holds because, in the hypothesis that at b_0 a new branch arises, one has that $\sin \theta_b \approx \sin \theta_b^p \geq 0$ in the $H_{0,1}^1$ norm for $|b - b_0|$ small enough and for every solution θ of Eq. (2.2) verifying the boundary conditions $\theta(0) = 0$ and $\theta'(1) = 0$.

This means that the new branch of solutions produced by the primary branch has to consist of local minima of the energy, at least for $|b - b_0|$ small enough. But this is not possible. Indeed, let θ_b^p be a minimizer and θ_b a local minimizer. Let us consider the function

$$f(\lambda) := \lambda \rightarrow E_b(\lambda \theta_b^p + (1-\lambda)\theta_b),$$

with $\lambda \in [0, 1]$. Clearly $f(\lambda)$ has two local minima for $\lambda = 0$ and $\lambda = 1$ (with $f(1) < f(0)$), and therefore it must have a maximum for a certain $\lambda^* \in (0, 1)$. If $|b - b_0|$ is suitably small then the function $\theta^* := \lambda^* \theta_b^p + (1-\lambda^*)\theta_b$ is such that $\|\theta^* - \theta_b^p\|_{H_{0,1}^1}$ is arbitrarily small, but in this case the sign of the second variation (3.10) tells us that all the directional (Gateaux) derivatives of E are positive in θ^* , and therefore λ^* cannot be a maximum for $f(\lambda)$. \square

In order to parametrize the possible equilibrium configurations when b varies in \mathbb{R}^+ , let us consider the initial value problem (2.2) with initial conditions $\theta(0) = 0$ and $\theta'(0) = K$. Let $\theta(s, K, b)$ be the corresponding unique solution. As we want to determine the solutions of the boundary condition problem expressed by (2.2), (2.3) and (2.4), we will plot (see Fig. 6), in the plane K, b , the computed curves

$$F(K, b) := \theta'(1, K, b) = 0. \quad (3.11)$$

This is a preliminary step toward the establishment of a stability chart.

We remark that the level set $F(K, b) = 0$ identifies a one-dimensional manifold (not necessarily connected) in the plane (K, b) , representing all the solutions of the boundary value problem (2.2)–(2.4), which includes all (possibly local) minima

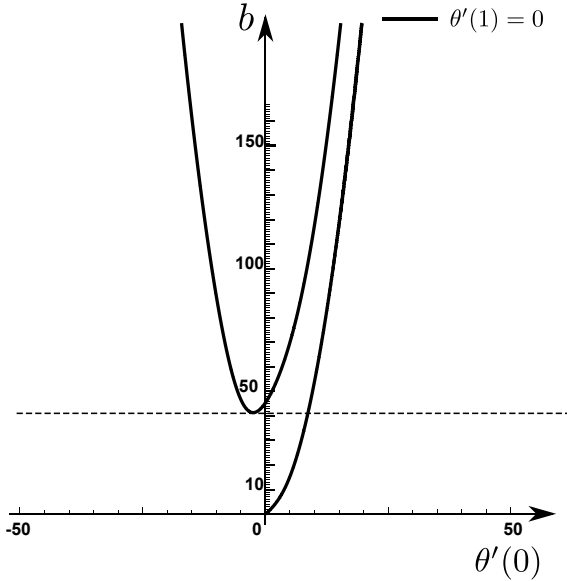


Fig. 6. With a continuous line are represented points in the plane $(\theta'(0), b)$ corresponding to solutions of the boundary value problem (2.2)–(2.4). The primary branch is on the right, while a secondary branch formed (as we will see) by both stable and unstable equilibrium shapes is also visible. Numerical evidence allows an estimate for the value $b_0 \approx 41$ at which the secondary branch appears; the corresponding initial value of the curvature is ≈ -2.6 (for details on the numerical procedure, see Sec. 6).

of the energy functional. We have detected a first curve of solutions, the primary branch, constituted by all global minima of the energy.

Proposition 6. $K_b = \theta'_b(0)$ diverges with b .

Proof. Let us integrate the two members of (2.2) to get:

$$\theta'_b(1) - \theta'_b(0) = -b \int_0^1 (1 - s) \cos \theta_b ds. \tag{3.12}$$

Recalling (2.3) and applying Chebyshev integral inequality (given that $1 - s$ and $\cos \theta_b$ are both decreasing in s) we obtain:

$$K_b = \theta'_b(0) \geq b \int_0^1 (1 - s) ds \int_0^1 \cos \theta_b ds = \frac{b}{2} \int_0^1 \cos \theta_b ds. \tag{3.13}$$

The last member can be written as

$$\begin{aligned} \frac{b}{2} \int_0^1 \cos \theta_b \frac{ds}{d\theta_b} d\theta_b &= \frac{b}{2} \int_0^{\theta_b(1)} \frac{\cos \theta_b}{\theta'_b} d\theta_b \\ &\geq \frac{b}{2K_b} \int_0^{\theta_b(1)} \cos \theta_b d\theta_b = \frac{b}{2K_b} \sin \theta_b(1), \end{aligned} \tag{3.14}$$

the last inequality holding because θ'_b is non-increasing (by Eq. (2.2)). By (3.12) and (3.13) we get $(K_b)^2 \geq \frac{b}{2} \sin \theta_b(1)$. To prove that K_b is unbounded when b diverges we only have to exclude that $\theta_b(1) \rightarrow 0$ when $b \rightarrow \infty$. Let us prove this by absurd.

Suppose thus that b_n is a sequence of positive reals such that $\lim_{n \rightarrow \infty} b_n = +\infty$, and let $\lim_{n \rightarrow \infty} \theta_{b_n}(1) = 0$. We recall that $\theta_{b_n}(s)$ is positive and strictly increasing in s . This implies that $\theta_{b_n}(s) \rightarrow 0$ pointwise for every s in $[0, 1]$. Since θ_{b_n} is monotone and smooth for every n , this implies that the convergence to the limit function $\theta(s) \equiv 0$ holds in the $H^1_{0,1}$ norm. Therefore, it should be $E_{b_n}(\theta_{b_n}) \rightarrow 0$ if $b_n \rightarrow +\infty$. But, since (2.8) immediately implies that for small b the energy is negative, the previous Lemma 2 excludes this. \square

3.2. Further properties of the primary branch

The next two results will concern the behavior of the system when b varies. Specifically, we will compute the derivative $\frac{\partial E(\theta)}{\partial b}$ of the energy evaluated in the minimizer, and will study the derivative $\frac{\partial \bar{\theta}}{\partial b}$ of the minimizer itself with respect to b .

Proposition 7. *Let θ be the minimizer of the energy (2.1). The derivative $\frac{\partial E(\theta)}{\partial b}$ is given by $\int_0^1 (s-1) \sin \theta(s) ds$.*

Proof. We write the derivative with respect to b of the deformation energy as follows:

$$\begin{aligned} \frac{\partial}{\partial b} E_{\text{DEF}} &= \frac{\partial}{\partial b} \int_0^1 \frac{\theta'^2(s)}{2} ds = \int_0^1 \theta'(s) \frac{\partial \theta'(s)}{\partial b} ds \\ &= \int_0^1 \left[\left(\theta'(s) \frac{\partial \theta(s)}{\partial b} \right)' - \theta''(s) \frac{\partial \theta(s)}{\partial b} \right] ds \\ &= \int_0^1 b(1-s) \cos \theta(s) \frac{\partial \theta(s)}{\partial b} ds \\ &= \int_0^1 b(1-s) \frac{\partial}{\partial b} (\sin \theta(s)) ds. \end{aligned} \quad (3.15)$$

For the potential energy we have instead:

$$\begin{aligned} \frac{\partial}{\partial b} E_{\text{POT}} &= \frac{\partial}{\partial b} \left(\int_0^1 -b(1-s) \sin \theta(s) ds \right) \\ &= \int_0^1 \left[-(1-s) \sin \theta(s) - b(1-s) \frac{\partial}{\partial b} \sin \theta(s) \right] ds. \end{aligned} \quad (3.16)$$

Since $E = E_{\text{DEF}} + E_{\text{POT}}$, Eqs. (3.15) and (3.16) imply

$$\frac{\partial}{\partial b} E_b = - \int_0^1 (1-s) \sin \theta(s) ds < 0. \quad (3.17)$$

The last inequality follows from the fact that $0 \leq \theta < \frac{\pi}{2}$ by Proposition 2, and confirms Lemma 2. \square

Proposition 8. *Let $\theta(b, s)$ be the minimizer of the energy (2.1). Then $\frac{\partial \theta(b, s)}{\partial b} > 0 \forall s \in (0, 1]$.*

Proof. Let $b_2 > b_1$ and let θ_{b_i} be the minimizers of E_{b_i} ($i = 1, 2$). By absurd we suppose that

$$\exists \bar{s} \in (0, 1] : \theta_{b_2}(\bar{s}) < \theta_{b_1}(\bar{s}). \quad (3.18)$$

Since $\theta_{b_i} \in C^\infty[0, 1]$, it is not empty the set S of the intervals $I(\bar{s})$ containing \bar{s} , included in $[0, 1]$ and such that $\theta_{b_2}(s) < \theta_{b_1}(s) \forall s \in I(\bar{s})$. Clearly there will exist an element of S which is the largest (with respect to the inclusion relation); let us call (s_1, s_2) this element. It will be $s_1 < \bar{s} < s_2$ and, by continuity, $\theta_{b_1}(s_1) = \theta_{b_2}(s_1)$ and if $s_2 < 1$ then $\theta_{b_2}(s_2) = \theta_{b_1}(s_2)$ (we remark that it can be that $s_1 = 0$ and $s_2 = 1$). Let us define $\tilde{\theta}(s)$ by:

$$\tilde{\theta} : \begin{cases} \theta_{b_2}(s) & \forall s \in [0, 1] \setminus (s_1, s_2), \\ \theta_{b_1}(s) & \forall s \in (s_1, s_2). \end{cases} \quad (3.19)$$

It is immediate to see that $\tilde{\theta} \in C^0[0, 1]$ and $\tilde{\theta} \in C^\infty$ piecewise, so that $\tilde{\theta} \in H_{0,1}^1$.

Let us evaluate now the difference

$$\begin{aligned} E_{b_2}(\theta_{b_2}) - E_{b_2}(\tilde{\theta}) &= \frac{1}{2} \int_{s_1}^{s_2} [(\theta'_{b_2})^2 - (\theta'_{b_1})^2] ds \\ &\quad - \int_{s_1}^{s_2} b_2(1-s) \sin \theta_{b_2} ds + \int_{s_1}^{s_2} b_2(1-s) \sin \theta_{b_1} ds. \end{aligned} \quad (3.20)$$

The sum of the last two terms is positive since $\theta_{b_1} > \theta_{b_2}$ and $0 \leq \theta_{b_i} < \frac{\pi}{2}$ imply that $\sin \theta_{b_1} > \sin \theta_{b_2}$. Now, recalling Eq. (2.2) and boundary conditions (2.3), we can write $\theta'(s)$ as follows:

$$\theta'(s) = -\theta'(1) + \theta'(s) = -\int_s^1 \theta''(\sigma) d\sigma = \int_s^1 b(1-\sigma) \cos \theta d\sigma. \quad (3.21)$$

We can therefore write the first term of the right-hand side of (3.20) as:

$$\frac{1}{2} \int_{s_1}^{s_2} \left[\int_s^1 b_2(1-\sigma) \cos \theta_{b_2} d\sigma \right]^2 ds - \frac{1}{2} \int_{s_1}^{s_2} \left[\int_s^1 b_1(1-\sigma) \cos \theta_{b_1} d\sigma \right]^2 ds. \quad (3.22)$$

By hypothesis $b_2 > b_1$. Moreover, since $0 \leq \theta < \frac{\pi}{2}$, we have that $\theta_{b_2} < \theta_{b_1}$ in $(s_1, s_2) \Rightarrow \cos \theta_{b_2} > \cos \theta_{b_1}$. Therefore we have

$$\int_s^1 b_2(1-\sigma) \cos \theta_{b_2} d\sigma > \int_s^1 b_1(1-\sigma) \cos \theta_{b_1} d\sigma.$$

Since the two integrals are positive, the previous inequality holds true for their squares. Therefore, the quantity in formula (3.22) is positive, and so is the difference $E_{b_2}[\theta_{b_2}] - E_{b_2}[\tilde{\theta}]$, which is absurd since by hypothesis θ_{b_2} is the minimizer of E_{b_2} . \square

4. Other Branches

In Proposition 9 below we prove that, for each fixed b sufficiently large, there exist stationary points of the energy functional (2.1) for which θ admits negative values in contrast with the solutions of the primary branch. These new solutions correspond to local minimizers of the energy, thus representing new stable solutions for *Elastica*. Referring to Fig. 6, they correspond to suitable points on the represented new branch. For topological reasons, the set of stable solutions we detect via variational arguments, cannot stop. Thus other stationary configurations are necessarily present. Indeed, since the function $F(K, b) = \theta'(1, K, b)$ is real analytic, the level set $\{(K, b) \in \mathbb{R} \times (0, +\infty) \mid F(K, b) = 0\}$, which contains the local minimizers, cannot have extreme points (see e.g. Ref. 32, Corollary 2, Example 1), hence it is unbounded. The stability character of these stationary configurations in this branch is for now unknown. However, we will establish in Sec. 5 some sufficient conditions (depending on b) for the stability of particular classes of solutions. In particular, we will show that if a solution has certain properties, then it is necessarily unstable. Numerical evidence (see Figs. 15, 16 in Sec. 6) shows the existence of these unstable solutions.

In order to state the main proposition of this section, let us consider the open convex cone \mathcal{C} :

$$\mathcal{C} = \{\theta \mid \theta \in H_{0,1}^1, \theta(s) < 0 \text{ for any } s \in (0, 1]\},$$

and look for the minima of E restricted to such a cone. Let us define

$$e_b(\mathcal{C}) := \inf_{\xi \in \mathcal{C}} E(\xi) > -\infty,$$

the last inequality obviously holding because of Remark 1. The functional E admits a minimum in $\bar{\mathcal{C}}$, the closure of \mathcal{C} (see for instance Ref. 20, Theorem 7.3.8), i.e. there exists $\bar{\theta} \in \bar{\mathcal{C}}$ such that $E(\bar{\theta}) = e_b(\mathcal{C})$.

Since any element $\tilde{\theta}$ of the primary branch is positive, then $\tilde{\theta} \notin \bar{\mathcal{C}}$ and hence $\bar{\theta} \neq \tilde{\theta}$. Moreover, for small b we have a unique solution to the Euler–Lagrange equations, and it is positive. Then it follows that, for b small, $\bar{\theta}$ must be in $\partial\mathcal{C}$.

Proposition 9. *There exists $b_0 > 0$, sufficiently large, such that for any $b > b_0$ there exists a local minimum of the energy θ which is solution of Eq. (2.2), with $\theta(0) = 0$ and $\theta'(1) = 0$. Moreover θ is negative and decreasing in $(0, 1]$.*

Proof. The main effort of the proof is in showing that $\bar{\theta} \notin \partial\mathcal{C}$. Before that we cannot use Eq. (2.2) because we cannot consider variations.

The basic starting point is that $E(\bar{\theta}) < 0$, provided that b is sufficiently large. We begin by proving this claim.

Consider the function $\xi \in \mathcal{C}$ defined by:

$$\begin{cases} \xi(s) = -3\pi \frac{s}{2R}, & s \in (0, R), \\ \xi(s) = -3/2\pi & s \in (R, 1). \end{cases} \quad (4.1)$$

The total energy can be computed explicitly

$$E(\xi) = \frac{9}{4} \frac{\pi^2}{R} + b \int_0^R (1-s) \sin\left(3\pi \frac{s}{2R}\right) ds - b \int_R^1 (1-s) ds.$$

Now we can choose R so small that the third term is dominating over the second one. In fixed R we choose b so large that E is negative.

In physical terms the above profile corresponds to a configuration of the beam folding around the origin for $3/4$ of the whole circle (of radius R), and then continuing vertically up to the end (see Fig. 7). The corresponding function $\xi(s)$ above defined is certainly not an equilibrium point for E , but its existence implies that it has to be $E(\bar{\theta}) < 0$.

As second step we show that $\bar{\theta}$ cannot cross the axis $\theta = -3/2\pi$.

In fact, in this case, the shape of the *Elastica* described by the function $\xi = -3/2\pi$ inside the set $\{s : \bar{\theta}(s) < -3/2\pi\}$ and $\xi = \bar{\theta}(s)$ outside that set, would be energetically more convenient because both the elastic and the potential energies are reduced.

As third step we prove that $\bar{\theta}$ must cross the axis $\theta = -\pi$. Otherwise, since $\bar{\theta} \in \bar{\mathcal{C}}$, by hypothesis it is $\bar{\theta} \leq 0$, and therefore $\sin \bar{\theta}(s) \leq 0$ for all $s \in (0, 1)$. However this is not possible because, in this case, the energy could not be negative.

Let s_0 be the first value of s such that $\bar{\theta}(s) = -\pi$. We show that $\bar{\theta}$ is non-increasing for $s > s_0$. Suppose the contrary. Then $\bar{\theta}$ has local minimizers for $s > s_0$.

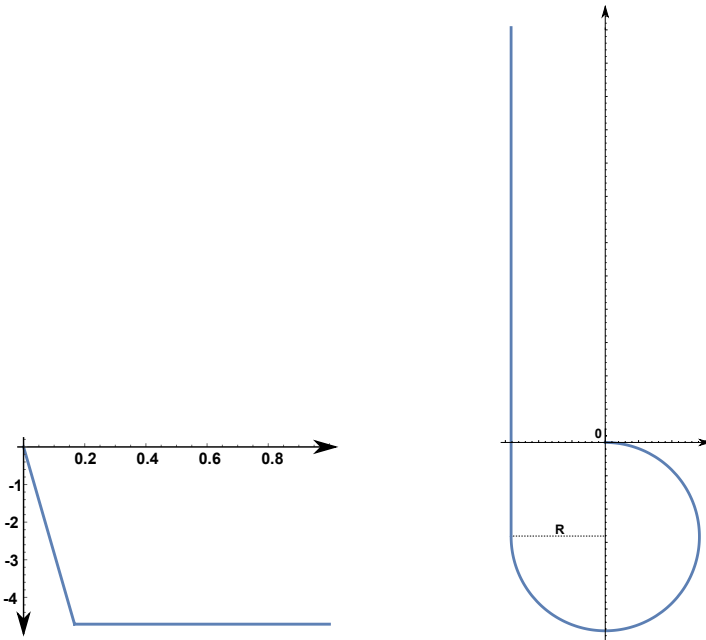


Fig. 7. The function $\xi(s)$ defined in (4.1) (left) and the corresponding deformed shape of the *Elastica* (right).

We select some of them, $\bar{s}_1, \dots, \bar{s}_n$ (and denote $m_i = \bar{\theta}(\bar{s}_i)$, $i = 1, \dots, n$) as follows: let \bar{s}_1 be the first minimizer larger than s_0 , \bar{s}_2 is the first minimizer (if any) larger than \bar{s}_1 such that $m_2 < m_1, \dots, \bar{s}_{i+1}$ is the first minimizer larger than \bar{s}_i such that $m_{i+1} < m_i$, for $i = 1, \dots, n - 1$. Let us now define the function

$$\xi(s) = \begin{cases} \bar{\theta}(s) & \text{for } s \notin \bigcup_{i=1}^n (\bar{s}_i, \bar{s}_{i+1}), \quad \bar{s}_{n+1} := 1, \\ \min_{s \in (\bar{s}_i, \bar{s}_{i+1})} \{m_i, \bar{\theta}(s)\}, & \text{for } s \in (\bar{s}_i, \bar{s}_{i+1}). \end{cases}$$

The construction is illustrated in Fig. 8. Clearly $\xi \in H^1$ since by definition $\xi(s_i) = \bar{\theta}(s_i)$ for any i .

The configuration ξ is energetically more convenient because the elastic energy is decreased in the constant intervals and the potential energy is decreased because $-\sin(\cdot)$ is positive above $-\pi$ and increasing in $(-\frac{3}{2}\pi, -\pi)$.

Next we prove that $\bar{\theta}$ is not increasing also in $(0, s_0)$. Suppose the contrary. Since $\bar{\theta} \in \bar{\mathcal{C}}$, it is not increasing in a right neighborhood of zero, the set of local minimizers for $\bar{\theta}$ in $(0, s_0)$ is not empty since $\bar{\theta}(s_0) = -\pi$. Let s_m be the first minimizer; the set of local maximizers is also not empty. Let s_M be the first maximizer. It is obviously $s_m < s_M < s_0$.

Case (a). Let us assume that $\theta(s_m) > \pi/2$.

Since $\bar{\theta}$ is monotonic in $[0, s_m]$, there exists a unique \bar{s} such that $\bar{\theta}(\bar{s}) = \bar{\theta}(s_M)$. Then we consider the function $\xi(s)$ defined by:

$$\begin{aligned} \xi(s) &= \bar{\theta}(s) && \text{for } s \in [0, \bar{s}], \\ \xi(s) &= \bar{\theta}(s_M) && \text{for } s \in (\bar{s}, s_M], \\ \xi(s) &= \bar{\theta}(s) && \text{for } s \in (s_M, 1]. \end{aligned}$$

The function ξ would clearly be energetically more convenient than $\bar{\theta}$.

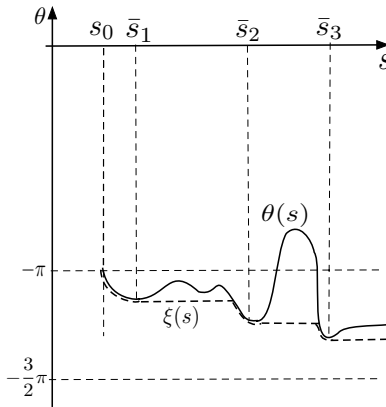


Fig. 8. θ continuous line, ξ dashed line.

Case (b). Suppose instead that $\theta(s_m) \leq \pi/2$.

Since $\bar{\theta}(s_0) = -\pi$, it is not empty the set N of points such that $\bar{\theta}(s) = \bar{\theta}(s_m)$. Let \bar{s} be the minimum of N . Then we consider the function $\xi(s)$ defined by:

$$\begin{aligned}\xi(s) &= \bar{\theta}(s) && \text{for } s \in [0, s_m], \\ \xi(s) &= \bar{\theta}(s_m) && \text{for } s \in (s_m, \bar{s}], \\ \xi(s) &= \bar{\theta}(s) && \text{for } s \in (\bar{s}, 1].\end{aligned}$$

Again the function ξ would be energetically more convenient than $\bar{\theta}$.

In conclusion, the function $\bar{\theta}$ is non-increasing in $(0, 1)$. Hence the only possibility to be in $\partial\mathcal{C}$ is that there is $\lambda > 0$ such that $\bar{\theta}(s) = 0$ for $s \in (0, \lambda)$. We now show that this is not possible.

Suppose that such a λ exists. We define

$$\xi(s) = \bar{\theta}(s + \lambda) \quad \text{for } s \in (0, 1 - \lambda) \quad \text{and} \quad \xi(s) = \bar{\theta}(1) \quad \text{for } s \in (1 - \lambda, 1). \quad (4.2)$$

An explicit computation leads us to (defining $B := \sin \bar{\theta}(1)$):

$$E(\xi) = \frac{1}{2} \int_0^1 |\xi'|^2 ds - b \int_0^{1-\lambda} (1-s) \sin(\bar{\theta}(s+\lambda)) ds - bB \int_{1-\lambda}^1 (1-s) ds.$$

Moreover, using that $\int_0^1 |\xi'|^2 ds = \int_0^1 |\bar{\theta}'|^2 ds$, by means of an obvious change of variables

$$E(\xi) - E(\bar{\theta}) = -b\lambda \int_\lambda^1 \sin \bar{\theta}(s) ds - bB \int_{1-\lambda}^1 (1-s) ds.$$

We show that the above quantity is negative. Indeed the last term is negative because $\bar{\theta}(1) \in (-\frac{3}{2}\pi, -\pi)$. As for the first term of the right-hand side, we write

$$T = \int_\lambda^1 \sin \bar{\theta}(s) ds = \int_\lambda^{s^*} \sin \bar{\theta}(s) ds + \int_{s^*}^1 \sin \bar{\theta}(s) ds, \quad (4.3)$$

where s^* is a point for which $\bar{\theta}(s^*) = -\pi$. We remark that, because of the monotonicity of $\bar{\theta}$, it is $\lambda < s^*$. Suppose by absurd that $T < 0$, namely

$$-\int_\lambda^{s^*} \sin \bar{\theta}(s) ds > \int_{s^*}^1 \sin \bar{\theta}(s) ds.$$

Then it holds

$$\begin{aligned}-\int_\lambda^{s^*} (1-s) \sin \bar{\theta}(s) ds &> -\int_\lambda^{s^*} (1-s^*) \sin \bar{\theta}(s) ds \\ &> \int_{s^*}^1 (1-s^*) \sin \bar{\theta}(s) ds > \int_{s^*}^1 (1-s) \sin \bar{\theta}(s) ds.\end{aligned}$$

Therefore

$$-b \int_0^1 (1-s) \sin \bar{\theta}(s) ds > 0,$$

but this contradicts the negativity of $E(\bar{\theta})$.

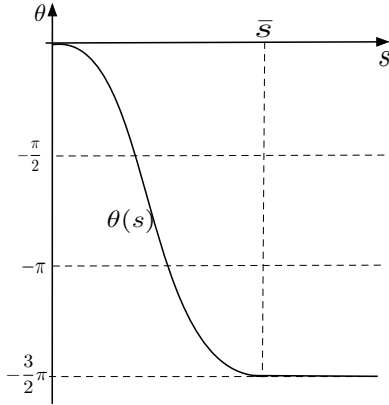


Fig. 9. $\theta = -\frac{3}{2}\pi$ for $s \geq \bar{s}$.

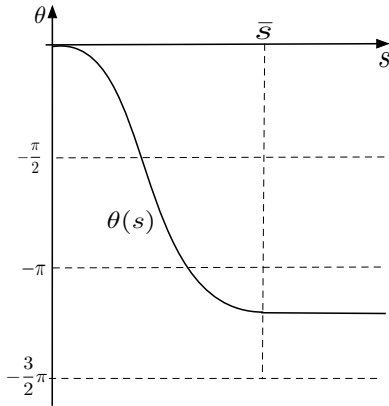


Fig. 10. The only possible θ .

Summarizing, we are left with the two possibilities depicted in Figs. 9 and 10.

Note that in both cases $\bar{\theta}$ is decreasing so that it cannot vanish in $(0, 1]$. This is enough to conclude that $\bar{\theta} \in \mathcal{C}$. Therefore we are now allowed to use Eqs. (2.2) and (2.3). The same uniqueness argument, already used for the primary branch, excludes also the possibility that $\bar{\theta}$ takes the constant value $-3/2\pi$ over a finite interval.

In conclusion $\bar{\theta}$ is strictly decreasing in $(0, 1]$ and $\lim_{s \rightarrow 1} \bar{\theta}'(s) = 0$. The continuity $b \rightarrow \bar{\theta}_b$ follows the same lines as shown in Proposition 4. \square

We want now to further study the solution just discussed, and prove that it is obtained by “gluing” together the solutions of two different problems. Let $\tilde{\theta}(s)$ be a solution of the boundary value problem:

$$\theta''(s) = -b(L - s) \cos \theta(s), \quad \theta(0) = 0, \quad \theta'(L) = 0, \quad (4.4)$$

such that:

- (a) $\tilde{\theta}(s)$ is decreasing;
- (b) its range is contained in $[0, -\frac{3}{2}\pi]$;
- (c) there exists a unique \bar{s} such that $\tilde{\theta}(\bar{s}) = -\pi$.

Note that these hypotheses are satisfied by the solution corresponding to the deformed shape represented in Fig. 15.

Proposition 10. *Suppose that there exists a solution of the boundary value problem (4.4) satisfying requirements (a), (b) and (c) given before. Then the relative deformed shape restricted to $[\bar{s}, L - \bar{s}]$ corresponds (up to a reflection) to the deformed shape of a beam of length $L - \bar{s}$ in the minimizer of the energy (primary solution).*

Proof. Let us set $\phi(s) = -\tilde{\theta}(s) - \pi$. Obviously ϕ is increasing, $\phi'' = -\tilde{\theta}''$ and $\cos \tilde{\theta} = -\cos \phi$. We have therefore that:

$$\phi''(s) = -b(L - s) \cos \phi(s) \tag{4.5}$$

holds with boundary conditions:

$$\phi(0) = -\pi, \quad \phi'(L) = 0. \tag{4.6}$$

Let us also set $\xi = s - \bar{s}$ and $\gamma(\xi) = \phi(\bar{s} + \xi)$. We consider now the restriction of $\gamma(\xi)$ on the interval $I_{\bar{s}} = [0, L - \bar{s}]$. It is immediate to verify that $\gamma(\xi)$ solves the boundary value problem:

$$\gamma''(\xi) = -b(L - \bar{s} - \xi) \cos \gamma(\xi), \quad \gamma(0) = 0, \quad \gamma'(L - \bar{s}) = 0. \tag{4.7}$$

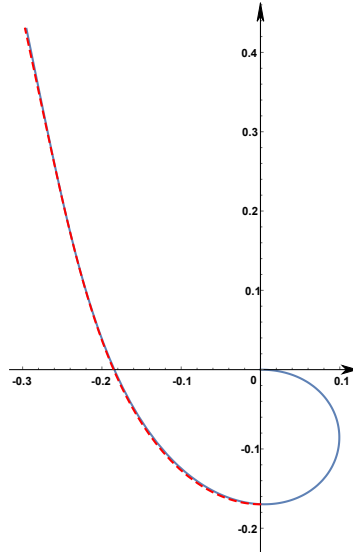


Fig. 11. Superposition of the curled stable solution (continuous line) and the absolute minimum solution (dashed line).

Moreover, γ is increasing in $I_{\bar{s}}$ and its range is contained in $[0, \frac{\pi}{2}]$. Therefore, recalling Proposition 2, $\gamma(\xi)$ corresponds to the (unique) absolute minimum of the energy functional when the length of the *Elastica* is equal to $L - \bar{s}$, which completes the proof. \square

As an internal consistency check of the numerical tools employed, we plotted a superposition between the curled stable solution and the absolute minimum solution of suitable reduced length (and rotated) in Fig. 11.

5. Results on Stability for Two Classes of Solutions

Let us recall the second variation of the energy functional E :

$$\mathcal{V} = \int_0^1 [(h')^2 + b(1-s)\sin\theta(s)h^2]ds. \tag{5.1}$$

We start by proving the following result, which can be applicable for solutions θ (possibly different from the local/global minimizers analyzed in the previous sections) such that $\sin\theta$ is positive in a neighborhood of 1.

Proposition 11. *Let $\theta(s)$ be a stationary point for E for a given b . If there exists $\lambda \in (0, 1)$ such that $\sin\theta$ is non-negative in $[\lambda, 1]$, then \mathcal{V} is positive if $b < \frac{\pi^2}{2\lambda^3(2-\lambda)}$.*

Proof. Since $\mathcal{V}[h] = \mathcal{V}[|h|]$, we can limit ourselves to variations that are non-negative.

We can suppose that $\sin\theta$ is negative in the whole interval $(0, \lambda)$, as if not \mathcal{V} will be increased by replacing $\sin\theta$ with $-\sin\theta$ on the subsets of $(0, \lambda)$ in which it is negative.

The stability of the solution θ is then equivalent to

$$\int_0^1 (h')^2 ds + b \int_{\lambda}^1 (1-s)\sin\theta(s)h^2 ds > b \int_0^{\lambda} (1-s)|\sin\theta(s)|h^2 ds, \tag{5.2}$$

which holds if so does

$$\int_0^{\lambda} (h')^2 ds > b \int_0^{\lambda} (1-s)h^2 ds. \tag{5.3} \quad \square$$

Before proceeding, let us prove the following.

Lemma 3. *Without losing generality, we can establish (5.3) only for variations h for which there exists a C^0 non-decreasing representative.*

Proof. Let us suppose that h has a C^0 representative (which we for simplicity will also denote by h) that decreases in a sub-interval (α, β) of $(0, \lambda)$. We can then define $\bar{h} \in C^0$ as

$$\bar{h} := \begin{cases} h & \forall s \in (0, \alpha), \\ 2h(\alpha) - h(s) & \forall s \in (\alpha, \beta), \\ h(s) + 2[h(\alpha) - h(\beta)] & \forall s \in (\beta, \lambda). \end{cases} \tag{5.4}$$

It is easily seen that $\bar{h} \in H^1$ and that it is non-negative and non-decreasing in (α, β) . This implies that, for $s \in (\alpha, \beta)$,

$$\bar{h}^2(s) = 4[h(\alpha)]^2 + h^2(x) - 4h(\alpha)h(s) \geq h^2(s), \quad (5.5)$$

and since obviously $\bar{h}' = h'$, one gets

$$\int_{\alpha}^{\beta} (\bar{h}')^2 ds > b \int_{\alpha}^{\beta} (1-s)\bar{h}^2 ds \Rightarrow \int_{\alpha}^{\beta} (h')^2 ds > b \int_{\alpha}^{\beta} (1-s)h^2 ds, \quad (5.6)$$

from which, observing that $\bar{h} \geq h$ in (β, λ) and that piecewise monotonic functions are dense in H^1 , the thesis follows. \square

We can now complete the proof of Proposition 11. For H^1 functions h that vanish in only one of the extrema of a real interval, a weak version of Poincaré inequality holds,^a namely there exists C such that

$$\|h\|_{L^p(0,\lambda)} \leq C\|h'\|_{L^p(0,\lambda)}, \quad (5.7)$$

which, for $p = 2$ provides

$$\left(\int_0^{\lambda} h^2 ds \right)^{\frac{1}{2}} \leq C \left(\int_0^{\lambda} (h')^2 ds \right)^{\frac{1}{2}}, \quad (5.8)$$

where $\frac{2\lambda}{\pi}$ is the optimal value for the constant.^b We have thus

$$\int_0^{\lambda} h^2 ds \leq \frac{4l^2}{\pi^2} \int_0^{\lambda} (h')^2 ds. \quad (5.9)$$

Therefore, (5.3) holds if so does

$$\frac{\pi^2}{4\lambda^2} \int_0^{\lambda} h^2 ds > b \int_0^{\lambda} (1-s)h^2 ds. \quad (5.10)$$

Since $1-s$ is decreasing, and recalling that h is non-decreasing, by Chebyshev's integral inequality we have

$$\int_0^{\lambda} (1-s)h^2 ds \leq \int_0^{\lambda} (1-s) ds \int_0^{\lambda} h^2 ds. \quad (5.11)$$

Therefore, (5.10) holds if

$$\frac{\pi^2}{4\lambda^2} \int_0^{\lambda} h^2 ds > b \int_0^{\lambda} (1-s) ds \int_0^{\lambda} h^2 ds. \quad (5.12)$$

Solving the previous inequality with respect to b , we get

$$b < \frac{\pi^2}{4\lambda^2} \left(\lambda - \frac{\lambda^2}{2} \right)^{-1} = \frac{\pi^2}{2\lambda^3(2-\lambda)}. \quad (5.13)$$

which completes the proof. \square

^aThis is easily seen applying the classical Poincaré inequality to $\tilde{h}(x) := h(x)$ for $x \in [0, \lambda]$ and $h(2\lambda - x)$ for $x \in (\lambda, 2\lambda]$.

^bThe optimal Poincaré constant would be simply $\frac{\lambda}{\pi}$ for functions vanishing in both extrema of the interval.

We want now to establish a check on instability. Let θ be a stationary point for \mathcal{E} . We will prove the following.

Proposition 12. *Let us suppose that there exist λ, μ, ν such that $0 < \lambda < \mu < \nu < 1$, and that $\sin \theta > 0$ in $(0, \lambda)$ and $\sin \theta < 0$ in (μ, ν) . Then θ is not a minimizer for E if^c:*

$$b > \frac{12}{\lambda(3\lambda^2 - 16\lambda + 12) \int_{\mu}^{\nu} |\sin \theta| ds}.$$

Proof. We consider a variation $\bar{h}(s)$ defined as:

$$\bar{h} := \begin{cases} \frac{M}{\lambda} s & \forall s \in (0, \lambda), \\ M & \forall s \in (\lambda, 1). \end{cases} \quad (5.14)$$

Let us compute \mathcal{V} for this variation^d:

$$\mathcal{V}[\bar{h}] = \frac{M^2}{\lambda} + b \left(\frac{M}{\lambda} \right)^2 \int_0^{\lambda} s^2 (1-s) \sin \theta ds + bM^2 \int_{\lambda}^1 (1-s) \sin \theta ds. \quad (5.15)$$

Recalling the hypotheses on the sign of $\sin \theta$, \mathcal{V} is negative if

$$\frac{M^2}{\lambda} + b \left(\frac{M}{\lambda} \right)^2 \int_0^{\lambda} s^2 (1-s) ds < bM^2 \int_{\mu}^{\nu} (1-s) |\sin \theta| ds, \quad (5.16)$$

that is

$$\frac{M^2}{\lambda} + bM^2 \left(\frac{\lambda}{3} - \frac{\lambda^2}{4} \right) < bM^2 \int_{\mu}^{\nu} (1-s) |\sin \theta| ds, \quad (5.17)$$

which holds if so does

$$\frac{1}{\lambda} + b \left(\frac{\lambda}{3} - \frac{\lambda^2}{4} \right) < b(1-\lambda) \int_{\mu}^{\nu} |\sin \theta| ds. \quad (5.18)$$

Solving for b , one gets

$$b > \frac{12}{\lambda(3\lambda^2 - 16\lambda + 12) \int_{\mu}^{\nu} |\sin \theta| ds}. \quad (5.19)$$

□

We remark that the right-hand side of this inequality involves a function depending on b . In this case, contrarily to the previous one, in order to apply the check one needs not only to know the behavior of the sign of $\sin \theta$, but also an estimate of the integral of its negative part.

^cIt is actually easy to get rid of μ and obtain a similar result supposing that $\sin \theta$ simply changes its sign at ν ; however, we prefer the current formulation in order to be able to apply the inequality when the zero of $\sin \theta$ is known with an error (that can be controlled).

^dWe will see that the inequality is not depending on the value M .

6. Some Numerical Results

The previous results can be applied to check the stability character of a stationary point θ , when they are not obtained as local/global minimizers. We will apply them in particular to a solution found numerically, which will be described below.

To solve numerically the boundary value problem (2.2)–(2.4) we used a standard shooting technique. Specifically, we first solved a set S of initial value problems with suitably parametrized initial data, i.e. the problem given by (2.2), (2.4) and $\theta'(0) = K$. Next we searched for the solution of the boundary value problem among the solutions of S . The nonlinear second-order Cauchy problem has been solved using the built-in function of *Mathematica* `NDSolve` for the numerical solution of differential equations. This function can use different methods for solving differential equations, but basically all of them employ an adaptive step size in order to stay within a certain error range. The method for the solution is automatically chosen taking into account different properties of the problem, but it is mainly based on the evaluation of its stiffness. `NDSolve` returns a function interpolating the values evaluated at the extrema of the steps. Parametrizing the Cauchy problem with respect to $\theta'(0) = K$, with $-40 \leq K \leq 40$, we have determined the values $\theta'(1, K, b)$. The error on these values depends of course on the step size chosen for K . Specifically, by means of the option `AccuracyGoal` of package `NDSolve`, we can control the desired final output up to an (adimensional) absolute error chosen *a priori* (we selected 10^{-8}); this was done for the estimate of all the quantities involved in the numerical check of the inequalities, i.e. θ , $\sin \theta$ and $\int \sin \theta$.

With $b = 60$, numerical simulations show that there is a solution $\bar{\theta}(s)$ such that $\sin \bar{\theta}$ is non-negative in $[0.3, 1]$, with an error (see above) sufficiently small to comfortably allow certainty on the sign at the left extremum of the interval. Since $\bar{\theta}$ appears in this case to be everywhere negative, the previous Proposition 9 tells us that the solution can be a local minimizer. Indeed, since in this case $\frac{\pi^2}{2\lambda^3(2-\lambda)} \approx 107.5$, Proposition 11 implies then that this is a stable configuration of the *Elastica* (not belonging to the primary branch).

The graph of $\sin \bar{\theta}$ is shown in Fig. 12.

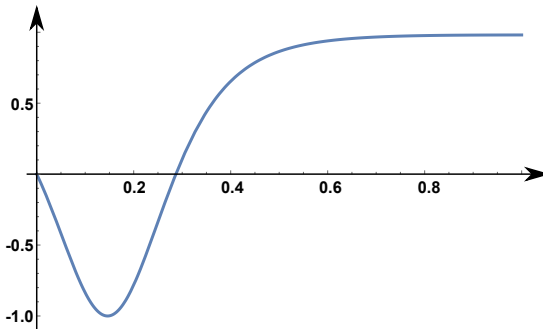


Fig. 12. Graph of $\sin \bar{\theta}$ (stationary point for $b = 60$).

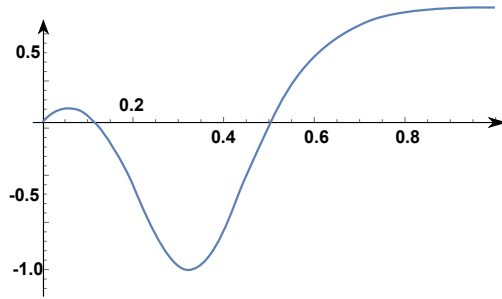


Fig. 13. Graph of $\sin \hat{\theta}$ (stationary point for $b = 60$).

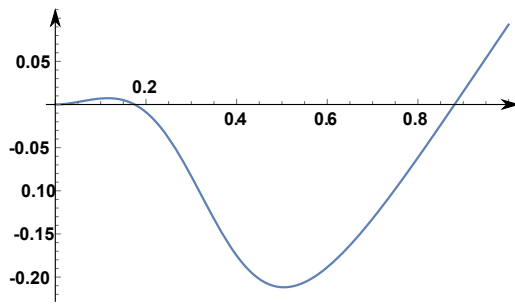


Fig. 14. Graph of $\int_0^s \sin \hat{\theta} ds$.

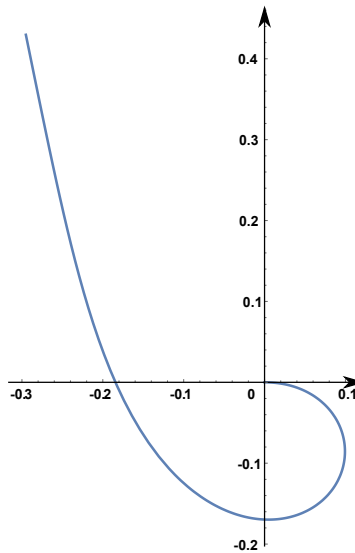


Fig. 15. Deformed shape of the *Elastica* corresponding to $\bar{\theta}$.

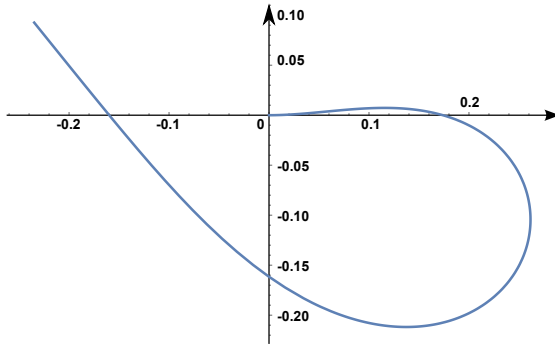


Fig. 16. Deformed shape of the *Elastica* corresponding to $\hat{\theta}$.

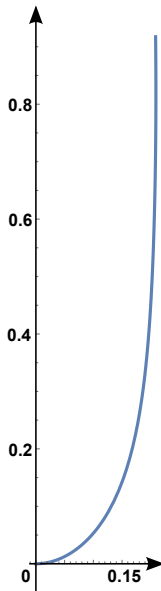


Fig. 17. Deformed shape of the *Elastica* corresponding to $\tilde{\theta}$.

With the same value $b = 60$, another solution $\hat{\theta}(s)$ is numerically found, and simulations show that $\sin \hat{\theta}$ is positive in $(0, 0.11)$ and negative in $(0.14, 0.5)$ with an error (see above) sufficiently small to comfortably allow certainty on the sign at the extrema of the intervals (notice that in this case Proposition 9 is not applicable because the solution is not everywhere negative). Numerical results show that $\int_{0.14}^{0.55} |\sin \hat{\theta}(s)| ds$ is not smaller than 0.2. Since in this case the right-hand side of the inequality (5.19) is ≈ 53.25 , this means, by the previous Proposition 12, that this solution is not stable.

The graphs of $\sin \hat{\theta}$ and $\int_0^s \sin \hat{\theta} ds$ are shown in Figs. 13 and 14.

Summarizing, with $b = 60$ (above the value $b \approx 41$ given in Fig. 6) we have numerical evidence of three solutions, two of which stable and one unstable.

The plots of the deformed shapes of the *Elastica* relative to the three solutions $\bar{\theta}$, $\hat{\theta}$ and $\tilde{\theta}$ are shown in Figs. 15–17.

7. Conclusions

Direct method of calculus of variations provides a natural tool for the analysis of the classical problem of the *Elastica* in the large deformation posed by Euler in 1744. In this paper, we applied direct method to establish the existence of global and local minimizers of a clamped *Elastica* subjected to uniformly distributed load. We also gave sufficient conditions for stability or instability of particular classes of stationary configurations. In particular, we proved that some equilibrium configurations found by means of numerical simulations are unstable if they exist. It seems to us that structural mechanics could significantly benefit from a wider application of the aforementioned theoretical tools.

Several new questions have been opened within the present research, the final objective being the full characterization of the equilibria of *Elastica* in large deformation under a distributed load.

Acknowledgment

We thank M. Ponsiglione for useful discussions.

References

1. B. E. Abali, W. H. Müller and V. A. Eremeyev, Strain gradient elasticity with geometric nonlinearities and its computational evaluation, *Mech. Adv. Mater. Mod. Process.* **1** (2015).
2. J. J. Alibert, P. Seppecher and F. dell’Isola, Truss modular beams with deformation energy depending on higher displacement gradients, *Math. Mech. Solids* **8** (2003) 51–73.
3. S. S. Antman, *Nonlinear Problems of Elasticity* (Springer, 1995).
4. D. Bernoulli, The 26th letter to Euler, in *Correspondence Mathématique et Physique*, Vol. 2 (P. H. Fuss, 1742).
5. J. Bernoulli, Quadratura curvae, e cujus evolutione describitur inflexae laminae curvatura, in *Die Werke von Jakob Bernoulli* (Birkhäuser, 1692), pp. 223–227.
6. K. E. Bisshopp and D. C. Drucker, Large deflection of cantilever beams, *Quart. Appl. Math.* **3** (1945) 272–275.
7. M. Born, Untersuchungen über die Stabilität der elastischen Linie in Ebene und Raum, unter verschiedenen Grenzbedingungen, Ph.D. thesis, University of Göttingen (1906).
8. B. Dacorogna, *Direct Methods in the Calculus of Variations*, Vol. 78 (Springer Science & Business Media, 2007).
9. F. dell’Isola, I. Giorgio, M. Pawlikowski and N. L. Rizzi, Large deformations of planar extensible beams and pantographic lattices: Heuristic homogenization, experimental and numerical examples of equilibrium, *Proc. Roy. Soc. A* **472** (2016) 20150790.

10. F. dell'Isola, T. Lekszycki, M. Pawlikowski, R. Grygoruk and L. Greco, Designing a light fabric metamaterial being highly macroscopically tough under directional extension: First experimental evidence, *Z. Math. Phys.* **66** (2015) 3473–3498.
11. F. dell'Isola, D. Steigmann and A. Della Corte, Synthesis of fibrous complex structures: Designing microstructure to deliver targeted macroscale response, *Appl. Mech. Rev.* **67** (2016) 21 pp.
12. L. Euler, Methodus inveniendi lineas curvas maximi minimive proprietate gaudentes, sive solutio problematis isoperimetrici lattissimo sensu accepti (Marc-Michel Bousquet et Soc., 1744). Additamentum 1.
13. L. C. Evans, *Partial Differential Equations* (Amer. Math. Soc., 2010).
14. M. G. Faulkner, A. W. Lipsett and V. Tam, On the use of a segmental shooting technique for multiple solutions of planar elastica problems, *Comput. Meth. Appl. Mech. Eng.* **110** (1993) 221–236.
15. D. G. Fertis, *Nonlinear Structural Engineering* (Springer-Verlag, 2006).
16. I. Fonseca and G. Leoni, *Modern Methods in the Calculus of Variations: L^p Spaces* (Springer Science & Business Media, 2007).
17. S. Forest and R. Sievert, Nonlinear microstrain theories, *Int. J. Solids Struct.* **43** (2006) 7224–7245.
18. I. Fried, Stability and equilibrium of the straight and curved elastica-finite element computation, *Comput. Meth. Appl. Mech. Eng.* **28** (1981) 49–61.
19. P. Germain, The method of virtual power in continuum mechanics. Part 2: Microstructure, *SIAM J. Appl. Math.* **25** (1973) 556–575.
20. A. J. Kudrila and M. Zabaranin, *Convex Functional Analysis* (Springer Science & Business Media, 2006).
21. P. Ladevèze, *Nonlinear Computational Structural Mechanics: New Approaches and Non-Incremental Methods of Calculation* (Springer Science & Business Media, 2012).
22. J. L. Lagrange, *Mécanique Analytique*, Vols. 1–2 (Mallet-Bachelier, 1853).
23. G. W. Milton, Adaptable nonlinear bimode metamaterials using rigid bars, pivots, and actuators, *J. Mech. Phys. Solids* **61** (2013) 1561–1568.
24. R. D. Mindlin and N. N. Eshel, On first strain-gradient theories in linear elasticity, *Int. J. Solids Struct.* **4** (1968) 109–124.
25. M. G. Mora and S. Müller, A nonlinear model for inextensible rods as a low energy Γ -limit of three-dimensional nonlinear elasticity, *Ann. l'IHP Anal. Nonlinaire* **21** (2004) 271–293.
26. C. Pideri and P. Seppecher, A second gradient material resulting from the homogenization of an heterogeneous linear elastic medium, *Contin. Mech. Thermodynam.* **9** (1997) 241–257.
27. C. Pideri and P. Seppecher, Asymptotics of a non-planar rod in nonlinear elasticity, *Asympt. Anal.* **48** (2006) 33–54.
28. A. C. Pipkin, Plane traction problems for inextensible networks, *Quart. J. Mech. Appl. Math.* **34** (1981) 415–429.
29. D. W. Raboud, M. G. Faulkner and A. W. Lipsett, Multiple three-dimensional equilibrium solutions for cantilever beams loaded by dead tip and uniform distributed loads, *Int. J. Nonlinear Mech.* **31** (1996) 297–311.
30. R. S. Rivlin, Networks of inextensible cords, in *Collected Papers of R. S. Rivlin* (Springer, 1997), pp. 566–579.
31. D. Scerrato, I. Giorgio and N. L. Rizzi, Three-dimensional instabilities of pantographic sheets with parabolic lattices: Numerical investigations, *Z. Math. Phys.* **67** (2016) 1–19.

32. D. Sullivan, Combinatorial invariants of analytic spaces, in *Proc. Liverpool Singularities Symp. I* (Springer, 1971), p. 165.
33. L. Tonelli, *Opere scelte: Calcolo delle variazioni*, Vol. 2 (Edizioni Cremonese, 1961).
34. E. Turco, F. dell'Isola, A. Cazzani and N. L. Rizzi, Hencky-type discrete model for pantographic structures: Numerical comparison with second gradient continuum models, *Z. Math. Phys.* **67** (2016) 1–28.

Appendix

Some qualitative properties of the equilibrium configurations of extensible Euler beams under distributed load in large deformation

Appendix

1 Overview

In Chapter 5 we showed that a clamped Euler *Elastica* under distributed load in large deformations can have equilibrium configurations different from the absolute minimizer of the total energy, which are instead local minima. We also saw that the deformed shape associated to such local minima can be such that the beam “turns” around the clamped edge. One may wonder whether deformed shapes with multiple turns are possible equilibrium configurations for the *Elastica*. The answer is no, and in this Appendix it will be shown indeed that equilibrium configurations (stationary points of the energy functional) cannot turn more than one time around the clamped edge, neither in the inextensible nor in the extensible case. Moreover, this result will be used to deduce some qualitative properties of the absolute minimizer in the extensible case.

2 A priori estimates on the range of stationary points

2.1 Inextensible case

Let us consider the boundary value problem arising when considering a clamped inextensible Euler beam under uniformly distributed load in large deformation:

$$\begin{cases} \theta''(s) = -b(1-s)\cos\theta(s) \\ \theta(0) = 0 \\ \theta'(1) = 0 \end{cases} \quad (1)$$

We remark that here we are using the same notations as in Chapter 5.

Proposition 1: If θ is a solution of (1), then $\theta(s) = \frac{\pi}{2}$ and $\theta(s) = \frac{-3\pi}{2}$ for every $s \in [0, 1]$.

Proof:

Let us define the function:

$$V(s) := \frac{1}{2}(\theta'(s))^2 + b(1-s)\sin\theta(s) - b(1-s)$$

By direct computation:

$$\begin{aligned} V'(s) &= \theta'(s)\theta''(s) + b(1-s)\cos\theta(s)\theta'(s) - b\sin\theta(s) + b = \\ &= \theta''(s)[\theta'(s) + b(1-s)\cos\theta(s)] + b(1-\sin\theta(s)) \geq 0 \end{aligned}$$

Let $\bar{s} \in (0, 1) : \theta(\bar{s}) \in \left(\frac{\pi}{2}, -\frac{3\pi}{2}\right)$. We have $\sin(\theta(\bar{s})) = 1$ and:

$$V(\bar{s}) = \frac{1}{2}(\theta'(\bar{s}))^2 + b(1 - \bar{s}) - b(1 - \bar{s}) = \frac{1}{2}(\theta'(\bar{s}))^2 \leq V(1) = 0 \quad \theta'(\bar{s}) = 0.$$

Let us now consider the Cauchy problem given by the ODE in (1) with boundary data $\theta(\bar{s}) = \frac{\pi}{2}$ (or $\theta(\bar{s}) = -\frac{3\pi}{2}$) and $\theta'(\bar{s}) = 0$. Clearly $\theta(s) \equiv \frac{\pi}{2}$ (or $\theta(s) \equiv -\frac{3\pi}{2}$) is the only solution in $[\bar{s}, 1]$. But then, assuming analyticity of $\theta(s)$ on a sufficiently large interval¹, the solution should be constantly $\frac{\pi}{2}$ on $[0, 1]$, which is absurd.

The proof is complete.

Remark 1. The function $V(s)$ allows us to give an estimate of the curvature in $s = 0$. Indeed:

$$V(0) = \frac{1}{2}(\theta'(0))^2 - b, \quad V(1) = 0 \quad \frac{1}{2}(\theta'(0))^2 \leq b$$

Remark 2. The previous reasoning holds true if we replace $b(1-s)$ with any weakly differentiable, positive and decreasing function $f(s)$, and therefore for any suitably regular distributed load $b(s)$ such that $b(s) \geq 0$ (we need that f is decreasing since in V' we have to estimate the sign of f').

2.2 Extensible case

In this section we want to study the boundary value problem (BVP) for the extensible Euler beam clamped in one side and free at the other one. In particular, we want to establish an *a priori* bound of the range of the equilibrium solutions $\theta(s)$, which as a particular consequence will prove that multiple folding around the clamp, with the deformed beam turning always in the same verse, is impossible. We will introduce a non-autonomous analog of a Lyapunov function $V_e(s)$, and will use it to prove the result.

The BVP, in the extensible case, can be written as:

$$\begin{cases} \theta''(s) = -b(1-s)\cos\theta(s) - \lambda b^2(1-s)^2\sin\theta(s)\cos\theta(s) \\ \theta(0) = 0 \\ \theta'(1) = 0 \end{cases} \quad (2)$$

where λ is a positive constant depending on the ratio between extensional and bending stiffness.

¹We remark that the right hand side of the ODE in (1) is analytic on its whole domain $[0, 1] \times \mathbb{R}$ and the radius of convergence is $+\infty$. Therefore, the bound for the amplitude of the analyticity interval, i.e. M^{-1} where M is the Lipschitz constant, is enough to prove analyticity of the solution on its whole domain in a standard fashion by applying multiple times the Cauchy-Kowalevski theorem.

Proposition 2: If θ is a solution of (2), then $\theta(s) = \frac{\pi}{2}$ and $\theta(s) = \frac{-3\pi}{2}$ for every $s \in [0, 1]$.

Proof:

Let us define $V_e(s)$ as

$$V_e(s) := \frac{1}{2}(\theta')^2(s) + b(1-s)\sin\theta(s) - b(1-s) + \frac{\lambda b^2}{2}(1-s)^2 \sin^2\theta(s) - \frac{\lambda b^2}{2}(1-s)^2$$

By direct computation:

$$V_e'(s) = \theta'[\theta'' + b(1-s)\cos\theta(s) + \lambda b^2(1-s)^2 \sin\theta(s)\cos\theta(s)] + b(1-\sin\theta(s)) + \lambda b^2(1-s)(1-\sin^2\theta(s)) \geq 0$$

Since $V_e(1) = 0$, and since the right hand side of the considered ODE is Lipschitz and analytic in its whole domain, the reasoning used in the inextensible case can be repeated and one has that $\theta(s) = \frac{\pi}{2}$ or $\theta(s) = \frac{-3\pi}{2}$ is impossible for every $s \in [0, 1]$.

The proof is complete.

This result excludes that equilibrium configurations (either stable or unstable) can turn more than one time around the clamped edge, which is by no means intuitively obvious at first sight. An example of an “impossible” equilibrium shape is shown in Fig.1.

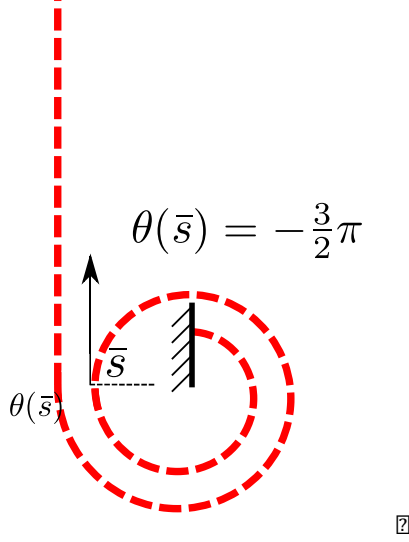


Figure 1: Example of an “impossible” equilibrium shape for an Euler beam under distributed load: propositions 1 and 2 prove that such a deformed shape, in which the beams turns two times around the clamp, cannot be an equilibrium configuration neither in the inextensible nor in the extensible case.

Remark 3. In the extensible case, the following bound is analogously obtained for the initial curvature:

$$V_e(0) = \frac{1}{2}(\theta'(0))^2 - b - \frac{\lambda b^2}{2}, \quad V_e(1) = 0 \quad -\sqrt{2b + \lambda b^2} \leq \theta'(0) \leq \sqrt{2b + \lambda b^2}$$

3 Properties of the minimizer in the extensible case

The total energy for a clamped extensible Euler beam with uniformly distributed load \mathbf{b} can be written as:

$$E(\theta, \alpha) := \int_0^1 \left[\frac{(\theta')^2}{2} + \frac{(\alpha - 1)^2}{2\lambda} - \mathbf{b} \cdot \boldsymbol{\chi} \right] ds \quad (3)$$

Here we are using the same notation employed in Chapter 5, and moreover $\alpha(s) := \boldsymbol{\chi}'(s)$ is the local strain and $\lambda > 0$ accounts for the ratio between bending and extensional stiffness. Let $\mathbf{b} = b\mathbf{e}_2$ ($\mathbf{e}_1, \mathbf{e}_2$ being the canonical basis of the affine plane). Performing an integration by parts and suitably choosing the primitive of $b(s)$, the energy can be written as:

$$E(\theta, \alpha) = \int_0^1 \left[\frac{(\theta')^2}{2} + \frac{(\alpha - 1)^2}{2\lambda} - b\alpha(1 - s) \sin \theta \right] ds \quad (4)$$

Imposing $\delta E = 0$ one deduces the algebraic relation

$$\alpha = 1 + b(1 - s) \sin \theta \quad (5)$$

which therefore is verified in every stationary point of E .

Let us define \tilde{E} substituting α into E :

$$\tilde{E}(\theta) := \int_0^1 \left[\frac{(\theta')^2}{2} - \frac{\lambda b^2}{2} (1 - s)^2 \sin^2 \theta - b(1 - s) \sin \theta \right] ds \quad (6)$$

Notice that the differential equation in (2) is the Euler-Lagrange equation associated to the energy functional (6).

Remark 4: It is clear that $\delta \tilde{E} = 0$ provides the same stationary points that one finds imposing $\delta E = 0$. Moreover, since E is strictly convex in α , assuming $\lambda b \leq 1$ it is easily proven the following:

Proposition 3: Let (θ, α) be the minimizer of E . Then θ is the minimizer for \tilde{E} . Moreover, if θ is the minimizer for \tilde{E} , then there exists $\alpha \in L^2$ such that (θ, α) is the minimizer of E .

We want now to study the qualitative properties of the absolute minimizer of the functional E .

Proposition 4: Let (θ, α) be the absolute minimizer of E . Then:

- $0 < \theta(s) < \frac{\pi}{2}$ for all $s \in (0, 1]$
- $\theta'(s) > 0$ for all $s \in [0, 1)$
- $\theta''(s) < 0$ for all $s \in [0, 1]$.

Proof:

Let (θ, α) be the absolute minimizer of E . Then, by Proposition 3, θ is a minimizer for \tilde{E} , and thus solves (2) in a strong form and it is $C^{\infty 2}$.

First of all, we want to show that $\theta(s)$ cannot be negative anywhere. Let us suppose that there exists $s_0 \in [0, 1]$ such that $\theta(s_0) < 0$. Then by continuity $\theta < 0$ on at least one interval. Let us consider now the function ξ defined as:

²This is proven exactly in the same way it was proven in the inextensible case in Chapter 5.

$$\begin{cases} \xi(s) = \theta(s), & s \in [0, 1] : \theta(s) > -\frac{\pi}{2} \\ \xi(s) = \frac{\pi}{2} & s \in [0, 1] : \theta(s) \leq -\frac{\pi}{2} \end{cases} \quad (7)$$

Since $\theta \in H^1$, it is easily seen that $\xi \in H^1$, that $\xi(0) = 0$, and that $\tilde{E}(\xi) < \tilde{E}(\theta)$. But, by Proposition 3, this is absurd. Therefore, $\theta(s) \geq 0$ for every $s \in [0, 1]$, and since $\theta(0) = 0$ and $\theta''(0) = -b < 0$, it has to be $\theta' > 0$ in a right neighborhood of zero.

Recalling Proposition 2, we have the following bound for the absolute minimizer:

$$s \in [0, 1], \quad \theta(s) \in [0, \frac{\pi}{2}) \quad (8)$$

Suppose now that $\theta'(s_0) < 0$ for some $s_0 \in (0, 1)$. Then, by continuity, θ has a maximum in some $s_1 \in (0, s_0)$. Therefore, since $\theta'(1) = 0$, there should be an inflection point $s_2 \in (s_1, 1]$. Collecting terms in the right hand side of equation (2), it is easily seen that, in all inflection points, it has to be either $\sin \theta(s) = \frac{-1}{\lambda b(1-s)}$ or $\cos \theta(s) = 0$. But recalling the bound (8), it is clear that both these possibilities are excluded (we recall that λ and b are positive). Suppose now that there exists $s_0 \in (0, 1)$ such that $\theta'(s_0) = 0$. Since we excluded both inflection points for θ and negative values for θ' , it has to be $\theta'(s) = 0$ for $s \geq s_0$. But then θ would be constant on an interval and by analyticity properties (recalled before), according to the boundary data this would imply $\theta \equiv 0$ in all $[0, 1]$, which is absurd. Therefore it is $\theta' > 0$ for all $s \in [0, 1)$ and the proof is complete.